

**TEMPERATURE DISTRIBUTION IN VERTICAL AND HORIZONTAL HIGH
PRESSURE VESSELS AND ITS IMPACT ON FOOD SAFETY**

by

MEENAKSHI KHURANA

**A dissertation submitted to the
Graduate School - New Brunswick
Rutgers, The State University of New Jersey**

in partial fulfillment of the requirements

for the degree of

Doctor of Philosophy

Graduate Program in Food Science

written under the direction of

Professor Mukund V. Karwe

and approved by

New Brunswick, New Jersey

October 2012

ABSTRACT OF THE DISSERTATION

Temperature Distribution in Vertical and Horizontal High Pressure Vessels and its Impact on Food Safety

By MEENAKSHI KHURANA

Dissertation Director:

Professor Mukund V. Karwe

The temperature distribution during High Hydrostatic Pressure Processing (HHPP) is of particular concern when high pressure process is carried out at higher temperatures, such as those associated with pressure assisted thermal pasteurization (PATP) and pressure assisted thermal sterilization (PATS). The pressure assisted thermal processes combine high pressure and heat to achieve pasteurization/sterilization temperature in order to eliminate the bacteria while maintaining better quality. During these processes, inactivation by temperature is the primary mechanism. Therefore for such processes, it is important to examine the temperature variation within the vessel to evaluate its impact on product safety.

The objective of this research was to predict the temperature distribution in vertical and horizontal high pressure vessels during pressure assisted thermal processing and to

quantify the temperature non-uniformity and its impact on microbial inactivation. The CFD software ANSYS[®]-Fluent was used to numerically predict the flow, temperature and *C. botulinum* inactivation distributions. Coefficient of variation (COV) was used to quantify and compare the process uniformity for various cases. Further, alkaline phosphatase (ALP), an enzyme present in raw milk was used as an indicator for experimentally verifying process uniformity.

The results obtained from the numerical simulations showed that the temperature non-uniformity arises in both vertical and horizontal high pressure vessels during HHPP due to the water added for compression, adiabatic compression heating, and conduction heat loss at vessel wall and ensuing natural convection cooling near the vessel wall. Based on the COV approach, (i) the temperature of water added for compression was found to have a major impact on the temperature distribution and inactivation of *C. botulinum*, (ii) adding an insulation to the vessel diminished the non-uniformity in temperature and *C. botulinum*, and (iii) process non-uniformity was found to be higher for a vertical vessel as compared to a horizontal vessel of same dimensions. Also, the experiments with alkaline phosphatase (ALP) in the vertical vessel showed location dependent inactivation, further confirming the existence of process non-uniformity.

The results from this research will help in process validation and process filing with regulatory agencies (USDA-FSIS and US-FDA) to develop guidelines for producing safe PATP and PATS processed foods.

ACKNOWLEDGEMENTS

It is a great privilege to thank all the people who made this dissertation possible and because of whom my graduate experience has been the one I will cherish forever.

Foremost, my deepest gratitude to my advisor, Dr. Mukund Karwe, for his excellent guidance, motivation, patience and for always being there to listen and give advice. I am grateful to him for giving me the opportunity to work on this research as well as on projects outside the scope of this research. I would also like to thank him for encouraging me to grow as a teacher and instilling in me to work hard with his mantra, there's always one more mountain to climb!

Special thanks to my dissertation and oral proposal committee members, Dr. Paul Takhistov, Dr. Kit Yam, Dr. Donald Schaffner, Dr. Alberto Cuitino from Rutgers University and Dr. Ramaswamy Anantheswaran from Penn State University for their guidance and valuable suggestions.

I am also thankful to the former and current departmental staff members for their various forms of support during my graduate study-- Paulette Arico, Irene Weston, Karen Ratzan, Karin Conover, Debbie Koch, Miriam Gonzalez, Yakov Uchitel, Dave Petrenka and Frank Caira.

I appreciate the financial support from NJAES (Rutgers-New Jersey Agricultural Experiment Station) and ELF (Equipment Leasing Fund) for funding high pressure equipment. I am also grateful to the sponsors of various scholarships and awards that I received during the course of this study.

I am also thankful to my cheerful group of fellow students who helped me stay motivated and focused through all these years. I greatly value their friendship and will cherish all the laughter, joy and mischief we shared.

Finally, this dissertation would not have been possible without the love, support, patience and encouragement from my family. Their love was my driving force and to them I dedicate this thesis. I hope this makes them proud!

TABLE OF CONTENTS

ABSTRACT OF THE DISSERTATION	ii
ACKNOWLEDGEMENTS	iv
TABLE OF CONTENTS	vi
LIST OF FIGURES	xii
LIST OF TABLES	xxiii
1. INTRODUCTION	1
1.1 Development of High Hydrostatic Pressure Processing	1
1.2 Basic Principles of HHPP	5
1.3 Potential Applications of HHPP	6
1.4 Effect of HHPP on Food Products	11
1.5 High Pressure Process and Equipment Description	12
1.6 Economics of High Pressure Processing	20
1.7 Thermal Transport during HHPP	22
2. LITERATURE REVIEW	29

2.1 Mathematical Modeling of HHPP	29
2.2 Microbial Inactivation with Pressure	36
2.3 Spore Inactivation with Pressure	38
2.4 Enzyme Inactivation with Pressure and its Potential as pTTI	40
3. RATIONALE AND OBJECTIVES	44
3.1 Research Rationale	44
3.2 Research Objectives	45
4. EXPERIMENTAL MATERIALS AND METHODS	48
4.1 Rutgers-High Pressure Processing Facility	48
4.1.1 Pressure Vessel Design and Dimensions	50
4.1.2 Working Description of High Pressure Process	51
4.1.3 Pressure Measurements	52
4.1.4 Temperature Measurements	53
4.2 Special Experimental Set Up	54
4.2.1 Time Constant Experiments	54
4.2.2 Initial High Temperature Experiments	56
4.2.3 Alkaline Phosphatase (ALP) Experiments	56
4.2.3.1 Introduction to Alkaline Phosphatase	56
4.2.3.2 Raw Milk Sample and its Placement in Vertical Vessel	59
4.2.3.3 Alkaline Phosphatase Activity Assay	59

5. THEORETICAL CONSIDERATIONS	63
5.1 Strength of Buoyancy Induced Flow (laminar or turbulent flow)	63
5.2 Governing Equations	64
5.2.1 Conservation of Mass	64
5.2.2 Conservation of Momentum	65
5.2.3 Conservation of Energy	66
5.3 Thermodynamics of High Pressure Process	68
5.3.1 Adiabatic Increase in Temperature	68
5.3.2 Pressure Work or Heat Generation (defined as boundary condition)	73
5.3.3 Velocity of Water Pumped into Vessel (defined as boundary condition)	74
5.4 Heat Transfer in Air Gap between Vessel and Shell (boundary condition)	75
5.5 Lag in Temperature Measurement	76
5.6 Impact of Temperature Distributions on Microbial Inactivation	87
5.6.1 Inactivation of <i>C. botulinum</i> spores	88
5.7 Quantification of Non-uniformity in Temperature and Inactivation of <i>C. botulinum</i>	89
5.7.1 Coefficient of Variation (COV), a Statistical Approach	90
6. NUMERICAL SIMULATION	93
6.1 Generation of Geometry and Meshing	93
6.1.1 Vertical High Pressure Vessel	94

6.1.2 Horizontal High Pressure Vessel	98
6.2 Importing Geometry/Mesh and General Settings	99
6.3 Defining Model	100
6.4 Defining Materials	102
6.4.1 Temperature Dependence of Material Thermophysical Properties	103
6.4.2 Pressure-Temperature Dependence of Material Thermophysical Properties	105
6.4.1.1 Create a C Source File	106
6.4.1.2 Compile the Source File	106
6.4.1.3 Hook the UDF to ANSYS®-Fluent Solver	107
6.5 Define Cell Zone Conditions	109
6.6 Define Boundary Conditions	109
6.7 Define Solution Methods	110
6.8 Run Calculation	111
7. RESULTS AND DISCUSSIONS	114
7.1 Parameters Governing High Pressure Process	114
7.2 Thermocouple Response & Parameters Governing Thermocouple Lag	118
7.2.1 Thermocouple Response	119
7.2.2 Quantification and Implications of Lag in Temperature	119
7.2.3 Parameters Governing Thermocouple Lag	121
7.2.4 Non-dimensional Temperature Difference	123

7.3 Numerically Predicted Results for Vertical and Horizontal Vessel	126
7.3.1 Validation of Numerical Model	127
7.3.2 Temperature and <i>C. botulinum</i> Distributions in Vertical Vessel	128
7.3.2.1 High Pressure “Cold Pasteurization”	129
7.3.2.2 Pressure Assisted Thermal Pasteurization (PATP)	132
7.3.2.3 Pressure Assisted Thermal Sterilization (PATs)	135
7.3.2.4 Effect of Thermophysical Properties	139
7.3.2.5 Effect of Water Inlet	144
7.3.2.6 Effect of Vessel Size	155
7.3.2.7 Effect of Insulating Sleeve	157
7.3.2.8 Effect of Inserting Pouches	164
7.3.2.9 Effect of Multiple Pressure Pulses (or Pressure Cycling)	164
7.3.3 Temperature and <i>C. botulinum</i> Distributions in Horizontal Vessel	
7.3.3.1 Pressure Assisted Thermal Sterilization (PATs)	169
7.3.3.2 Effect of Vessel Size	170
7.3.3.3 Effect of Insulating Sleeve	171
7.3.3.4 Effect of Inserting Pouches	178
7.3.4 Vertical vs. Horizontal Positioned Vessel	178
7.4 Temperature Non-Uniformity Mapping using Alkaline Phosphatase	180
8. CONCLUSIONS AND IMPACT	185
9. FUTURE WORK	188
10. BIBLIOGRAPHY	189

LIST OF FIGURES

Figure 1-1: Hydrostatic pressure at various levels and the pressure range used for foods.	2
Figure 1-2: Few examples of high pressure processed products currently in US market...	5
Figure 1-3: HHPP equipment assembly with vertically oriented pressure vessel (cylinder in blue).	14
Figure 1-4: HHPP equipment assembly with horizontally oriented pressure vessel.	14
Figure 1-5: Typical variation of pressure with time during HHPP.	17
Figure 1-6: Changes in high pressure equipment and operating costs in past few years..	22
Figure 1-7: Typical pressure and temperature variation with time during HHPP.	26
Figure 4-1: Rutgers 10 liter high hydrostatic pressure processing facility.	49
Figure 4-2: Details of Rutgers high hydrostatic pressure processing set up.	51
Figure 4-3: Schematic of Rutgers HHPP vessel with major dimensions.	52
Figure 4-4: High pressure thermocouple assembly (attached to the top closure) (a) made vertical for measuring the time constant of each thermocouple and (b) showing depth of thermocouples.	55
Figure 4-5: Experimental set up to heat the steel vessel using a water bath attached to a heating coil, (a) showing heating coil and (b) coil inserted.	57
Figure 4-6: Wire (metal) frame designed to position samples at several locations in the vertical high pressure vessel (a) View 1, (b) View 2, (c) points corresponding in the vessel geometry.	60

Figure 5-1: (a) Dimensions of HHPP vessel. Shaded area represents the radial section for numerical simulation, (b) computational domain used for simulation, Ri = 71 mm, Ro = 223 mm.	65
Figure 5-2: Adiabatic compression heating values (calculated from slope of the lines) for water, obtained from Food Biotechnology and Food Engineering, TU, Berlin.....	71
Figure 5-3: Anticipated response of the thermocouple to a ramp input during pressurization, pressure hold, and pressure release.	77
Figure 6-1: (a) Dimensions of HHPP vessel. Shaded area represents the radial section for numerical simulation, (b) computational domain used for simulation, Ri = 71 mm, Ro = 223 mm.	95
Figure 6-2: Computational mesh used for vertical vessel numerical simulation with points A, B, C shown by ⊕ corresponding to thermocouple tips in experimental assembly.....	97
Figure 6-3: Computational mesh for horizontal vessel numerical simulation.....	99
Figure 6-4: Problem setup window as appearing in the ANSYS®-Fluent program.	100
Figure 6-5: Energy equation enabled in the Energy dialogue box.....	100
Figure 6-6: Viscous model window showing k-epsilon model and its settings.....	101
Figure 6-7: Create/Edit Material window showing steel properties.	103
Figure 6-8: Create/Edit Material window: to define polynomial profile for change in water properties with temperature.	104
Figure 6-9: Compiled UDF dialogue box showing the attached UDFs.....	107

Figure 6-10: Create/Edit Materials window showing how to hook UDFs to the material properties.	108
Figure 6-11: Solver window as appears in ANSYS®-Fluent.	110
Figure 6-12: Residual monitors window as appearing in the ANSYS®-Fluent to define convergence criteria.	111
Figure 6-13: Iteration window as appearing in the ANSYS®-Fluent program.	112
Figure 7-1: The true temperature of water predicted using equations (5-31),(5-51),(5-72) and the thermocouple response predicted using equations (5-49), (5-70), (5-74) obtained when time constant was 10s and 20s respectively.	120
Figure 7-2: Dimensionless temperature difference at the end of (a) pressurization, (b) pressure hold, and (c) pressure release as a function of their respective governing parameters.	125
Figure 7-3: Comparison of corrected experimental and numerically predicted time-temperature variations at $T_i = 313 \text{ K}$ (40°C), $P = 586 \text{ MPa}$, for the thermocouple located (a) near top (A), (b) in between (B), and (c) near bottom (C) of the vessel in water.	128
Figure 7-4: Isotherms in water and s.steel wall for 10 L vertical vessel with water inlet from top at $T_i = 298 \text{ K}$, $P = 700 \text{ MPa}$, $Q = 400,000 \text{ W/m}^3$ for ($0 \leq t \leq 180 \text{ s}$), (a) before pressurization (0 s), (b) end of pressurization (180 s), & (c) after 600 s hold time (780 s).	131
Figure 7-5: Streamlines in water for 10 L vertical vessel at $T_i = 298 \text{ K}$, $P = 700 \text{ MPa}$, $Q = 400,000 \text{ W/m}^3$ for ($0 \leq t \leq 180 \text{ s}$), (a) before pressurization (0 s), (b) end of pressurization (180 s), & (c) after 600 s of hold period (780 s)..	132

Figure 7-6: Isotherms in water and s.steel wall for 10 L vertical vessel with water inlet from top at $T_i = 313$ K, $P = 700$ MPa, $T_{inlet} = 298$ K, $Q = 480,000$ W/m³ for $(0 \leq t \leq 180$ s), (a) before pressurization (0 s), (b) end of pressurization (180 s), & (c) after 600 s hold time (780 s). 134

Figure 7-7: Streamlines in water for 10 L vertical vessel at $T_i = 313$ K, $P = 700$ MPa, $T_{inlet} = 298$ K, $Q = 480,000$ W/m³ for $(0 \leq t \leq 180$ s), (a) before pressurization (0 s), (b) end of pressurization (180 s), & (c) after 600 s of hold period (780 s). 135

Figure 7-8: Isotherms in water and s.steel wall for 10 L vertical vessel with water inlet from top at $T_i = 368$ K, $P = 700$ MPa, $Q = 860,000$ W/m³ for $(0 \leq t \leq 180$ s), (a) before pressurization (0 s), (b) end of pressurization (180 s), & (c) after 600 s hold time (780 s). 137

Figure 7-9: Streamlines in water for 10 L vertical vessel at $T_i = 368$ K, $P = 700$ MPa, $T_{inlet} = 298$ K, $Q = 860,000$ W/m³ for $(0 \leq t \leq 180$ s), (a) before pressurization (0 s), (b) end of pressurization (180 s), & (c) after 600 s of hold period (780 s). 138

Figure 7-10: COV of temperature for vertical vessel at various initial temperatures (T_i), $P = 700$ MPa, & T_{inlet} (water added for compression) = 298 K..... 140

Figure 7-11: Isotherms in water and s.steel wall for 10 L vertical vessel at the end of pressurization (180 s) at $T_i = 313$ K, $P = 700$ MPa, $T_{inlet} = 298$ K, $Q = 400,000$ W/m³ for $(0 \leq t \leq 180$ s), (a) constant, (b) temperature dependent, & (c) pressure-temperature dependent thermophysical properties..... 142

Figure 7-12: Isotherms in water and s.steel wall for 10 L vertical vessel at the end of hold time (780 s) at $T_i = 313$ K, $P = 700$ MPa, $T_{inlet} = 298$ K, $Q = 400,000$ W/m³ for ($0 \leq t \leq 180$ s), (a) constant, (b) temperature dependent, & (c) pressure-temperature dependent thermophysical properties. 143

Figure 7-13: COV of temperature for 10 L vertical vessel at $P = 700$ MPa, $T_i = 313$ K, T_{inlet} (water added for compression) = 298 K (25°C), for constant, temperature dependent & pressure-temperature dependent thermophysical properties. 144

Figure 7-14: Isotherms in water and s.steel wall for 10 L vertical vessel at the end of pressurization (180 s) at $T_i = 368$ K, $P = 700$ MPa, $T_{inlet} = 298$ K, $Q = 860,000$ W/m³ for ($0 \leq t \leq 180$ s), (a) no water inlet, (b) water inlet from top, & (c) water inlet from bottom. 146

Figure 7-15: Isotherms in water and s.steel wall for vertical vessel at the end of hold time (780 s) at $T_i = 368$ K, $P = 700$ MPa, $T_{inlet} = 298$ K, $Q = 860,000$ W/m³ for ($0 \leq t \leq 180$ s), (a) no water inlet, (b) water inlet from top, & (c) water inlet from bottom. 147

Figure 7-16: Streamlines in water and s.steel wall for 10 L vertical vessel at the end of pressurization (180 s) at $T_i = 368$ K, $P = 700$ MPa, $T_{inlet} = 298$ K, $Q = 860,000$ W/m³ for ($0 \leq t \leq 180$ s), (a) no water inlet, (b) water inlet from top, & (c) water inlet from bottom. 148

Figure 7-17: Streamlines in water and s.steel wall for vertical vessel at the end of hold time (780 s) at $T_i = 368$, $P = 700$ MPa, $T_{inlet} = 298$ K, $Q = 860,000$

W/m ³ for (0 ≤ t ≤ 180 s), (a) no water inlet, (b) water inlet from top, & (c) water inlet from bottom.	149
Figure 7-18: Numerically predicted dimensionless temperature variation along the vertical mid-plane at the end of pressure hold period (780 s) for water inlet from top and water inlet from bottom at P = 700 MPa and T _i = 368 K.	150
Figure 7-19: Numerically predicted dimensionless temperature variation along the radial mid-plane at the end of pressure hold period (780 s) for water inlet from top and water inlet from bottom at P = 700 MPa and T _i = 368 K.	151
Figure 7-20: COV of temperature plotted against time for 10 L vertical high pressure vessel with no water inlet, water inlet from top and water inlet from bottom at T _i = 368 K, P = 700 MPa, T _{inlet} = 298 K, Q = 860,000 W/m ³ for (0 ≤ t ≤ 180 s).....	152
Figure 7-21: Contours for <i>C. botulinum</i> inactivation in water and s.steel wall for 10 L vertical vessel at the end of hold time (780 s) at T _i = 368 K P = 700 MPa, T _{inlet} = 298 K Q = 860,000 W/m ³ for (0 ≤ t ≤ 180 s), (a) no water inlet, (b) water inlet from top, & (c) water inlet from bottom.	153
Figure 7-22: COV of <i>C. botulinum</i> inactivation plotted against time for vertical high pressure vessel with no water inlet, water inlet from top and water inlet from bottom T _i = 368 K, P = 700 MPa, T _{inlet} = 298 K, Q = 860,000 W/m ³ for (0 ≤ t ≤ 180 s).	154

Figure 7-23: Numerically predicted dimensionless temperature variation along the horizontal mid-plane for vessels with different inner radii for $P = 700$ MPa, $T_i = 333$ K, $T_{inlet} = 298$ K, at the end of (a) pressurization (180 s), (b) hold period (780 s) for conduction only and conjugate heat transfers..... 156

Figure 7-24: Isotherms in water and s.steel vessel for vertical vessel at $T_i = 368$ K, $P = 700$ MPa, $T_{inlet} = 298$ K, $Q = 860,000$ W/m³ for ($0 \leq t \leq 180$ s), (a) without insulation, & (b) with insulation (12.7 mm thick) at the end of pressurization (180 s)..... 158

Figure 7-25: Isotherms in water and s.steel wall for vertical vessel at $T_i = 368$ K, $P = 700$ MPa, $T_{inlet} = 298$ K, $Q = 860,000$ W/m³ for ($0 \leq t \leq 180$ s), (a) without insulation, & (b) with insulation (12.7 mm thick) at the end of 600 s hold time (780 s). 159

Figure 7-26: Mean (volume average) temperature for 10 L vertical vessel at $P = 700$ MPa, $Q = 860,000$ W/m³ for pressurization ($0 \leq t \leq 180$ s), 600 s hold time ($t = 780$ s) & $T_i = 368$ K (95°C), $T_{inlet} = 298$ K (25°C), 368 K (95°C), 393 K (120°C) with or without insulation..... 161

Figure 7-27: Standard deviation in mean temperatures for 10 L vertical vessel at $P = 700$ MPa, $Q = 860,000$ W/m³ for pressurization ($0 \leq t \leq 180$ s), 600 s hold time ($t = 780$ s) & $T_i = 368$ K (95°C), $T_{inlet} = 298$ K (25°C), 368 K (95°C), 393 K (120°C) with or without insulation. 161

Figure 7-28: COV of temperature for 10 L vertical vessel at $P = 700$ MPa, $Q = 860,000$ W/m³ for pressurization ($0 \leq t \leq 180$ s), 600 s hold time

($t = 780$ s) & $T_i = 368$ K (95°C), $T_{\text{inlet}} = 298$ K (25°C), 368 K (95°C),
 393 K (120°C) with or without insulation..... 162

Figure 7-29: Mean log reduction of *C. botulinum* for 10 L vertical vessel at $P = 700$ MPa,
 $Q = 860,000$ W/m³ for pressurization ($0 \leq t \leq 180$ s), 600 s hold time
($t = 780$ s) & $T_i = 368$ K (95°C), $T_{\text{inlet}} = 298$ K (25°C), 368 K (95°C),
 393 K (120°C) with or without insulation..... 162

Figure 7-30: Standard deviation in mean log reduction of *C. botulinum* for 10 L
vertical vessel at $P = 700$ MPa, $Q = 860,000$ W/m³ for pressurization
($0 \leq t \leq 180$ s), 600 s hold time ($t = 780$ s) & $T_i = 368$ K (95°C),
 $T_{\text{inlet}} = 298$ K (25°C), 368 K (95°C), 393 K (120°C) with or without
insulation..... 163

Figure 7-31: COV of *C. botulinum* inactivation for 10 L vertical vessel at $P = 700$ MPa,
 $Q = 860,000$ W/m³ for pressurization ($0 \leq t \leq 180$ s), 600 s hold time
($t = 780$ s) & $T_i = 368$ K (95°C), $T_{\text{inlet}} = 298$ K (25°C), 368 K (95°C),
 393 K (120°C) with or without insulation..... 163

Figure 7-32: Isotherms in water, oil pouches, and s.steel wall for 10 L vertical vessel
at $P = 700$ MPa, $T_i = 333$ K (60°C), $T_{\text{inlet}} = 298$ K (25°C), Q (water) =
 $450,000$ W/m³ for ($0 \leq t \leq 180$ s), Q (olive oil) = $750,000$ W/m³ for
($0 \leq t \leq 180$ s), at the end of (a) pressurization ($t = 180$ s), (b) pressure
hold ($t = 780$ s)..... 165

Figure 7-33: Numerically predicted time-temperature data at a selected point
($z = 546$ mm, $r = 61$ mm) in the 10 L vertical vessel for 5 pressure

pulses (700 MPa) of 2 min hold time each, $T_i = 368 \text{ K}$ (95°C),
 $T_{\text{inlet}} = 298 \text{ K}$ (25°C) & $Q = 860,000 \text{ W/m}^3$ for pressurization..... 166

Figure 7-34: COV of temperature for 10 L vertical vessel at $T_i = 368 \text{ K}$ (95°C),
 $T_{\text{inlet}} = 298 \text{ K}$ (25°C), $Q = 860,000 \text{ W/m}^3$ for pressurization – single
pressure pulse ($P = 700 \text{ MPa}$) for 10 min hold time, 5 pulses (700 MPa)
for 2 min hold time each. 166

Figure 7-35: Mean of *Clostridium botulinum* inactivation for 10 L vertical vessel at
 $T_i = 368 \text{ K}$ (95°C), $T_{\text{inlet}} = 298 \text{ K}$ (25°C), $Q = 860,000 \text{ W/m}^3$ for
pressurization - single pressure pulse ($P = 700 \text{ MPa}$) for 10 min hold
time, 5 pulses (700 MPa) for 2 min hold time each..... 167

Figure 7-36: COV of *Clostridium botulinum* inactivation for 10 L vertical vessel at
 $T_i = 368 \text{ K}$ (95°C), $T_{\text{inlet}} = 298 \text{ K}$ (25°C), $Q = 860,000 \text{ W/m}^3$ for
pressurization - single pressure pulse ($P = 700 \text{ MPa}$) for 10 min hold
time, 5 pulses (700 MPa) for 2 min hold time each..... 167

Figure 7-37: Isotherms in water and s.steel wall for 10 L horizontal vessel (vertical
slices) of at $T_i = 368 \text{ K}$, $P = 700 \text{ MPa}$, Q (water) = $860,000 \text{ W/m}^3$ for
($0 \leq t \leq 180 \text{ s}$), with water inlet from both sides $T_{\text{inlet}} = 298 \text{ K}$, (a) location
of vertical slices w.r.t. pressure cavity, (b) end of pressurization (180 s),
& (c) after 600 s hold time (end of 780 s)..... 170

Figure 7-38: Isotherms in water and s.steel wall for horizontal vessel (vertical slices)
of 350 L at $T_i = 333 \text{ K}$, $P = 586 \text{ MPa}$, Q (water) = $480,000 \text{ W/m}^3$ for
($0 \leq t \leq 180 \text{ s}$), with water inlet from both sides $T_{\text{inlet}} = 298 \text{ K}$, (a) end of
pressurization (180 s) & (b) after 600 s hold time (end of 780 s)..... 171

Figure 7-39: 2D symmetric slice of horizontal vessel showing (a) radial mid-plane and (b) vertical mid-plane for plotting variable radius vessel results.....	172
Figure 7-40: Numerically predicted dimensionless temperature variation along the radial mid plane for horizontal vessels with different inner radii, $T_i = 368$ K, $P = 700$ MPa, at the end of hold time (780 s).....	173
Figure 7-41: Numerically predicted dimensionless temperature variation along the vertical plane for horizontal vessels with different inner radii, $T_i = 368$ K, $P = 700$ MPa, at the end of hold time (780 s).	173
Figure 7-42: Isotherms in water and s.steel vessel for 10 L horizontal vessel (slices) at $T_i = 368$ K, $P = 700$ MPa, $T_{inlet} = 298$ K, (a) no insulation, & (b) with insulation (12 mm thick) at the end of pressurization (180 s).	175
Figure 7-43: Isotherms in water and s.steel vessel for horizontal vessel (slices) at $T_i = 368$ K, $P = 700$ MPa, $T_{inlet} = 298$ K, (a) no insulation, & (b) with insulation (12 mm thick) at the end of hold period (780 s).	176
Figure 7-44: COV of temperature for horizontal vessel at $P = 700$ MPa, $T_i = 368$ K, $T_{inlet} = 298$ K (25°C), 368 K (95°C), with or without insulation.....	177
Figure 7-45: COV of <i>C. botulinum</i> inactivation for horizontal vessel at $P = 700$ MPa, $T_i = 368$ K, $T_{inlet} = 298$ K (25°C), 368 K (95°C), with or without insulation.....	177
Figure 7-46: Isotherms in oil pouches and s.steel wall for horizontal vessel at $T_i = 333$ K, $P = 700$ MPa, $T_{inlet} = 298$ K, Q (water) = 450,000 W/m ³ for ($0 \leq t \leq 180$ s), Q (olive oil) = 750,000 W/m ³ for ($0 \leq t \leq 180$ s), at the end of pressure hold period (780 s).....	179

Figure 7-47: COV of temperature for 10 L high pressure vessel when operated in vertical and horizontal positions where $P = 700$ MPa, $T_i = 368$ K, and $T_{inlet} = 298$ K.	180
Figure 7-48: The standard curve for 4-MU, relating concentration of 4-MU to relative fluorescence units.....	181
Figure 7-49: (a) Inactivation of ALP at (b) selected locations for vertical vessel at $P = 600$ MPa, $T_i = 328$ K (55°C), $T_{inlet} = 25^\circ\text{C}$. Letters a,b,c on each bar show statistical significance with $p < 0.05$	182
Figure 7-50: Confidence intervals for raw milk samples located at C1, C2, C3, C4, S1, S2, S3, and S4.....	184

LIST OF TABLES

Table 1-1: Adiabatic compression heating values for selected food substances obtained from various sources (Rasanayagam et al., 2003).....	24
Table 5-1: Theoretically calculated (using equation (5-20)) adiabatic compression heating values of water at different initial temperatures.....	70
Table 5-2: Adiabatic compression heating values for water extracted from pressure- temperature graph shown in Figure 5.2.	71
Table 5-3: Adiabatic compression heating values of water obtained from NIST- IAPSW standard database plots.	72
Table 7-1: Parameters governing the temperature difference at the end of pressurization, pressure hold, and pressure release stages of HHPP.	123

1. INTRODUCTION

High hydrostatic pressure processing (HHPP or HPP or HHP or Pascalization) is non-thermal food preservation and processing technology that can inactivate food borne pathogens and spoilage micro-organisms without significantly altering organoleptic properties and nutritional value of foods. Therefore, it can be used to improve quality and safety of food products, and to extend the shelf life of products. During HHPP, foods (solids or liquids, packaged or unpackaged) may be subjected to pressures up to 1000 MPa (145,000 psi). To get an idea of how high is this high pressure, one has to imagine pressure on a dime if three big elephants (weighing 4-5 tons each) are made to stand on it! Also, the pressure used for foods is 7-10 times higher than the pressure in the deepest part of ocean called Mariana trench (Knorr, 1999) as shown in **Figure 1-1**. Although the proof of concept of HHPP was demonstrated more than hundred years ago, its utility and successful applications have been demonstrated only in last couple of decades.

1.1 Development of High Hydrostatic Pressure Processing

HHPP was first demonstrated as a possible food preservation process in 1899 by Bert H. Hite at West Virginia Agricultural Experimental Station (Hoover et al., 1989; Knorr, 1999). Hite showed that high pressure treatment can delay the souring of milk at ambient temperatures (Knorr, 2003). Bridgman (1914) observed coagulation of egg white with high pressure treatment. The technology did not attract wide recognition in this period due to non-availability of suitable high pressure equipment (Rastogi et al., 2007) but it re-surfaced in food industry as an emerging technology in the late 1980s. Between 1982-

1988, D. Farkas, D. Hoover, and D. Knorr at the University of Delaware attempted to repeat Hite's work using a cold isostatic press and showed that pressures of 350 MPa (50,000 psi) can inactivate a wide range of pathogenic and spoilage microbes (Farkas, 2005). During the same period, studies were undertaken in Japan on preservation of foods by high pressure.

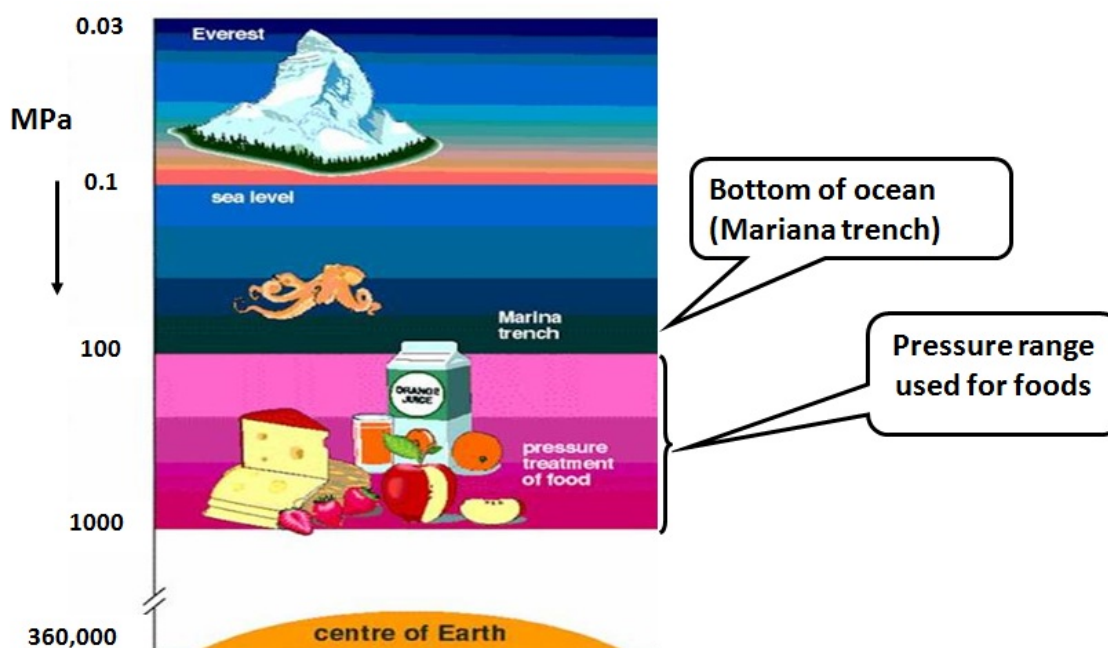


Figure 1-1: Hydrostatic pressure at various levels and the pressure range used for foods.

In 1992, commercialized high pressure processed products (high acid products including apple, strawberry, and pineapple jams) were marketed in Japan (Hayashi, 2002). Since then, high pressure processing has also been applied to fruit preserves, ingredients for rice cakes, raw squid, grape juice, and mandarin orange juice in Japan (Hayakawa et al., 1996; Rastogi et al., 2007). High pressure processed foods are in the market in Japan

since 1992 (Suzuki, 2002), and in Europe and in the United States since 1996 (Knorr, 1999; Knorr et al., 2002).

In the US, the impetus for high pressure technology came from the US Army research center in Natick, MA, in order to develop better quality MREs (Meal Ready to Eat) for the troops. In 1993, they initiated a study to preserve foods using high pressure. They teamed up with researchers at the University of Delaware and the Oregon State University to study the effect of pressure on microbes and to demonstrate pressure preservation of food products. Work over the next two years resulted in the successful preservation of spaghetti with meat sauce, spanish rice, yogurt with peaches and a fruit mix. Samples were shown to be microbiologically stable for up to 120 days at room temperature (Farkas, 2007).

The first commercial high pressure product in the US was Avo Classic Guacamole (a heat sensitive product) with extended refrigerated shelf life and manufactured by Avomex, Inc., Keller, TX. Recently, a leading Mexican manufacturer of juices and nectars, Grupo Jumex, utilized Avure's (high pressure processing equipment manufacturer) "Fresher Under Pressure" technology for their juice and smoothie product line. Also, growing concern for seafood safety led the seafood manufacturers to explore this technology and show many benefits such as almost 100% meat separation from shell for lobsters, oysters, clams and increased yield without any mechanical damage to the product. Other, commercially available high pressure processed products in Europe and the US include juice, tomato salsa, smoothies, fruit & vegetable purees, oysters and ready to eat meats.

In the US, high pressure process is currently commercialized by Hormel Foods (as TrueTaste™ technology on its Hormel® Natural Choice® products), Motivati Seafoods Inc. (for Gold Band Oysters®, Gold Band Frozen Half Shell Oysters®, Perfectly Shucked Oyster Meat®, and Gold Band Frozen Half Shell Clams®), Fresherized Foods™ (for Wholly Guacamole, Wholly Salsa), SimplyFresco™ (as Cucina Fresca™ Pasta Sauce & Cucina Fresca™ Salsa), Mission Avocados (as Culinary Fresh™ on its Mr. Avocado products), Cargill (Fressure™ fresh ground beef) and others. Some of the products are shown in **Figure 1-2**.

Companies using HHPP in other countries include FressureFoods™ in New Zealand (All natural Avocado Spread, All natural Mild Guacamole & All natural Spicy Guacamole), PreshaFruit™ in Australia (Preshafruit® Juices & Preshafruit® Fruit Coulis), MacLab in Australia (Stabilised Mussel Powder), Campofrio in Spain (Vuelta y Vuelta), FruityLine® in Netherlands and more. The high pressure treated products currently available are mainly for refrigerated and high acid foods because of the inability of the process to destroy spores without added heat (Zhu et al., 2008). Some of the companies in the US that provide HHPP tolling services (contract manufacturing) are AmeriQual Foods (Evansville, IN), HPP Food Services (Wilmington, CA), American Pasteurization Co. (APC) (Milwaukee, WI), GoodFoods™ Group (Chicago, IL) and Millard (Headquarters: Omaha, NE, facilities around North America).

The high pressure technology is expanding rapidly for new product development and product improvements in different segments of food industry such as dairy sector (cheese, yogurt, mayonnaise), fruits & vegetables (wet salads, smoothies, sauces),

seafood, juice and beverage. Also, because of the advantages of high pressure process over thermal processing such as better retention of color, flavor, texture etc., the technology is becoming a topic of major interest for cosmetic and pharmaceutical industry.



Figure 1-2: Few examples of high pressure processed products currently in US market.

1.2 Basic Principles of HHPP

The two basic principles that govern the effect of high pressure processing of foods are Pascal's isostatic principle and Le Chatelier's principle (Venugopal, 2006). Before discussing the principles let's understand the types of foods that can be processed under high pressure. HHPP can be used for both liquid and solid foods (with sufficient moisture for uniform pressure transmission). But foods containing air pockets such as whole strawberries, breads, whole eggs, marshmallows are not suitable for the process because during high pressure the air is squeezed out and the product containing air does not come back to the original shape after pressure is released.

The Pascal's isostatic principle answers the question, why foods do not get crushed under high pressure? According to Pascal's principle high pressure acts uniformly and instantly throughout the mass of a food, i.e., the process time is independent of the volume and shape of the food product. Isostaticity has been assumed for several years for HHPP, but with the increasing applications of HHPP for different food products the recent topic of discussion is whether the pressure is transmitted uniformly in a heterogeneous food product such as foods containing bones or fibers. This issue remains unresolved and is an active research area.

The physico-chemical changes occurring during HHPP follow the Le Chatelier's principle, which states that any reaction, conformational change, or phase transition that is accompanied by a decrease in volume will be favored at high pressures, while reactions involving an increase in volume will be inhibited (Lopez-Malo et al., 2000).

Another important principle that is applicable during high pressure processing is the heat of compression. Although many food and non-food materials are incompressible at atmospheric pressure, they get compressed under very high pressure (e.g., water). The work done to increase the pressure, i.e., compress the substance gets converted into heat which results in increase in temperature of the substance. This principle is discussed in detail in section 1.7.

1.3 Potential Applications of HHPP

The initial emphasis of high pressure treatment was directed mostly towards food preservation by destruction of microorganisms, with the aim of extending shelf life of the

food product while achieving minimum impact on product quality. With subsequent research, its potential for physical modification of structure and function of food and food constituents as well as the possibility for development of new processes such as pressure assisted freezing, thawing, and rehydration etc., were recognized (Rastogi et al., 2007). Other influences of pressure on food materials include protein denaturation or modification, enzyme activation or inactivation, changes in enzyme substrate interactions and changes in the properties of polymer carbohydrates and fats (Butz and Tauscher, 2002).

The application of high pressure processing also has considerable potential as an alternative to conventional thermal treatment in terms of instantaneous pressure transmission, i.e., time for pressurization treatment is independent of size and shape of food product (hence a larger product does not need longer processing time than a smaller product), reduced process times, retention of freshness, texture, flavor, and color (Butz et al., 1997). Also, high pressure does not alter the food structure significantly as pressure is applied isostatically, i.e., equally from all the directions which provides a uniform effect. Therefore, HHPP offers a unique way to produce new, safe, high quality products, with minimum detrimental effects that are associated with thermal processing such as loss of original flavor and color.

Some of the potential applications of high pressure processing are discussed in detail in the next few sections.

(a) Quality Retention and Enhancement

In general, chemical reactions associated with reduction in volume are favored during HHPP. However, high pressure does not affect the covalent bonds in foods (Knorr, 1999). Therefore, the retention of color, nutrients and taste in high pressure processed foods is better compared to thermally processed foods. Van Loey et al. (1998) showed that pressures up to 800 MPa and temperatures below 50°C had no effect on the color (chlorophyll) of broccoli juice. Butz et al. (2002a) found that chlorophyll was stable at 75°C and 600 MPa for long treatment times (10-40 min) and that vitamin C was stable after high pressure processing. Krebbers et al. (2003) observed an increase in the brightness of red color of tomato puree treated at 700 MPa, for 1 min at 80-90°C. Ahmed et al. (2005) reported no significant change in color of fresh and canned mango pulp with high pressure (100-200 MPa). Rodrigo et al. (2007) found a maximum of 8.8% increase in color of strawberry with pressure-temperature treatment of 300-700 MPa and 65°C.

(Butz et al., 2002) showed no major changes in nutritional values and in antioxidant activity of crushed or liquid extracts of tomato and carrot after HHPP. Butz and Tauscher (2002) found that under pressure, aspartame decayed to its non-sweet components faster in milk but in acidic medium like juices or carbonated drinks it was insensitive to pressure. They also showed that during HHPP of carrot puree, carotenoids were well protected since they are buried in lipophilic environments, which implies that the food matrix offers protection against loss of quality. In another study on orange juice (freshly squeezed), sensory panel could not perceive difference between pressure treated and unpressurized juice (Ludikhuyze and Hendrickx, 2002). In addition, control juice showed

signs of fermentation after 2 weeks at 6°C and became organoleptically unacceptable, however, the pressure treated juice remained free from fermentation for 5 weeks at 6°C.

(b) Modification of Structure and Function of Foods

High pressure has a potential for modification of structure and function of food and food constituents such as protein denaturation and starch gelatinization (Knorr, 1999). Enzymes are a special group of proteins which have been shown to activate under lower pressures (100-200 MPa) while higher pressures generally induce complete to partial enzyme inactivation (Knorr, 1999). Protein denaturation with pressure is affected by pH, presence of salt, substrate concentration, and subunit structure of enzyme (Hoover et al., 1989). Process parameters like pressure, time, and temperature affect restructuring of proteins, which may lead to high value products (Messens et al., 1997). Molina and Ledward (2003) studied the gelation of soy proteins and found that pressurizing the proteins before heat treatment or pressure treatment alone gave different results from heating alone. The pressure denatured protein has more features of native protein than of temperature denatured protein (Ludikhuyze and Hendrickx, 2002).

Aqueous starch dispersions could be gelatinized at room temperature under high pressure (Solt, 1998). They further found that pressure induced gels of waxy maize and potato starch were stronger than heat induced gels. Bárcenas et al. (2010) studied the effect of pressures between 50-250 MPa for 1-4 min on wheat dough and bread made from this pressure treated dough. They found that dough hardness and adhesiveness significantly increased, the treated dough gave breads with different appearance, e.g., the crumb acquired brownish color and heterogeneous cell gas distribution resulted in new crumb

structure. They suggested that HHPP in the range 50–200 MPa could be an alternative technique for obtaining novel textured cereal based products. Thus, combination of heat and high pressure can offer novel textures and novel products.

(c) Pressure Assisted Processes

(i) Freezing and Thawing

HHPP offers a possibility for new process options like high pressure assisted freezing and thawing, and pressure shift freezing and thawing (Knorr, 1999). Pressure assisted process is normal freezing or thawing occurring under a constant but higher than atmospheric pressure while pressure shift freezing or thawing is achieved during sudden pressure release (depressurization). Decrease in melting and freezing point of water with pressure to a minimum of -22°C at 207.5 MPa (Cheftel et al., 2000; Denys et al., 1997; LeBail et al., 2002a; LeBail et al., 2002b) leads to rapid ice nucleation resulting in small and uniform ice crystals during pressure release and causes less structural damage to the food compared to conventional slow freezing. It was found that pressure shift freezing (140MPa, -14°C) resulted in smaller and more uniform ice crystals compared to air blast freezing (Chevalier et al., 2002). Fernández et al. (2006) showed that the pressure-shift freezing is more advantageous than pressure assisted freezing due to expansion and temperature drop obtained and homogeneous ice-crystals.

In general, thawing occurs more slowly than freezing, further damaging the food. Pressure induced thawing reduces the loss of water holding capacity and improves color and flavor preservation in fruits (Rastogi et al., 2007). Also, high pressure treatment has been shown to reduce the thawing time of frozen meat to one-third of time necessary at

atmospheric pressure and also to reduce drip loss (Chourot et al., 1997; Denys et al., 1997; LeBail et al., 2002b). Finally, another potential application of high pressure could be storage at subzero ($< 0^{\circ}\text{C}$) temperatures without freezing (because pressure decreases the freezing point of water) which can be explored not only for foods but also for cells, animal tissues/skin for transplant etc.

(ii) Dehydration and Rehydration

Dehydration process like osmotic dehydration is a slow process. Application of high pressure causes permeabilization of cell structure thus allowing enhanced mass transfer. It has been shown that after pressure treatment at 600 MPa for 15 min, the drying rate of sliced potatoes increased significantly (Rastogi et al., 2007). Similarly, enhanced water removal and solid gain was observed during osmotic dehydration of pineapple (Rastogi et al., 2007). Most dehydrated foods are rehydrated before consumption. Loss of solids during rehydration is a major problem associated with dehydrated foods. Increased water uptake during soaking of glutinous rice was found after a pressure treatment of up to 600 MPa (Rastogi et al., 2007).

Another, major application of high pressure is inactivation of micro-organisms, spores, and enzymes. The effect of high pressure on several microbes, spores, and enzymes will be discussed in a later section.

1.4 Effect of HHPP on Food Products

As discussed in the previous section, HHPP can result in products with novel structure and texture, or increased functionality of certain ingredients providing the possibility for development of new food products (Rastogi et al., 2007).

HHPP has been shown to be useful for improving shelf life of yogurt and defrosting frozen seafood (Hayakawa et al., 1996). It has also been shown to improve rennet or acid coagulation of whey proteins and increase cheese yield (Trujillo et al., 2000). HHPP can be used to design or improve existing products like cream caramel with fresher taste and better texture (Ponce et al., 1998). HHP treatment may increase mass transfer and juice yield, and enhance drying (Knorr, 2003). HHPP can result in improved release of metabolites from plants and reduced fat uptake of French fries (Knorr, 1999). A reduction of 40% in oil uptake during frying was observed, when thermally blanched frozen potatoes were replaced by high pressure blanched potatoes (Rastogi et al., 2007). Sanchez-Moreno et al. (2002) have found that carotenoid and vitamin A in orange juice could be extracted better with increasing pressure from 100 to 400 MPa.

The above sections (1.1, 1.2, 1.3) discussed the development, applications, and effects of HHPP on different foods. The next section will discuss the high pressure process considerations, kind of equipments used for high pressure process, and their limitations.

1.5 High Pressure Process and Equipment Description

High pressure food processing is typically carried out as a batch process where foods, solids or liquids are subjected to pressures between 100 and 1000 MPa. Although the effect of high pressure on foods up to 1000 MPa (145,000 psi) has been investigated on laboratory scale vessels, for the commercial applications the equipment design limitations restrict the pressure levels to 690 MPa (100,000 psi). High pressure equipment with pressures up to 690 MPa and temperatures in the range of 5 to 120°C for process times up

to 60 min are currently available to the food industry for large scale processing (Henry and Chapman, 2002).

Commercial high pressure units are available with pressure vessels that can operate in vertical or horizontal positions as shown in **Figure 1-3** and **Figure 1-4**, respectively. The vertical vessels came first and are more common for pilot size vessels (up to 320 L). As the demand for high pressure processed products increased and the technology became commercial, there was a need for higher capacity vessels. From high pressure vessel design, safety and mechanical strength point of view, it is always recommended to increase length of the cylinder instead of radius. Designing tall vessels is possible but can pose various problems such as unstable vessel, difficulty in loading, and changes in the existing facilities with low roof lines. To solve the problem for existing facilities with low roof lines, few companies designed the space efficient layout of equipment by placing the pump and other supporting mechanical equipment at a sub-level (basement) and operated it from top.

Later, horizontal vessels were built to serve installations where vertical space is limited (buildings with low roof lines) and minimum plant alteration is required. Over time, other advantages of horizontal vessel were recognized such as it allows single direction in-line product flow which is favored by most regulatory agencies for all food processes because it allows separation of processed and unprocessed food products.

The vertical and horizontal high pressure vessels are commercially available either as a conventional batch system or semi-continuous system. With batch systems, both solid &

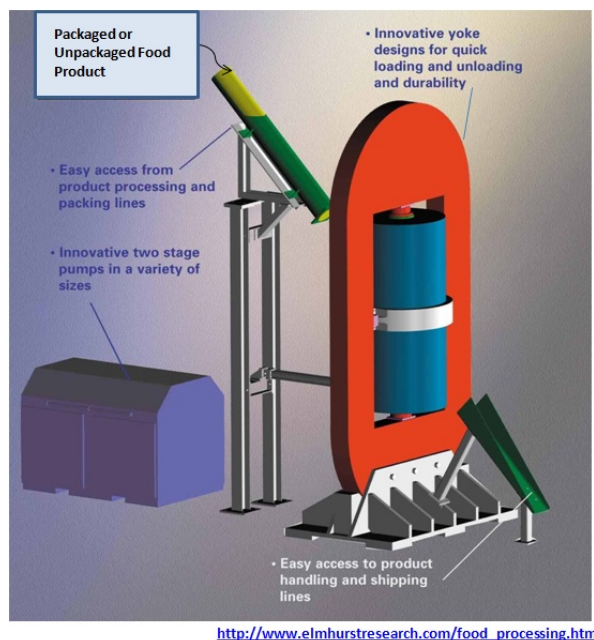


Figure 1-3: HHPP equipment assembly with vertically oriented pressure vessel (cylinder in blue).

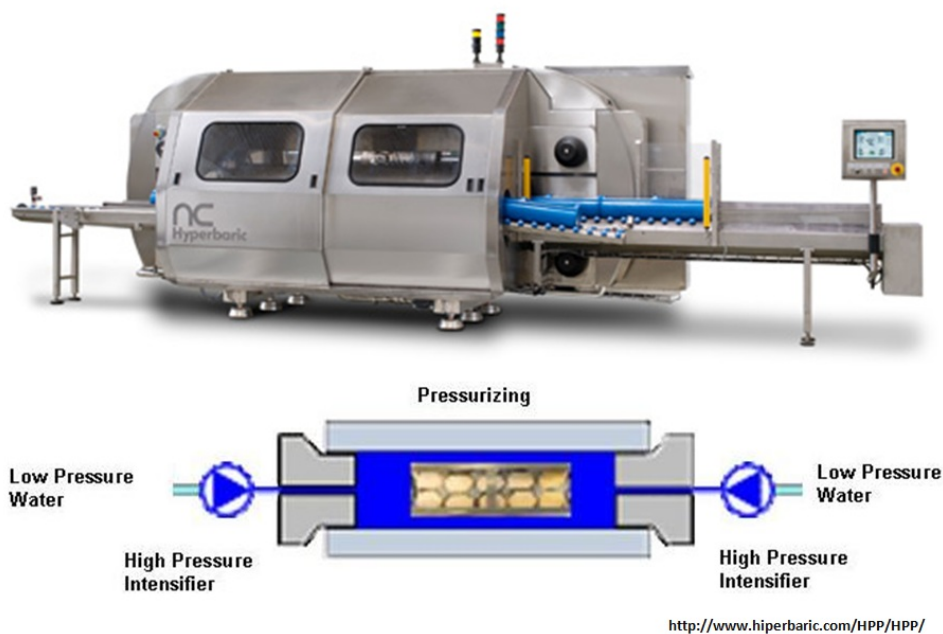


Figure 1-4: HHPP equipment assembly with horizontally oriented pressure vessel.

liquid pre-packaged food products can be treated whereas only low viscous pumpable liquid foods (no package) can be treated with semi-continuous systems.

During a batch high pressure process, food products are generally vacuum packed (some products like shell fish are banded and placed in a mesh bag) in flexible pouches or containers and loaded in the vessel, the vessel is then filled with a pressure transmitting medium. Water is frequently used as a pressure transmitting fluid in the food industry from its mechanical safety and economic point of view (Makita, 1992). The high pressure process is then accomplished in three stages: compression (pressurization) stage where pressure is increased from ambient to the desired high pressure as shown in **Figure 1-5**. During the pressurization stage the work done to increase the pressure (compress the food and pressurizing medium) gets converted into heat and increases the temperature of the food and pressurizing medium. These thermal effects associated with high pressure process are discussed in detail in section 1.7. The pressurization stage is followed by a pressure holding stage where the pressure is held constant at the elevated pressure level for several minutes. Finally, the pressure is reduced to atmospheric during depressurization stage. The product is then taken out for further treatment or packaging.

Currently, available semi-continuous systems typically use two or more pressure vessels that are sequenced to deliver a continuous product. This is accomplished by operating three vessels such that while the first vessel is loading, the second vessel is under compression, and the third is discharging at any point in time (Balasubramaniam et al., 2008). In the US, Avure Technologies (Kent, WA) manufactures semi-continuous systems for processing clear liquids such as juices. A low pressure food grade pump is

used (as juice is pumped from one vessel to another) to fill the vessel. When filled, the input port is closed and high pressure process water is introduced behind the free piston to compress the food. After the pressure is held constant for the required period, the system is decompressed by releasing the pressure on the high pressure process water. The liquid after treatment is discharged from the pressure vessel into a sterile hold tank. Then the treated liquid food can be filled aseptically into pre-sterilized containers.

High pressure can be generated in the system by three ways: direct compression, indirect compression, and heating of pressure transmitting medium. In direct compression a piston with a large end and a small end is used. The large end of the piston is connected to a low pressure pump and small end is used to apply pressure on the transmitting medium by the action of hydraulic pressure applied over large end of piston. Indirect compression uses a high pressure intensifier to pump the pressurizing medium from a reservoir directly into a closed and deaerated vessel to reach a given pressure (Venugopal, 2006). This system also uses a piston to increase the pressure, as in direct compression, but the displacement of the piston is achieved by pumping water with an intensifier (high pressure pump) into the vessel. The third pressurization method which has not been used in food industry so far, involves the heating of the pressure transmitting medium inside the vessel to cause expansion of the medium due to increase in temperature and the closed vessel does not allow the medium to expand (Venugopal, 2006).

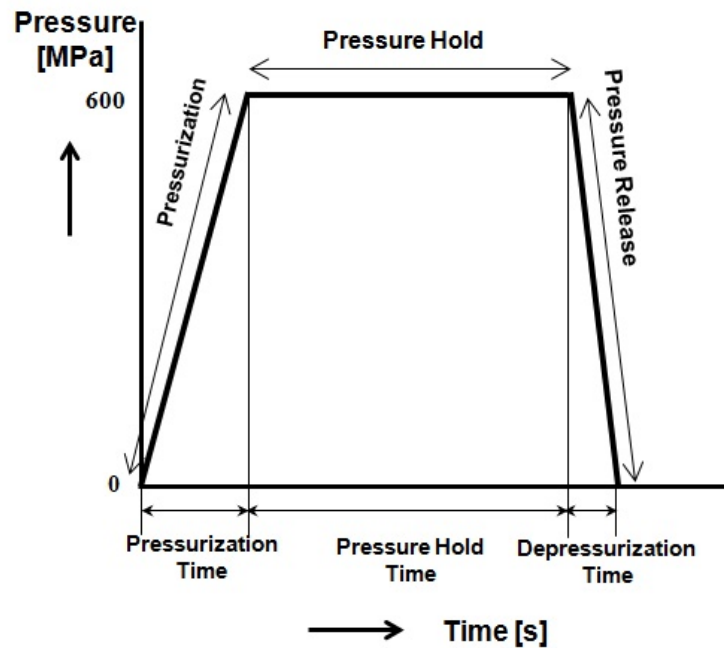


Figure 1-5: Typical variation of pressure with time during HHPP.

Typical batch high pressure equipment consists of a cylindrical steel vessel with high tensile strength, two end closures, a means for restraining end closures (a closing yoke to cope with high axial forces), direct or indirect pressure pumps for pressure generation, and necessary pressure and temperature controls (Henry and Chapman, 2002). The cylindrical steel vessel used can be a monobloc cylinder with several advantages such as simple construction, high precision in strength calculations and low production costs but they can be used only for smaller size vessels. They are not suitable for large size vessels due to problems like reduction in strength. Very high fluid pressures produce high forces and thus need thick walled cylinders. In monobloc cylinders, the Hoop stress at outside of the wall thickness is appreciably less than that at the inside surface, hence, wall material is not used to the fullest strength (Fryer and Harvey, 1997). One method to mitigate this has been through residual stresses imposed by multilayered cylinder (compression fitted)

and wire winding of cylinder (trade name QUINTUS[®] - Flow Pressure Systems). In a multi layered vessel two or more cylinders are shrinkage fitted (compression fitted) which give rise to high compressive residual stresses within the inner cylinder due to compression fitting and increase the fatigue strength, thus assuring safety even when fatigue failure occurs within the cylinder. Wire winding of cylinders also results in compressive residual stresses within the wall of the cylinder and thus high tensile stresses do not arise when wire wound cylinders are subjected to internal pressures, giving them higher strength (Koizumi and Nishihara, 1991). It also provides 'leak before break' failure mode to for large cross-section vessels and thus ensures safety.

In addition to the above design features required for high pressure vessel, another consideration for the high pressure process to be effective is that the food substances must contain liquid (e.g., water or oil) for pressure transmission and not have major internal air pockets. Food substances containing entrapped air/air pockets such as strawberries or marshmallows would be crushed under high pressure due to differences between the compressibility of air and water, and when under pressure the air from these pockets escape causing cell rupture which cannot be reversed after pressure is released. But an air filled balloon does not burst under pressure because it is perfect elastic and consists of a closed cell from which air cannot escape. Also, dry solids do not have sufficient moisture to make high pressure processing effective for microbial destruction.

Two of the major manufacturers of high pressure equipment are:

- (i) Avure Technologies Incorporated (Kent, Washington):

Avure Technologies Incorporated is a wholly owned subsidiary of Flow International Corporation (United States and Sweden). It is also the producer of 'Fresher under PressureTM' technology.

Avure's high pressure product line includes small lab units (2L – 690 MPa, 10-90°C) for local testing and large commercial-scale systems with pressure vessel capacities from 35 liters up to nearly 700 liters (35L – 600MPa, 215L-600MPa, 320L-400MPa, 350L-600MPa, and 687L-300MPa). Avure manufactures both batch and continuous systems.

(ii) NC Hyperbaric (Spain):

The NC Hyperbaric high pressure processing equipment WAVE 6000 RANGE includes WAVE 6000/55 (55L volume), WAVE 6000/135 (135L volume), WAVE 6000/420, WAVE 6000/300, and WAVE 6000/300T (2 vessels with 300L volume operating in tandem). The above units operate in horizontal position, have a maximum working pressure of 600 MPa and temperature range of 5-30°C.

Other high pressure equipment manufactures include Elmhurst Research, Inc. (Albany, NY, United States), Engineered Pressure Systems International (Belgium)/ Engineered Pressure Systems Incorporated (Boston, MA, United States), UHDE Hockdrucktechnik (Germany), Stansted Fluid Power (United Kingdom), Resato International (Netherlands), Kobe Steel (Japan), ACB Pressure System-Alstom (France), and UNIPRESS (Poland) (Hendrickx and Knorr, 2002).

1.6 Economics of High Pressure Processing

For a new technology such as high pressure to be successful commercially it should reduce the cost of the food product and/or provide opportunities for improving its quality and safety. Although, currently high pressure processing is more expensive compared to conventional thermal processing, it offers value added products (by retaining nutritional components, color, flavor and texture) with longer shelf life. This is the reason for high pressure being used for niche products such as seafood and guacamole. For example, the seafood industry in the U.S is using the high pressure process for processing oysters since 2000 and now clams, mussels, crabs, and lobsters because of the advantages of ease of shucking (meat separation from shell), safety (inactivation of sea borne pathogens as *Vibrio*), and increased yield (Kural and Chen, 2008).

A typical investment for a commercial high pressure processing unit is in the range \$500,000 to \$ 2.5 million (depending on the equipment capacity) of which 50-60% is contributed by the high pressure vessel, closures, and yoke. Therefore, pressure vessel is the most crucial component of the unit.

The main factors that govern the cost of processing per liter along with the capital cost are the capacity of the system, energy requirements, and the maintenance. Similar to other food processing technologies, increasing the vessel volume decreases the cost per liter. The energy cost and the maintenance cost for high pressure unit is affected by the number of pulses (pressure cycles) and the total cycle (pressurization, pressure hold and pressure release) time (De Heij et al., 2003). Generally, the energy cost is low and

comprise about 2-4% of the total costs. The maintenance of the system demands frequent replacement of the static or dynamic seals which is about 5% of the investment cost per year. In 1998 ABB (Asea Brown Boveri) group advised purchasers of their internal intensifier units (subject to their usage) to replace seals monthly when operating at 400 MPa and weekly for 600 MPa (Hendrickx, 2001).

In the early stages of commercial application of high pressure processing technology for foods only few companies were using this technology because the cost of high pressure processed food product was approximately 10 times more than the high temperature treated products which were 2-4 cents per liter (Hendrickx, 2001). With the advancement in the high pressure equipment technology and more commercial acceptance of high pressure products, Balasubramaniam et al. (2008) quoted the HHPP treatment cost as 4-10 cents/lb which is not very different from thermal processing. To reduce the cost of high pressure products several authors suggest increasing the capacity while reducing the capital cost. **Figure 1-6** shows the decreasing equipment and operating costs of high pressure technology over the last 12 years.

The developments in equipment design and industrial adaptation of the process are causing decrease in overall cost of the process. Therefore, successful applications and the growing market for high pressure processed products suggest that the initial investment costs may be sustainable. Also, it appears that the consumers are willing to pay extra for new products with better quality and more convenience than existing products (Norton and Sun, 2008).

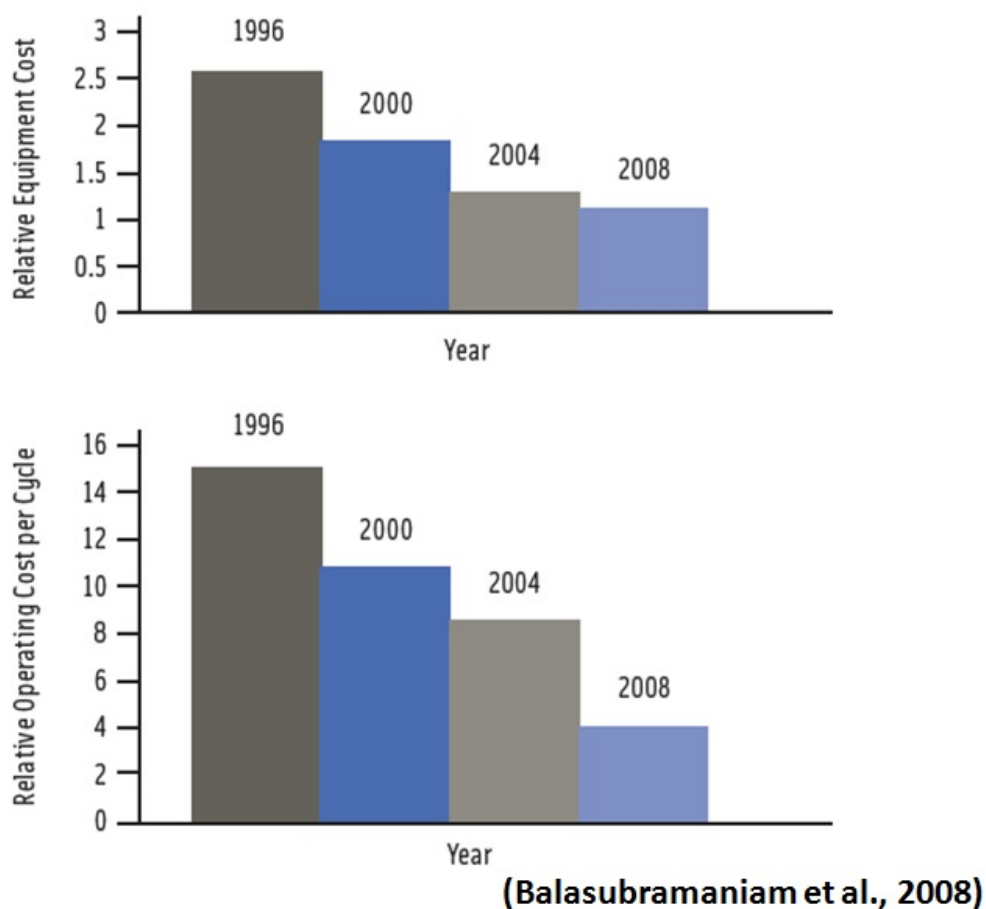


Figure 1-6: Changes in high pressure equipment and operating costs in past few years.

1.7 Thermal Transport during HHPP

Although, HHPP is termed as a non-thermal process, thermodynamics dictates that all compressible substances undergo increase/decrease in temperature during compression/expansion. Most of the food substances including water are incompressible at lower pressures but at high pressures they undergo substantial compression. For example, water which is a polar substance gets compressed by 15% at 600 MPa whereas hexane (non-polar) is compressed by 25% at 600 MPa (Ludikhuyze and Hendrickx,

2002). When high pressure is applied to a food substance, the molecules of the food get compressed, i.e., their intermolecular distance decreases and heat is generated due to work done against the intermolecular forces. The heat so generated is known as adiabatic heat of compression which results in an increase in temperature of the food. This rise in temperature is reversed upon depressurization as the heat is absorbed. Temperature increase in °C per 100 MPa increase in pressure is generally known as the compression heating value of a substance. The compression heating value for different foods depends on factors such as process pressure, compressibility, initial temperature, composition of food, and their properties like viscosity, thermal conductivity and heat capacity (Rasanayagam et al., 2003). **Table 1-1** shows adiabatic compression heating values for different food substances. Some dependence of compression heating value of a food on process pressure is expected as for water this value changes with increase in pressure (Barbosa-Cánovas and Rodriguez, 2005).

The compression heating values for foods range from 2-40°C. For water this value is 2-3°C whereas for oils and fats it is 6-9°C due to their higher compressibility, lower thermal conductivity and lower heat capacity. Compression heating value of lipids is independent of length of hydrocarbon chain but higher degree of unsaturation of hydrocarbon chain lowers the compression heating value for lipids (Heremans, 2002). For solvents such as hexane this value could be as high as 40°C. It has also been shown that the compression heating value of water increases with increasing initial temperature while compression heating value of oil is not significantly affected by initial temperature (Rasanayagam et al., 2003). In food industry, water is most commonly used as a pressure transmitting

medium because of its safety, low cost, and comparable compression heating value to most foods like juices. Also, if the pressure transmitting fluid has high compression heating value like oils, the microbial inactivation data could include unintended thermal effects (Ting, 2002).

Table 1-1: Adiabatic compression heating values for selected food substances obtained from various sources (Rasanayagam et al., 2003).

Substance at 25°C	Temperature change (°C) per 100 MPa
Water	~ 3.0
Orange Juice	~ 3.0
2% Fat Milk	~ 3.0
Tomato Salsa	~ 3.0
Salmon	~ 3.2
Chicken Fat	~ 4.5
Beef Fat	~ 6.3
Olive Oil	~ 6.0 to 8.7
Soy Oil	~ 6.2 to 9.0
Hexane	~ 40.0

The heat generated due to adiabatic compression heating of the pressurizing medium results in temperature difference between the food sample, pressurizing medium and the vessel wall, and is continuously dissipated through the thick metal walls of the vessel by

heat conduction if the wall is cooler. This happens during pressurization and also during pressure hold time when there is no heat generation. Therefore, upon depressurization, the temperature drops below the initial temperature as shown in **Figure 1-7**. The heat loss at the wall gives rise to non-uniform temperature distribution with the fluid at the center of vessel being warmer than the fluid near the wall. Also, free convection sets in near the vessel wall affecting the temperature distribution. Makita (1992) observed that, although temperature of high pressure medium at the wall of the vessel decreases quickly due to high thermal conductivity of the vessel metal, at the center, the temperature of the medium reaches a maximum temperature that is close to the sum of initial temperature of medium and increase in temperature due to compression heating. In addition, during indirect pressurization, compression is achieved by pumping liquid (mostly water) into the vessel through an intensifier pump till the required pressure is attained. This additional water pumped into the vessel to achieve compression can be at a temperature different from the temperature of the water in the vessel further affecting the temperature distribution.

When high pressure treatment is applied to microorganisms that can be inactivated by application of high pressure alone, temperature distribution in the vessel is of little practical relevance unless it has detrimental effects on quality. Therefore, at lower initial temperatures, i.e., room temperature, temperature non-uniformity in the process does not pose any threat to the safety of the product.

However, bacterial spores can survive pressures above 1000 MPa at ambient temperatures (Balasubramanian and Balasubramaniam, 2003). Only moderate pressures

(~600 MPa) are needed at moderate temperatures ($>70^{\circ}\text{C}$) if a combined pressure-temperature treatment (Ghani and Mohammed, 2007) is used for inactivation of bacterial spores. In that case, non-uniform temperature distribution during the process can cause non-uniform inactivation of the spores that are resistant to lower pressures but are susceptible to high pressure and high temperature combination treatment. Thus, it becomes necessary to understand the temperature distribution established in the vessel to design process control strategies in order to achieve high degree of process uniformity.

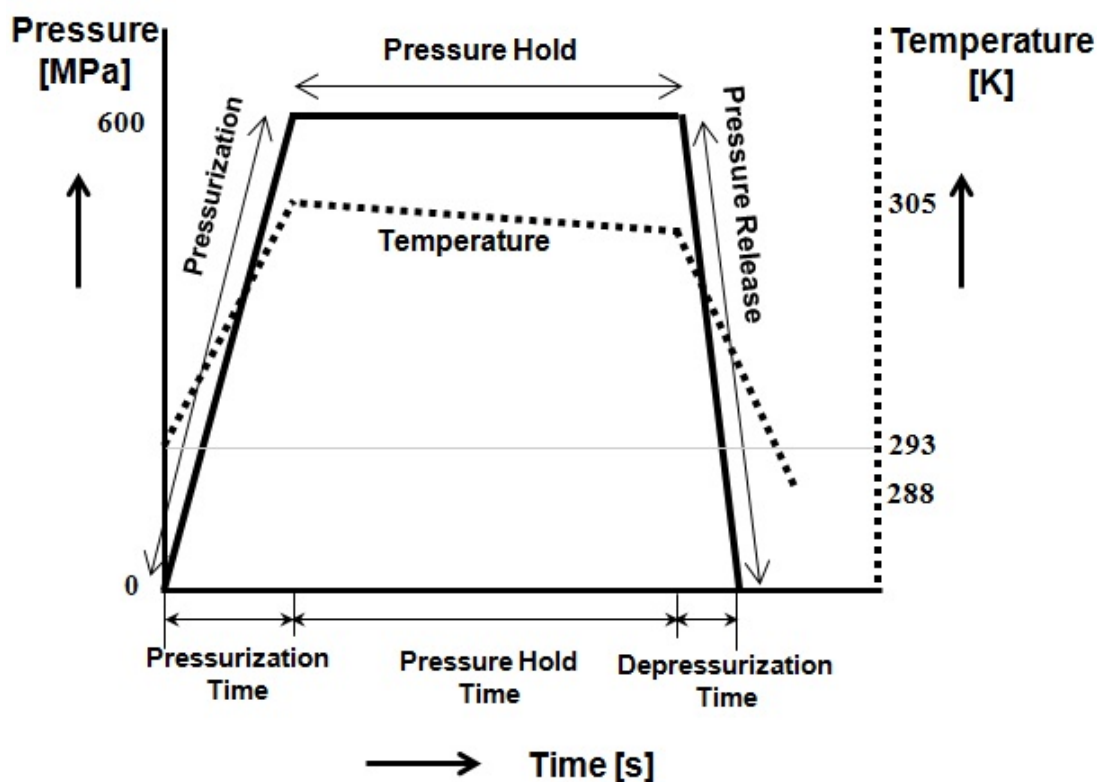


Figure 1-7: Typical pressure and temperature variation with time during HHPP.

As foods undergo relatively low nutrient destruction at temperatures below 100°C (373 K), HHPP can be applied at moderate temperatures to a number of food products, especially those contaminated with spores, which are usually sterilized thermally at a

temperature near 121°C (394 K). Ghani and Farid (2007) stated that adiabatic heating caused by fluid compression at high pressure can cause significant temperature distribution throughout the treated food. By taking into account the non-uniform temperature distribution during the process, it can be assured that the objective of the process has been accomplished everywhere within the food product (Denys et al., 2000b). Recently, US FDA (U.S. Food and Drug Administration) accepted high pressure processing as a novel food sterilization process. The excerpt below has been taken from IFT's newsletter (http://members.ift.org/IFT/Pubs/Newsletters/weekly/nl_030409.htm).

“The National Center for Food Safety and Technology (NCFST), Illinois Institute of Technology (IIT), and Avure Technologies, Inc., announced that the U.S. Food and Drug Administration (FDA) has accepted the research institute's filing of a new food sterilization process. It represents the first petition to the FDA for the commercial use of **pressure-assisted thermal sterilization (PATS)** processes for application in the production of low acid foods. The technology improves the quality of thermally processed foods while eliminating the food safety risks associated with bacteria such as *Clostridium botulinum* and its toxins. The PATS process, which combines mild heat with high pressure to produce commercially sterile low acid food products, underwent a validation process and safety assessment by NCFST researchers and its Dual Use Science and Technology (DUST) consortium members. PATS represents an alternative to retort processing, which involves exposure of the food to high temperatures. The successful FDA filing allows NCFST to proceed with the production of demonstration products using the PATS process”.

In the present section the high pressure process, its advantages, and application to the food industry were discussed along with the high pressure equipment and economics. The next section will discuss the high pressure research that has been reported in literature.

2. LITERATURE REVIEW

In last decade, high pressure processing of foods has gained broad acceptance from the food industry as an innovative and alternative food processing technology. Although, both the food industry and the scientific community have shown adequate evidence on the benefits of the technology, the scientific validation of the process uniformity is still an active and growing area of research. Researchers have been using mathematical modeling and experimental approach to understand the process uniformity.

2.1 Mathematical Modeling of HHPP

Mathematical modeling studies facilitate understanding of the thermal transport of a system better but they should be supported with experimental data (Pehl et al., 2002). Modeling of hydrodynamic and thermal changes during HHPP has been attempted by several researchers (Hartmann, 2002; Hartmann and Delgado, 2003; Hartmann et al., 2003; Khurana and Karwe, 2009; Otero et al., 2002a; Otero et al., 2002b; Otero et al., 2002c; Pehl et al., 2000). These researchers followed a deterministic approach based on governing equations for the high pressure process for their numerical models. One of the main difficulties when modeling thermal transport in high pressure process is lack of appropriate thermophysical properties of different food materials under pressure.

Pehl et al. (2002) were the first to examine the dynamic effects of fluid convection and heat transfer in high pressure process. They used a high pressure optical cell of 2 ml volumetric capacity. They developed high pressure digital particle image thermography and high pressure digital particle image velocimetry which allowed determination of time

scales for hydrodynamic and thermal compensation of liquids under high pressures up to 800 MPa. These experimental analyses were compared with the numerical investigations of Hartmann (2002) and Hartmann and Delgado (2002b) and were found to be in good agreement.

Hartmann and Delgado (2002a) investigated the effect of convective heat transfer during high pressure on enzyme inactivation using finite volume numerical scheme. They investigated the effect of geometrical scale of the vessel and pressurizing medium viscosity on the thermal non-uniformity during high-pressure treatment. In their model they used viscosity as a function of temperature and pressure. They found that larger vessel size increased the inactivation rate due to higher average temperature, as a result of relatively less heat loss at the walls (Hartmann and Delgado, 2002a, 2003; Hartmann et al., 2003).

Hartmann et al. (2003) studied the effect of convective and diffusive transport on inactivation of *Escherichia coli* in packed food (milk) under high pressure. They used a finite volume numerical approach and included heat conduction equation for package in the model. Also, in their model they used density, heat capacity and viscosity of water (medium) as a function of temperature and pressure. They found that non-uniformities of more than one log cycle in inactivation of *E. coli* can be observed depending on the package material parameters, on the position and arrangement of the packages in the vessel. For packed liquid food systems with lower thermal conductivity packaging material, induced natural convection may lead to non-uniformities, depending on the viscosity of the packed food. In absence of these thermal non-uniformities, the

inactivation would be higher and processing time could be reduced for larger scale vessels (Hartmann et al., 2003; Hartmann and Delgado, 2003).

Hartmann and Delgado (2004) have numerically simulated the mechanical effects of the compression of a yeast cell under high hydrostatic pressure, using a finite element method. They found that the deformation of cell under pressure deviated strongly from the isotropic volume reduction. This is because the presence of different material resistances in a cell generates a heterogeneous distribution of strains and further substantial deformations.

Hartmann et al. (2004) studied the experimental and numerical analysis of thermofluid dynamics in a high pressure autoclave 3.3 L in volume with water inlet from bottom, at pressure levels of 500 MPa and 300 MPa for pressure hold time of 820 s. They achieved an excellent agreement between numerical and experimental temperature fields and showed that the temperature measuring device does not affect the temperature measurements significantly. Also, they observed a temperature difference of 6-7 K at the end of the process in the autoclave. Further, they assessed the process uniformity by including the kinetics of *B. subtilis* α -amylase for the standard case (non-adiabatic, using viscosity of water), adiabatic case (assuming the process to be adiabatic) and high viscosity case (assuming higher viscosity for water). The results showed the average activity to be lowest for the adiabatic case followed by the standard case.

Denys et al. (2000a) modeled conductive heat transfer during HHPP using a finite difference numerical approach. They considered an overall heat transfer coefficient

model to account for heat transfer between pressurizing medium and vessel wall. Pressure dependent thermal conductivity and thermal expansion coefficient of the product were determined experimentally and incorporated in the numerical scheme. They showed numerically that with pressure cycling, 8 cycles each of 30 s compression time and 2 min holding time at 500 MPa pressure, higher inactivation rate for *Bacillus subtilis* α -amylase were achieved compared to one step application at same pressure and same total process time. This was associated to the temperature increase during compression. They also observed that the maximum temperature reached during the pressure cycling process was lower than when same pressure was established in one step. This was because of the heat loss during the pressure hold. On the other hand, higher heterogeneity in terms of temperature was observed with cycling (Denys et al., 2000b).

Improvements are needed for the contribution of the convection heat transfer in the high-pressure fluid (Denys et al., 1997). Several researchers (Hartmann and Delgado, 2002a, b; Pehl et al., 2002) have indicated that more viscous foods give more thermal heterogeneity. 50% sucrose solution gave 6 times larger temperature gradient compared to water under the same conditions (Pehl et al., 2002). Therefore, viscosity of food under pressure should be a known parameter and thermofluidodynamical processes need to be investigated.

Adriano Ardia (2004) for his doctoral thesis studied the ways in which pressure can be used to achieve sterilization of the resistant microbial species in foods in which thermal processing fails to obtain high-quality of the product. He showed that the high pressure treatment alone cannot cause a significant reduction of *A. acidoterrestris* spores in orange

juice, whereas a combination of high pressure (700 MPa) and strong heating (initial temperature of 90-95°C) reduces the number of survivors by 6 log in 5 min. Adriano also studied the combined pressure-temperature inactivation (100-1400 MPa, 90-130°C) of *B. stearothermophilus* spores in different buffer solutions and observed an unexpected behavior. It was noticed that an increase in temperature at each pressure level resulted in an increase in inactivation but when different pressure levels were plotted at fixed temperature, the highest pressure did not always result in the higher inactivation. Adriano attributed the unexpected phenomenon to the instability of the phosphate buffer at high pressure-temperature conditions.

Ghani and Farid (2007) modeled convective and conductive heat transfer in a three dimensional high pressure vessel loaded with pieces of solid beef fat. The results showed that the solid beef fat sample was heated more than the water due to their higher compression heating value. Also, for water, they observed that the effect of forced and free convection on temperature distribution was felt only in the early stages of compression.

Knoerzer et al. (2007) observed using numerical simulation, a circulation region at the base of the vessel due to water entering and the flow to be primarily driven by buoyancy forces. They also showed a significant reduction in *C. botulinum* spore count when the process was carried out with PTFE insulation in the vessel whereas no significant reduction was seen in vessel without PTFE insulation.

Klotz et al. (2007) constructed a model to describe the non log-linear inactivation kinetics

of pressure treated bacteria, assuming that the inactivation rate changes inversely with the square root of time. They found their model to be a good fit with the experimental data and also validated the model with experimental data from other publications.

Rauh et al. (2009) numerically studied the effect of thermofluidodynamical inhomogeneities during the high pressure process on uniformity in enzyme (β -glucanase, α -amylase, lipoxygenase, polyphenoloxidase) inactivation. They observed that the thermophysical properties, e.g., viscosity play a major role in heterogeneities, and more uniform temperature conditions do not necessarily lead to more effective inactivation.

Juliano et al. (2009) analyzed and compared four kinetic models (traditional first-order, Weibull distribution, nth order model, and combined log linear and nth order) for inactivation of *C. botulinum* in their computational model of a high pressure sterilization process. The process conditions selected were pressure of 600 MPa, initial temperature 90°C and hold time of 220 s. The results showed that the first-order model achieved a 12D reduction faster compared to the other models and gave a greater difference (~8.5 log) in inactivation between inside and outside the packages compared to other models that showed only 1 - 1.5 log. Also, Weibull or the nth order model showed a more uniform inactivation distribution.

Knoerzer et al. (2010a) studied the compression heating of water and water/propylene glycol mixtures during high pressure processing. They observed that at lower pressures mixtures with glycol concentration below 50% showed similar compression heating as water whereas with glycol concentration more than 50% a significant increase in

compression heating value. At higher pressures the compression heating values were very similar for all the concentrations, i.e., 10^{-4} MPa⁻¹.

Knoerzer et al. (2010b) studied the carrier optimization during high pressure thermal processing with aim of maximizing heat retention and improving temperature uniformity. They developed an integrated software routine that progressively alters the carrier wall thickness and showed an optimized design of a polymeric carrier in a 35 L high pressure unit. They showed that to achieve maximum temperature uniformity with respect to process time and distribution around 15% usable volume of the vessel has to be sacrificed.

Knoerzer et al. (2010c) studied the adiabatic compression heating behavior of high-density polyethylene (HDPE), polypropylene (PP) and polytetrafluoroethylene (PTFE) during high pressure processing. The process conditions used were initial temperatures from 5-90°C, pressures up to 750 MPa, and hold time of 60 s. They showed that overall adiabatic heating values for HDPE and PP are higher than water except for pressures greater than 600 MPa and temperature greater than 70°C where compression heating values of PP and water almost overlaps. Whereas compression heating value for PTFE is lower than water for temperatures more than 30°C. Also, between the three plastics the compression heating value for PTFE is significantly lower than HDPE and PP at pressures greater than 100 MPa.

The research progress discussed above for the mathematical modeling of high pressure process has been done for the high pressure vessel with vertical orientation. The

modeling of high pressure vessel with horizontal orientation is a current topic of research and has not been reported in the literature.

2.2 Microbial Inactivation with Pressure

High pressure processing has gained popularity in last 15 years as a method to microbiologically stabilize foodstuff. Pressures between 300 and 600 MPa can inactivate yeasts, moulds, and most vegetative bacteria including most infectious food borne pathogens (Smelt, 1998). Among the vegetative bacteria, Gram-positive bacteria are more resistive to HPP than Gram-negative bacteria due to the presence of rigid teichoic acids in the peptidoglycan layer of their cell wall (Shigehisa et al., 1991). Smaller size and coccoidal shape bacteria offer more resistance to HPP than the large rod-shaped ones because of their reduced surface area for cell leakage.

Pressure induced inactivation mechanism of microorganisms is a complex phenomenon, which includes protein denaturation, phase change, morphological changes, and membrane effects (Hoover et al., 1989). Studies involving the mechanism of cell lysis show that pressure affects microorganisms in different ways. High pressure can cause an inactivation in membrane transport systems that results in sublethal injury or it can affect metabolic activity and damage the cell membrane (Hartmann and Delgado, 2003). Intracellular gas vacuoles can collapse at pressures of 0.6 MPa (Hoover et al., 1989). Some microorganisms, such as *L. monocytogenes*, show higher inactivation rates at low temperature high pressure treatments (Knorr, 1999).

Karatzas and Bennik (2002) isolated the high pressure resistant (piezotolerant) strain

(AK01) of *L. monocytogenes* Scott A at 400 MPa, 20 min in buffer and semi-skim milk (1-2 % fat) and observed higher HHP tolerance (piezotolerance) in the stationary phase than in the exponential phase. In semi-skim milk, exponential-phase cells showed lower reductions upon pressurization than in buffer showing the effect of substrate composition.

Knorr (1999) stated that metabolite production of some microorganisms can be increased with high pressure and inactivation of some microorganisms is not correlated with temperature or pressure interaction. This will create unique opportunities for selective inactivation of some microorganisms in a mixture (Knorr, 1999).

It is clear from literature that the shape of pressure inactivation curve depends on factors such as type of organism, the composition of suspending medium, pressure intensity, and the treatment temperature (Smelt, 1998). Cell death rate increases with pressure but it does not always follow a first order kinetics; sometimes, there is a tailing off in inactivation (Kalchayanand et al., 1998). The ability of bacteria to survive HHPP can be greatly increased when treated in nutritionally rich media, e.g., meat, containing substances like carbohydrates, proteins, and fat (Simpson and Gilmour, 1997). Therefore, although first-order inactivation curves do occur, but curves with upward concavity and tails are more common (Klotz et al., 2007).

Chen and Hoover (2003) observed that increasing temperature increased pressure inactivation of *L. monocytogenes* in UHT milk. They obtained an 8 log reduction at 500 MPa, 50°C and 5 min treatment time. They also observed the tailing effect in the survival curves indicating that linear model was not a good fit.

Inactivation of hepatitis A virus (HAV) and feline calicivirus, a Norovirus surrogate, by high hydrostatic pressure has been shown by Kingsley et al., (2002). They found 7 log reduction after processing at 450 MPa for 5 minutes for HAV and at 275 MPa for 5 minutes for feline calicivirus. The NIH conducted a study using HHPP (690-1200 MPa) to inactivate infectious prions responsible for bovine spongiform encephalopathy (BSE) (Brown et al., 2003; Schauwecker, 2004). These experiments were carried out at elevated temperatures (121-137°C) suggesting that combination of high temperature and high pressure is needed for the inactivation of BSE prions. This process is sometimes called pressure assisted thermal processing (PATP).

2.3 Spore Inactivation with Pressure

As discussed above high pressure has the ability to inactivate a range of vegetative cells, but spores are resistant to pressurization up to 1200 MPa (Martin et al., 2002; Smelt, 1998). A pressure of even 1200 MPa was not sufficient to kill *Bacillus subtilis* spores (Heinz and Knorr, 2005). High pressures up to 600 MPa can inactivate vegetative cells and enzymes without heat, but not bacterial spores (Hayakawa et al., 1996). Some researchers have shown that spores are resistant to high pressures partly because of the protective effect of membranes and coat layers surrounding the core, presence of dipicolinic acid, and the low water content in the spore coat compared to vegetative cells (Hayakawa et al., 1996). Therefore, it is necessary to study combination of high pressure with other treatments that can lead to commercial sterility.

The most accepted/used combination with high pressure to achieve sterilization is temperature. The process is sometimes called pressure assisted thermal sterilization (PATs). The inactivation can be achieved either by a combination of high temperature with high pressure (Heinz and Knorr, 2005) or by applying pressure in pulses. The pre-treatment by pressures of 50-300 MPa often stimulates the germination of bacterial spores. Since the resistance of the dormant spore is much greater than the resistance of the germinated spore or growing cell of the same strain (Doona and Feeherry, 2007). The germinated spores can then be killed by relatively mild heat treatments or pressure treatments (Smelt, 1998).

The coupled action of hydrostatic pressure and temperature was investigated in order to activate spores and consequently to inactivate their vegetative form in second step with higher operating pressure (Spilimbergo et al., 2002). It was concluded that at higher temperature, faster germination is obtained and also, salts, glucose and amino acids were found to enhance the rate of germination (Spilimbergo et al., 2002).

High pressure processing can be used with heat to inactivate spores of *Bacillus stearothermophilus* at 90°C for 30 min at 150 MPa to bring about 2 log reduction from an original count of 10^6 , and of *B. subtilis* at 70°C and 150 MPa (Balasubramanian and Balasubramanian, 2003; Knorr, 1999).

Reddy et al. (1999) showed that no reduction of *Clostridium botulinum* type E spores in phosphate buffer at 827 MPa and temperatures below 35°C was achieved. However, a 5

log reduction was observed when the temperature was increased from 35 to 55°C with pressure hold time of 10 min.

In the patent literature (Meyer, 2000, 2001), it has been suggested that to achieve commercial sterility with high pressure at least two pressure pulses (700–1000 MPa) when product is preheated to a temperature of 70–90°C, are required. The suggestion is based on the observation that no surviving spores were detected immediately following the single pulse treatment whereas growth occurred in treated samples after one week indicating only sublethal injury to cells.

High pressure combined with temperature is really attractive with regards to sterilization as it has shown to inactivate spores and also been shown to have less deleterious effects on food quality compared to high temperature treatments. High pressure has significant potential as a value added food processing procedure.

2.4 Enzyme Inactivation with Pressure and its Potential as pTTI

Like spores (discussed in section 2.3), some enzymes cannot be inactivated by pressure alone and need a combination of high pressure and elevated temperatures for inactivation. Many researchers have studied the effect of high pressure and/or combined pressure-temperature on inactivation of enzymes and concluded that the response depends on the origin of enzyme, nature of substrates, pH, pressure, temperature, and time of processing. It has been shown that low pressures tend to activate some enzymes, whereas high pressures induce inactivation.

Researchers have found that pressure cycling results in lower activity for enzymes such as trypsin, chymotrypsin, *Bacillus subtilis* α -amylase as compared to the single pressure cycle, whereas, repeated pressure build up had no effect on the activity of pectin methyl esterase (PME) (Hendrickx et al., 1998).

Ludikhuyze et al. (1997) studied the isothermal-isobaric inactivation of *Bacillus subtilis* α -amylase in 0.01 M Tris-HCl buffer and 15% vol glycerol at pH 8.6, in pressure range of 1 – 750 MPa and temperature 25 – 85°C and found that the inactivation follows a first order model.

Nienaber and Shellhammer (2001) studied the inactivation kinetics of PME in orange juice at pressures of 400, 500, 600 MPa and temperatures of 25, 37.5, 50°C for various times. They concluded that inactivation kinetics follow first order kinetics and pressure (400 – 600 MPa) combined with temperature (< 50°C) accelerated the PME inactivation. Their calculated D-values ranged from 4.6 min (600 MPa at 50°C) to 117.5 min (400 MPa at 25°C).

Indrawati et al., (2000) studied the inactivation kinetics of LOX (lipoxygenase) in green bean juice for pressures up to 650 MPa and temperature range -10 to 70°C. They found that the inactivation followed first order model. They also found that high-pressure treatment at subzero temperature resulted in an antagonistic effect on LOX inactivation whereas no such effect was found above room temperature.

Riahi and Ramaswamy (2004) studied the high pressure inactivation kinetics of amylase in apple juice at 100–400 MPa, 0–60 min and 6–40°C. They found that pressure

inactivation of amylase in apple juice was significantly ($p < 0.01$) influenced by pH, pressure level, holding time and temperature. Also, inactivation of amylase by pressure treatment were found to follow a bi-phasic model and instantaneous inactivation due to pressure pulse action and a subsequent first order inactivation rate during the pressure hold.

This section so far discussed the inactivation of various enzymes under high pressure but enzymes due to their different levels of pressure and temperature sensitivity have been investigated for their potential as pressure-temperature-time indicators (pTTI).

Grauwet et al. (2009) studied the potential of *Bacillus subtilis* α -Amylase (BSA) as an indicator for high hydrostatic pressure pasteurization process in a vertical single vessel system. Pressure range of 400-600 MPa with temperatures from 10-40°C for 1-15 min were investigated. Based on the pressure-temperature stability of BSA, the kinetic model selected to describe the p-T dependency of inactivation rate constant and positioning of indicator along radial or axial direction, BSA was found to be suitable as an indicator of non-uniformity of high pressure process. In another study, Grauwet et al., (2010) studied the ovomucoid based pTTI for high pressure high temperature process. They characterized the inactivation kinetics (first order inactivation model) of ovomucoid system under isothermal- isobaric conditions and observed temperature dependent inactivation at constant pressure. The ovomucoid system can possibly be used to map temperature uniformity in a high pressure vessel by positioning the indicator at different coordinates in the vessel.

It is clear from the literature cited in this section that high pressure processing is a developing technology with many more research opportunities to fill in the gaps. The next section will discuss the hypotheses and objectives of this research.

3. RATIONALE AND OBJECTIVES

3.1 Research Rationale

The temperature and its distribution in a high pressure vessel are most relevant when a combination of high pressure and high temperature (during PATP, PATS) is needed to inactivate microbes, spores, or enzymes which are resistant to high pressure alone. The main rationale for this study was that the temperature distribution inside a HHPP vessel becomes non-uniform during the process due to adiabatic compression heating, concomitant heat loss to the thick wall of the vessel and addition of water to the vessel during pressurization. The non-uniformity in temperature within the pressurizing medium and the food product can impact the microbial and enzyme inactivation. Non-uniform temperature distribution in the vessel can also lead to non-uniform inactivation of microorganisms and hence compromise product safety.

Determining accurate temperature distribution in a high pressure vessel can help to differentiate the effect of temperature and pressure and generate understanding of the synergy between pressure and temperature on inactivation kinetics of enzymes, nutritional and flavor compounds, and microorganisms. The results obtained from this research will be useful in the evaluation of process performance and help with process validation and process filing with regulatory agencies (USDA-FSIS and FDA) to develop guidelines for producing high pressure processed foods which are safe to consume. The results will also be important for food processors and equipment manufacturers to

understand the effects of non-uniform thermal treatment on foods processed using PATP, PATS.

3.2 Research Objectives

The overall objective of this research was to predict the temperature distribution in a commercial high pressure food processing vessel during a typical high pressure process and its impact on microbial inactivation. To evaluate the process performance and its effectiveness following specific objectives were studied for this research project:

Objective 1: Prediction of Temperature and Flow Fields in Vertical & Horizontal Vessels

In this objective, a numerical simulation program was used to predict the temperature and flow fields in the pressurizing medium (water) during the high pressure process. The commercial high pressure systems are available with high pressure vessels that can operate in vertical and horizontal orientation, therefore, simulation models were generated for both orientations. The sub-objectives here were:

- (a) To carry out numerical simulation of thermal transport in a high pressure vessel to predict temperature and flow fields during high pressure at room temperature (also called cold pasteurization), pressure assisted thermal pasteurization (PATP), and pressure assisted thermal sterilization (PATS) processes.
- (b) To predict the effect of initial operating temperature, properties (density, heat capacity, thermal conductivity and viscosity) of food material, and water added to vessel on temperature distribution during HHPP.

- (c) To evaluate the effect of an insulating sleeve in the vessel on temperature non-uniformity in vessel.

Objective 2: Validation of Numerically Predicted Temperature

- (a) To validate the predicted results with experimental data at selected locations in the vessel while taking into account the lag between the true temperature and the temperature measured by the high pressure thermocouple assembly.

Objective 3: Quantification of Process Non-Uniformity in terms of Temperature and Microbial & Enzyme Inactivation

In this objective, both numerical and experimental strategies were used to quantify the non-uniformity in temperature during the high pressure process. The results from Objective 1 provide a qualitative/visual measure of non-uniformity in temperature at a particular time during the high pressure process. Therefore, to understand the impact of non-uniformity in temperature, it is important to quantify the results and take into account the temperature variation throughout the process. The sub-objectives here were:

- (a) To numerically quantify the process temperature non-uniformity and its impact on microbial inactivation (*C. botulinum* spores)

The time-temperature data obtained from the numerical simulation program were used to quantify the impact of non-uniformity in temperature on *C. botulinum* spores. The *C. botulinum* spores were chosen for this study as they are the most heat and pressure resistant organisms of concern for the low acid foods and are known to be inactivated by a combination of high pressure and high temperature. The conventional thermal processing F-value approach was used for the quantification of lethality.

- (b) To experimentally quantify the impact of temperature non-uniformity on inactivation of Alkaline phosphatase (ALP) in raw milk

In this objective, an effort was made to experimentally measure the temperature at several locations in the pressurizing medium (water) in the vessel. For this purpose it was desirable to choose an indicator microbial/enzyme system (i) which is sensitive to temperature change ($\sim 5\text{-}10^\circ\text{C}$), and (ii) whose inactivation pressure and temperature range fall within equipment pressure and temperature range. The available literature on the effect of pressure on alkaline phosphatase suggests that ALP is pressure resistant and temperature susceptible within the range of pressures possible on the currently available high pressure equipments. Therefore, alkaline phosphatase was chosen as an indicator to study the impact of non-uniformity in temperature.

Next chapter discusses the material and methods used to accomplish the above objectives.

4. EXPERIMENTAL MATERIALS AND METHODS

The research methodology included both experimental and numerical approaches. The precise control of parameters like ambient temperature and initial temperature of fluid during experiments was difficult because of variable ambient conditions. Therefore, the experiments were performed first and the initial experimental conditions were then used as an input to the numerical simulation program for prediction of temperature distribution and flow field inside the vessel. For validation of numerical simulation program, the experiments were carried out with water acting as both pressurizing medium and test sample. For quantification of temperature non-uniformity, the experiments were carried out using raw milk as test sample and water as pressurizing medium.

4.1 Rutgers-High Pressure Processing Facility

High hydrostatic pressure processing unit used for experimental investigations is put together using equipment manufactured by Elmhurst, Inc., Albany, NY and is shown in **Figure 4-1**. The unit comprises of a 10 liter high pressure vessel (operated vertically) with an external heating/chilling tank and a 20 HP intensifier pump to build a maximum pressure of 690 MPa (100,000 psi) in 3 min or less. The high pressure vessel is designed for a temperature range of 5°C to 90°C and is programmed for pressure hold times of 1 to 60 min. It also has pressure cycling capability. The detailed setup of the unit is shown in **Figure 4-2**, which shows the 10 liter processing vessel, the intensifying pump, the yoke and the data logger. The processing vessel can be tilted for easy loading and unloading of samples. The intensifier pump pumps the filtered tap water into the pressure vessel to

raise the pressure. The function of the yoke is to restrain the pressure vessel assembly (top and bottom closures) and cope with high axial forces during high pressure process. A PLC control panel was used to control, display, and maintain the process pressure and time during the process along with start up and emergency shutdown procedures. A data acquisition system (National Instruments-LabVIEW™ 7 Express) based on analog to digital conversion technology (converts an input analog voltage or current to a digital number proportional to the magnitude of the voltage or current) was used for recording real time pressure and temperature.



Figure 4-1: Rutgers 10 liter high hydrostatic pressure processing facility.

4.1.1 Pressure Vessel Design and Dimensions

The high hydrostatic pressure processing vessel was a cylindrical shaped vessel with overall length of the cylinder 1090 mm and the external diameter 445 mm. The pressure cavity in the vessel had diameter of 142 mm and length of 823 mm as shown in **Figure 4-3**, surrounded by thick solid wall made of four layers of steel. These layers from inside to outside are two layers of SA-705 forging XM 16 stainless steel with a thickness of 13.72 mm and 22.10 mm, respectively, and two layers of FA-723 carbon steel with a thickness of 19.81 mm and 91.44 mm, respectively. The solid steel wall was surrounded by an outer steel shell with an air gap of 2.38 mm between solid steel wall and the shell, as shown schematically in **Figure 4-3**. The vessel also had the top and bottom closures to provide an ideal seal while the vessel is pressurized. The top closure had a 6.6 mm opening through which the inlet pipe connected to intensifying pump goes through and adds the additional water into the pressure cavity to bring it to desired pressure.

In the present study, the vessel bottom closure was fixed, whereas, the top closure was removable for loading and unloading. In both bottom and top closures, sealing was accomplished by a combination of o-ring and separate metal and polymer back up rings. The o-ring was always made of a softer material (an elastomer) and deforms under pressure, filling and sealing any irregularities on the connecting surfaces. The metal and polymer back up rings are designed to expand and contract as pressure increases or decreases, thus continuously confining the o-ring in place with no clearance. The steel sleeve shown in **Figure 4-3**, was part of the top closure assembly that fits into the pressure cavity after the samples are loaded into the cavity.

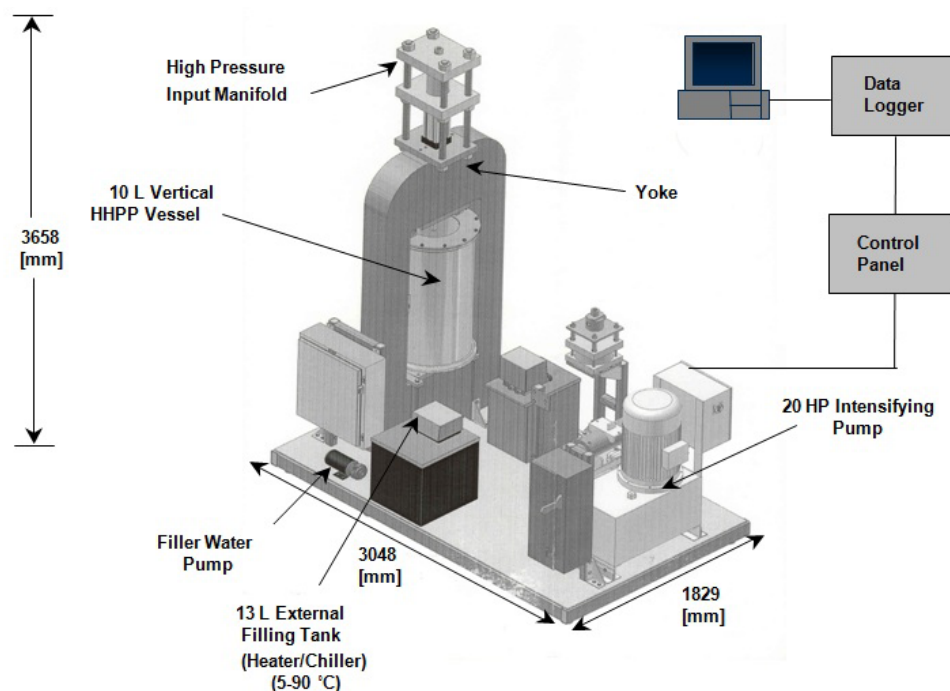


Figure 4-2: Details of Rutgers high hydrostatic pressure processing set up.

4.1.2 Working Description of High Pressure Process

The high pressure vessel was kept in horizontal position when not in use. Samples were loaded into the pressure cavity in this position, top closure inserted and then the vessel is made almost vertical to fill the pressure cavity with water through an opening in the top closure using a hose or a low pressure pump. After filling, the vessel was made completely vertical to align the opening in the top closure with the input pipe through which the pumped water enters the vessel at high pressure. Using the PLC panel, the desired final pressure (kpsi) and hold time (min) were set. The vessel was pressurized using an intensifier (20 HP high pressure pump). High pressure water from intensifier pump was pumped into the vessel through the input pipe and the top closure until the set pressure was achieved. A typical pressurization time to achieve 600 MPa (87,000 psi)

was 180 s. The pressurization time can be reduced by reducing the volume of the pressure cavity, which can be achieved by inserting aluminum ingots in the cavity. Pressure in the vessel can be held constant for defined period of time (1 – 60 min). During pressure hold time, the pressure may slightly drop. If the pressure drops by 1% of the set value, the intensifier pump comes on to repressurize it to desired pressure level. At the end of hold time, the depressurization valve opens and the additional water added to the vessel for pressurization goes out and the vessel depressurized in few seconds.

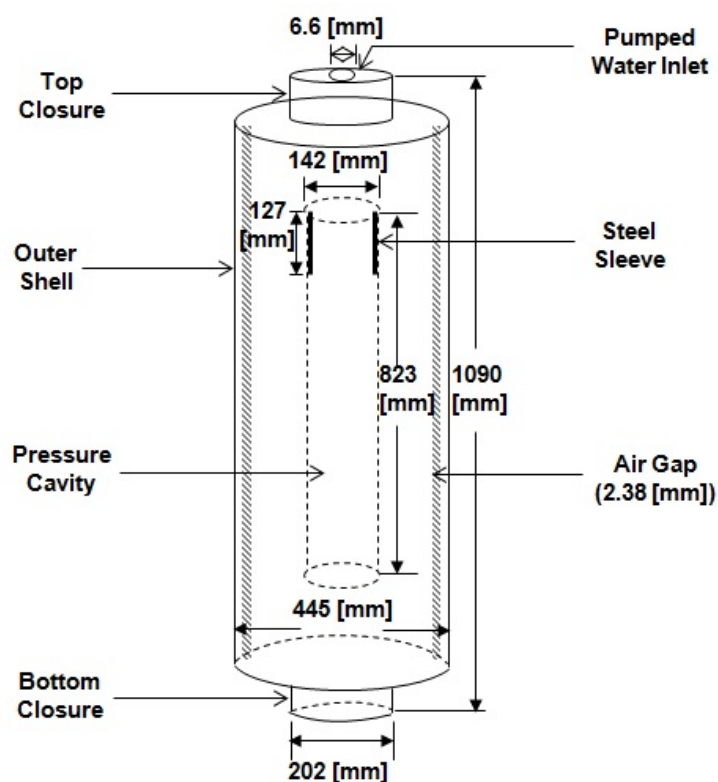


Figure 4-3: Schematic of Rutgers HHPP vessel with major dimensions.

4.1.3 Pressure Measurements

The pressure in the system during the process was measured using a transducer which measured the line pressure which was assumed to be the same pressure as the pressure in

the vessel. It is possible that pressure inside the vessel would be slightly less than the line pressure during pressurization, however, the pressures should be the same at the end of pressurization. Also, the concomitant increase of temperature of water inside the vessel was an indirect indication of pressure increase in the vessel. Pressure data as a function of time were recorded at a frequency of 4 Hz, over the entire period of pressurization, pressure hold and depressurization, by a data acquisition system from National Instruments (LabVIEW™ 7 Express), Austin, TX.

4.1.4 Temperature Measurements

The pressure vessel was equipped with three thermocouple probes that were threaded to the inside of the top closure. These thermocouples facilitated measurement of temperature of water in the vessel during the high pressure process. The probes used type K (Ni-Cr/Ni-Al) thermocouples (ungrounded) in high pressure tubing (inner diameter 2.1 mm). The temperature range for the type K thermocouple is -200°C to 1200°C . Often type K thermocouples are used in high pressure vessels because their calibration is not sensitive to pressure. The tips of the thermocouples were located at three different depths (203 mm, 318 mm and 546 mm from the top of the pressure cavity) as shown in **Figure 4-4(b)** and 10 mm away from the inner wall of the vessel. Temperature data as a function of time for all three thermocouples were recorded at a frequency of 4 Hz over the entire period of pressurization, pressure hold and depressurization by a data acquisition system from National Instruments (LabVIEW™ 7 Express).

4.2 Special Experimental Set Up

Special experimental setups were needed for performing the experiments (i) to calculate the time constant of the thermocouples, (ii) to carry out higher initial temperature studies, and (iii) to carry out the enzyme (alkaline phosphatase) studies. The individual set up are described in the subsequent sections.

4.2.1 Time Constant Experiments

The dynamic response of a high pressure thermocouple assembly is a function of the design of the thermocouple. In our case the delay in the response was due to the high pressure tubing surrounding the thermocouples. The time constant values for the three thermocouples were determined in a specially designed experiment and the values were used as an input in the equations (5-49) and (5-70) to find the true temperature as discussed in later section 5.5.1.

The response of a thermocouple to step change in temperature is given by

$$\frac{[T_{\infty} - T]}{T_{\infty} - T_{ip}} = e^{(-t/\tau)} \quad (4-1)$$

where, T_{∞} is the temperature of constant water bath, T is the temperature of thermocouple probe, T_{ip} is the initial temperature of thermocouple probe, t is the time, and τ represents the time constant of the thermocouple.

To experimentally obtain the value of the time constant τ for each thermocouple, the high pressure thermocouple assembly was taken out of the high pressure vessel and made vertical by hanging it using a support system as shown in **Figure 4-4**. In three separate

experiments, each thermocouple was immersed in constant water bath (ice point bath, boiling water bath and a fixed temperature bath at 50°C (323 K)) and the time-temperature data were recorded using LabVIEW™ 7 Express. Each experiment was repeated three times. The time constant τ value for each thermocouple was obtained by plotting natural logarithm of left hand side term of equation (4-1) as a function of time (t) and then predicting the parameter (slope) by analyzing the experimental data using linear regression. The negative reciprocal of the slope of the best fit line is the time constant τ .

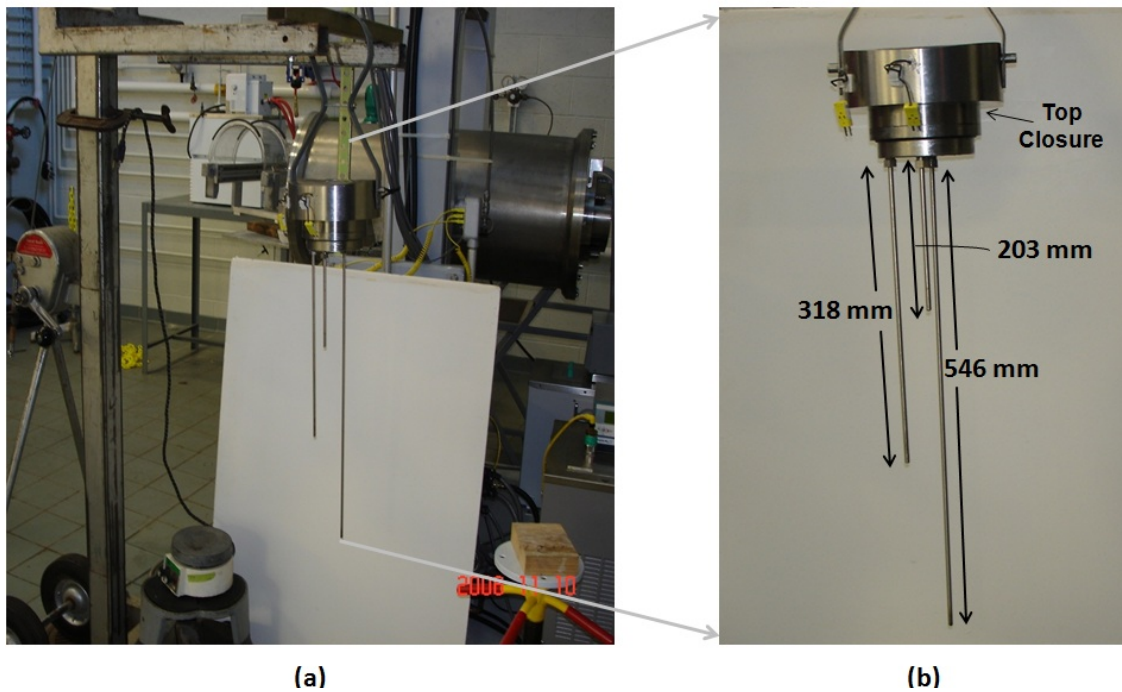


Figure 4-4: High pressure thermocouple assembly (attached to the top closure) (a) made vertical for measuring the time constant of each thermocouple and (b) showing depth of thermocouples.

The analysis of variance (ANOVA) was performed to estimate the significance of the effect of high pressure thermocouple tube length and heating medium temperature on the time constant value.

4.2.2 Initial High Temperature Experiments

For high pressure experiments at initial temperatures higher than ambient temperature, the steel vessel had to be heated to the desired initial temperature prior to experimental run because if water at higher temperature is filled in the cold vessel, the water (~ 11 kg) rapidly loses heat to the giant steel vessel (~ 1000 kg) and the temperature of water drops rapidly. Therefore, an external water bath attached to a coil was used to circulate hot water in the vessel to pre-heat the vessel steel mass overnight and equilibrate it at the desired temperature before starting the experiments, as shown in **Figure 4-5**. After the vessel was heated overnight to bring the temperature of steel mass to desired initial temperature, a 13 liter external heating/chilling water tank was used to add the water at the desired initial temperature as a pressure transmitting medium just before the experiment to avoid heat losses. It was not possible to change the temperature of water added by the intensifier during pressurization.

4.2.3 Alkaline Phosphatase (ALP) Experiments

As described in Objective 3(b), alkaline phosphatase was chosen as an indicator to show non-uniform temperature distribution during high pressure high temperature process.

4.2.3.1 Introduction to Alkaline Phosphatase

Alkaline phosphatase (ALP, EC 3.1.3.1) is a hydrolase enzyme distributed widely in nature (blue-green algae, molds, bacteria, and tissues of members of animal kingdom). It is an indigenous milk enzyme and has attracted interest of several researchers for their use as process indicators to assess effectiveness of the process. The ALP enzyme is well

known as process indicators for the thermal treatment of milk. Indeed, under normal pasteurization conditions (high temperature short time or lower temperature longer time) ALP is slightly more thermostable than *Mycobacterium tuberculosis*, the most heat resistant non-sporogenic pathogenic microorganism in raw milk, and hence absence of ALP activity is used as a sign for adequate pasteurization (Ludikhuyze et al., 2000).

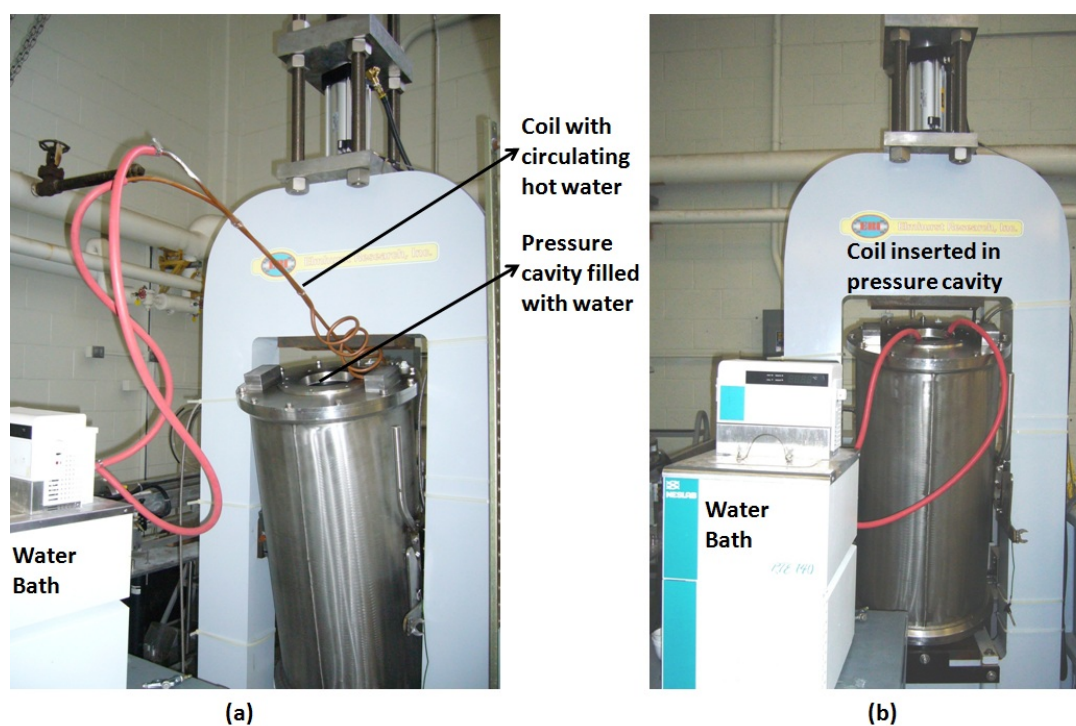


Figure 4-5: Experimental set up to heat the steel vessel using a water bath attached to a heating coil, (a) showing heating coil and (b) coil inserted.

Although, sufficient literature is available on the effectiveness of ALP as an indicator of process severity for heat pasteurization process, not much data is available on the feasibility of its use as an indicator for high temperature high pressure, i.e., PATS or PATP process. Johnston (1995) and Lopez-Fandino et al. (1996) studied the activity of alkaline phosphatase under pressure and concluded that alkaline phosphatase appears

quite pressure resistant, with no inactivation in raw milk after treatment at 400 MPa for 20-60 min at 20°C, although, complete inactivation was achieved above 700 MPa. Mussa and Ramaswamy (1997) studied the ultra-high pressure pasteurization of fresh milk at 100-400 MPa for 5-120 min with respect to pressure destruction of microorganisms, inactivation of alkaline phosphatase, changes in color and viscosity. They showed that ALP cannot be used effectively as an indicator for milk pressurization as it is not pressure sensitive.

Pressure-temperature inactivation of ALP in bovine milk was studied by Ludikhuyze et al. (2000). They used the thermal death time (D-value) terminology to include the pressure-temperature dependence in the kinetic model. The pressure and temperature range studied was 0.1 to 725 MPa and 25°C to 63°C respectively. The experiments were carried out on a multi-vessel high pressure unit (from Resato International B.V., Holland) containing 8 individual vessels (8 ml volume) and ALP activity was measured spectrophotometrically at 425 nm using p-nitrophenyl di-natriumphosphate as substrate. They observed an increase in D-value with increasing pressures up to 300 MPa and then decrease with further pressure increase suggesting low pressure largely protects the enzyme against inactivation. Rademacher and Hinrichs (2006) studied the reaction kinetics and inactivation of indigenous milk enzymes- alkaline phosphatase, γ -glutamyltransferase and phosphohexoseisomerase in pressure range 400-800 MPa and temperatures between 5 and 40°C. It was shown that amongst the three enzymes alkaline phosphatase was the most pressure stable.

For this purpose of this study, it was desirable to prefer an indicator microbial/enzyme system (i) which is sensitive to temperature change ($\sim 5\text{-}10^{\circ}\text{C}$), and (ii) whose inactivation pressure and temperature range fall within equipment pressure and temperature range. The literature cited above on alkaline phosphatase under pressure suggested that in the current pressure equipment range, ALP would be pressure resistant and temperature susceptible. Therefore, alkaline phosphatase was chosen as an indicator to study the impact of non-uniformity in temperature.

4.2.3.2 Raw Milk Sample and its Placement in Vertical Vessel

Fresh, organic raw bovine milk was procured from a local farm (Birchwood Farms, Newton, PA, U.S.A.). The milk was stored at refrigerated temperatures before the experiments. Milk used for experiments was no older than 24 h. For high pressure processing the raw milk was poured in 0.6 ml Polypropylene graduated microcentrifuge tubes with locking lids (Fisher Scientific, Catalogue no. 02-681-273). The samples in microcentrifuge tubes were tied to the special metal wire frame (shown in **Figure 4-6**) designed to hold the sample at a specific location and high pressure processed at 600 MPa, 55°C for 20 min. After processing, the samples were removed from cavity, kept on ice till the analysis was finished.

4.2.3.3 Alkaline Phosphatase Activity Assay

The residual activity of ALP was determined using BioVision's (BioVision Research Products, Mountain View, CA, USA) Alkaline Phosphatase Fluorimetric Assay Kit (Catalog # K422-500). The kit is based on the principle that ALP in milk sample cleaves

the phosphate group of the non-fluorescent 4-Methylumbelliferyl phosphate disodium salt (MUP) substrate resulting in 4-Methylumbelliferone (MU) which gives an intense fluorescent signal (Ex/Em = 360nm/440nm). The product formation is monitored continuously during a 30 min incubation period and enzyme activity is calculated from the rate of fluorescence increase.

The BioVision Alkaline phosphatase fluorimetric assay kit consists of ALP assay buffer (with glycine, magnesium chloride, zinc chloride, and Brij35) - stable for 2 months at 4°C, 5mM MUP substrate solution (stable for 2 months at -20°C), ALP enzyme solution (reconstituted enzyme is stable for 2 months at 4°C), and stop solution (storage at 4°C).

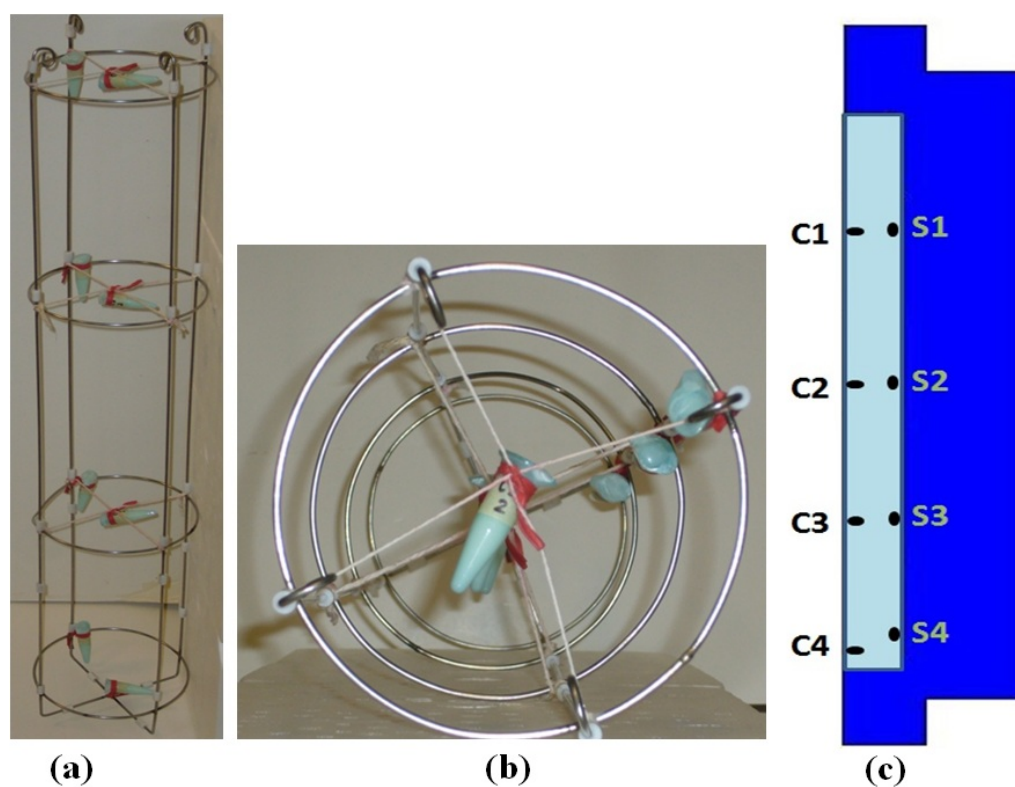


Figure 4-6: Wire (metal) frame designed to position samples at several locations in the vertical high pressure vessel (a) View 1, (b) View 2, (c) points corresponding in the vessel geometry.

Procedure to obtain the standard curve:

To obtain the 4-MU standard curve, 5 mM MUP solution was diluted with assay buffer to generate 50 μ M MUP solution. From the 50 μ M MUP solution, 0, 2, 4, 6, 8, 10 μ l were added into 96-well plate in triplicate to generate 0, 0.1, 0.2, 0.3, 0.4, 0.5 nmol/well MUP standard. The final volume in each well was brought to 120 μ l with assay buffer. 10 μ l of ALP enzyme solution was added to each well containing the MUP standard. The 96-well plate was covered with aluminum foil to protect from light and gently shaken for 2 min to mix the well contents. Using a fluorescence microtiter plate reader, the fluorescence intensity at Ex/Em 360/340 nm was measured for blank 96-well plate (end point reading) followed by fluorescence intensity monitored over time (30 min) for sample plate held at 25°C. The blank plate reading was subtracted from the sample plate reading to obtain the corrected fluorescence intensity reading. The relative fluorescence units (RFU, fluorescence intensity) obtained were plotted against the 4-MU standard curve. The ALP enzyme converts MUP substrate to equal amount of 4-Methylumbelliferone (4-MU).

Sample and sample background control preparation:

The raw milk sample was diluted 50-fold using assay buffer. A 10 μ l sample from the diluted milk was added into the 96-well plate in quintuplicate. The total volume was brought to 110 μ l with assay buffer. In order to avoid interference of components in sample, a sample background control was done. 10 μ l sample from the diluted milk was added into the 96-well plate in triplicates and 100 μ l assay buffer was added to bring the volume to 110 μ l. 20 μ l of stop solution was added to the background control wells and mixed to terminate ALP activity in the sample.

The given 5 mM MUP substrate solution was diluted to 0.5 mM with assay buffer. 20 μ l of the 0.5 mM MUP solution was added to each well containing the test samples and the background controls.

Alkaline phosphatase activity calculation:

The fluorescence intensity of test samples and the background controls prepared as directed in above section was measured at Ex/Em 360/340 nm using a fluorescence microtiter plate reader continuously for 30 min at 25°C. To calculate the residual activity, the sample background control fluorescence intensity (averaged) was subtracted from average sample fluorescence intensity and the obtained value was applied to the standard curve to get the amount of 4-MU generated by ALP sample. ALP activity of test samples was then calculated as

$$ALP \text{ activity} = \frac{A}{VT} \quad (mU/ml) \quad (4-2)$$

Where A: amount of 4-MU generated by samples (in nmol), V: volume of sample added in the assay well (in ml), and T: reaction time (in min).

Definition of U: The amount of enzyme causing the hydrolysis of 1 μ mol of MUP per minute at pH 10.0 and 25°C (glycine buffer).

The current chapter focused on the materials and methods used for the experimental part of this research. The next chapter will discuss the theory of high pressure processing which will form the basis for the numerical simulation calculations and provide inputs to the simulation program.

5. THEORETICAL CONSIDERATIONS

5.1 Strength of Buoyancy Induced Flow (laminar or turbulent flow)

In order to develop an appropriate mathematical model and to carry out numerical simulation, it is necessary to know whether the natural convection induced flow within the vessel is laminar or turbulent. Since no correlations are available in the literature for natural convection flow on the inner surface of a vertical cylinder, the inner cylinder surface was approximated as a vertical flat plate for the purpose of choosing the laminar or turbulent flow model. This approximation was based on the correlation that for heat transfer from isothermal surfaces a vertical cylinder may be treated as a vertical flat surface (Holman, 1981) if

$$\frac{D}{L} \geq \frac{35}{Gr_L^{1/4}} \quad (5-1)$$

where, D is the diameter of the cylinder, L is the length of the cylinder, Gr_L is the Grashof number with length as the characteristic dimension. The Grashof number is a dimensionless number used in free convection systems and is defined as the ratio of buoyant forces to viscous forces (Singh and Heldman, 2001).

$$Gr_L = \frac{L^3 g \beta (T_s - T_\infty)}{\nu^2} \quad (5-2)$$

where, g is the acceleration due to gravity, L is the characteristic dimension (length of cylinder), β is the thermal expansion coefficient, T_s is the surface temperature

(temperature of the wall), T_∞ is the fluid temperature far from surface of the object, and ν is the kinematic viscosity.

It was assumed that equation (5-1) was applicable for flow on the inner surface of the high pressure cavity. The values for ratios in equation (5-1) for our vessel were found to be $\frac{D}{L} = 0.38$, $\frac{35}{Gr_L^{1/4}} = 0.08$. Later, the assumption was found to be valid in our case after the simulations and experiments were performed. According to Singh and Heldman, (2001), for a flat plate in vertical orientation, transition to turbulent occurs around Gr_L equals 10^9 . In our case, this value was of the order of 10^9 at room temperature and 10^{11} at higher initial temperatures. Therefore, the flow was assumed to be turbulent in the mathematical model and in the numerical simulation.

5.2 Governing Equations

The physical domain for the problem under consideration is shown in **Figure 5-1(a)**. However, since the problem can be considered as axisymmetric, only a radial slice of the physical domain, as shown in **Figure 5-1(b)**, was used to solve the governing equations.

5.2.1 Conservation of Mass

Continuity equation is a general mass balance that holds in all problems with no net generation of mass and with no mass transfer (Brodkey and Hershey, 2003), and is given by

$$\frac{\partial \rho}{\partial t} + \nabla \cdot (\rho \bar{V}) = 0 \quad (5-3)$$

Where, ρ is the density, t is time, \bar{V} is the average velocity and ∇ is the operator.

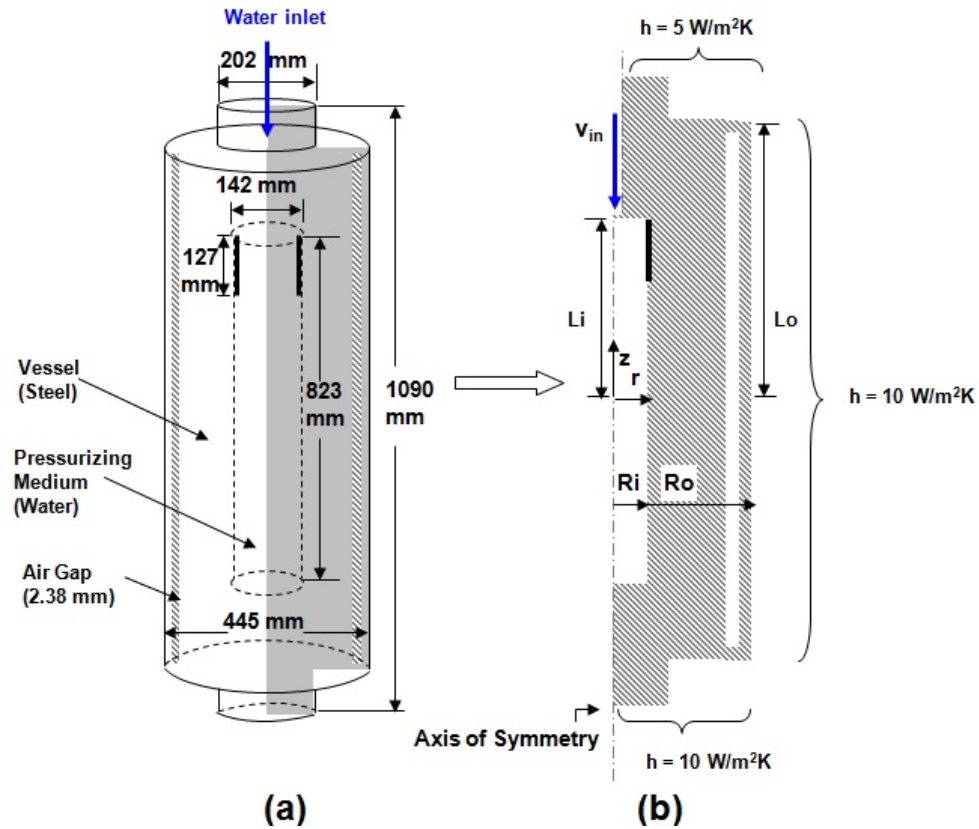


Figure 5-1: (a) Dimensions of HHPP vessel. Shaded area represents the radial section for numerical simulation, (b) computational domain used for simulation, $R_i = 71 \text{ mm}$, $R_o = 223 \text{ mm}$.

5.2.2 Conservation of Momentum

The Navier-Stokes equation in vector form for turbulent flow is given by

$$\rho \frac{D\bar{V}}{Dt} = \rho \left(\frac{\partial \bar{V}}{\partial t} + \bar{V} \cdot \nabla \bar{V} \right) = \bar{F} + (\bar{\nu} + \epsilon_m) \nabla^2 \bar{V} - \nabla \bar{P} \quad (5-4)$$

In the above equation, P is pressure, ν is kinematic viscosity, ϵ_m is the momentum eddy viscosity, \bar{F} represents the driving force for natural convection and bar on the quantities represents the time-averaged values for turbulent flow.

The driving buoyancy force for the vertical flow arises due to the difference between the body force and the force due to hydrostatic pressure gradient in ambient medium given by $g(\rho_a - \rho)$ (Jaluria, 1980), where ρ_a represents density of ambient medium. Although density of fluid was assumed to be constant in the continuity equation but in momentum equation, Boussinesq approximation was applied as density difference causes natural convection flow to occur. Gao, Mei, & Chen (2003) stated that in Boussinesq approximation, variations in fluid density are ignored, except insofar as they give rise to a gravitational force, therefore the force term in equation (5-4) is given by equation (5-5).

$$g(\rho_a - \rho) \cong -\rho\beta(T - T_a) \quad (5-5)$$

where, ρ_a is the density at far away location with temperature T_a . This approximation is accurate as long as the changes in the density are small. Therefore, final governing equation for momentum transfer in turbulent flow with Boussinesq approximation is given by

$$\rho \frac{D\bar{V}}{Dt} = \rho \left(\frac{\partial \bar{V}}{\partial t} + \bar{V} \cdot \nabla \bar{V} \right) = \underbrace{\hat{g}_z \beta (\bar{T} - T_i)}_{\text{only in z direction}} + (\bar{v} + \varepsilon_m) \nabla^2 \bar{V} - \nabla \bar{P} \quad (5-6)$$

where, g_z represents acceleration due to gravity along negative z direction, β is coefficient of thermal expansion, and T_i is the initial temperature of water.

5.2.3 Conservation of Energy

The energy conservation equation for turbulent flow is given by

$$\frac{D\bar{T}}{Dt} = \frac{\partial \bar{T}}{\partial t} + \bar{V} \cdot \nabla \bar{T} = \nabla \cdot (\alpha + \varepsilon_t) \nabla T + \frac{Q}{\rho C_p} + \beta \bar{T} \frac{D\bar{P}}{Dt} + \frac{\mu}{\rho C_p} \phi_v \quad (5-7)$$

In the above equation, α is thermal diffusivity, ϵ_t is the turbulent thermal diffusivity, Q is the source term (heat of chemical reaction or other volumetric heat sources), ϕ_v is viscous dissipation (thermal energy dissipated by viscous heating), C_p is heat capacity, β is coefficient of thermal expansion and μ is dynamic viscosity. The terms on the right hand side of equation (5-7) represent conduction of heat, heat source, pressure work, and viscous dissipation, respectively. In our case the second term is zero as there was no chemical heat source term. If we expand the third (pressure work) term we get,

$$\beta \bar{T} \frac{D\bar{P}}{Dt} = \beta \bar{T} \left[\frac{\partial \bar{P}}{\partial t} + \bar{V} \cdot \nabla \bar{P} \right] \quad (5-8)$$

$$= \beta \bar{T} \left[\frac{\partial \bar{P}}{\partial t} + \bar{V}_x \frac{\partial \bar{P}}{\partial x} + \bar{V}_y \frac{\partial \bar{P}}{\partial y} + \bar{V}_z \frac{\partial \bar{P}}{\partial z} \right] \quad (5-9)$$

Since there is no significant bulk pressure variation within the fluid (water), $(\partial \bar{P} / \partial x)$, $(\partial \bar{P} / \partial y)$, and $(\partial \bar{P} / \partial z)$ were taken as zero. Therefore, the pressure work term becomes

$$\beta \bar{T} \frac{D\bar{P}}{Dt} = \beta \bar{T} \frac{d\bar{P}}{dt} \quad (5-10)$$

The fourth term on the right hand side of equation (5-7) which represents viscous dissipation, was neglected due to low velocity gradients and low viscosity of water. Therefore, the governing equation for conservation of energy in turbulent flow is given by

$$\frac{D\bar{T}}{Dt} = \frac{\partial \bar{T}}{\partial t} + \bar{V} \cdot \nabla \bar{T} = \nabla \cdot (\alpha + \epsilon_t) \nabla \bar{T} + \beta \bar{T} \frac{d\bar{P}}{dt} \quad (5-11)$$

The energy conservation equation for solid region (vessel steel wall) with constant physical properties (properties for steel were assumed to be constant) is given by

$$\frac{1}{\alpha_s} \frac{\partial T}{\partial t} = \nabla^2 T \quad (5-12)$$

Where α_s is the thermal diffusivity of steel and ∇^2 is the Laplacian operator. The above equation represents the conduction heat transfer in the vessel wall.

5.3 Thermodynamics of High Pressure Process

5.3.1 Adiabatic Increase in Temperature

As discussed in section 1.7, work done during pressurization/depressurization causes increase/decrease in temperature in both the food and the pressurizing medium. For the purpose of modeling, this temperature change produced by pressure change can be derived by assuming high pressure vessel to be a closed system and the process to be locally adiabatic. The increase in temperature due to pressure can be estimated by a thermodynamic equation which can be derived from total derivative of the entropy of the pressurized system

$$ds = \left(\frac{\partial s}{\partial T} \right)_P dT + \left(\frac{\partial s}{\partial P} \right)_T dP \quad (5-13)$$

where, s is the specific entropy. For a reversible process, the entropy change would be zero,

$$\therefore \left(\frac{\partial s}{\partial T} \right)_P dT + \left(\frac{\partial s}{\partial P} \right)_T dP = 0 \quad (5-14)$$

From Maxwell's relations (Abbott Van Ness, 1972), we know that

$$\left(\frac{\partial s}{\partial P} \right)_T = - \left(\frac{\partial v}{\partial T} \right)_P \quad (5-15)$$

Substituting equation (5-15) in equation (5-14), we get

$$\left(\frac{\partial s}{\partial T}\right)_p dT - \left(\frac{\partial v}{\partial T}\right)_p dP = 0 \quad (5-16)$$

Also, we know that isobaric heat capacity is defined as (Abbott and Van Ness (1972)),

$$C_p = T \left(\frac{\partial s}{\partial T}\right)_p \quad (5-17)$$

and the coefficient of thermal expansion (β) is defined as

$$\beta = \frac{1}{v} \left(\frac{\partial v}{\partial T}\right)_p \quad (5-18)$$

Substituting equation (5-17) and (5-18) in equation (5-16), we get

$$\frac{C_p}{T} dT - \beta v dP = 0 \quad (5-19)$$

Rearranging equation (5-19), we obtain

$$\frac{dT}{dP} = \frac{T v \beta}{C_p} \quad (5-20)$$

It can be seen from equation (5-20) that dT/dP depends on physical quantities which are function of composition of the sample and further these physical properties also depend on temperature and pressure (Makita, 1992). This makes the calculation of dT/dP complicated. In the present work, dT/dP values in equation for pressure work (discussed later in section 5.3.2) were obtained from the literature data and assumed to be constant, i.e., were considered to be only a function of initial temperature of water.

(a) Theoretical Compression Heating Values of Water

The adiabatic compression heating values for water at different initial temperatures were calculated using equation (5-20), and are given in **Table 5-1**. The values of β , $\rho (= \frac{1}{v})$,

and C_p for water at different initial temperatures were taken from Singh and Heldman (2003). The main constraint during theoretical calculations of increase in temperature with pressure is the specific volume (v) under pressure, which should not be taken as constant under these conditions (Rasanayagam et al., 2003). It was observed that theoretical adiabatic compression heating values calculated using equation (5-20) show a discrepancy from values found in literature as shown in **Table 5-1** and **Table 5-2**.

Table 5-1: Theoretically calculated (using equation (5-20)) adiabatic compression heating values of water at different initial temperatures.

Initial Temp. (°C)	T (K)	β (K⁻¹)	ρ (kg/m³)	C_p (J/kg K)	dT/dP (K/100 MPa)
10	283.15	0.000095	999.7	4195	0.64
20	293.15	0.00021	998.2	4182	1.47
25	298.15	0.00028	997.1	4180	2.00
30	303.15	0.0003	995.7	4176	2.18
40	313.15	0.00039	992.2	4175	2.95
60	333.15	0.00053	983.2	4181	4.29

(b) Compression Heating Values for Water Obtained from Literature

The compression heating values for water are available in literature from different sources. Hendrickx and Knorr (2001) stated that for water at an initial temperature of 25°C the increase in temperature is 2°C /100 MPa whereas it was found to be 3°C/100 MPa at 25°C by Rasanayagam et al. (2003). Also, Rasanayagam et al. (2003) presented the compression heating value for water at 60°C as 4°C/100 MPa. The compression

heating values as calculated from data presented in **Figure 5-2** (Food Biotechnology and Food Process Engineering, TU, Berlin) are given in **Table 5-2**.

Adiabatic Heating during Compression

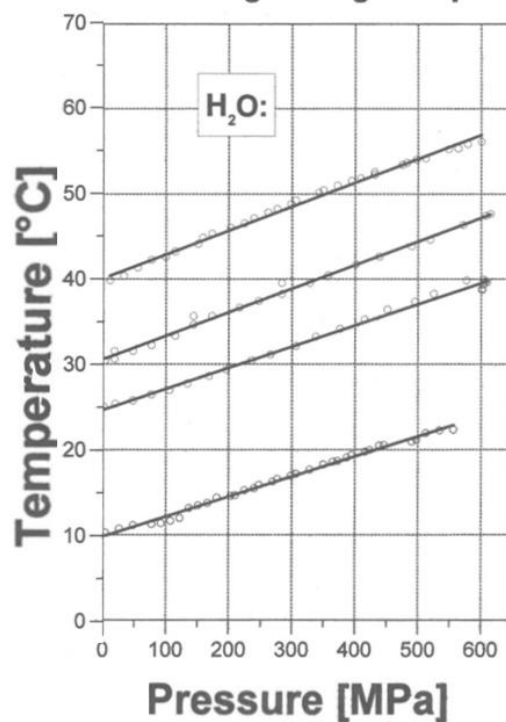


Figure 5-2: Adiabatic compression heating values (calculated from slope of the lines) for water, obtained from Food Biotechnology and Food Engineering, TU, Berlin.

Table 5-2: Adiabatic compression heating values for water extracted from pressure-temperature graph shown in Figure 5.2.

Initial Temp. (°C)	T (K)	dT/dP (K /100 MPa)
10	283.15	2.3
20	298.15	2.5
30	303.15	2.8
40	313.15	2.8

The compression heating values of water dT/dP at different initial temperature are also available from NIST-IAPSW standard reference database version 10 section 2.2 as given by Barbosa-Canovas and Rodriguez (2005). These are shown in **Table 5-3**. It shows that dT/dP values are also a function of pressure.

Table 5-3: Adiabatic compression heating values of water obtained from NIST-IAPSW standard database plots.

Initial Temp. (°C)	Initial Temp. (K)	dT/dP (K/100 MPa)					
		0.1-100 MPa	100-200 MPa	200-300 MPa	300-400 MPa	400-500 MPa	500-600 MPa
20	293.15	1.5	2.5	2.8	3	3.15	3.15
30	303.15	2.2	2.8	3.15	3.3	3.3	3.3
40	313.15	2.8	3.2	3.4	3.4	3.4	3.4
60	333.15	4.2	4.1	4	3.8	3.8	3.8
80	353.15	5.6	5.2	4.8	4.6	4.4	4.2

Thus, a variation was found between dT/dP values obtained from different sources in the literature. For the purpose of this research compression heating values obtained from NIST –IAPSW database **Table 5-3** were used since they include both the effect of initial temperature and increase in pressure.

5.3.2 Pressure Work or Heat Generation (defined as boundary condition)

The pressure work term, i.e., the last term in equation (5-11) was modified to take into account temperature increase during pressurization. From equation (5-11),

$$\text{Pressure Work} = \beta \bar{T} \frac{dP}{dt} \quad (5-21)$$

From the above expression, it is clear that we need the values of coefficient of thermal expansion, temperature and rate of pressurization in order to calculate pressure work term for a given food material or pressurizing medium. The values of temperature and rate of pressurization can be easily obtained by experiments whereas it is difficult to measure coefficient of thermal expansion, specifically for complex food systems. Therefore, mathematical approach was used to replace β in pressure work term by quantities which can be measured easier.

Rearranging equation (5-20) we get

$$\beta \bar{T} = \frac{C_p}{v} \frac{dT}{dP} \quad (5-22)$$

Substituting value of $\beta \bar{T}$ from equation (5-22) into equation (5-21), we obtain,

$$\text{Pressure Work (Q)} = \frac{C_p}{v} \frac{dT}{dP} \frac{dP}{dt} \quad (5-23)$$

$$\therefore \text{Pressure Work (Q)} = \rho C_p \frac{dT}{dP} \frac{dP}{dt} \quad (5-24)$$

where, ρ is the density of water and C_p is the heat capacity.

The values of density and heat capacity for water were taken from Singh and Heldman (2003) at initial temperature. The dT/dP values for water at different initial temperature were used as given in **Table 5-3**. The values of dP/dt for 20°C, 40°C and 60°C were

obtained from the experimental data. To calculate pressure work term for 80°C (353 K), dP/dt values were assumed to be constant (3.60 MPa/s) as we could not carry out the experiments for initial temperature more than 60°C (333 K) due to the experimental set up limitations. Pressure work term so calculated was fed to the numerical simulation program as source term.

5.3.3 Velocity of Water Pumped into Vessel (defined as boundary condition)

In the Rutgers HHPP unit the water is pumped into the vessel through the top closure using a high power intensifier pump to pressurize the vessel. The velocity at which the pressurizing fluid enters the vessel during pressurization can be calculated based on the rate of pressurization, compressibility of water, and the diameter of the inlet as follows:

$$v_{in} = \frac{C \cdot V_{water}}{\pi r^2 \cdot t_{cum}} \quad (5-25)$$

where, C is the fraction of water compression (0.15 for 700 MPa), V_{water} is the volume of water in the vessel (in m³), r is the radius of the opening in the closure for water inlet (in m), and t_{cum} is the pressure come up time (180 s for 700 MPa). Here, we assumed that water enter the vessel at a constant rate although it probably is not true.

Based on equation (5-25), the value of v_{in} was found to be 0.28 m/s for the 10 L vertical vessel and 0.14 m/s from each inlet for 10 L horizontal vessel. For 350 L horizontal vessel, 0.03 m/s from each end. The velocity values were specified as water inlet boundary condition in the numerical simulation model for the period of pressurization.

5.4 Heat Transfer in Air Gap between Vessel and Shell (boundary condition)

To determine if convection heat transfer takes place in the air gap between the main vessel and the shell, we need to calculate the Rayleigh number for the gap. Rayleigh number is dimensionless number, defined as a product of Grashof number and Prandtl number. For free/natural convection near a vertical wall, Rayleigh number is given by

$$Ra_x = Gr_x \cdot Pr = \frac{x^3 g \beta}{\nu^2} (T_s - T_\infty) \cdot Pr \quad (5-26)$$

where, Ra_x is the Rayleigh number, Gr_x is the Grashof number, Pr is the Prandtl number, and x is the characteristic length (air gap shown in **Figure 4-3**). The fluid properties needed to calculate Gr_x and Pr were evaluated at the film temperature, which is defined as

$$T_f = \frac{T_s + T_\infty}{2} \quad (5-27)$$

Gebhart et al. (1988) stated that for vertical rectangular enclosures, at small values of Ra , i.e., $Ra \leq 1000$, there is little increase in the heat transfer over that due to conduction alone.

In our case, for air gap of 2.38 mm even if we assume that temperature difference between air and shell surface was 100 K, the value of Ra_x obtained would be 141. Therefore, conduction heat transfer would dominate in the air gap. Hence, air was treated as a still continuum in numerical simulation and only the energy (conduction heat transfer) equation was solved there.

5.5 Lag in Temperature Measurement

The transient temperature that was measured by thermocouples during the high pressure experiments were corrected to account for the finite lag that exists between the actual temperature and the measured temperature. The lag arises due to the mass of the thermocouple assembly which consists of high pressure metal tubing surrounding the thermocouple wires.

Correction in experimentally measured temperature due to thermocouple response time

During the high pressure process, it was assumed for the sake of analysis that the temperature increases linearly as pressure is increased during the pressurization stage. During the pressure hold period, the temperature decreases, albeit slowly, but almost linearly. Therefore, we calculated the response of the thermocouples to linearly increasing and decreasing temperature input during pressurization, pressure hold time and depressurization.

Thermocouple response to ramp input

The dynamic response of a thermocouple to ramp input (linear temperature increase with time) can be modeled as a first-order system. A simplified heat transfer analysis was used to derive the response of a thermocouple to ramp input. The unsteady state energy equation for a thermocouple (lumped mass) subjected to heat transfer is

$$m_t C_p \frac{dT}{dt} = hA(T_w(t) - T) \quad (5-28)$$

where, m_t is mass of thermocouple, h is the heat transfer coefficient, $T_w(t)$ is the temperature of water in which thermocouple is immersed, as a function of time, and A is the surface area. **Figure 5-3** shows, schematically, the response of a thermocouple to ramp input.

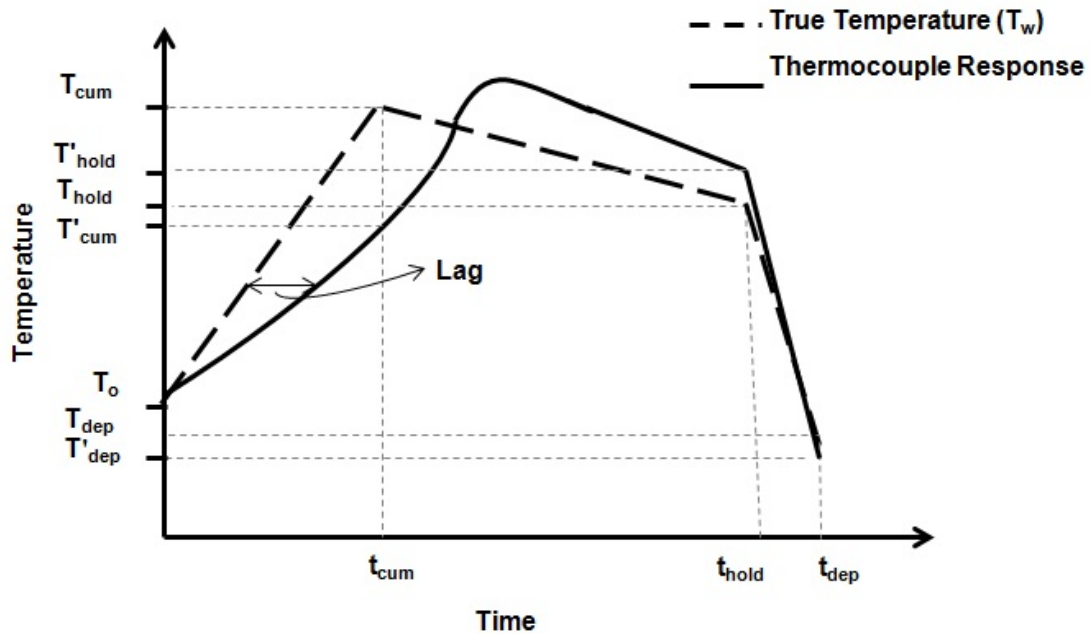


Figure 5-3: Anticipated response of the thermocouple to a ramp input during pressurization, pressure hold, and pressure release.

The thermocouple response to ramp input can be obtained analytically as follows:

(a) For $0 \leq t \leq t_{cum}$ [during pressurization]

Based on the experimental data the increase in temperature during pressurization was found to be linear therefore, from **Figure 5-3**, we can write

$$\frac{(T_w - T_0)}{(T_{cum} - T_0)} = \frac{(t - 0)}{(t_{cum} - 0)} \quad (5-29)$$

$$T_w = T_o + \frac{(T_{cum} - T_o)}{t_{cum}} t \quad (5-30)$$

Defining T' as the temperature read by the thermocouple during pressurization, from equation (5-28) we get

$$m_t C_p \frac{dT'}{dt} = hA \left[\left(T_o + \frac{(T_{cum} - T_o)}{t_{cum}} t \right) - T' \right] \quad (5-31)$$

$$m_t C_p \frac{dT'}{dt} = hA T_o + hA \frac{(T_{cum} - T_o)}{t_{cum}} t - hA T' \quad (5-32)$$

Dividing both sides of the equation (5-32) by mC_p , we get

$$\frac{dT'}{dt} + \frac{hA}{m_t C_p} (T' - T_o) = \frac{hA}{m_t C_p} \left(\frac{T_{cum} - T_o}{t_{cum}} t \right) \quad (5-33)$$

$$\text{Let } (T' - T_o) = \theta' \quad (5-34)$$

$$\therefore \frac{dT'}{dt} = \frac{d\theta'}{dt} \quad (5-35)$$

Therefore, equation (5-33) becomes

$$\frac{d\theta'}{dt} + \frac{hA}{m_t C_p} \theta' = \frac{hA}{m_t C_p} \left(\frac{T_{cum} - T_o}{t_{cum}} t \right) \quad (5-36)$$

Equation (5-36) is of the form Leibnitz Linear Equation (Grewal, 1995), i.e.,

$$\frac{dy}{dx} + Py = S(x)$$

whose solution is given by

$$y \cdot (\text{I.F.}) = \int S \cdot (\text{I.F.}) \cdot dx + c$$

where, I.F. (integrating factor) = $e^{\int P \cdot dx}$

Therefore, from equation (5-36) we define I.F. = $e^{\int \frac{hA}{m_t C_p} dt}$

$$= e^{\left(\frac{hA}{m_t C_p}\right)t} = e^{\frac{t}{\tau}}$$

where,

$$\frac{m_t C_p}{hA} = \tau = \text{time constant of thermocouple} \quad (5-37)$$

and the solution can be written as

$$\theta' e^{\frac{t}{\tau}} = \frac{1}{\tau} \left(\frac{T_{\text{cum}} - T_o}{t_{\text{cum}}} \right) \int e^{\frac{t}{\tau}} dt + c \quad (5-38)$$

Integrating the above equation by parts, we get

$$\therefore \theta' e^{\frac{t}{\tau}} = \frac{1}{\tau} \left(\frac{T_{\text{cum}} - T_o}{t_{\text{cum}}} \right) \left[t \int e^{\frac{t}{\tau}} dt - \int \left(\frac{dt}{dt} \int e^{\frac{t}{\tau}} dt \right) dt \right] + c \quad (5-39)$$

$$\therefore \theta' e^{\frac{t}{\tau}} = \frac{1}{\tau} \left(\frac{T_{\text{cum}} - T_o}{t_{\text{cum}}} \right) \left[\tau t e^{\frac{t}{\tau}} - \tau^2 e^{\frac{t}{\tau}} \right] + c \quad (5-40)$$

$$\therefore \theta' e^{\frac{t}{\tau}} = \left(\frac{T_{\text{cum}} - T_o}{t_{\text{cum}}} \right) \left[t e^{\frac{t}{\tau}} - \tau e^{\frac{t}{\tau}} \right] + c \quad (5-41)$$

$$\therefore \theta' = \left(\frac{T_{\text{cum}} - T_o}{t_{\text{cum}}} \right) [t - \tau] + c e^{-\frac{t}{\tau}} \quad (5-42)$$

Replacing $\theta' = (T' - T_o)$ in equation (5-42), we get

$$T' - T_o = \left(\frac{T_{\text{cum}} - T_o}{t_{\text{cum}}} \right) [t - \tau] + c e^{-\frac{t}{\tau}} \quad (5-43)$$

$$\therefore T' = T_o + \left(\frac{T_{\text{cum}} - T_o}{t_{\text{cum}}} \right) [t - \tau] + c e^{-\frac{t}{\tau}} \quad (5-44)$$

At $t = 0$; $T' = T_o$, we get

$$T_o = T_o + \left(\frac{T_{cum} - T_o}{t_{cum}} \right) [0 - \tau] + ce^{-\frac{0}{\tau}} \quad (5-45)$$

$$\therefore c = \tau \left(\frac{T_{cum} - T_o}{t_{cum}} \right) \quad (5-46)$$

Substituting expression for 'c' in equation (5-44), we get

$$T' = T_o + \left(\frac{T_{cum} - T_o}{t_{cum}} \right) [t - \tau] + \left[\tau \left(\frac{T_{cum} - T_o}{t_{cum}} \right) e^{-t/\tau} \right] \quad (5-47)$$

$$\therefore T' = T_o + \tau \left(\frac{T_{cum} - T_o}{t_{cum}} \right) \left[\frac{t}{\tau} - 1 + e^{-t/\tau} \right] \quad (5-48)$$

Thus the response of a thermocouple to a ramp input or linearly increasing temperature, i.e., during pressurization is given by equation (5-48).

(b) For $t_{cum} \leq t \leq t_{hold}$ [during pressure hold]

Assuming that temperature decreases linearly with time during pressure hold, as shown in

Figure 5-3, we can write

$$\frac{(T_w - T_{cum})}{(T_{hold} - T_{cum})} = \frac{(t - t_{cum})}{(t_{hold} - t_{cum})} \quad (5-49)$$

\therefore Temperature of water T_w varies with time t as follows

$$T_w = T_{cum} + \left(\frac{T_{hold} - T_{cum}}{t_{hold} - t_{cum}} \right) [t - t_{cum}] \quad (5-50)$$

Defining T'' as the temperature read by the thermocouple during the pressure hold phase, from equation (5-28) we can write

$$m_t C_p \frac{dT''}{dt} = hA \left[\left(\frac{T_{hold} - T_{cum}}{t_{hold} - t_{cum}} \right) (t - t_{cum}) + T_{cum} - T'' \right] \quad (5-51)$$

$$\text{Let } t - t_{\text{cum}} = t'' \quad (5-52)$$

$$\therefore dt = dt'' \quad (5-53)$$

$$m_t C_p \frac{dT''}{dt''} = hA \left[\left(\frac{T_{\text{hold}} - T_{\text{cum}}}{t_{\text{hold}} - t_{\text{cum}}} \right) t'' + T_{\text{cum}} - T'' \right] \quad (5-54)$$

Divide both sides of equation (5-54) by mC_p , we get

$$\frac{dT''}{dt''} + \frac{hA}{m_t C_p} (T'' - T_{\text{cum}}) = \frac{hA}{m_t C_p} \left(\frac{T_{\text{hold}} - T_{\text{cum}}}{t_{\text{hold}} - t_{\text{cum}}} \right) t'' \quad (5-55)$$

$$\text{Let } T'' - T_{\text{cum}} = \theta'' \quad (5-56)$$

$$\therefore \frac{dT''}{dt''} = \frac{d\theta''}{dt''} \quad (5-57)$$

Substituting the expression from equation (5-57) in equation (5-55), we get

$$\frac{d\theta''}{dt''} + \frac{hA}{m_t C_p} \theta'' = \frac{hA}{m_t C_p} \left(\frac{T_{\text{hold}} - T_{\text{cum}}}{t_{\text{hold}} - t_{\text{cum}}} \right) t'' \quad (5-58)$$

Following the method described earlier to solve Leibnitz Linear Equation and using

$$\begin{aligned} \text{Integrating Factor (I.F)} &= e^{\int \frac{hA}{m_t C_p} dt''} \\ &= e^{\left(\frac{hA}{m_t C_p} \right) t''} = e^{\frac{t''}{\tau}} \end{aligned}$$

we can write,

$$\theta'' e^{\frac{t''}{\tau}} = \frac{1}{\tau} \left(\frac{T_{\text{hold}} - T_{\text{cum}}}{t_{\text{hold}} - t_{\text{cum}}} \right) \int e^{\frac{t''}{\tau}} t'' dt'' + c \quad (5-59)$$

Integrating by parts, we get

$$\theta'' e^{\frac{t''}{\tau}} = \frac{1}{\tau} \left(\frac{T_{\text{hold}} - T_{\text{cum}}}{t_{\text{hold}} - t_{\text{cum}}} \right) \left[t'' \int e^{\frac{t''}{\tau}} dt'' - \int \left(\frac{dt''}{dt''} \int e^{\frac{t''}{\tau}} dt'' \right) dt'' \right] + c \quad (5-60)$$

$$\therefore \theta'' e^{\frac{t''}{\tau}} = \frac{1}{\tau} \left(\frac{T_{\text{hold}} - T_{\text{cum}}}{t_{\text{hold}} - t_{\text{cum}}} \right) \left[\tau t'' e^{\frac{t''}{\tau}} - \tau^2 e^{\frac{t''}{\tau}} \right] + c \quad (5-61)$$

$$\therefore \theta'' e^{\frac{t''}{\tau}} = \left(\frac{T_{\text{hold}} - T_{\text{cum}}}{t_{\text{hold}} - t_{\text{cum}}} \right) \left[t'' e^{\frac{t''}{\tau}} - \tau e^{\frac{t''}{\tau}} \right] + c \quad (5-62)$$

$$\therefore \theta'' = \left(\frac{T_{\text{hold}} - T_{\text{cum}}}{t_{\text{hold}} - t_{\text{cum}}} \right) [t'' - \tau] + c e^{-t''/\tau} \quad (5-63)$$

Replacing $\theta'' = (T'' - T_{\text{cum}})$ in equation (5-63), we get

$$T'' - T_{\text{cum}} = \left(\frac{T_{\text{hold}} - T_{\text{cum}}}{t_{\text{hold}} - t_{\text{cum}}} \right) [t'' - \tau] + c e^{-t''/\tau} \quad (5-64)$$

$$\therefore T'' = T_{\text{cum}} + \left(\frac{T_{\text{hold}} - T_{\text{cum}}}{t_{\text{hold}} - t_{\text{cum}}} \right) [t'' - \tau] + c e^{-t''/\tau} \quad (5-65)$$

From **Figure 5-3**, at $t = t_{\text{cum}}$; $T'' = T'_{\text{cum}}$

\therefore From equation (5-52), at $t'' = 0$; $T'' = T'_{\text{cum}}$

$$\begin{aligned} T'_{\text{cum}} &= T_{\text{cum}} + \left(\frac{T_{\text{hold}} - T_{\text{cum}}}{t_{\text{hold}} - t_{\text{cum}}} \right) [0 - \tau] + c e^{-0/\tau} \\ c &= T'_{\text{cum}} - T_{\text{cum}} + \tau \left(\frac{T_{\text{hold}} - T_{\text{cum}}}{t_{\text{hold}} - t_{\text{cum}}} \right) \end{aligned} \quad (5-66)$$

Substituting expression for 'c' in equation (5-65), we get

$$T'' = T_{\text{cum}} + \left(\frac{T_{\text{hold}} - T_{\text{cum}}}{t_{\text{hold}} - t_{\text{cum}}} \right) [t'' - \tau] + \left[T'_{\text{cum}} - T_{\text{cum}} + \tau \left(\frac{T_{\text{hold}} - T_{\text{cum}}}{t_{\text{hold}} - t_{\text{cum}}} \right) \right] e^{-t''/\tau} \quad (5-67)$$

$$\text{Replace } t'' = t - t_{\text{cum}} \quad (5-68)$$

$$T'' = T_{\text{cum}} + \left(\frac{T_{\text{hold}} - T_{\text{cum}}}{t_{\text{hold}} - t_{\text{cum}}} \right) [t - t_{\text{cum}} - \tau] + \left[T'_{\text{cum}} - T_{\text{cum}} + \tau \left(\frac{T_{\text{hold}} - T_{\text{cum}}}{t_{\text{hold}} - t_{\text{cum}}} \right) \right] e^{-(t-t_{\text{cum}})/\tau} \quad (5-69)$$

Thus response of a thermocouple during pressure hold is given by equation (5-69), where T_{cum} is the temperature as read by the thermocouple at end of pressurization, obtained from equation (5-48) at t equal to t_{cum} .

(c) For $t_{hold} \leq t \leq t_{dep}$ [during pressure release]

Based on experimental data, assuming that temperature decreases linearly with time during pressure release as shown in **Figure 5-3**, we can write

$$\frac{(T_w - T_{hold})}{(T_{dep} - T_{hold})} = \frac{(t - t_{hold})}{(t_{dep} - t_{hold})} \quad (5-70)$$

\therefore Temperature of water T_w decreases with time t during pressure release as follows

$$T_w = T_{hold} + \left(\frac{T_{dep} - T_{hold}}{t_{dep} - t_{hold}} \right) [t - t_{hold}] \quad (5-71)$$

Defining T''' as the temperature read by the thermocouple during the pressure release phase, from equation (5-28) we can write

$$m_t C_p \frac{dT'''}{dt} = hA \left[\left(\frac{T_{dep} - T_{hold}}{t_{dep} - t_{hold}} \right) (t - t_{hold}) + T_{hold} - T''' \right] \quad (5-72)$$

Following the steps followed for pressurization and pressure hold, for depressurization we get

$$T''' = T_{hold} + \left(\frac{T_{dep} - T_{hold}}{t_{dep} - t_{hold}} \right) [t - t_{hold} - \tau] + \left[T''_{hold} - T_{hold} + \tau \left(\frac{T_{dep} - T_{hold}}{t_{dep} - t_{hold}} \right) \right] e^{-(t-t_{hold})/\tau} \quad (5-73)$$

Thus response of a thermocouple during pressure release is given by equation (5-73), where T''_{hold} is the temperature as read by the thermocouple at end of hold period, obtained from equation (5-69) at t equals t_{hold} .

Equations (5-48), (5-69), and (5-73) can be used to predict the response of a thermocouple having time constant τ during pressurization, pressure hold, and pressure release respectively, given the actual variation of temperature that the thermocouple is supposed to measure. Typically, during a high pressure experiment, the temperature measured by a thermocouple, i.e., variations of T' , T'' , and T''' with t are recorded. However, the main interest is to know the true variation of temperature (T_w) with time, from the experimentally recorded data (T' , T'' , and T''' with t). Therefore, the equations (5-48), (5-69), and (5-73) obtained above were mathematically rearranged to get the true variation in temperature, from the temperature data recorded by a thermocouple, as described below.

Analysis to find true variation of temperature of water as a function of time from the experimental data

Given T' , T'' , and T''' from experimental data, we can calculate “true” variation of water temperature as a function of time by rearranging equations (5-48), (5-69), and (5-73).

(a) For $0 \leq t \leq t_{\text{cum}}$ [during pressurization]

From equation (5-48), we know that

$$T' = T_o + \tau \left(\frac{T_{\text{cum}} - T_o}{t_{\text{cum}}} \right) \left[\frac{t}{\tau} - 1 + e^{-t/\tau} \right] \quad (5-74)$$

Since the slope of equation (16), $\left(\frac{T_{\text{cum}} - T_o}{t_{\text{cum}}} \right)$ was assumed to be constant during pressurization, we can replace it by $\left(\frac{T_w - T_o}{t} \right)$, where T_w is the true temperature corresponding to T' at time t . Therefore, we get

$$\therefore T_w - T_o = \frac{(T' - T_o)t}{\tau \left[\frac{t}{\tau} - 1 + e^{-t/\tau} \right]} \quad (5-75)$$

$$\therefore T_w = T_o + \frac{(T' - T_o)t}{\tau \left[\frac{t}{\tau} - 1 + e^{-t/\tau} \right]} \quad (5-76)$$

Equation (5-76) was used to predict the corrected or “true” variation of water temperature with time ‘t’ during pressurization from the measured variation of T’.

(b) For $t_{cum} \leq t \leq t_{hold}$ [during pressure hold]

From equation (5-69), we know that

$$T'' = T_{cum} + \left(\frac{T_{hold} - T_{cum}}{t_{hold} - t_{cum}} \right) [t - t_{cum} - \tau] + \left[T'_{cum} - T_{cum} + \tau \left(\frac{T_{hold} - T_{cum}}{t_{hold} - t_{cum}} \right) \right] e^{-(t-t_{cum})/\tau} \quad (5-77)$$

$$T'' - T_{cum} - T'_{cum} e^{-(t-t_{cum})/\tau} + T_{cum} e^{-(t-t_{cum})/\tau} = \left(\frac{T_{hold} - T_{cum}}{t_{hold} - t_{cum}} \right) [t - t_{cum} + \tau e^{-(t-t_{cum})/\tau} - \tau] \quad (5-78)$$

Since slope of above equation $\left(\frac{T_{hold} - T_{cum}}{t_{hold} - t_{cum}} \right)$ was assumed to be constant for all points

during pressure hold, we can replace it by $\left(\frac{T_w - T_{cum}}{t - t_{cum}} \right)$, where T_w is true temperature

corresponding to T'' at time t.

$$T'' - T_{cum} - T'_{cum} e^{-(t-t_{cum})/\tau} + T_{cum} e^{-(t-t_{cum})/\tau} = \left(\frac{T_w - T_{cum}}{t - t_{cum}} \right) [t - t_{cum} + \tau e^{-(t-t_{cum})/\tau} - \tau] \quad (5-79)$$

$$T'' + T_{cum} \left(e^{-(t-t_{cum})/\tau} - 1 \right) - T'_{cum} e^{-(t-t_{cum})/\tau} = \left(\frac{T_w - T_{cum}}{t - t_{cum}} \right) [t - t_{cum} + \tau e^{-(t-t_{cum})/\tau} - \tau] \quad (5-80)$$

$$T_w = T_{cum} + (t - t_{cum}) \left[\frac{T'' + T_{cum} \left(e^{-\frac{(t-t_{cum})}{\tau}} - 1 \right) - T'_{cum} e^{-\frac{(t-t_{cum})}{\tau}}}{t - t_{cum} + \tau e^{-\frac{(t-t_{cum})}{\tau}} - \tau} \right] \quad (5-81)$$

Equation (5-81) was used to predict the corrected or “true” variation of water temperature with time ‘t’ during pressurization from the measured variation of T”.

(c) For $t_{hold} \leq t \leq t_{dep}$ [during pressure release]

From equation (5-73), we know that

$$T''' = T_{hold} + \left(\frac{T_{dep} - T_{hold}}{t_{dep} - t_{hold}} \right) [t - t_{hold} - \tau] + \left[T''_{hold} - T_{hold} + \tau \left(\frac{T_{dep} - T_{hold}}{t_{dep} - t_{hold}} \right) \right] e^{-\frac{(t-t_{hold})}{\tau}} \quad (5-82)$$

$$T''' - T_{hold} - T''_{hold} e^{-\frac{(t-t_{hold})}{\tau}} + T_{hold} e^{-\frac{(t-t_{hold})}{\tau}} = \left(\frac{T_{dep} - T_{hold}}{t_{dep} - t_{hold}} \right) [t - t_{hold} + \tau e^{-\frac{(t-t_{hold})}{\tau}} - \tau] \quad (5-83)$$

Since slope of above equation $\left(\frac{T_{dep} - T_{hold}}{t_{dep} - t_{hold}} \right)$ was assumed to be constant for all points

during pressure release, we can replace it by $\left(\frac{T_w - T_{hold}}{t - t_{hold}} \right)$, where T_w is true temperature

corresponding to T''' at time t.

$$T''' - T_{hold} - T''_{hold} e^{-\frac{(t-t_{hold})}{\tau}} + T_{hold} e^{-\frac{(t-t_{hold})}{\tau}} = \left(\frac{T_w - T_{hold}}{t - t_{hold}} \right) [t - t_{hold} + \tau e^{-\frac{(t-t_{hold})}{\tau}} - \tau] \quad (5-84)$$

$$T''' + T_{hold} \left(e^{-\frac{(t-t_{hold})}{\tau}} - 1 \right) - T''_{hold} e^{-\frac{(t-t_{hold})}{\tau}} = \left(\frac{T_w - T_{hold}}{t - t_{hold}} \right) [t - t_{hold} + \tau e^{-\frac{(t-t_{hold})}{\tau}} - \tau] \quad (5-85)$$

$$T_w = T_{\text{hold}} + (t - t_{\text{hold}}) \left[\frac{T''' + T_{\text{hold}} \left(e^{-\frac{(t-t_{\text{hold}})}{\tau}} - 1 \right) - T'_{\text{hold}} e^{-\frac{(t-t_{\text{hold}})}{\tau}}}{t - t_{\text{hold}} + \tau e^{-\frac{(t-t_{\text{hold}})}{\tau}} - \tau} \right] \quad (5-86)$$

Equation (5-86) was used to predict the corrected or “true” variation of water temperature with time ‘t’ during pressurization from the measured variation of T'''.

Therefore, the true variation of temperature of water at thermocouple locations during pressurization, pressure hold and pressure release can be predicted by equations (5-76), (5-81), and (5-86), respectively, from the measured variation of temperatures T', T'', and T''' with time t.

So far, in this chapter we discussed some of the theoretical knowledge that will be useful when setting up the numerical simulation program such as governing equations, laminar or turbulent flow, heat generation term etc. The following section discusses the theory behind some of the techniques that were used for evaluation of the results obtained from the numerical simulation program.

5.6 Impact of Temperature Distributions on Microbial Inactivation

Although the existence of temperature distributions during a process provide enough information to make a statement if a process is uniform or non-uniform, it is important to understand the impact of that temperature distribution on a parameter which is relevant to the process, e.g., if the temperature distribution exists during a high pressure process where inactivation of target microorganism can be achieved just by pressure (assuming

temperatures are not too high to cause any quality damage), the existing temperature distribution is of no consequence. Whereas, during a pressure assisted thermal process where primary mechanism for inactivation is temperature, it is important to take into account the impact of temperature distribution on the inactivation of microbe of concern.

5.6.1 Inactivation of *C. botulinum* spores

The temperature history during high pressure process obtained from the numerical simulation program was used to quantify the impact of non-uniformity in temperature on the non-uniformity in the inactivation of *C. botulinum* spores.

A combined high pressure high temperature (HPHT) treatment has been shown to achieve inactivation of baro-resistant *C. botulinum* spores in low-acid foods. For instance, Margosch et al., (2004) showed the inactivation of *C. botulinum* spores in mashed carrots at pressurization temperatures in the range of 90-116°C together with pressures of 500-700 MPa. Koutchma et al. (2005) showed that the HPHT (or PATS) process may be validated by applying concepts used in conventional thermal processing of low-acid foods such as decimal reduction time and temperature sensitivity. Their results suggest that the traditional F-value approach can be applied to the HPHT process where only the thermal component of the process is accounted and the pressure effect on the inactivation is ignored. Based on the above approach, a high pressure process of 700 MPa, 121°C, and 3min pressure hold time gives a F value of 3 min corresponding to a 12 D reduction of *C. botulinum* spores using the conventional thermal processing approach. Therefore,

traditional F-value approach applied in thermal processing was used for quantification of inactivation of *C. botulinum* during pressure assisted thermal processing.

$$F = \int_0^t 10^{\frac{T(t)-T_{ref}}{z_T}} dt = -D \log_{10} \frac{N}{N_0} \quad (5-87)$$

The z-value of 10°C and D-value of 0.2 min for *C. botulinum* spores at T_{ref} of 121°C were used for the calculations.

Using the above approach, the log reduction (L_R) of *C. botulinum* spores can be expressed as

$$L_R = -\log_{10} \frac{N}{N_0} = \frac{\int_0^t 10^{\frac{T(t)-T_{ref}}{z_T}} dt}{D_{ref}} \quad (5-88)$$

where, N is the final concentration of *C. botulinum* spores, N_0 is the initial concentration of *C. botulinum* spores, D_{ref} is the decimal reduction time for *C. botulinum* spores at T_{ref} , z_T is the increase in temperature required to reduce the D for *C. botulinum* spores by 90% at T_{ref} , T_{ref} is reference temperature.

Using equation (5-88), a user defined function (UDF) was written in C language and attached to the numerical program to include the calculation for inactivation of *C. botulinum* spores as discussed in next chapter.

5.7 Quantification of Non-uniformity in Temperature and Inactivation of *C. botulinum*

The temperature and microbial distribution contours generated using the numerical program represent the qualitative and snapshot visualization of process uniformity/non-

uniformity in the vessel. Although the numerical program allows access to the time-dependent data for variables involved (such as temperature history for the process) for generation of the visual representations, there is a need to convert this data into some meaningful parameter to quantify non-uniformity and compare various cases. Therefore, coefficient of variation (COV) approach was used to quantify the process temperature and microbial distributions.

5.7.1 Coefficient of Variation (COV), a Statistical Approach

The COV method was used to quantify the non-uniformity in temperature and inactivation of *C. botulinum* spores as well as quantitatively compare the process uniformity for cases such as high pressure vessel without and with insulation. By definition,

$$COV = \frac{\text{Standard Deviation (S.D.)}}{\text{Mean}} \quad (5-89)$$

The method is frequently used in different research areas to compare the results with different means. Higher COV values signify more non-uniformity (Geedipalli et al., 2007). Based on the above definition (equation (5-89)), the process uniformity of a process variable ϕ can be given as

$$COV_{\phi} = \frac{1}{\bar{\phi}} \sqrt{\frac{1}{V} \sum_i [V_i (\phi_i - \bar{\phi})^2]} \quad (5-90)$$

where, V is the volume of the given domain, V_i is the volume of one mesh element in given domain, ϕ_i is the value of process variable in V_i and bar indicates the volume weighted average value.

Expanding equation (5-90), we get

$$COV_{\phi} = \frac{1}{\bar{\phi}} \sqrt{\frac{1}{V} \sum_i [V_i (\phi_i^2 + (\bar{\phi})^2 - 2\phi_i \bar{\phi})]} \quad (5-91)$$

$$= \frac{1}{\bar{\phi}} \sqrt{\frac{1}{V} \left(\sum_i V_i \phi_i^2 + (\bar{\phi})^2 \sum_i V_i - 2\bar{\phi} \sum_i V_i \phi_i \right)} \quad (5-92)$$

$$= \frac{1}{\bar{\phi}} \sqrt{\sum_i \frac{V_i \phi_i^2}{V} + (\bar{\phi})^2 \sum_i \frac{V_i}{V} - 2\bar{\phi} \sum_i \frac{V_i \phi_i}{V}} \quad (5-93)$$

By definition,

$$\bar{\phi} = \sum_i \frac{V_i \phi_i}{V} \quad (5-94)$$

$$\bar{\phi}^2 = \sum_i \frac{V_i \phi_i^2}{V} \quad (5-95)$$

$$COV_{\phi} = \frac{\sqrt{\bar{\phi}^2 - (\bar{\phi})^2}}{\bar{\phi}} \quad (5-96)$$

Therefore, COV in temperature (T) and inactivation (L_R) of *C. botulinum* spores can be given by equations (5-97), (5-98) respectively.

$$COV_T = \frac{\sqrt{\overline{T^2} - (\bar{T})^2}}{\bar{T}} \quad (5-97)$$

$$COV_{L_R} = \frac{\sqrt{\overline{L_R^2} - (\bar{L}_R)^2}}{\bar{L}_R} \quad (5-98)$$

The quantities $\overline{T^2}$, $(\bar{T})^2$, $\overline{L_R^2}$ and $(\bar{L}_R)^2$ are easy to calculate from the numerical simulation program.

Although COV method is useful for comparison of data sets with different means, it is important to be aware of the limitations of this method. One of the problems in interpreting COV arises when mean value of the variable is very small. In that case, COV value becomes very large, falsely implying large non-uniformity from practical point of view.

The subsequent chapter talks about the application of the theoretical knowledge gained from this chapter to set up the numerical simulation program.

6. NUMERICAL SIMULATION

Numerical simulation typically involves building a simplified geometry of the physical domain and then solving the set of governing equations that describe the physics of the problem. The main reason for using numerical simulation model for high pressure process was to understand the temperature and velocity distributions within the vessel which are very difficult to determine experimentally at every location in the vessel.

Numerical simulation of heat transfer and fluid flow were carried out for a vertical and a horizontal high pressure vessel (water in the pressure cavity and the vessel wall) using a finite volume based commercial computational fluid dynamics (CFD) software ANSYS®-Fluent (Version 12.0.16, ANSYS, Inc., Canonsburg, PA). The governing equations of conservation of mass, momentum, and energy (Equations 5-3, 5-6, 5-11 and 5-12) were numerically solved in the computational domains to predict thermal and flow fields within the pressurizing medium (water) and the energy (conduction) equation was solved for the vessel wall.

Numerical simulation of heat transfer and fluid flow during a high pressure process involved the following steps:

6.1 Generation of Geometry and Meshing

Generating a simplified geometry from the actual geometry and a good quality mesh are important parts of CFD problems. For this research, the computational geometries and meshes for numerical simulation of vertical and horizontal high pressure vessels were

generated using a commercial grid generator and geometry modeler software Gambit (Version 2.3.30, FLUENT Inc., Lebanon, NH). Gambit allows different approaches for generating simplified geometry of the physical problem followed by grid generation.

For creating 2D geometries a bottom up approach was followed, i.e., generate low dimensional entities and build on top of them (e.g., 1. create vertexes, 2. link vertexes to make edges, 3. create faces from edges, 4. mesh edges, and 5. mesh faces) whereas a top down approach was used for 3D geometries, wherein upper dimensional entities (such as volumes) were built first and then Boolean operations (unite volumes, split volumes, subtract volumes, and intersect volumes) were used to define other entities.

The 2D and 3D computational domains generated were discretized into small control volumes to allow the numerical simulation program ANSYS®-Fluent to solve the governing equations in each of those volumes and then provide an integrated solution. Various grid generation schemes such as quad/hex, tri/tet (mapped or paved) were tried and the final scheme selection was made on the basis of mesh characteristics such as area (2D), volume (3D), aspect ratio, equiangle skew etc. In general, a mesh is considered problematic if it has very high skewness (>0.95), high aspect ratio (>100) and negative areas/volumes.

6.1.1 Vertical High Pressure Vessel

The vertical high pressure vessel, due to its axial symmetry was modeled as a 2D axisymmetric cylinder with water inlet from top of the vessel. The axisymmetric condition assumes that no flow/thermal gradients exist in the azimuthal direction. The

numerical simulations were carried out in a radial slice of the cylinder and the details of the radial geometry are shown in **Figure 6-1(b)**. The simplification of full 3D cylindrical geometry to a 2D radial slice resulted in much less computer memory being used up and less CPU time to solve the conservation equations.

The computational domain was discretized using a structured uniform quadrilateral face mesh as shown in **Figure 6-2**. As a starting point, a coarse (2568 nodes) mesh was created in Gambit and later while carrying out the numerical simulation using ANSYS[®] -

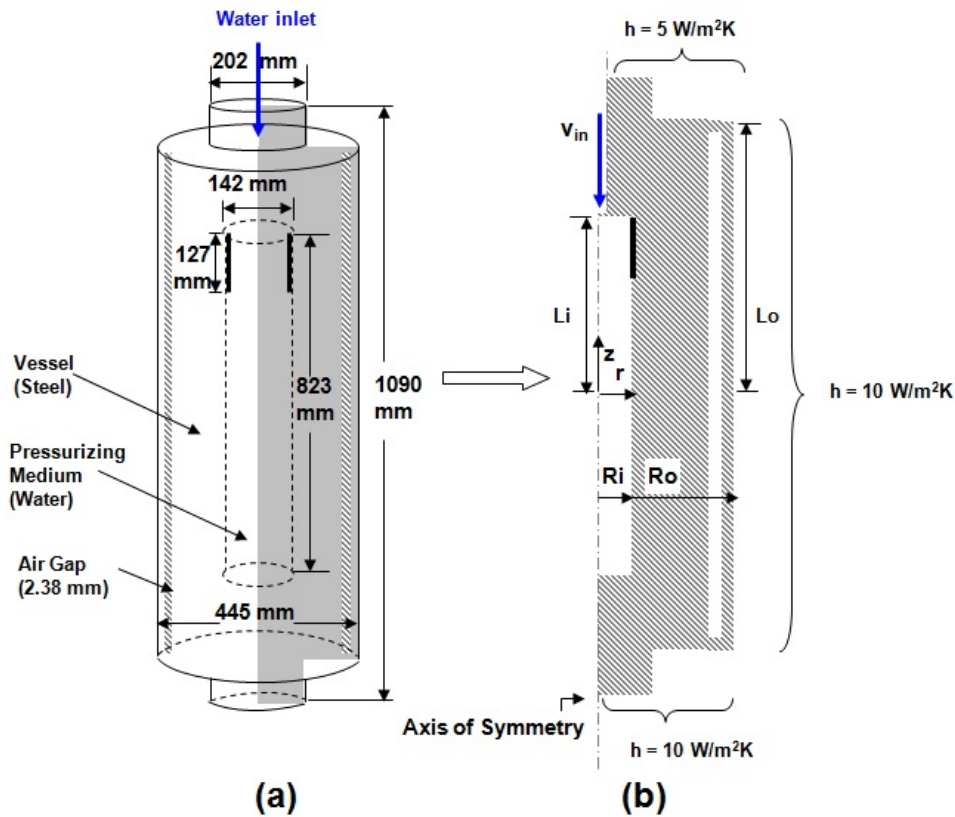


Figure 6-1: (a) Dimensions of HHPP vessel. Shaded area represents the radial section for numerical simulation, (b) computational domain used for simulation, $R_i = 71 \text{ mm}$, $R_o = 223 \text{ mm}$.

Fluent, the computational mesh was adapted (more nodes and cells added) repeatedly based on the developing velocity gradients in the water column until a grid independent solution was obtained. The final grid had 40,216 nodes.

To evaluate the effect of an insulating sleeve and oil pouches in the vessel, the existing geometry was modified. For vessel with insulation, initially the numerical simulation with insulation of thickness 3.17 mm, 6.75 mm and 12.7 mm were carried out, however, most simulations were carried out with 12.7 mm thick insulation because it gave maximum insulation effect without significantly altering the process volume. The geometry with 12.7 mm insulation had 4300 nodes to start with and 47,115 nodes after adaptation. Properties of Teflon[®] (which is DuPont[™] brand name for the polymer PTFE) were used for the insulating sleeve. The insulation was assumed to be rigid, i.e., conduction heat transfer equation was solved. The adiabatic compression heating of PTFE which is $\sim 4^{\circ}\text{C}/100\text{ MPa}$ at 90°C (Knoerzer et al., 2010) was not included in the numerical model for this study as the fraction of insulating sleeve to volume of vessel was not significant. For oil pouches, it was assumed that seven cylindrical pouches (90 mm in length, 70 mm in radius) containing oil were placed in the vertical vessel. The 2D axisymmetric geometry (**Figure 6-2(b)**) was modified to include seven 2D axisymmetric pouches in the vessel pressure cavity. The distance between the pouches was 24 mm. The grid with pouches had 8540 nodes at start and 102,000 nodes after adaptation. Governing equations for natural convection flow were solved in the pouches. The adiabatic compression heating value and heat generation term for olive oil were calculated to be

13K/100 MPa and $750,000 \text{ W/m}^3$, respectively, using its thermophysical properties defined in section 6.4.

For the purpose of validation of the numerical program, three thermocouple points were marked in the computational domain located at exactly the same position as in the experimental setup, as shown in **Figure 6-2**. During the numerical simulation temperature vs. time data at these points were recorded.

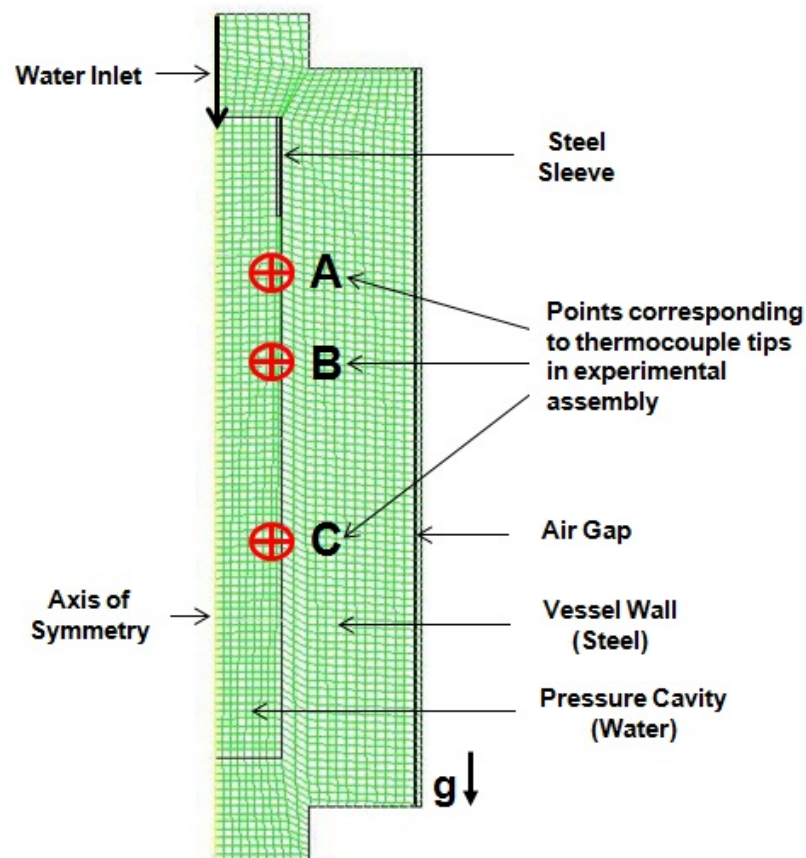


Figure 6-2: Computational mesh used for vertical vessel numerical simulation with points A, B, C shown by \oplus corresponding to thermocouple tips in experimental assembly.

6.1.2 Horizontal High Pressure Vessel

The horizontal high pressure vessel was modeled as a 3D cylinder with water inlet to the vessel from both end closures (currently available horizontal vessels in market have water inlet from both ends). The horizontal vessel geometry could not be simplified to axisymmetric geometry as horizontal system loses its axisymmetry because of the water inlet from both the sides. In the absence of water inlets the horizontal high pressure vessel can be modeled as a 2D slice, i.e., no azimuthal component, which was not the case here. It was possible to simplify the full 3D geometry to 3D symmetric by splitting the cylinder geometry for purposes of numerical simulation in half and then defining the plane of symmetry.

The numerical simulation was done for two different size vessels. For 10 L vessel, simulations were carried out for the 10 L vessel with dimensions same as the vertical vessel mentioned above considering that it was operating in horizontal position and water inlet was from both end closures. For 350 L commercial vessel, the major dimensions were obtained from a leading HHPP equipment manufacturer. The length and diameter of pressure cavity were 2998 mm, 390 mm, respectively, and outer cylinder were 3608 mm, 1000 mm, respectively. The diameter of opening for water inlet in both end closures was 40 mm.

The computational domain was discretized using a Tet/Hybrid Tgrid mesh as shown in **Figure 6-3**. Initially, the mesh was coarse (80,000 nodes) and later while carrying out the numerical solution using ANSYS®-Fluent the computational mesh was adapted

repeatedly based on the developing velocity gradients in the water column during the process until a grid independent solution was obtained. The final grid had 257,130 nodes.

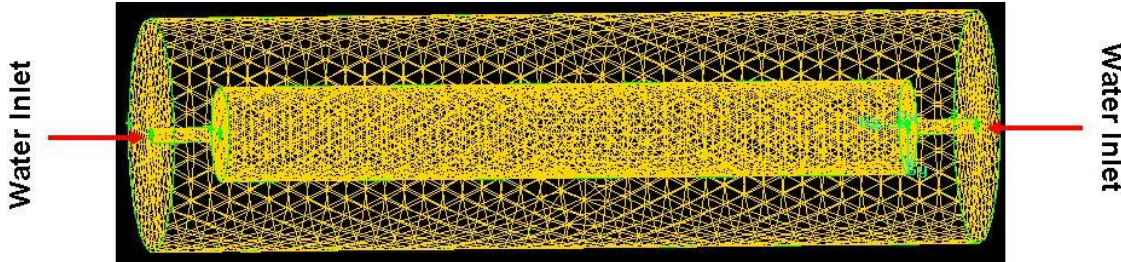


Figure 6-3: Computational mesh for horizontal vessel numerical simulation.

The next section describes steps in setting up and running the numerical simulation program.

6.2 Importing Geometry/Mesh and General Settings

FLUENT Launcher was used to start the 2D (for vertical vessel simulation) or 3D (for horizontal vessel simulation) version of ANSYS[®]-Fluent. The computational mesh/grid geometry generated in Gambit was read into the program and was displayed in the embedded graphics window as shown in **Figure 6-4**. It also shows the general problem setup window that appears after importing the geometry into ANSYS[®]-Fluent program. The mesh/grid was checked for domain extents, volume statistics and face area statistics. Since the grid geometry was created in centimeters, grid scaling was used to convert it to SI units (meters) as required by the program. A pressure based solver and absolute velocity formulation was used (see ANSYS[®]-Fluent manual for details).

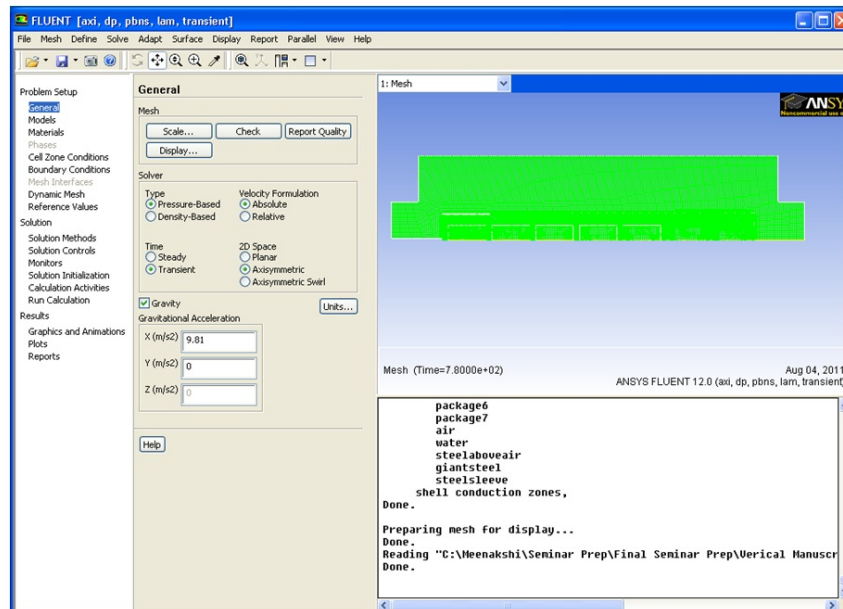


Figure 6-4: Problem setup window as appearing in the ANSYS®-Fluent program.

6.3 Defining Model

Since we were dealing with a thermal transport problem, energy equation option was enabled in the Energy dialogue box (**Figure 6-5**) to activate the heat transfer calculations.

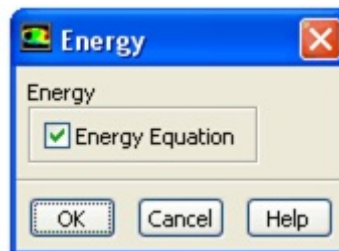


Figure 6-5: Energy equation enabled in the Energy dialogue box.

Another question during model selection was whether the flow within the vessel was laminar or turbulent. For the vertical vessel, the inner cylinder surface was approximated as a vertical flat plate for the purpose of selecting the laminar or turbulent flow model; for details refer to section 5.1. Based on the theoretical calculations it was found that the

flow in the vertical and horizontal vessel under given conditions was turbulent. Therefore, relevant turbulence model and options were activated. So far no single turbulence model is universally accepted as appropriate for all classes of problems. The choice of turbulence model depends on certain considerations such as the physics of the flow, the established practice for a specific class of problem, the level of accuracy required, the available computational resources, and the amount of time available for the simulation. For the purpose of this research, the turbulence was included using the realizable k- ϵ model - where k is the turbulent kinetic energy and ϵ is the dissipation rate (Jaluria & Torrance, 1986). For near wall solution, a standard wall function condition was enabled (see **Figure 6-6**).

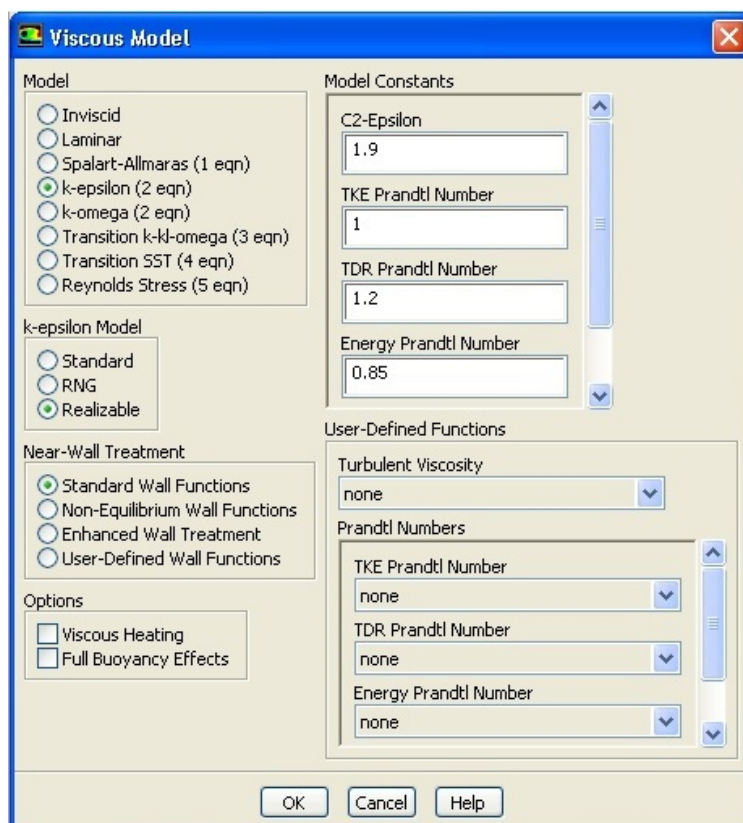


Figure 6-6: Viscous model window showing k-epsilon model and its settings.

6.4 Defining Materials

The materials panel allows the user to define the materials and their properties using either ANSYS[®]-Fluent Database or User-Defined Database/Functions. The materials used for this research were water, s.steel, Teflon[™], oil, polyethylene and air. The pressure dependent property data for some of these materials is not readily available in literature, therefore, the properties of s.steel ($\rho = 8020 \text{ kg/m}^3$, $C_p = 502.48 \text{ J/kg-K}$, $k = 16.27 \text{ W/m-K}$), air ($\rho = 1.092 \text{ kg/m}^3$, $C_p = 1014 \text{ J/kg-K}$, $k = 0.0265 \text{ W/m-K}$), oil ($\rho = 920 \text{ kg/m}^3$, $C_p = 1793 \text{ J/kg-K}$, $k = 0.22 \text{ W/m-K}$, $\mu = 0.08 \text{ Pa.s}$, $\beta = 0.00072 \text{ 1/K}$), polyethylene ($\rho = 940 \text{ kg/m}^3$, $C_p = 1900 \text{ J/kg-K}$, $k = 0.42 \text{ W/m-K}$) and Teflon[™] ($\rho = 2190 \text{ kg/m}^3$, $C_p = 995 \text{ J/kg-K}$, $k = 0.27 \text{ W/m-K}$) were taken from literature at the initial temperature and assumed to be constant through the process. These properties were given as an input in the materials panel (as shown for steel in **Figure 6-7**).

The properties of water under pressure are well documented and the data are available from International Association for Properties of Water and Steam (IAPWS). Thermophysical properties of water such as density, heat capacity, thermal conductivity, viscosity, and coefficient of thermal expansion are functions of both temperature and pressure. In this research, initially only temperature dependence of these properties was included in the numerical model. Later on, change in properties with both pressure and temperature were considered. Finally the three models (constant properties, temperature dependent properties, and pressure-temperature dependent properties) were compared. The sections below discuss the temperature dependent and combined pressure-

temperature dependent equations used and how they were defined in the ANSYS®-Fluent solver.

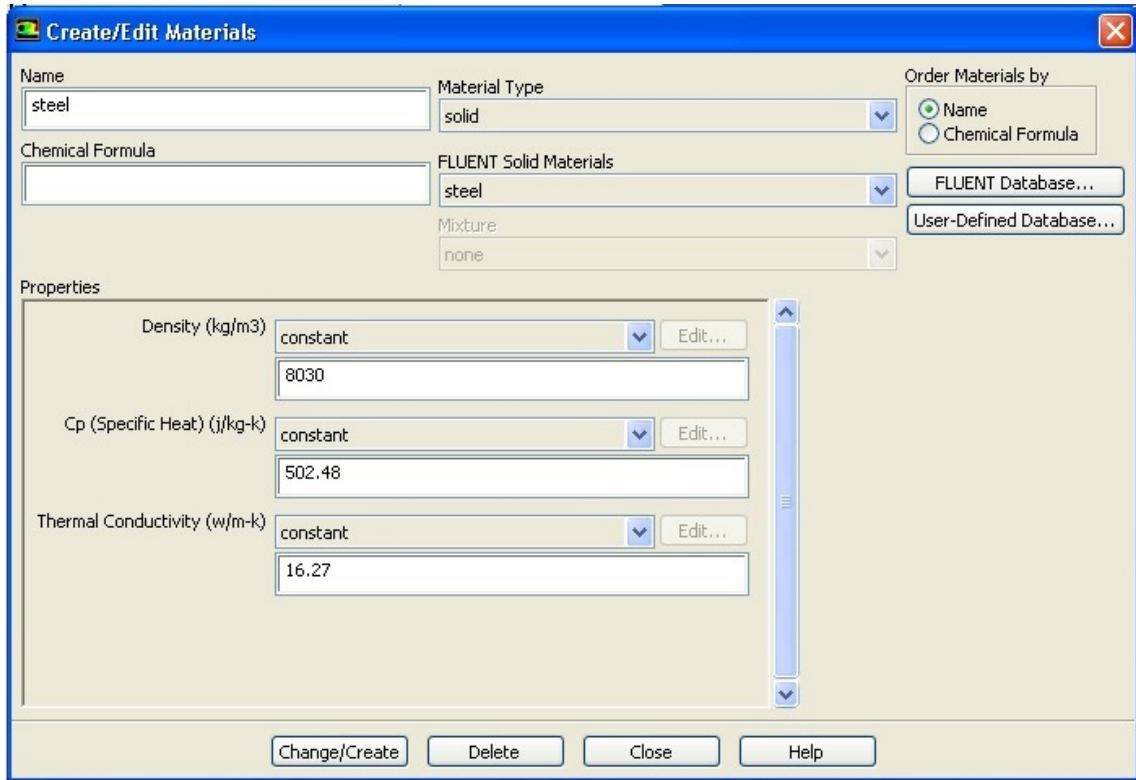


Figure 6-7: Create/Edit Material window showing steel properties.

6.4.1 Temperature Dependence of Material Thermophysical Properties

This part of the study was carried out based on assumption that no significant changes in density, specific heat, thermal conductivity, viscosity and thermal expansion coefficient of water occurred while under pressure. The equations for change in these properties with temperature ($^{\circ}\text{C}$) were obtained from Singh and Heldman (2003) and given as follows,

$$\rho(\text{kg}/\text{m}^3) = 997.18 + (3.14 \times 10^{-3})T - (3.75 \times 10^{-3})T^2 \quad (6-1)$$

$$C_p(\text{kJ}/[\text{kg}^{\circ}\text{C}]) = 4.1762 - (9.08 \times 10^{-5})T + (5.47 \times 10^{-6})T^2 \quad (6-2)$$

$$k(W/[m^{\circ}C]) = 0.571 + (1.76 \times 10^{-3})T - (6.7 \times 10^{-6})T^2 \quad (6-3)$$

The polynomial profile panel for defining material properties in ANSYS®-Fluent (as shown in **Figure 6-8**) was used to define the temperature dependence of density, heat capacity, and thermal conductivity of water.

Natural convection flow in water and oil was modeled by employing the Boussinesq approximation. Therefore, water density was treated as a constant value in all solved equations, except for buoyancy term in momentum equation (refer to section 5.2.2 for details).

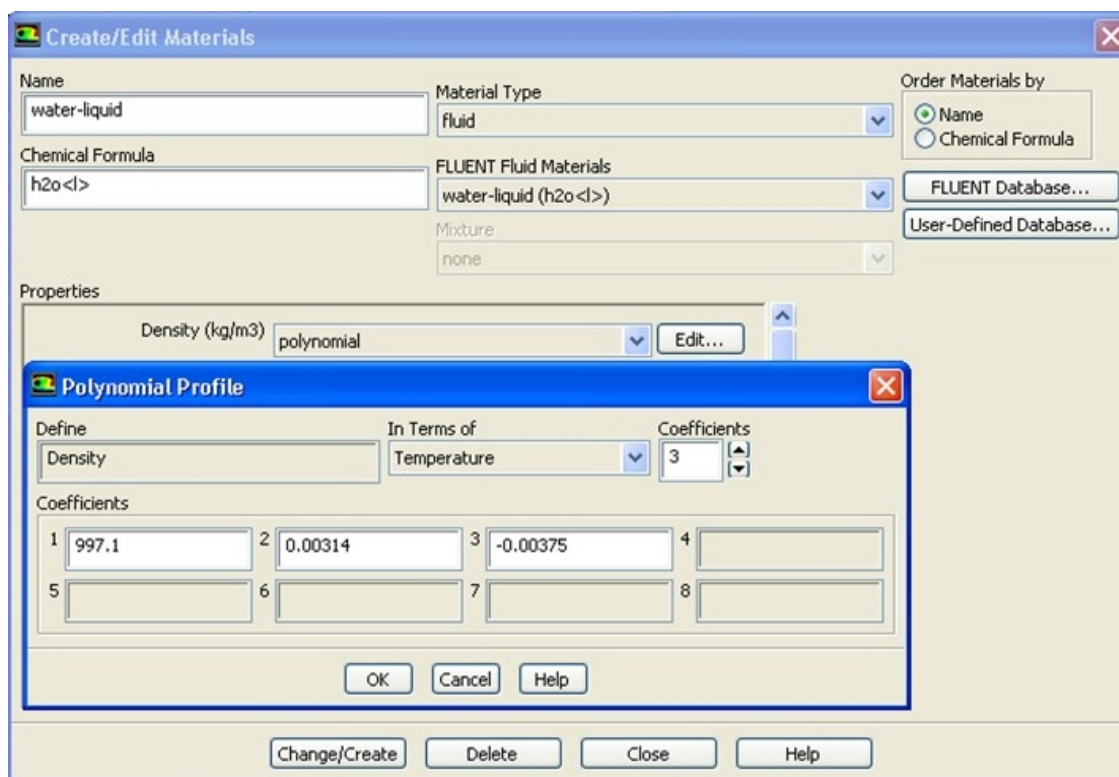


Figure 6-8: Create/Edit Material window: to define polynomial profile for change in water properties with temperature.

6.4.2 Pressure-Temperature Dependence of Material Thermophysical Properties

The fluid flow and heat transfer equations used to predict the temperature distribution during the high pressure process were adapted to include the combined pressure-temperature dependence of the thermophysical properties of water.

NIST (National Institute of Standards and Technology) Standard Reference Database 10 (NIST/ASME Steam Properties Database, Version 2.22) was used to obtain the data for thermophysical properties of water in the pressure and temperature range of 0.1-600MPa and 0°C -120°C (273-393 K), respectively. Multiple regression analysis was carried out in Excel™ and MATLAB to obtain the equations for combined pressure (in MPa) and temperature (in K) dependent density (kg/m³), thermal conductivity (W/m-K), and viscosity (kg/m-s) of water, as given below.

$$\rho(P, T) = 1161.37 - 0.28(P) - 0.5(T)(R^2 = 0.989) \quad (6-4)$$

$$k(P, T) = 0.19 + 3 * 10^{-4}(P) + 1.4 * 10^{-3}(T) (R^2 = 0.980) \quad (6-5)$$

$$\mu(P, T) = 0.0037 + 4.23 * 10^{-7}(P) - 9.7 * 10^{-6}(T)(R^2 = 0.939) \quad (6-6)$$

The pressure in above equations was replaced by a linear time dependent pressure profile, $P = 3.6t - 21.3$ which was obtained from the experimental data. This was done because we introduce the pressure increase in the program as heat source (pressure work) term. The numerical simulation program does not solve for pressure. The final equations formed in terms of temperature (in K) and time (in s) were:

$$\rho(T, t) = 1155.41 - 0.5(T) + (t) \quad (6-7)$$

$$k(T, t) = 0.18 + 1.4 * 10^{-3}(T) + 1.1 * 10^{-3}(t) \quad (6-8)$$

$$\mu(T, t) = 3.7 * 10^{-3} - 9.7 * 10^{-6}(T) + 1.5 * 10^{-6}(t) \quad (6-9)$$

The above equations were incorporated into the numerical simulation program using user-defined functions (UDFs) module of the ANSYS[®]-Fluent. UDFs are C-codes that can be used to customize the ANSYS[®]-Fluent solver, i.e., to provide customized material properties, source terms, boundary conditions etc., to the solver. The knowledge of various ‘Macros’ defined by the software were used to access the geometry variables (such as cell, node, face, area, volume, etc.) and the cell variables (such as pressure, density, temperature, etc.).

6.4.1.1 Create a C Source File

After determining the pressure-temperature-time dependent equations for the properties, WordPad text editor was used to create a file containing C code that implements the function. The source code file was saved with a .c extension (e.g., cell_density.c) in the working folder. The source codes can be referred to in Appendix I.

6.4.1.2 Compile the Source File

In the compiled UDFs dialogue box, click add Source Files (Figure 6-9). This will open the Select File dialog box. Select the UDF source files to be used (e.g. viscosity.c, density.c). Click build. This process will compile the code and will build a shared library in the working folder. As the compile/build process begins, a warning dialog box will appear, reminding that the UDF source file must be in the folder that contains case and

data files (i.e., the working folder). Click OK to close the dialog box and resume the compile/build process. The results of the build will be displayed in the console. The compilation history is stored in the log file that is saved in the working folder. Click Load to load the shared library into ANSYS® Fluent. The console will report that the library has been opened and the function (e.g., viscosity.c) is loaded.

6.4.1.3 Hook the UDF to ANSYS®-Fluent Solver

Now that the UDF was compiled, it was ready to be hooked to the material properties dialogue box. In the create/edit materials dialogue box, a new material was created, i.e., water-liquid. On the properties tab, user-defined was selected from the drop-down list next to a particular property (**Figure 6-10**) and then choose the name of the UDF that corresponds to the property. The user defined property will be used in the subsequent solution calculation.

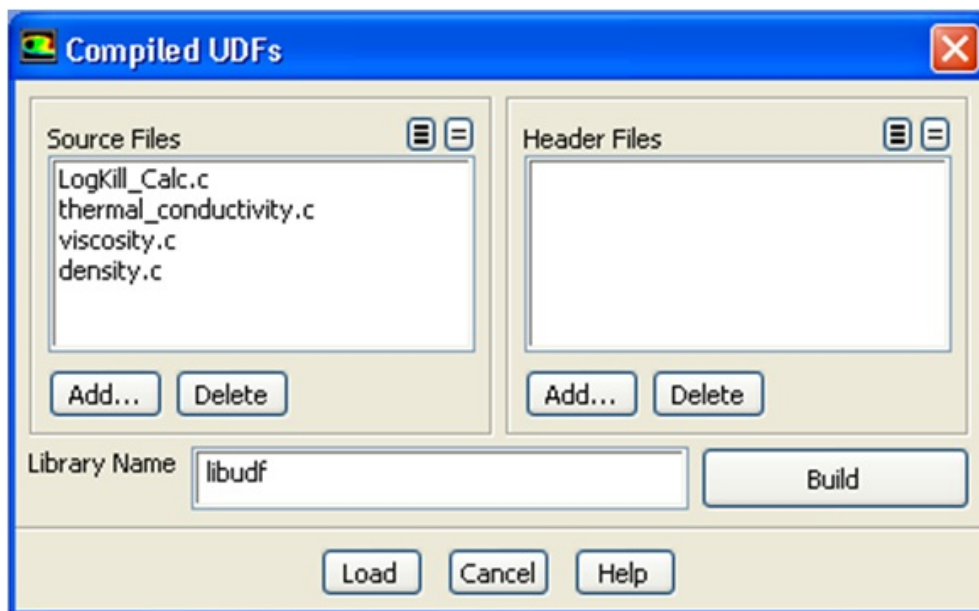


Figure 6-9: Compiled UDF dialogue box showing the attached UDFs.

For the $\log(\text{No}/N)$ value calculation UDF, the computed values were stored in the memory so that they can be used by the UDF during iterations and later for postprocessing. In order to access the memory location in a cell for storing F-value the macro `C_UDMI` was used in UDF source code. The Number of User-Defined Memory Locations (User Memory 0, User Memory 1) were specified in the User-Defined Memory dialogue box. The F-value calculation source code also consists of a `DEFINE_EXECUTE_AT_END` Macro. This macro is hooked to the program through the user define function hooks dialogue box. Click the edit button next to Execute At End to open the Execute At End Functions dialog box. Select the functions to hook to the model from the Available Execute at End Functions list. Click add and then OK to close the dialog box.

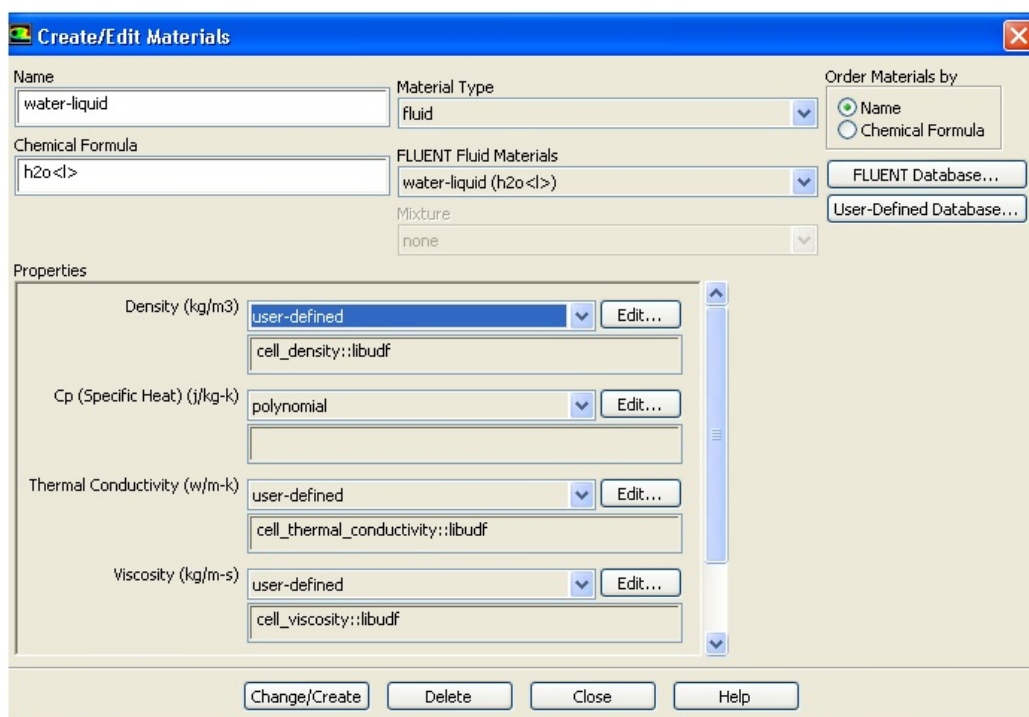


Figure 6-10: Create/Edit Materials window showing how to hook UDFs to the material properties.

6.5 Define Cell Zone Conditions

Set the cell zone conditions for the continuum zones. Also, select the source term option for the fluid zone for the period of pressurization and deselect during hold period. The amount of heat generated due to pressure work defined as source term in the program can be calculated and is discussed in Chapter 5 (Section 5.3).

6.6 Define Boundary Conditions

Subsequently, boundary conditions for the domain were defined. The axis boundary condition was defined on the centerline of the axisymmetric geometry. The gravity was defined in the axial direction for vertical vessel and in radially downward direction for horizontal vessel. A coupled thermal boundary condition was defined between the water column and the steel vessel, i.e., both the continuum domains (solid steel and water as fluid) were coupled by the common edge. Also, for insulation model coupled boundary condition was defined between water and Teflon[®], and Teflon[®] and solid steel interfaces. The air gap in the high pressure vessel was very thin, therefore, the heat transfer was assumed to be taking place via conduction mechanism, and hence, conduction heat transfer equation were solved in the air gap. On the outside surface of the vessel, thermal convection boundary condition for walls was used with heat transfer coefficient of 10 W/m²K on the vertical side and bottom walls, and 5 W/m²K on the top wall. The approximate values of h on the outer surface were calculated using the relations provided by Churchill and Chu as given in the textbook by Holman (1981) (Khurana, 2008). It was found that the results were not sensitive to small variation in value of h. A water inlet

boundary condition was defined for the period of pressurization to compensate for the reduction in volume, the value of v_{in} equal to 0.28 m/s was defined for vertical vessel as calculated in section 5.3.

6.7 Define Solution Methods

In the spatial discretization box, Least Squares Cell Based was chosen from the drop down list for Gradient. Second order upwind solution scheme was selected for density, momentum, and energy. For the transient formulation, second order implicit solver as shown in **Figure 6-11** was used to solve for thermal and velocity fields.

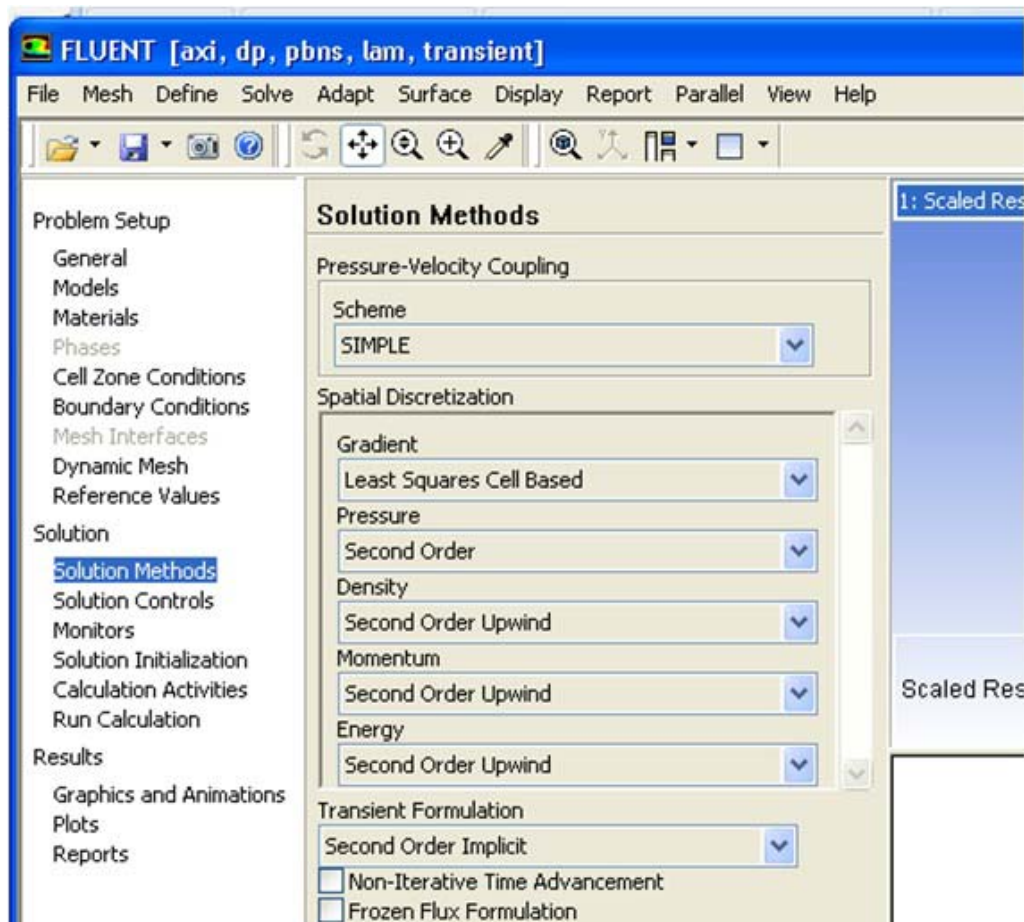


Figure 6-11: Solver window as appears in ANSYS®-Fluent.

To indicate the convergence of the solution, convergence criteria were defined for residuals such as continuity, x-velocity, y-velocity, energy, k and ϵ . The absolute convergence criteria (if the residual value is less than the user defined value then the solution is considered to be converged) of 10^{-6} was defined for all the residuals as shown is **Figure 6-12**.

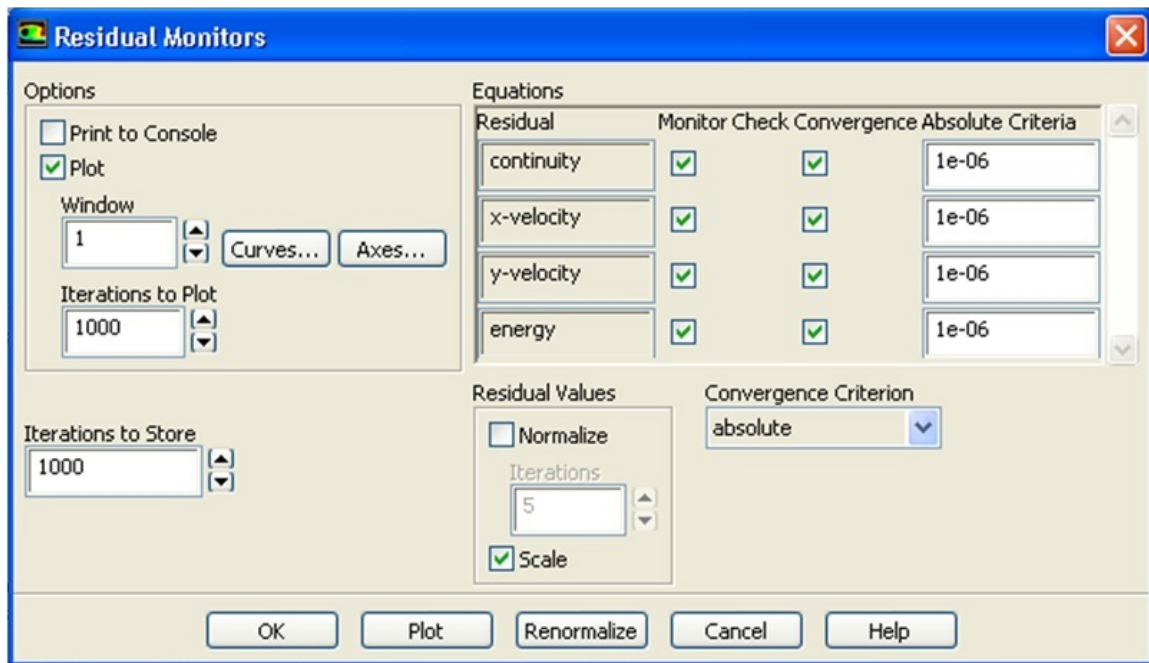


Figure 6-12: Residual monitors window as appearing in the ANSYS®-Fluent to define convergence criteria.

6.8 Run Calculation

The model was initialized at the given initial temperature of water and vessel steel mass and iterated. A time step size of 0.1 s was used as shown in **Figure 6-13**. Number of time steps were defined based on needs of the individual case.

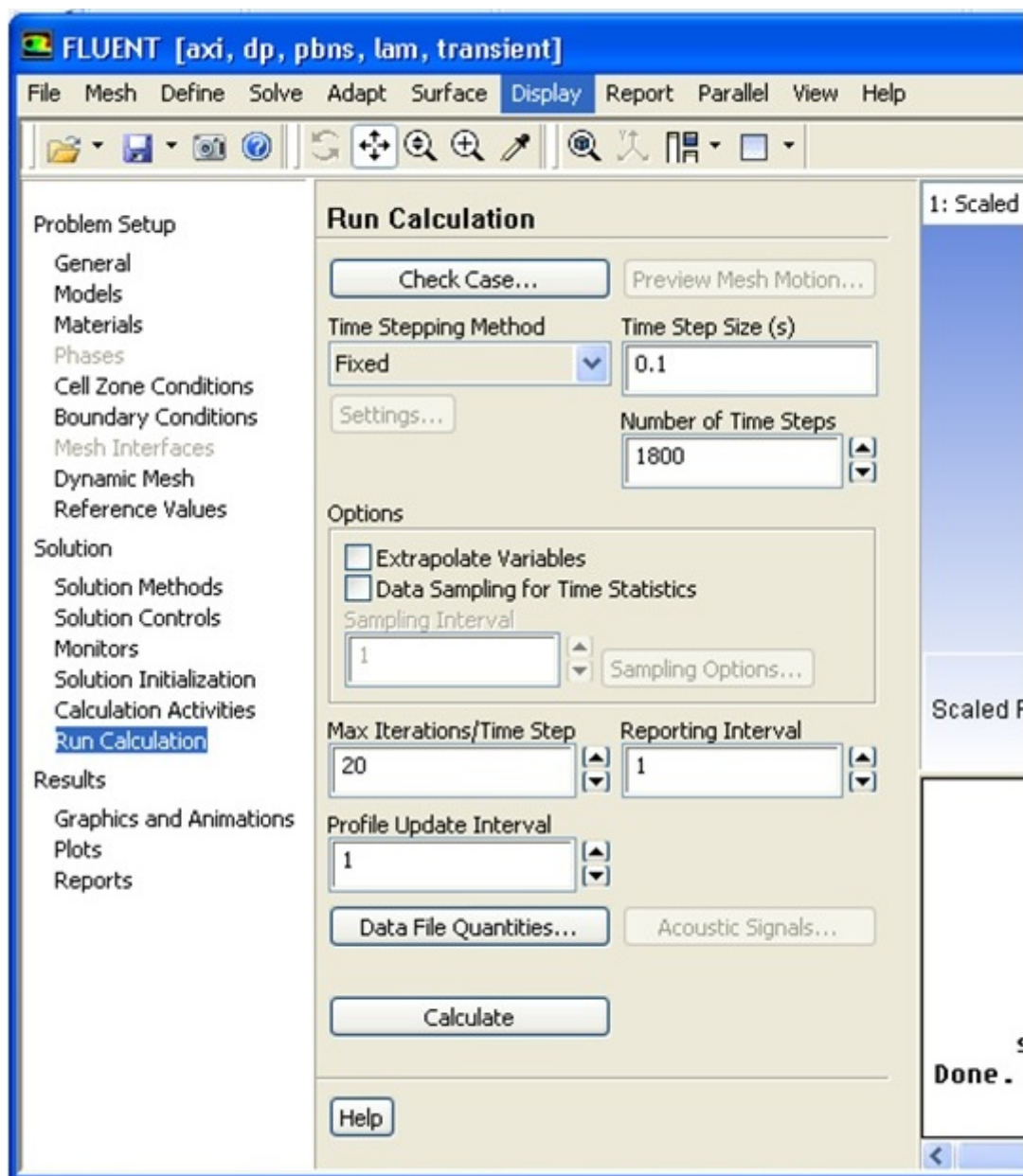


Figure 6-13: Iteration window as appearing in the ANSYS®-Fluent program.

Computational time needed to run typical vertical 2-d axisymmetric geometry simulation was approximately 36 hrs on a desktop computer with Intel® Pentium® 4 processor and 2 GB RAM. We were not able to run horizontal 3D geometry simulations on the above system. Computational time to run 3D simulation for the horizontal vessel was

approximately 18 hours on a DELL Inc. workstation with Intel[®] Xeon[®] processor and 16 GB RAM. On the same system the time needed to run vertical 2D axisymmetric geometry simulation was approximately 8-10 hrs.

Once a converged solution was obtained, the contours for temperature and inactivation of *C. botulinum* were generated using the graphics tab under results. Also, time-temperature-log reduction of *C. botulinum* history was extracted from the program to calculate the coefficient of variation.

Next chapter will discuss the results obtained from this research.

7. RESULTS AND DISCUSSIONS

The results obtained from this research are presented in four sections. First, the parameters governing the high pressure process, second, the parameters that govern the lag in temperature measurement by thermocouple, third, the numerical simulation for temperature and inactivation of *C. botulinum* distributions under different conditions and subsequently, the results obtained for ALP experiments will be discussed.

7.1 Parameters Governing High Pressure Process

The dimensional analysis of the high pressure process was carried out to obtain the generalized non-dimensional parameters that govern the process. As a first step in the dimensional analysis the governing conservation equations and the boundary conditions were made dimensionless. The differential conservation equations that describe the vertical high pressure vessel, assuming axisymmetry and constant properties, and the initial and boundary conditions that describe the flow and heat transfer situation are:

Continuity Equation (Conservation of Mass)

$$\frac{1}{r} \frac{\partial}{\partial r} (\rho r v_r) + \frac{\partial}{\partial z} (\rho v_z) = 0 \quad (7-1)$$

Conservation of Momentum Equation (r-direction)

$$\rho \left(\frac{\partial v_r}{\partial t} + v_r \frac{\partial v_r}{\partial r} + v_z \frac{\partial v_r}{\partial z} \right) = - \frac{\partial P}{\partial r} + \mu \left[\frac{\partial}{\partial r} \left(\frac{1}{r} \left(\frac{\partial}{\partial r} (r v_r) \right) \right) + \frac{\partial^2 v_r}{\partial z^2} \right] \quad (7-2)$$

Conservation of Momentum Equation (z-direction)

$$\rho \left(\frac{\partial v_z}{\partial t} + v_r \frac{\partial v_z}{\partial r} + v_z \frac{\partial v_z}{\partial z} \right) = -\frac{\partial P}{\partial z} + \mu \left[\frac{1}{r} \left(\frac{\partial}{\partial r} \left(r \frac{\partial v_z}{\partial r} \right) \right) + \frac{\partial^2 v_z}{\partial z^2} \right] + \rho g_z \beta (T - T_i) \quad (7-3)$$

Conservation of Energy Equation

$$\frac{\partial T}{\partial t} + v_r \frac{\partial T}{\partial r} + v_z \frac{\partial T}{\partial z} = \frac{k}{\rho C_p} \left[\frac{1}{r} \frac{\partial}{\partial r} \left(r \frac{\partial T}{\partial r} \right) + \frac{\partial^2 T}{\partial z^2} \right] + \frac{Q}{\rho C_p} \quad (7-4)$$

Initial Conditions:

$$\text{At } t = 0: T = T_i ; v_r = v_z = 0$$

Boundary Conditions:

$$\text{At } r = 0 : \frac{\partial T}{\partial r} = 0 ; \frac{\partial v_z}{\partial r} = 0 \quad (\text{axisymmetry})$$

$$\text{At } r = R_i : v_r = v_z = 0 \text{ (no slip); } \left(-k_{\text{fluid}} \frac{\partial T}{\partial r} \right)_{\text{fluid}} = \left(-k_{\text{solid}} \frac{\partial T}{\partial r} \right)_{\text{solid}} \text{ (heat flux continuity);}$$

$$T_{\text{fluid}} = T_{\text{solid}} \text{ (temperature continuity)}$$

$$\text{At } r = R_o : \left(-k_{\text{solid}} \frac{\partial T}{\partial r} \right)_{\text{solid}} = h(T - T_i)$$

$$\text{At } z = L_i : v_r = v_z = 0 \text{ (no slip); } \left(-k_{\text{fluid}} \frac{\partial T}{\partial z} \right)_{\text{fluid}} = \left(-k_{\text{solid}} \frac{\partial T}{\partial z} \right)_{\text{solid}} \text{ (heat flux continuity);}$$

$$T_{\text{fluid}} = T_{\text{solid}} \text{ (temperature continuity)}$$

The above boundary condition, i.e., at $z = L_i$ is true, except for the inflow part which is defined in the boundary condition below.

Velocity Inflow (At $z = L_i$): $v_z = V_{\text{in}}$ for $0 < r < 3.3 \text{ mm}$, $0 < t < t_{\text{cum}}$; $t_{\text{cum}} = 180 \text{ s}$;

$$v_z = V_{\text{in}} = 0 \text{ for } t \geq t_{\text{cum}}$$

To make the governing equations and the boundary conditions dimensionless we divide all the variables that have dimension velocity by characteristic velocity (v_o), the radial

distance variable by the characteristic radius (R_i), the axial distance variable by the characteristic length (L_i), and time by characteristic time (t_0). The pressure can be made dimensionless using the term ρv_0^2 , based on constant density and characteristic velocity.

Similarly, temperature can be made dimensionless based on constant thermal conductivity, constant heat source term, and characteristic length as shown below. The dimensionless quantities were indicated by asterisk,

$$r^* = \frac{r}{R_i} ; \quad z^* = \frac{z}{L_i} ; \quad t^* = \frac{t}{t_0} = \frac{\alpha t}{L_i^2} ; \quad v_r^* = \frac{v_r}{v_0} = \frac{v_r}{\sqrt{g\beta\left(\frac{L_i^2 Q}{k}\right)L_i}} ; \quad v_z^* = \frac{v_z}{v_0} = \frac{v_z}{\sqrt{g\beta\left(\frac{L_i^2 Q}{k}\right)L_i}} ;$$

$$P^* = \frac{P}{\rho v_0^2} = \frac{P}{\rho g\beta\left(\frac{L_i^2 Q}{k}\right)L_i} ; \quad T^* = \frac{T - T_i}{\left(\frac{L_i^2 Q}{k}\right)}$$

Introducing dimensionless quantities in the continuity equation results in,

$$\frac{1}{r^*} \frac{\partial}{\partial r^*} (r^* v_r^*) + \left(\frac{R_i}{L_i}\right) \frac{\partial v_z^*}{\partial z^*} = 0 \quad (7-5)$$

$$\text{Let } \frac{R_i}{L_i} = \gamma \quad (7-6)$$

The dimensionless continuity equation becomes

$$\frac{1}{r^*} \frac{\partial}{\partial r^*} (r^* v_r^*) + (\gamma) \frac{\partial v_z^*}{\partial z^*} = 0 \quad (7-7)$$

Introducing dimensionless quantities into the r-direction momentum equation results in,

$$\frac{1}{Gr^{1/2} Pr} \left(\frac{R_i}{L_i}\right) \frac{\partial v_r^*}{\partial t^*} + v_r^* \frac{\partial v_r^*}{\partial r^*} + \left(\frac{R_i}{L_i}\right) v_z^* \frac{\partial v_r^*}{\partial z^*} = -\frac{\partial P^*}{\partial r^*} + \frac{1}{Gr^{1/2}} \left(\frac{L_i}{R_i}\right) \left[\frac{\partial}{\partial r^*} \left(\frac{1}{r^*} \left(\frac{\partial}{\partial r^*} (r^* v_r^*) \right) \right) \right] + \frac{1}{Gr^{1/2}} \left(\frac{R_i}{L_i}\right) \frac{\partial^2 v_r^*}{\partial z^{*2}} \quad (7-8)$$

Using equation (7-6), the dimensionless momentum equation in r-direction becomes

$$\frac{\gamma}{Gr^{1/2}Pr} \frac{\partial v_r^*}{\partial t^*} + v_r^* \frac{\partial v_r^*}{\partial r^*} + \gamma v_z^* \frac{\partial v_r^*}{\partial z^*} = -\frac{\partial P^*}{\partial r^*} + \frac{1}{Gr^{1/2}\gamma} \left[\frac{\partial}{\partial r^*} \left(\frac{1}{r^*} \left(\frac{\partial}{\partial r^*} (r^* v_r^*) \right) \right) \right] + \frac{\gamma}{Gr^{1/2}} \frac{\partial^2 v_r^*}{\partial z^{*2}} \quad (7-9)$$

Introducing dimensionless quantities into the z-direction momentum equation results in,

$$\frac{1}{Gr^{1/2}Pr} \frac{\partial v_z^*}{\partial t^*} + \left(\frac{L_i}{R_i} \right) v_r^* \frac{\partial v_z^*}{\partial r^*} + v_z^* \frac{\partial v_z^*}{\partial z^*} = -\frac{\partial P^*}{\partial z^*} + \frac{1}{Gr^{1/2}} \left(\frac{L_i}{R_i} \right)^2 \left[\frac{1}{r^*} \frac{\partial}{\partial r^*} \left(r^* \frac{\partial v_z^*}{\partial r^*} \right) \right] + \frac{1}{Gr^{1/2}} \frac{\partial^2 v_z^*}{\partial z^{*2}} + T^* \quad (7-10)$$

Using equation (7-6), the dimensionless momentum equation in z-direction becomes

$$\frac{1}{Gr^{1/2}Pr} \frac{\partial v_z^*}{\partial t^*} + \frac{1}{\gamma} v_r^* \frac{\partial v_z^*}{\partial r^*} + v_z^* \frac{\partial v_z^*}{\partial z^*} = -\frac{\partial P^*}{\partial z^*} + \frac{1}{Gr^{1/2}} \left(\frac{1}{\gamma} \right)^2 \left[\frac{1}{r^*} \frac{\partial}{\partial r^*} \left(r^* \frac{\partial v_z^*}{\partial r^*} \right) \right] + \frac{1}{Gr^{1/2}} \frac{\partial^2 v_z^*}{\partial z^{*2}} + T^* \quad (7.11)$$

Introducing dimensionless quantities into the energy equation results in,

$$\frac{1}{Gr^{1/2}Pr} \frac{\partial T^*}{\partial t^*} + \left(\frac{L_i}{R_i} \right) v_r^* \frac{\partial T^*}{\partial r^*} + v_z^* \frac{\partial T^*}{\partial z^*} = \frac{1}{Gr^{1/2}Pr} \left[\left(\frac{L_i}{R_i} \right)^2 \left(\frac{1}{r^*} \frac{\partial}{\partial r^*} r^* \frac{\partial T^*}{\partial r^*} \right) + \frac{\partial^2 T^*}{\partial z^{*2}} \right] + \frac{1}{Gr^{1/2}Pr} \quad (7.12)$$

Using equation (7-6), the dimensionless energy equation becomes

$$\frac{1}{Gr^{1/2}Pr} \frac{\partial T^*}{\partial t^*} + \left(\frac{1}{\gamma} \right) v_r^* \frac{\partial T^*}{\partial r^*} + v_z^* \frac{\partial T^*}{\partial z^*} = \frac{1}{Gr^{1/2}Pr} \left[\left(\frac{1}{\gamma} \right)^2 \left(\frac{1}{r^*} \frac{\partial}{\partial r^*} r^* \frac{\partial T^*}{\partial r^*} \right) + \frac{\partial^2 T^*}{\partial z^{*2}} \right] + \frac{1}{Gr^{1/2}Pr} \quad (7.13)$$

Introducing dimensionless quantities into initial conditions gives:

$$\text{At } t^* = 0: T^* = 0; v_r^* = v_z^* = 0$$

$$v_z^* = \frac{V_{in}}{\sqrt{g\beta \left(\frac{L_i^2 Q}{k} \right) L}} \quad \text{for } 0 < r^* < R_i R_{inlet}, 0 < t < t_{cum}; t_{cum} = 180 \text{ s};$$

$$v_z^* = 0 \quad \text{for } t > t_{cum}$$

Introducing dimensionless quantities into boundary conditions gives:

$$\text{At } r^* = 0: \frac{\partial T^*}{\partial r^*} = 0; \frac{\partial v_z^*}{\partial r^*} = 0 \quad (\text{axisymmetry})$$

$$\text{At } r^* = 1: v_r^* = v_z^* = 0 \text{ (no slip); } \left(\frac{\partial T^*}{\partial r^*} \right)_{\text{fluid}} = \frac{k_{\text{solid}}}{k_{\text{fluid}}} \left(\frac{\partial T^*}{\partial r^*} \right)_{\text{solid}} \text{ (heat flux continuity)}$$

$$T^*_{\text{fluid}} = T^*_{\text{solid}} \text{ (temperature continuity)}$$

$$\text{At } r^* = \frac{R_o}{R_i} : \left(-\frac{\partial T^*}{\partial r^*} \right)_{\text{solid}} = \text{Bi} \cdot T^*$$

$$\text{At } z^* = 1: v_r^* = v_z^* = 0 \text{ (no slip); } \left(\frac{\partial T^*}{\partial z^*} \right)_{\text{fluid}} = \frac{k_{\text{solid}}}{k_{\text{fluid}}} \left(\frac{\partial T^*}{\partial z^*} \right)_{\text{solid}} \text{ (heat flux continuity)}$$

$$T^*_{\text{fluid}} = T^*_{\text{solid}} \text{ (temperature continuity)}$$

Thus, the dimensionless parameters that govern the solution are : γ , $\frac{1}{Gr^{1/2} Pr}$, Pr , Bi ,

$$\frac{k_{\text{solid}}}{k_{\text{fluid}}}, \frac{V_{\text{in}}}{\sqrt{g\beta \left(\frac{L_i^2 Q}{k} \right) L_i}}$$

The parameters obtained can be used for the scale up of the high pressure process.

7.2 Thermocouple Response & Parameters Governing Thermocouple Lag

The theoretical analysis of temperature measured by the high pressure thermocouple assembly during high hydrostatic pressure processing (HHPP) was carried out and the thermocouple response equations were non-dimensionalized to obtain the parameters that govern the difference in temperature measured by the thermocouple and actual temperature at the end of pressurization and pressure hold period.

7.2.1 Thermocouple Response

A program in MATLAB[®] was written to predict the response of thermocouple under given conditions. **Figure 7-1** shows the plot of the temperature of water obtained from equations (5-31), (5-51), (5-72) and the predicted thermocouple response obtained from equations (5-49), (5-70), (5-74) when initial temperature (T_o), t_{cum} , t_{hold} , t_{dep} were 60°C, 180s, 780s, and 785s respectively. The value for time constant (τ) for our thermocouple assembly was 10s as obtained from the experimental data, the details of experimental set up and procedure are explained in the Chapter 4 (section 4.2.1). However, for the purpose of showing the effect of time constant on temperature we chose two values of τ namely 10s and 20s (**Figure 7-1**). It is clear from **Figure 7-1** that as the value of time constant increases, the difference between the true temperature and the temperature recorded by the thermocouple increases. Also, it was observed that the thermocouple under predicts the temperature during the pressurization phase and over predicts during pressure hold. However, given enough hold time, the thermocouple will eventually read the same temperature as true temperature.

7.2.2 Quantification and Implications of Lag in Temperature

Equations (5-77), (5-82), and (5-87) obtained from the inverse theoretical analysis (section 5.5) were used to correct the experimentally obtained temperature variation during a high pressure process where the pressure was increased from ambient (0.1MPa) to 586MPa in 180s, held constant at this pressure for 600s, and then depressurized in 5s. The initial temperature for the experiment was 313K. Using the time constant value of

10s obtained for the given thermocouple assembly, the solution obtained showed that there was a lag of approximately 2K. In order to see the implications of this 2K difference obtained for our thermocouple assembly we calculated the F-value (time required to sterilize the selected organism at 394.3K (121.1°C)). For *C. botulinum* (z-value 10°C), the results showed that calculations using the temperature indicated by the

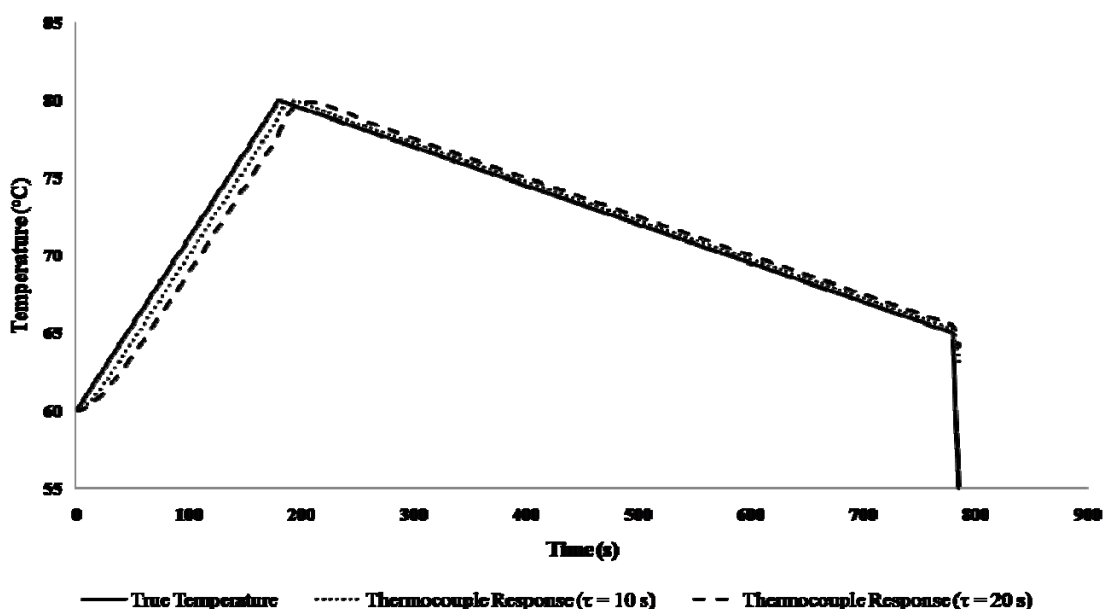


Figure 7-1: The true temperature of water predicted using equations (5-31), (5-51), (5-72) and the thermocouple response predicted using equations (5-49), (5-70), (5-74) obtained when time constant was 10s and 20s respectively.

thermocouple as obtained from the analytical solution, slightly ($\sim 2\%$) over predicted the F-value compared to the predictions based on the true temperature variation. The extent of over prediction depends on the value of time constant of the thermocouple and other process parameters. Although the difference in the F-value is small, the calculations based on the actual thermocouple response are on the unsafe side.

7.2.3 Parameters Governing Thermocouple Lag

The parameters governing the difference in temperature at the end of pressurization ($t = t_{\text{cum}}$), pressure hold ($t = t_{\text{hold}}$), and pressure release ($t = t_{\text{dep}}$) were obtained by non-dimensionalizing the thermocouple response equations derived in Section 5.5.

The response of a thermocouple to a linearly increasing/decreasing temperature during pressurization, pressure hold, and pressure release was given by equations (7-14), (7-15), (7-16) respectively (Refer to section 5.5 for details).

$$T' = T_o + \tau \left(\frac{T_{\text{cum}} - T_o}{t_{\text{cum}}} \right) \left[\frac{t}{\tau} - 1 + e^{-t/\tau} \right] \quad (7-14)$$

$$T'' = T_{\text{cum}} + \left(\frac{T_{\text{hold}} - T_{\text{cum}}}{t_{\text{hold}} - t_{\text{cum}}} \right) [t - t_{\text{cum}} - \tau] + \left[T'_{\text{cum}} - T_{\text{cum}} + \tau \left(\frac{T_{\text{hold}} - T_{\text{cum}}}{t_{\text{hold}} - t_{\text{cum}}} \right) \right] e^{-(t-t_{\text{cum}})/\tau} \quad (7-15)$$

$$T''' = T_{\text{hold}} + \left(\frac{T_{\text{dep}} - T_{\text{hold}}}{t_{\text{dep}} - t_{\text{hold}}} \right) [t - t_{\text{hold}} - \tau] + \left[T''_{\text{hold}} - T_{\text{hold}} + \tau \left(\frac{T_{\text{dep}} - T_{\text{hold}}}{t_{\text{dep}} - t_{\text{hold}}} \right) \right] e^{-(t-t_{\text{hold}})/\tau} \quad (7-16)$$

The dimensionless temperature difference (between true temperature and temperature measured by thermocouple) at the end of pressurization, pressure hold, and pressure release are indicated by $\Delta\theta_{\text{cum}}$, $\Delta\theta_{\text{hold}}$, and $\Delta\theta_{\text{dep}}$ respectively.

Evaluating equations (5-31) and (7-14) at $t = t_{\text{cum}}$ and subtracting we get

$$\Delta\theta_{\text{cum}} = \frac{T_{\text{cum}} - T'_{\text{cum}}}{T_{\text{cum}} - T_o} = \frac{\tau}{t_{\text{cum}}} \left(1 - e^{-\frac{t_{\text{cum}}}{\tau}} \right) \quad (7-17)$$

Def. $\frac{\tau}{t_{\text{cum}}} = \tau^*$, we get (7-18)

$$\Delta\theta_{\text{cum}} = \frac{T_{\text{cum}} - T'_{\text{cum}}}{T_{\text{cum}} - T_o} = \tau^* \left(1 - e^{-\frac{t}{\tau^*}} \right) \quad (7-19)$$

Similarly, evaluating equations (5-51) and (7-15) at $t = t_{\text{hold}}$ and subtracting we get

$$\Delta\theta_{\text{hold}} = \frac{T_{\text{hold}} - T''_{\text{hold}}}{T_{\text{cum}} - T_o} = \left(\frac{T_{\text{hold}} - T_{\text{cum}}}{T_{\text{cum}} - T_o} \right) \left[\frac{\tau^*}{\left(\frac{t_{\text{hold}}}{t_{\text{cum}}} - 1 \right)} \left(1 - e^{-\frac{t_{\text{hold}} - 1}{\tau^*}} \right) \right] + \Delta\theta_{\text{cum}} e^{-\frac{t_{\text{hold}} - 1}{\tau^*}} \quad (7-20)$$

Similarly, evaluating equations (5-72) and (7-16) at $t = t_{\text{dep}}$ and subtracting we get

$$\Delta\theta_{\text{dep}} = \frac{T_{\text{dep}} - T'''_{\text{dep}}}{T_{\text{cum}} - T_o} = \left(\frac{T_{\text{dep}} - T_{\text{hold}}}{T_{\text{cum}} - T_o} \right) \left[\frac{\tau^*}{\left(\frac{t_{\text{dep}}}{t_{\text{cum}}} - \frac{t_{\text{hold}}}{t_{\text{cum}}} \right)} \left(1 - e^{-\frac{t_{\text{dep}} - t_{\text{hold}}}{\tau^*}} \right) \right] + \Delta\theta_{\text{hold}} e^{-\frac{t_{\text{dep}} - t_{\text{hold}}}{\tau^*}} \quad (7.21)$$

Therefore, the parameters that govern the thermocouple response and their range during high pressure process are given in **Table 7-1**.

The ranges for the values of parameters in **Table 7-1** were defined based on the typical values of the time and temperature variables, e.g., time constant ($\tau = 1$ to 20 s), pressure come-up time ($t_{\text{cum}} = 10$ to 200 s) which depend upon the vessel size and target pressure, pressure hold time ($t_{\text{hold}} = t_{\text{cum}} + 60$ to 1200 s), and pressure release ($t_{\text{dep}} = t_{\text{cum}} + t_{\text{hold}} + 5$ to 20 s). The typical increase in temperature ($T_{\text{cum}} - T_o$) for water during pressurization range of 300 – 600 MPa is 10 to 20°C and drop in temperature ($T_{\text{hold}} - T_{\text{cum}}$) during pressure hold for hold time from 60 to 1200 s is 1 to 10°C. The dimensionless parameters obtained here can be used to evaluate which parameter will have more effect on the lag in the temperature during the high pressure process.

Table 7-1: Parameters governing the temperature difference at the end of pressurization, pressure hold, and pressure release stages of HHPP.

	Parameter	Range
1	$\tau^* \left(= \frac{\tau}{t_{\text{cum}}} \right)$	0.005 - 2
2	$\frac{T_{\text{hold}} - T_{\text{cum}}}{T_{\text{cum}} - T_o}$	0.05 - 1
3	$\frac{t_{\text{hold}}}{t_{\text{cum}}}$	1-120
4	$\frac{T_{\text{hold}} - T_{\text{dep}}}{T_{\text{cum}} - T_o}$	1
5	$\frac{t_{\text{dep}}}{t_{\text{cum}}}$	1.025 - 122

7.2.4 Non-dimensional Temperature Difference

Figure 7.2 (a, b, and c) shows the dimensionless temperature difference at the end of pressurization, pressure hold, and pressure release respectively, as a function of their respective governing parameters. The values of governing parameters were used from the above

The ranges for the values of parameters in **Table 7-1** were defined based on the typical values of the time and temperature variables, e.g., time constant ($\tau = 1$ to 20 s), pressure come-up time ($t_{\text{cum}} = 10$ to 200 s) which depend upon the vessel size and target pressure, pressure hold time ($t_{\text{hold}} = t_{\text{cum}} + 60$ to 1200 s), and pressure release ($t_{\text{dep}} = t_{\text{cum}} + t_{\text{hold}} + 5$ to

20 s). The typical increase in temperature ($T_{\text{cum}}-T_o$) for water during pressurization range of 300 – 600 MPa is 10 to 20°C and drop in temperature ($T_{\text{hold}}-T_{\text{cum}}$) during pressure hold for hold time from 60 to 1200 s is 1 to 10°C. The dimensionless parameters obtained here can be used to evaluate which parameter will have more effect on the lag in the temperature during the high pressure process.

Table 7-1: Parameters governing the temperature difference at the end of pressurization, pressure hold, and pressure release stages of HHPP.

	Parameter	Range
1	$\tau^* \left(= \frac{\tau}{t_{\text{cum}}} \right)$	0.005 - 2
2	$\frac{T_{\text{hold}} - T_{\text{cum}}}{T_{\text{cum}} - T_o}$	0.05 - 1
3	$\frac{t_{\text{hold}}}{t_{\text{cum}}}$	1-120
4	$\frac{T_{\text{hold}} - T_{\text{dep}}}{T_{\text{cum}} - T_o}$	1
5	$\frac{t_{\text{dep}}}{t_{\text{cum}}}$	1.025 - 122

It can be seen from **Fig. 7.2 (a)** that as the τ^* increases (i.e. time constant increases) the temperature lag between the true temperature and the temperature recorded by the thermocouple at the end of pressurization increases, as expected. Also, from **Figs. 7.2 (b) and 7.2 (c)** it is clear that the temperature difference at the end of pressure hold and

pressure release is negative which means that the thermocouple over predicts the true temperature. The non-dimensional parameters that govern the temperature difference at the end of pressurization, pressure hold, and pressure release obtained above can be used to predict the lag of thermocouple response. These results provide a universal solution for the response of a thermocouple with a given time constant, to temperature rise and fall associated with pressure increase and decrease in a high pressure vessel.

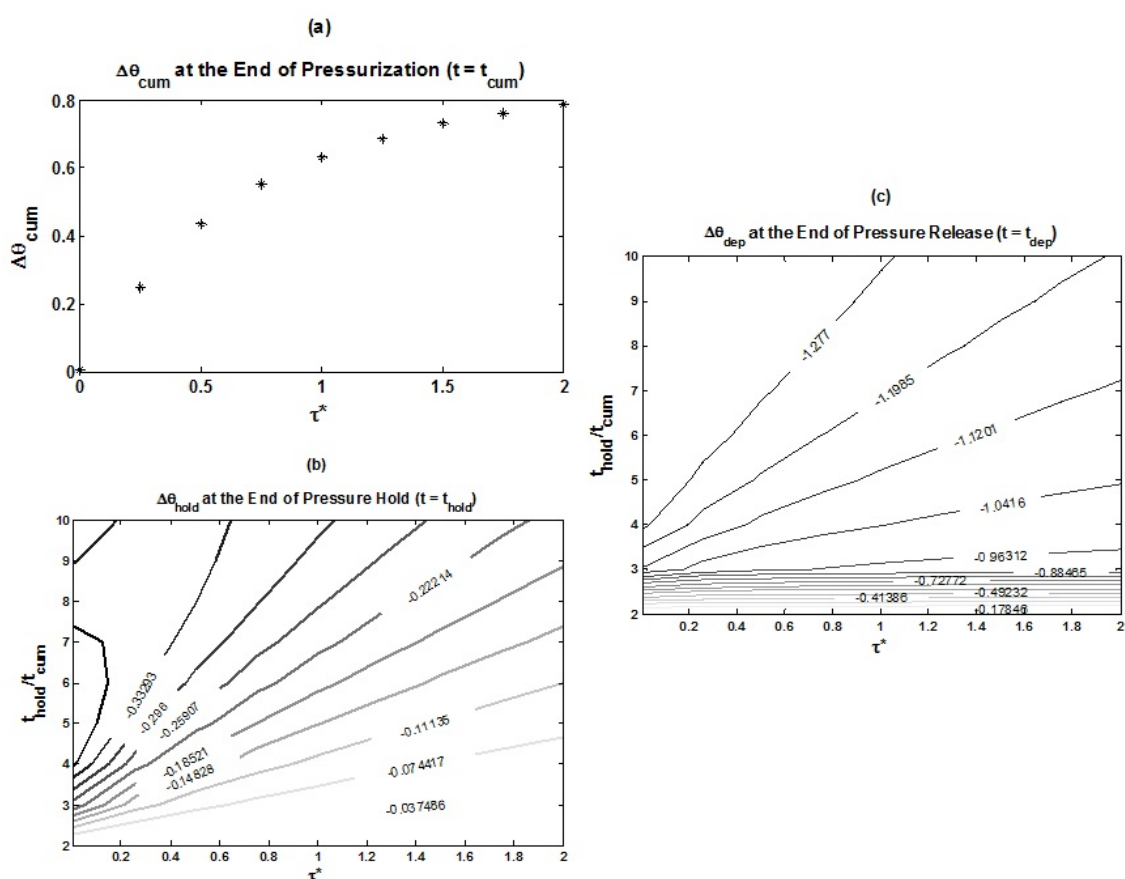


Figure 7-2: Dimensionless temperature difference at the end of (a) pressurization, (b) pressure hold, and (c) pressure release as a function of their respective governing parameters.

7.3 Numerically Predicted Results for Vertical and Horizontal Vessel

Although adiabatic compression heating during the high pressure process causes an instantaneous and volumetric temperature increase throughout the pressurizing medium, a temperature gradient is established between the medium (water) and the colder vessel wall which causes heat transfer to occur from water to the thick vessel wall. The water entering the vessel from top or bottom (for vertical vessel) and from both end closures (for horizontal vessel) is at room temperature, further contributing to these temperature differences. The resulting density difference due to the temperature variation within the pressurizing medium leads to a downward draft of fluid near the wall. Thus a circulation pattern sets up in the high pressure medium with fluid going down near the vessel side wall and rising in the middle. In the results presented in this section, the cooling effect caused by the entering fluid during compression is included in the model. The results for the numerical simulation are presented in the form of isotherms (lines of constant temperature), streamlines (lines whose tangents are everywhere parallel to the velocity vector) and temperature distributions compared in terms of COV values.

Before discussing the numerical results it is important to consider that for any research involving numerical scheme, validation of the results obtained from the numerical model with experimental data is critical to support and have confidence in the predictions made by the model. In our case, the validation of the model was carried out for vertical vessel high pressure unit at Rutgers University. Since we did not have access to the high pressure unit with horizontal vessel, it was assumed that the model developed for

horizontal vessel is valid as the model development techniques similar to the vertical vessel were used.

7.3.1 Validation of Numerical Model

Comparison of numerically predicted data with experimental data

The time temperature history during the pressurization and hold time of high pressure process were recorded experimentally at three thermocouple points in the Rutgers University HHPP vertical vessel and also predicted numerically at the same points, shown in **Figure 6-2**, for initial temperature of 313 K, in order to validate the numerical model. **Figure 7-3** shows the comparison between the corrected experimental (in which experimental data has been corrected for thermocouple response time using equations (5-76) and (5-81)) and numerically predicted variation of temperature with time at $T_i = 313 \text{ K}$ (40°C) and $T_{\text{inlet}} = 298 \text{ K}$ (25°C). The maximum correction in temperature for thermocouple lag was found to be about 2 K. A very good agreement between the corrected experimental temperatures and numerically predicted temperatures was obtained with initial temperature of 313 K (40°C). The validated numerical model was further used to study the high pressure process under various conditions.

Due to experimental limitations, it was not possible to carry out temperature measurement experiments at final temperature higher than 60°C (333 K). The seals in the top and bottom closures would start leaking as higher temperature would soften and expand them (even though the vessel was designed to operate up to 90°C (363K) according to Elmhurst Research Inc.).

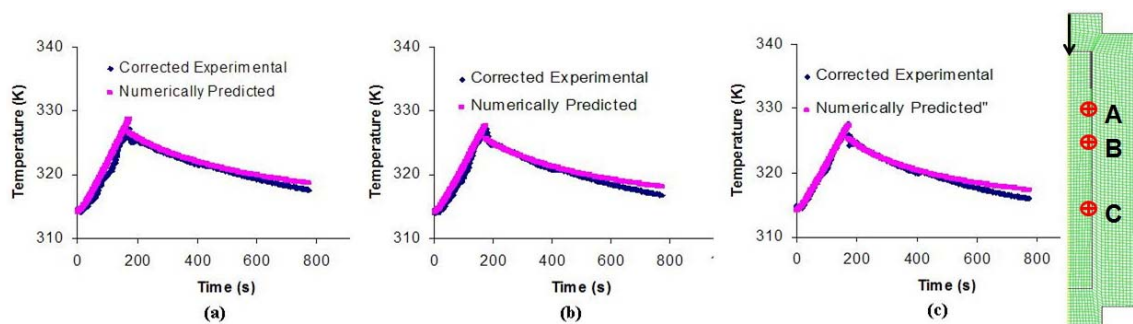


Figure 7-3: Comparison of corrected experimental and numerically predicted time-temperature variations at $T_i = 313$ K (40°C), $P = 586$ MPa, for the thermocouple located (a) near top (A), (b) in between (B), and (c) near bottom (C) of the vessel in water.

7.3.2 Temperature and *C. botulinum* Distributions in Vertical Vessel

For the vertical vessel, the numerical simulation was carried out in a 2D axisymmetric slice to predict the temperature distribution in water and vessel wall during the high pressure process. The thermal and physical properties of water were defined in the model as a function of both pressure and temperature. The natural convection heat transfer was included in the model by turning on the gravity and the pressure work as a source term in water boundary condition to pressurize vessel to 700 MPa. The water added to the vessel from top in order to increase the pressure was included in the model and in all simulations was assumed to be at room temperature (298 K (25°C)) unless otherwise specified. The inlet velocity of the water was calculated to be 0.28 m/s (refer to section 5.3.3).

As mentioned before, high pressure process based on the initial temperature can be categorized into three parts: High pressure “Cold Sterilization”, Pressure Assisted

Thermal Pasteurization (PATP), and Pressure Assisted Thermal Sterilization (PATS).

The results obtained for each part are presented below:

7.3.2.1 High Pressure “Cold Pasteurization”

High pressure process is termed as cold pasteurization when the high pressure process is carried out at initial temperature close to room temperature. Therefore, the conjugate heat transfer, i.e., convection in water and conduction in vessel wall for this case were simulated at initial temperature of water and s.steel vessel wall of 298 K (25°C). **Figure 7-4(a)** shows the isotherms in radial slice of high pressure vessel before pressurization, i.e., when pressure was 0.1 MPa (atmospheric pressure) and the water and s.steel mass were at 298 K. **Figure 7-4(b)** shows the isotherms in water and the s.steel vessel wall at the end of pressurization when pressure was increased from 0.1 to 700 MPa in 180 s. The water added to the vessel to compensate for compression was at 298 K. The heat source term Q was 400,000 W/m³.

Figure 7-4(c) shows the isotherms at the end of hold time when the pressure was maintained at 700 MPa for 600 s. From **Figure 7-4(b)** it is clear that at the end of pressurization the maximum temperature in the vessel reached 311 K, i.e., a temperature increase of about 13 K was observed. This increase in temperature does not happen uniformly throughout the vessel because of continuous inflow of water from top of the vessel while pressure is increasing, conduction heat loss at vessel wall, and convection currents setting in due to density differences. At the end of pressurization, the temperature distribution in the top half of the vessel is primarily affected by the incoming

water and this causes the maximum temperature to be towards the bottom where the dominant mechanism is conduction heat loss to vessel wall and natural convection currents. The average temperature at the end of pressurization in the vessel is 309 K. At the end of 600 s of hold period, the maximum temperature in the vessel dropped to 305 K and the hot region moved close to the top of the vessel. The average temperature at end of hold period in the vessel is 304 K. During the hold period as there is no water added to the vessel, the natural convection is the only source for induced momentum and flow field in the pressure cavity which gives a slow mixing effect to equilibrate the temperature.

To understand the flow pattern and its affect on temperature distribution in the vessel better, contours for streamlines and velocity vectors in water zone were plotted. **Figure 7-5** shows the corresponding streamlines in water before pressurization (everything is still, $v=0$ everywhere), at the end of pressurization and end of hold period. The contour plotted during pressurization phase showed that the water added to the vessel goes straight down for about one third of the length of the pressure cavity for approximately initial 30 s of pressurization period, spreads out as it loses momentum and the velocity decreases from 0.28 m/s at the inlet to approximately 0.08 m/s close to the one-third of the length. As the water inside the vessel is continuously increasing in temperature due to adiabatic compression heating, the density of water entering the vessel is slightly higher than the surrounding water. This along with an additional steel sleeve (part of top closure) in top part of the vessel results in forced convection currents leading to formation of a large eddy close to the top of the vessel (in top one-third length as shown

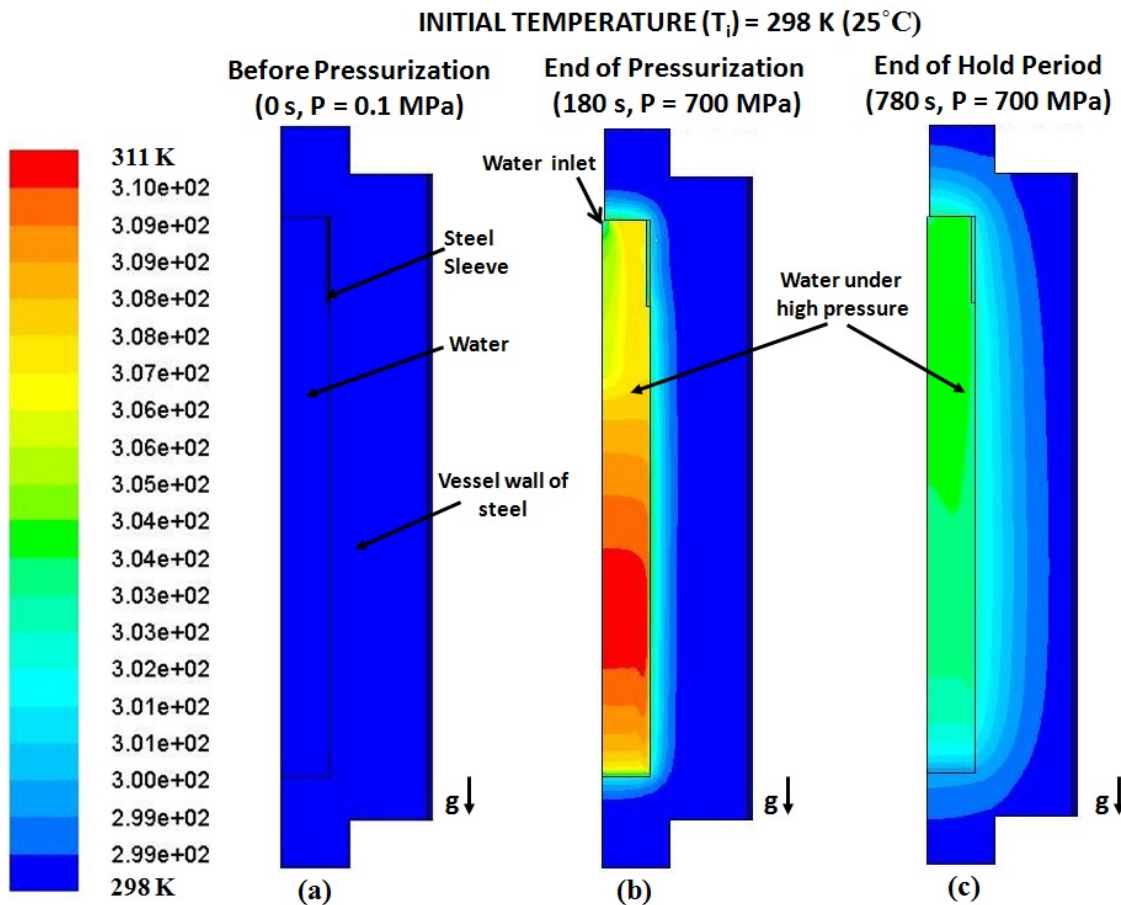


Figure 7-4: Isotherms in water and s.steel wall for 10 L vertical vessel with water inlet from top at $T_i = 298$ K, $P = 700$ MPa, $Q = 400,000$ W/m³ for ($0 \leq t \leq 180$ s), (a) before pressurization (0 s), (b) end of pressurization (180 s), & (c) after 600 s hold time (780 s).

in **Figure 7-5(b)**) and in the rest of the fluid a thin downward directed layer close to the vessel wall, rising up in the center of the vessel is observed. The velocity in the eddy close to the top of vessel is of the order of 10^{-2} m/s and 10^{-3} m/s in the rest of the fluid. As seen from **Figure 7-5(c)**, this large eddy disappears over the period of hold time with existence of single flow pattern (i.e., downward draft at the vessel wall and rising towards the center) with velocity values 0.003 m/s in the fluid.

(40°C), however the inlet water (water added to the vessel to compensate for compression) temperature was at 298 K (25°C). The pressure was held constant at 700 MPa for 600 s. **Figure 7-6(a)** shows that initially the temperature of the water and the s. steel mass is constant and uniform at 313 K (40°C). At the end of pressurization as shown in **Figure 7-6(b)**, the maximum temperature in the vessel reached 328 K (i.e., $\Delta T_{\max} = 15$ K) due to compression heating. Also, simultaneous cooling is caused due to the water (at 298 K (25°C)) pumped into the vessel from the inlet hole in top and heat loss to the vessel wall. Since the water is entering from the top under gravity, the top region of the vessel cools more than the bottom region and causes the hottest spot in the vessel to move towards the bottom. Due to the arising temperature variation within the vessel, the buoyancy force becomes active. The water adjacent to the wall loses heat to the vessel causing its density to increase and thus flow downward whereas the water in the bulk and near the center of the vessel is at the higher temperature and moves upward. Therefore, a flow pattern sets up in the fluid with the hot fluid rising at the center of the vessel and coming down near the cooler vessel wall. **Figure 7-6(c)** shows the isotherms after the pressure is maintained at 700 MPa for 600 s. It can be observed that the maximum temperature in the vessel dropped to 323 K at the end of 300 s and to 319 K at the end of 600 s.

Figure 7-7 shows the corresponding streamlines in water at the end of pressurization and end of hold period. It can be seen that at the end of pressurization (**Figure 7-7(b)**), the

after US-FDA accepted commercial use of PATS for low acid foods. **Figure 7-8** shows the isotherms in water and the s.steel wall when pressure was increased from 0.1 to 700 MPa in 180 s, the process was carried out at initial temperature of 368 K (95°C) and water inlet to the vessel was at 298 K (25°C). The pressure was held constant at 700 MPa for 600 s. Before the pressurization is initiated the temperature of water and vessel steel mass were at 368 K (95°C) as shown in **Figure 7-8(a)**. At the end of pressurization, the maximum temperature in the vessel reached 386 K, i.e., the temperature of water increased from 368 K to 386 K ($\Delta T_{\max} = 18$ K) due to compression heating as shown in **Figure 7-8(b)**.

Similar to the results discussed above for cold pasteurization and PATP, the temperature distribution during PATS at the end of pressurization became non-uniform with cold spot in the upper part of the vessel where water was entering to compensate for compression. The natural convection currents and conduction heat loss to the wall further contributed to the non-uniformity in temperature. **Figure 7-8(c)** shows the isotherms after the pressure was maintained at 700 MPa for 600 s. It can be observed that at the end of 600 s the maximum temperature in the vessel dropped to 372 K, a temperature difference of approximately 10°C existed in the vessel which can give rise to non-uniform inactivation and of concern for food safety.

Figure 7-9 shows the corresponding streamlines in water at the end of pressurization and end of hold period. It can be seen that at the end of pressurization (**Figure 7-9(b)**) flow in the water due to natural convection and flow of pumped water co-existed whereas at the

end of the hold period the movement was entirely governed by the natural convection currents (**Figure 7-9(c)**).

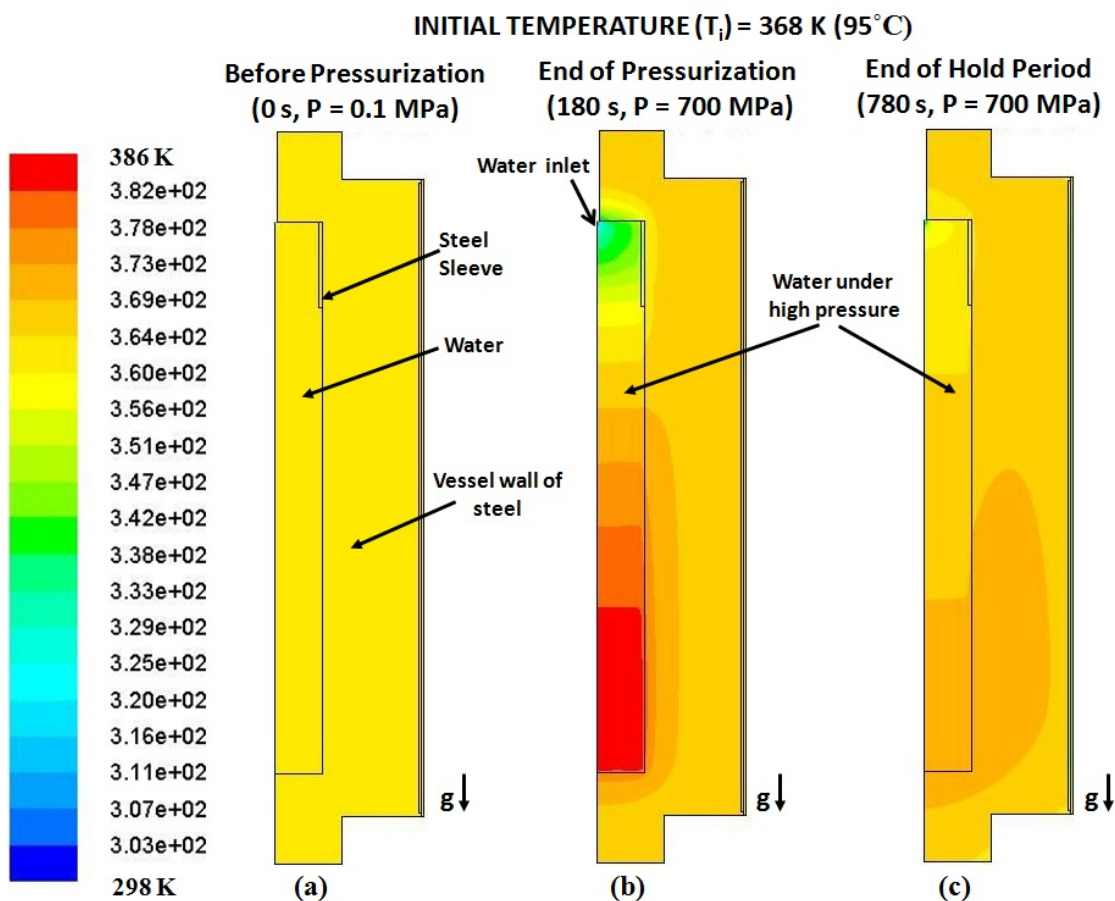


Figure 7-8: Isotherms in water and s.steel wall for 10 L vertical vessel with water inlet from top at $T_i = 368$ K, $P = 700$ MPa, $Q = 860,000$ W/m³ for ($0 \leq t \leq 180$ s), (a) before pressurization (0 s), (b) end of pressurization (180 s), & (c) after 600 s hold time (780 s).

Although a similar temperature distribution trend was observed for the cold pasteurization, PATP and PATS, it is important to notice and discuss a few differences. It is clear from the **Figure 7-4(b)**, **Figure 7-6(b)**, and **Figure 7-8(b)** (as the process was initiated at higher initial temperatures) that at the end of pressurization the region of

Also, it can be seen that at the end of 600 s hold time, the cold region in the vessel was towards the bottom of the vessel for cold pasteurization (**Figure 7-4(c)**) whereas for PATP (**Figure 7-6(c)**) and PATS (**Figure 7-8(c)**) the cold region was still towards the top of the vessel. This can be due to higher temperature difference between the initial temperature and inlet water temperature during pressurization, and temperature gradient within the vessel at the end of pressurization during PATP and PATS compared to cold pasteurization, the 600 s hold time was not enough for movement of fluid in the vessel to make the higher temperature fluid rise and push the cold spot towards the bottom of the vessel.

To further investigate the effect of higher initial temperature on temperature distribution in the vessel, COV in temperature for the process starting at different initial temperatures was plotted (as shown in **Figure 7-10**). It can be seen from **Figure 7-10** that when the inlet water temperature was fixed to 298 K, starting the process at higher initial temperatures lead to the higher COV value at fixed time implying that the non-uniformity in temperature increased as the initial temperature increased.

7.3.2.4 Effect of Thermophysical Properties

As mentioned earlier, predicting the temperature distributions during HHPP via heat transfer models requires pressure-temperature dependent thermophysical properties of foods and the pressurizing medium used. Foods are complex systems and obtaining these properties for foods as a function of pressure is very difficult and hence not much literature is available for most of the food materials. Therefore, as a starting point for

numerical simulations it is recommended to use the constant properties at atmospheric pressure or temperature dependent properties at atmospheric pressure.

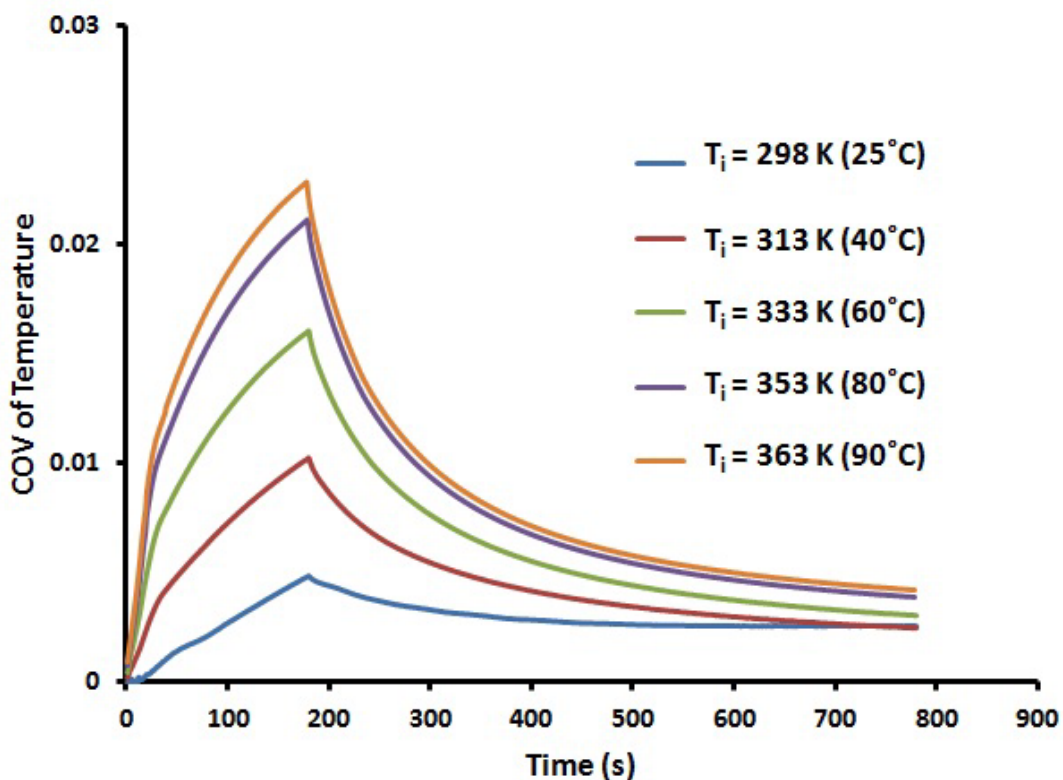


Figure 7-10: COV of temperature for vertical vessel at various initial temperatures (T_i), $P = 700 \text{ MPa}$, & T_{inlet} (water added for compression) = 298 K.

In this section, the numerical simulation for three different cases, (i) constant properties of water (i.e., properties at atmospheric pressure and at initial temperature of 313 K (40°C)), (ii) temperature dependent properties of water (at atmospheric pressure), and (iii) pressure-temperature dependent properties of water, were carried out. Water was used because it is the only food product whose thermophysical properties for a range of pressure and temperature are well studied and documented. Although the results obtained from this model will not be valid for other food products but it will provide an insight

into importance of using pressure-temperature dependent properties for products that have similar pressure temperature dependent properties.

Error! Reference source not found.(a, b, c) shows the isotherms in water and the s. steel wall for constant properties, temperature only dependent properties, and pressure-temperature dependent properties, respectively, when pressure was increased from 0.1 to 700 MPa in 180 s, the initial temperature was 313 K (40°C) and water entering the vessel for compression was at 298 K (25°C). The pressure was held constant at 700 MPa for 600 s. It is clear from the isotherms that the maximum temperature of 333 K was obtained when the temperature dependent properties were used followed by constant properties and pressure-temperature dependent properties which reached 330 K and 327 K, respectively at the end of 180 s. Similarly, the isotherms at the end of hold time of 600 s (**Error! Reference source not found.**) show that temperature dropped to 317 K for temperature dependent properties compared to the constant and pressure temperature dependent properties where it dropped to 319 K.

The isotherms for the three cases (**Figure 7-12**) show similar flow and temperature patterns but difference in temperature values. Therefore, it can be concluded that using constant properties or temperature only dependent properties instead of pressure-temperature dependent properties can be used to understand the phenomenon (flow and temperature trends) but using the temperature data for process safety calculations can lead to over/under prediction of safety parameters.

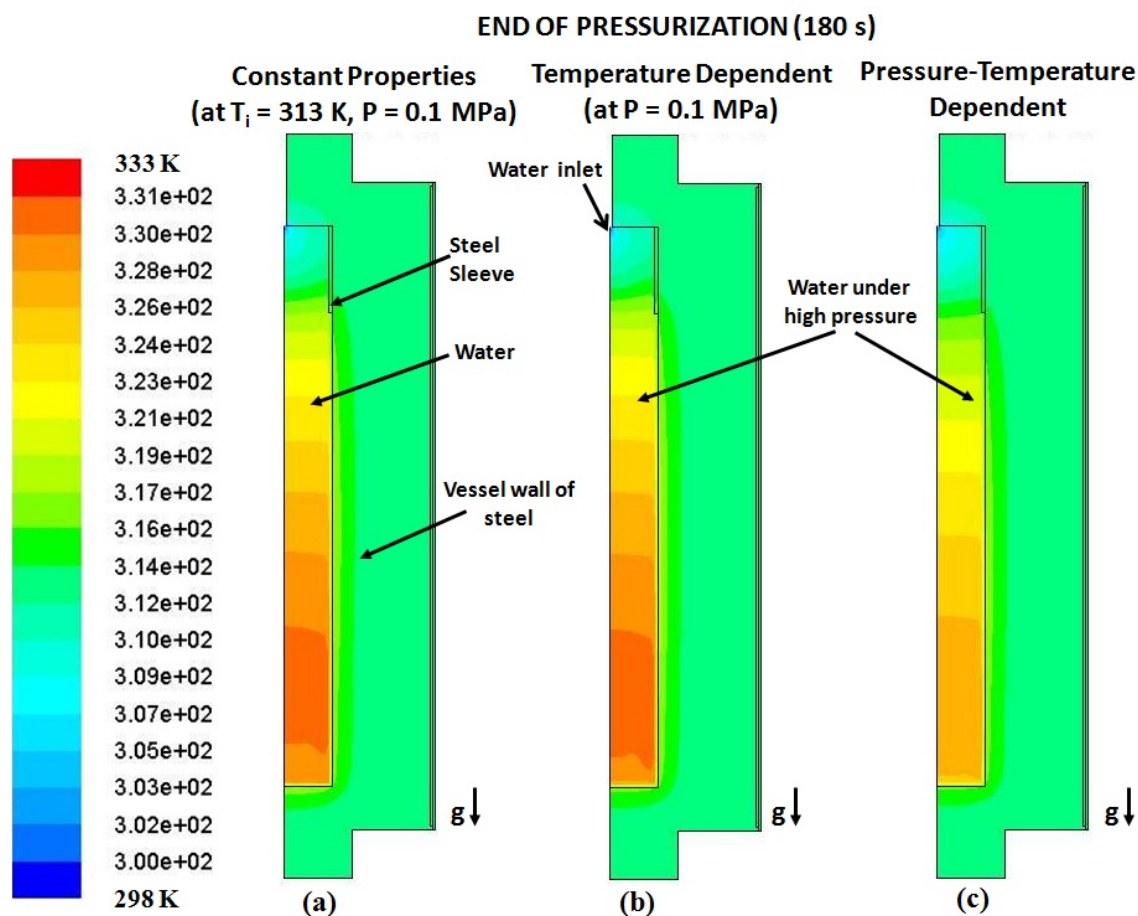


Figure 7-11: Isotherms in water and s.steel wall for 10 L vertical vessel at the end of pressurization (180 s) at $T_i = 313$ K, $P = 700$ MPa, $T_{inlet} = 298$ K, $Q = 400,000$ W/m³ for ($0 \leq t \leq 180$ s), (a) constant, (b) temperature dependent, & (c) pressure-temperature dependent thermophysical properties.

In order to better quantify the implications of using constant or temperature only dependent properties due to lack of pressure dependent properties, the temperature non-uniformity was expressed in terms of coefficient of variation (COV) values (shown in **Error! Reference source not found.**). It can be seen from **Error! Reference source not und.** that the COV values for constant properties, temperature only dependent properties,

and pressure-temperature dependent properties were comparable. This shows that the overall temperature distribution for the

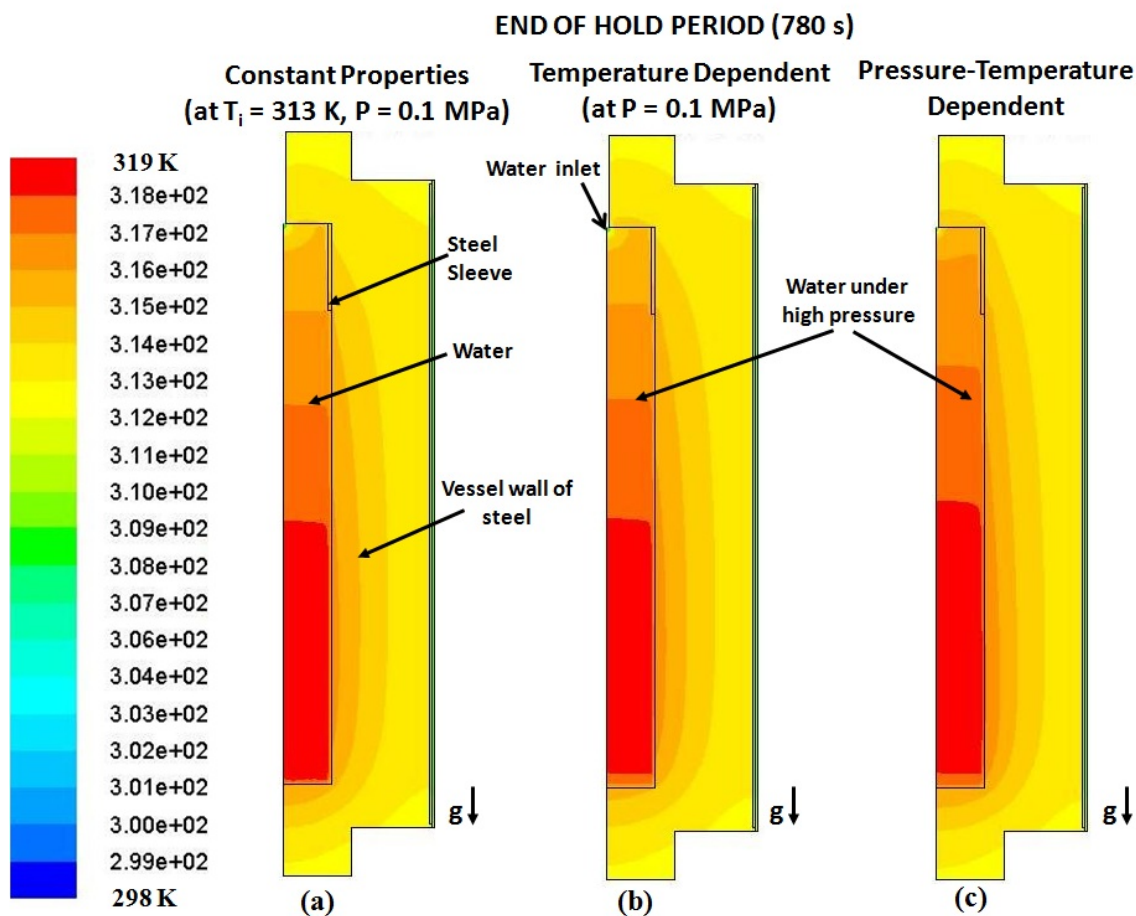


Figure 7-12: Isotherms in water and s.steel wall for 10 L vertical vessel at the end of hold time (780 s) at $T_i = 313$ K, $P = 700$ MPa, $T_{inlet} = 298$ K, $Q = 400,000$ W/m³ for ($0 \leq t \leq 180$ s), (a) constant, (b) temperature dependent, & (c) pressure-temperature dependent thermophysical properties.

three cases were very similar. The results do not give enough compelling reason to use constant or temperature dependent properties over pressure-temperature dependent properties. But since the temperature values for the temperature only dependent properties case were higher than the temperature values corresponding to the pressure-

temperature dependent properties case, it can be concluded that using temperature only dependent properties can over predict the safety parameters (like F-value) which is not desirable when targeting bacterial inactivation.

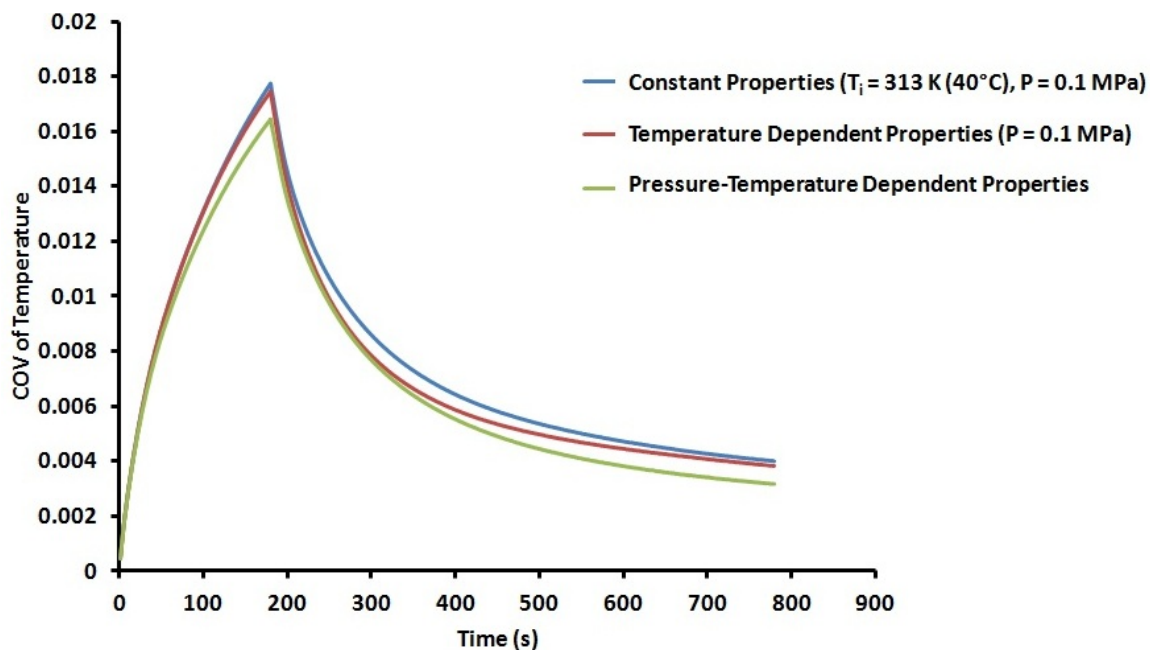


Figure 7-13: COV of temperature for 10 L vertical vessel at $P = 700$ MPa, $T_i = 313$ K, T_{inlet} (water added for compression) = 298 K (25°C), for constant, temperature dependent & pressure-temperature dependent thermophysical properties.

7.3.2.5 Effect of Water Inlet

As discussed in Chapter 1, vertical high pressure food processing vessels are available in two configurations, with water added to compensate for compression from 1) top and 2) bottom. In this research an attempt was made to compare the two configurations with respect to uniformity in temperature distribution and *C. botulinum* inactivation distribution. In addition to the configurations mentioned above, simulation was also carried out for a hypothetical case, i.e., vessel with no water inlet and for the purpose of

discussions it was assumed to be a pressure vessel where pressure was generated by piston (although piston motion was not included in the model).

The numerical simulation for the vertical vessel with water inlet from the bottom was carried out using the 2D radial slice used for water inlet from top. The only difference was that the direction of gravity was reversed. Similarly, for vertical vessel with no water inlet a velocity of 0 m/s was defined at the velocity boundary condition and pressure increase was defined by heat generation term.

Figure 7-14(a, b, c) shows the isotherms in the water and s.steel vessel for no water inlet, water inlet from top and water inlet from bottom respectively, when the pressure was increased from 0.1 to 700 MPa in 180 s and initial temperature was 368 K (95°C). It can be seen that at the end of pressurization (180 s), a maximum temperature of 392 K (**Figure 7-14(a) & (c)**) was achieved for no water inlet and water inlet from bottom vessels whereas for water inlet from top maximum temperature was 386 K (**Figure 7-14(b)**) The cooling due to the buoyancy force and heat loss to vessel wall was observed for all three configurations. The effect of water added to compensate for compression was found to be more pronounced for vessel with water inlet from top because the incoming colder water (298 K) flows under gravity and gets mixed with the bulk of the fluid, whereas for the water inlet from bottom again due to gravity, the added water remains closer to the bottom and does not get mixed with the bulk of fluid. **Figure 7-15(a, b, c)** shows the corresponding isotherms for the pressure hold phase. At the end of hold period, it was observed that maximum temperature dropped to 377 K for no water inlet (**Figure 7-15(a)**), 370 K for water inlet from top (**Figure 7-15 (b)**), and 380 K for water

inlet from bottom (Figure 7-15(c)).

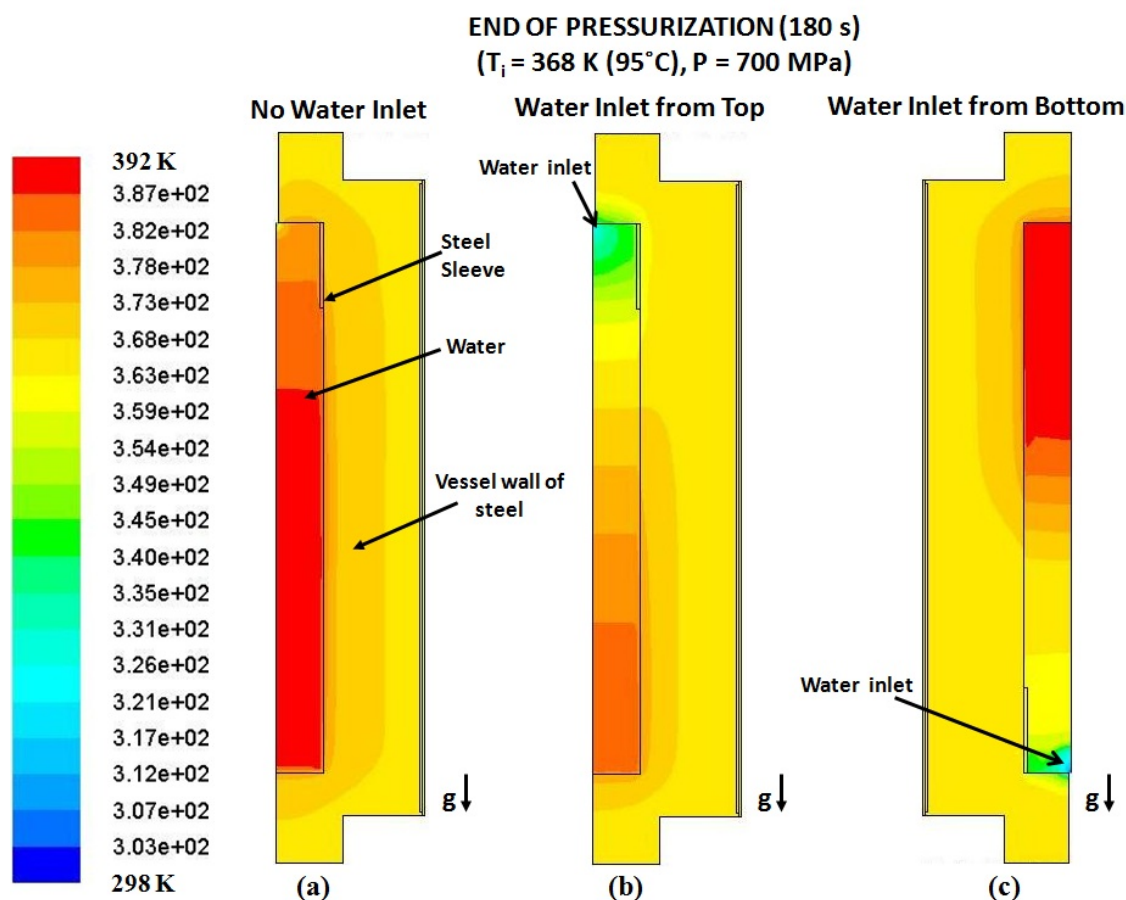


Figure 7-14: Isotherms in water and s.steel wall for 10 L vertical vessel at the end of pressurization (180 s) at $T_i = 368 \text{ K}$, $P = 700 \text{ MPa}$, $T_{\text{inlet}} = 298 \text{ K}$, $Q = 860,000 \text{ W/m}^3$ for ($0 \leq t \leq 180 \text{ s}$), (a) no water inlet, (b) water inlet from top, & (c) water inlet from bottom.

Figure 7-16 and Figure 7-17 show the corresponding streamlines in water at the end of pressurization and end of hold time, respectively. It shows that the colder water entering from the bottom of the vessel has less effect on the movement of fluid than the circulation caused due to buoyancy forces because the fluid entering from the bottom under the

gravity remains towards the bottom of the vessel and does not affect the fluid at a distance. **Figure 7-16(c)** shows that at the end of 600 s of hold period the velocity values were very low in water.

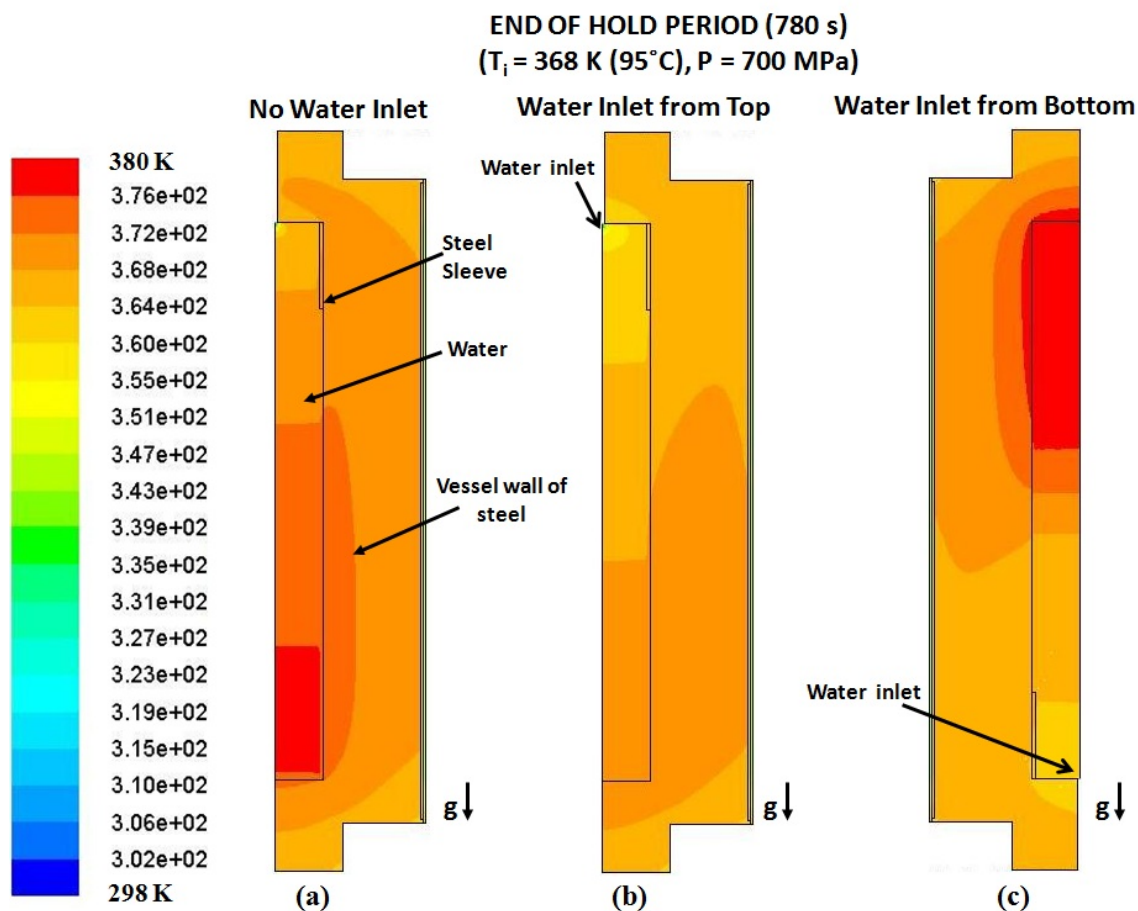


Figure 7-15: Isotherms in water and s. steel wall for vertical vessel at the end of hold time (780 s) at $T_i = 368 \text{ K}$, $P = 700 \text{ MPa}$, $T_{\text{inlet}} = 298 \text{ K}$, $Q = 860,000 \text{ W/m}^3$ for ($0 \leq t \leq 180 \text{ s}$), (a) no water inlet, (b) water inlet from top, & (c) water inlet from bottom.

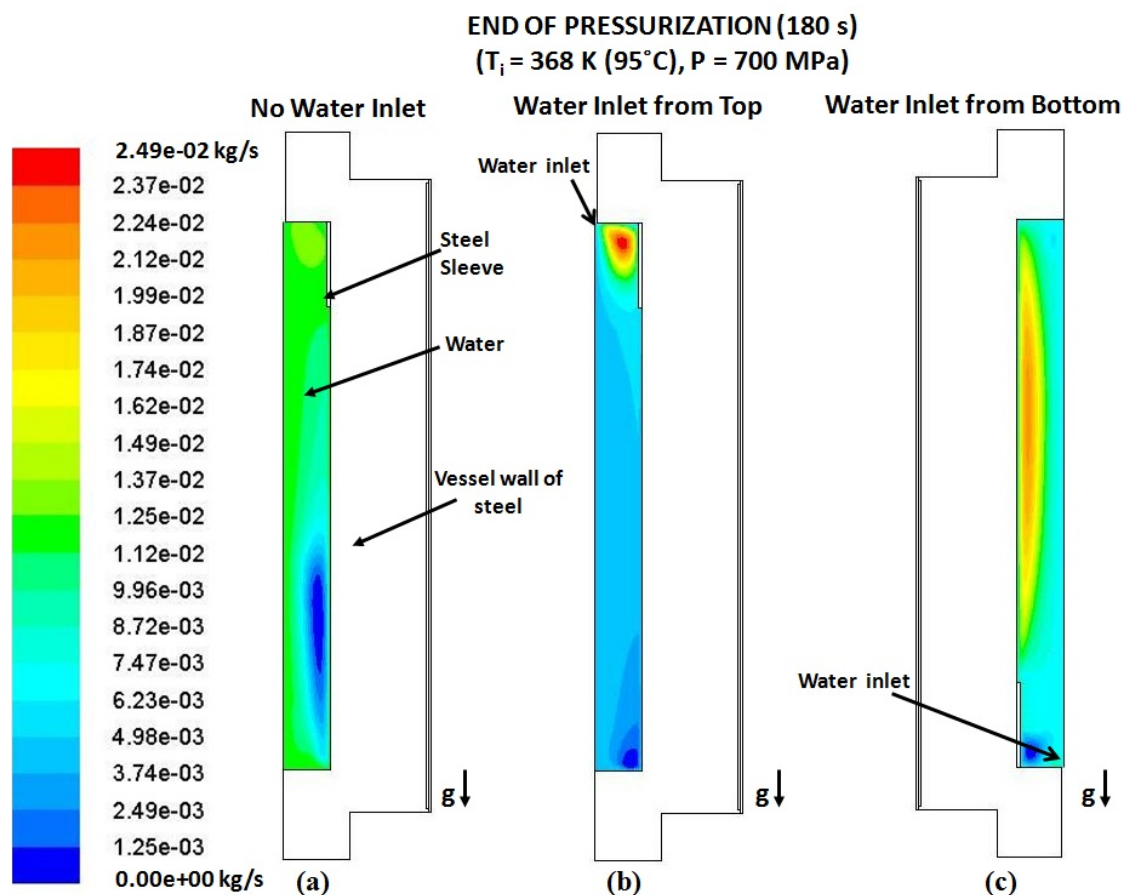


Figure 7-16: Streamlines in water and s.steel wall for 10 L vertical vessel at the end of pressurization (180 s) at $T_i = 368$ K, $P = 700$ MPa, $T_{inlet} = 298$ K, $Q = 860,000$ W/m³ for ($0 \leq t \leq 180$ s), (a) no water inlet, (b) water inlet from top, & (c) water inlet from bottom.

COV Comparison for Water Inlet from Top vs. Water Inlet from Bottom

The results obtained and discussed were compared in terms of 1) dimensionless temperature and 2) COV of temperature to understand the difference between the vertical vessels with water inlet from top and the water inlet from bottom. It is clear from the results above that the maximum temperature achieved during the water inlet from bottom was about 6 K higher than when the water inlet to the vessel was from the top. Also, the

hottest point in the vessel moved towards the top in case of water inlet from bottom as opposed to water inlet from the top closure.

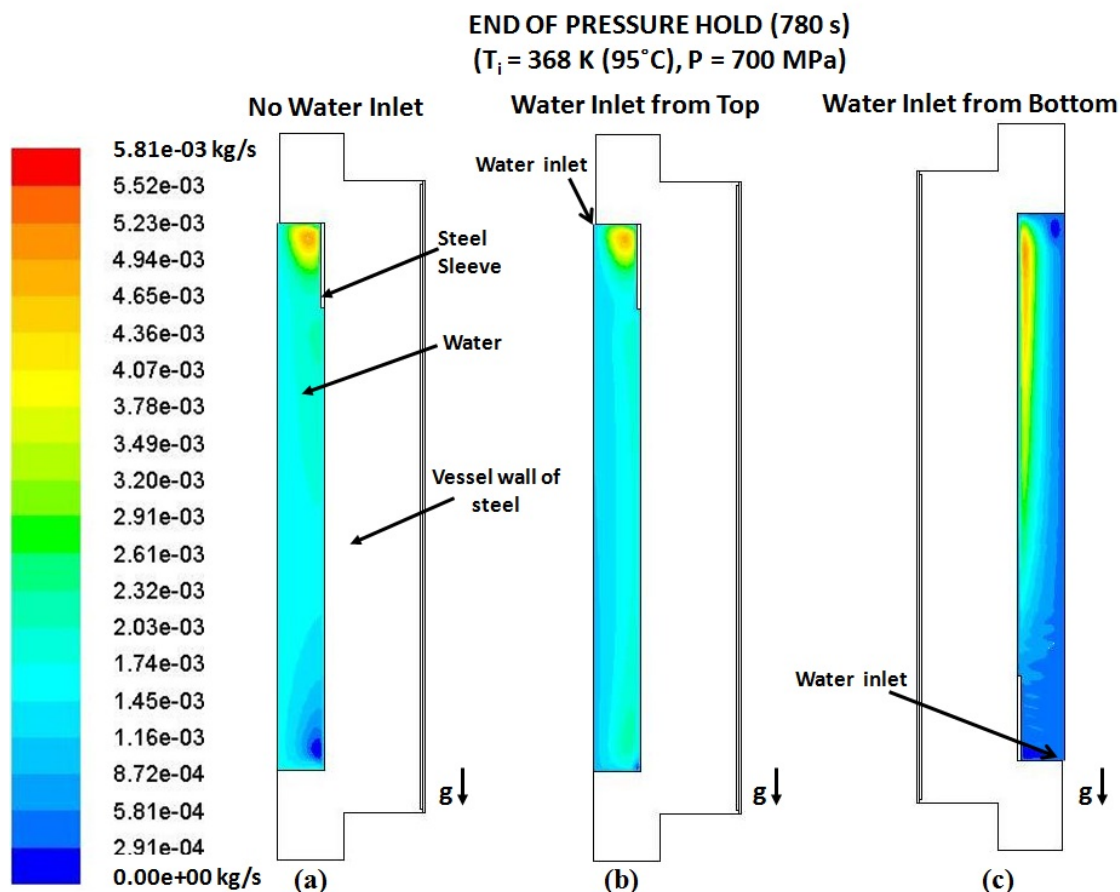


Figure 7-17: Streamlines in water and s.steel wall for vertical vessel at the end of hold time (780 s) at $T_i = 368$, $P = 700 \text{ MPa}$, $T_{\text{inlet}} = 298 \text{ K}$, $Q = 860,000 \text{ W/m}^3$ for $(0 \leq t \leq 180 \text{ s})$, (a) no water inlet, (b) water inlet from top, & (c) water inlet from bottom.

In order to compare the two cases in terms of uniformity in temperature, dimensionless temperature $[(T-T_i)/(T_{\text{max}}-T_i)]$ distributions were plotted along the axial and radial mid-planes of the 2D axisymmetric geometry, as shown in **Figure 7-18** and **Figure 7-19**. T_{max} was the maximum temperature and was obtained from the predicted time-temperature

history on the respective planes (axial and radial mid-planes). It can be seen from the **Figure 7-18** that in the axial (vertical) direction the water inlet from bottom tends to make the temperature distribution in the vessel more uniform as compared to the water inlet from top, whereas, the radial temperature distribution on the mid-plane in the vessel was found to be similar for the two cases, as shown in **Figure 7-19**.

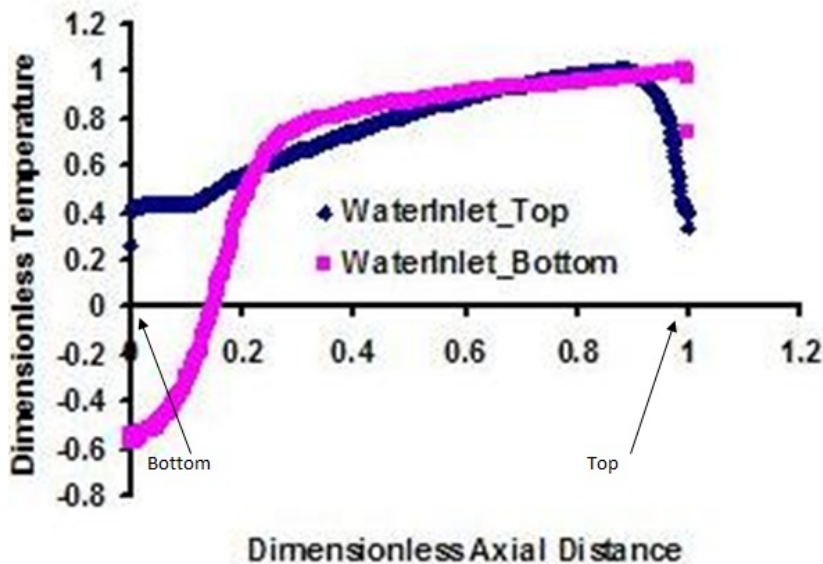


Figure 7-18: Numerically predicted dimensionless temperature variation along the vertical mid-plane at the end of pressure hold period (780 s) for water inlet from top and water inlet from bottom at $P = 700$ MPa and $T_i = 368$ K.

The second method used for comparison was coefficient of variation. **Figure 7-20** shows the COV of temperature for vertical vessel at $P = 700$ MPa, $T_i = 368$ K with no water inlet, water inlet from top and water inlet from bottom. It can be seen here that vessel with no water inlet has the lowest COV values followed by water inlet from top and water inlet from bottom, respectively, implying that vessel with no water inlet gives the most temperature uniformity. For water inlet from top, the COV values continuously

increased during pressurization due to cold water added into the vessel, peaking at end of pressurization and then decreased as the temperature tries to equilibrate. After approximately 220 s of hold time, COV values for water inlet from top approached COV values for no water inlet. Amongst water inlet from top and water inlet from bottom it can be observed that although the higher maximum temperature was achieved at the end of pressurization and hold period for water inlet from bottom, the higher COV values for water inlet from bottom throughout the process show that the temperature differences within the vessel were higher and thus COV values show more non-uniformity.

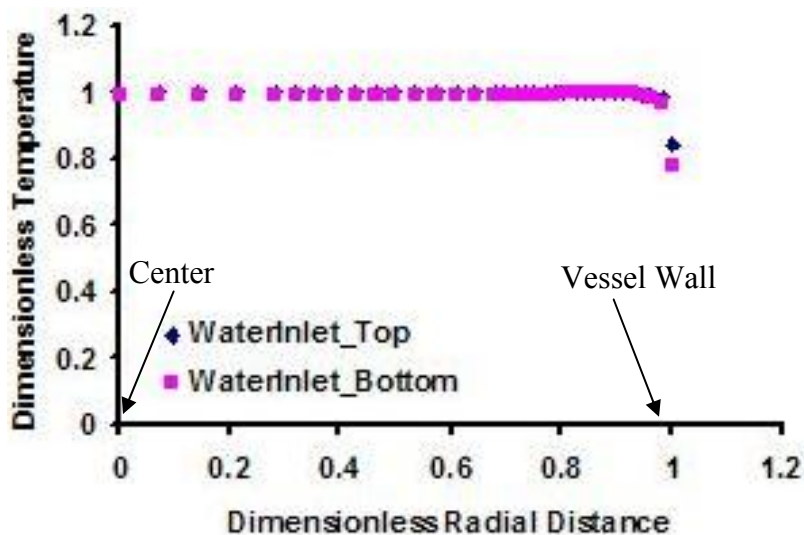


Figure 7-19: Numerically predicted dimensionless temperature variation along the radial mid-plane at the end of pressure hold period (780 s) for water inlet from top and water inlet from bottom at $P = 700$ MPa and $T_i = 368$ K.

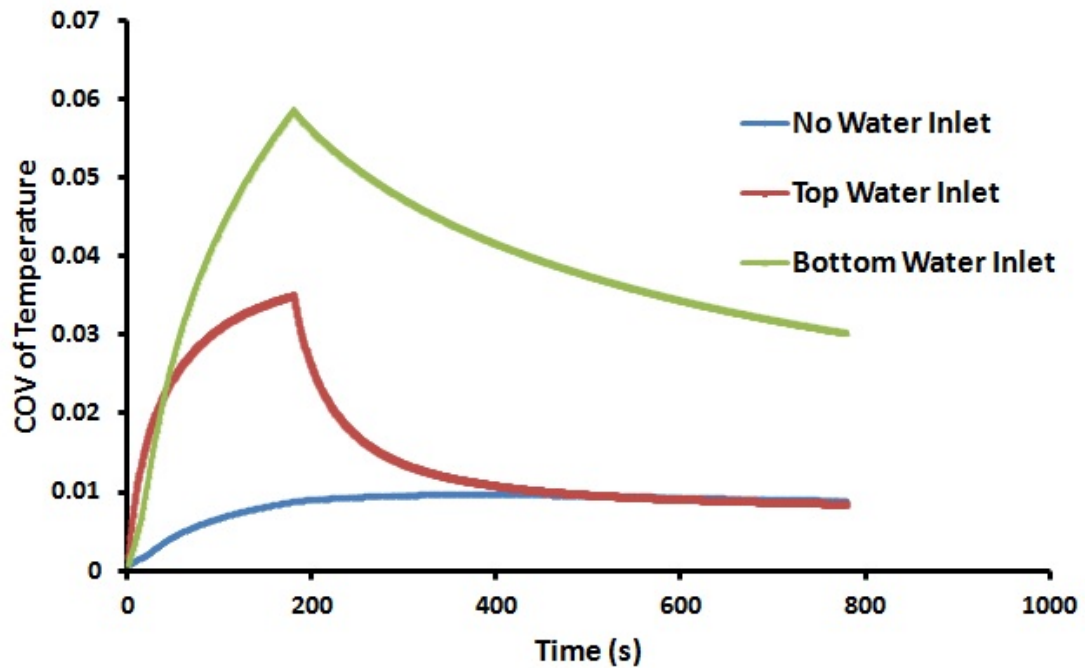


Figure 7-20: COV of temperature plotted against time for 10 L vertical high pressure vessel with no water inlet, water inlet from top and water inlet from bottom at $T_i = 368$ K, $P = 700$ MPa, $T_{inlet} = 298$ K, $Q = 860,000$ W/m³ for ($0 \leq t \leq 180$ s).

It was clear from the results and comparison seen above that temperature non-uniformity exists in the three configurations at different levels. In order to better quantify the implications of this non-uniformity in temperature on food safety, traditional F-value kinetics for *C. botulinum* was included in the numerical model. **Figure 7-21** shows the contours for *C. botulinum* inactivation in the vertical vessel at $P = 700$ MPa, $T_i = 368$ K for no water inlet, water inlet from top and water inlet from bottom. The **Figure 7-21** shows the $-\log N/N_0$ achieved at the end of the process for *C. botulinum*, based only on

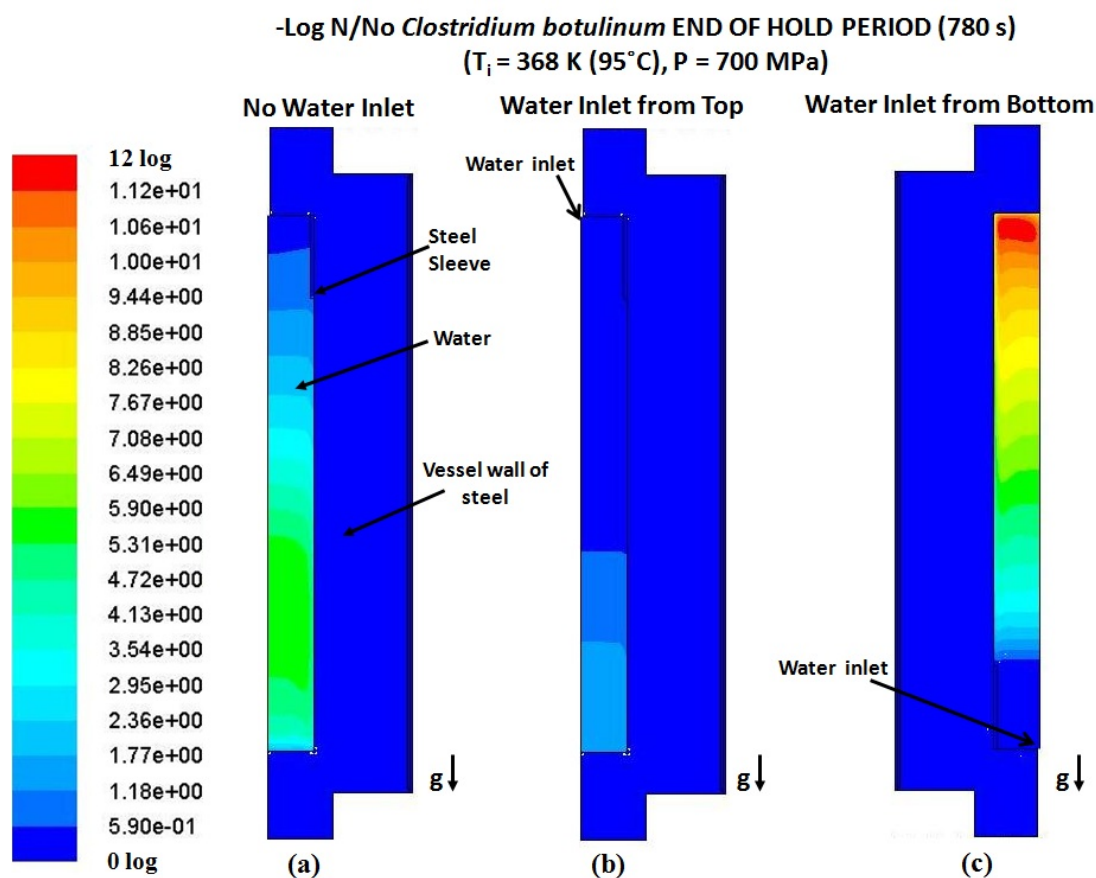


Figure 7-21: Contours for *C. botulinum* inactivation in water and s.steel wall for 10 L vertical vessel at the end of hold time (780 s) at $T_i = 368 \text{ K}$, $P = 700 \text{ MPa}$, $T_{\text{inlet}} = 298 \text{ K}$ $Q = 860,000 \text{ W/m}^3$ for $(0 \leq t \leq 180 \text{ s})$, (a) no water inlet, (b) water inlet from top, & (c) water inlet from bottom.

temperature history (no pressure affect was included in the inactivation kinetics). It can be seen from **Figure 7-21** that the non-uniform temperature resulted in non-uniform inactivation of *C. botulinum*. A maximum of 12 log reduction was achieved when the process was carried out with water inlet from bottom but only in the water very close to the top of the vessel. Similarly, although the maximum inactivation with no water inlet and water inlet from top was 6 log and 4 log respectively, on average, only about 8 log reduction was achieved for water inlet from bottom followed by 4 log for no water inlet

and 1 log for water inlet from top. From these results it is hard to compare the three configurations in terms of non-uniformity in inactivation; therefore, the results were studied further in terms of COV values.

Figure 7-22 shows the COV of *C. botulinum* inactivation for vertical vessel at $P = 700$ MPa, $T_i = 368$ K for no water inlet, water inlet from top and water inlet from bottom. It can be seen here that as we observed in COV of temperature, COV values of *C. botulinum* inactivation for no water inlet were lowest and hence most uniform process. Whereas for the water inlet from top and water inlet from bottom, the trend reversed compared to COV of temperature. The COV values for water inlet from top were higher than the water inlet from bottom.

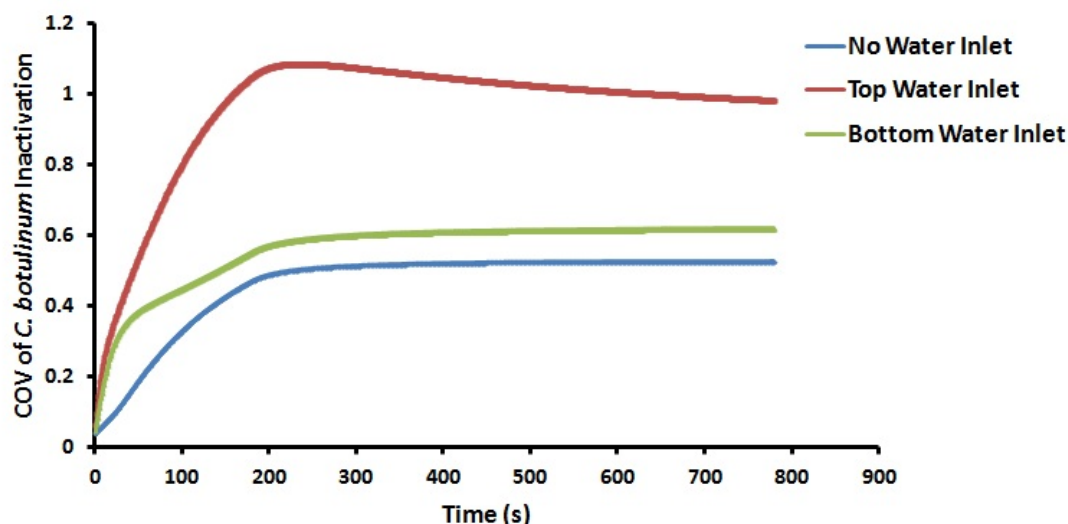


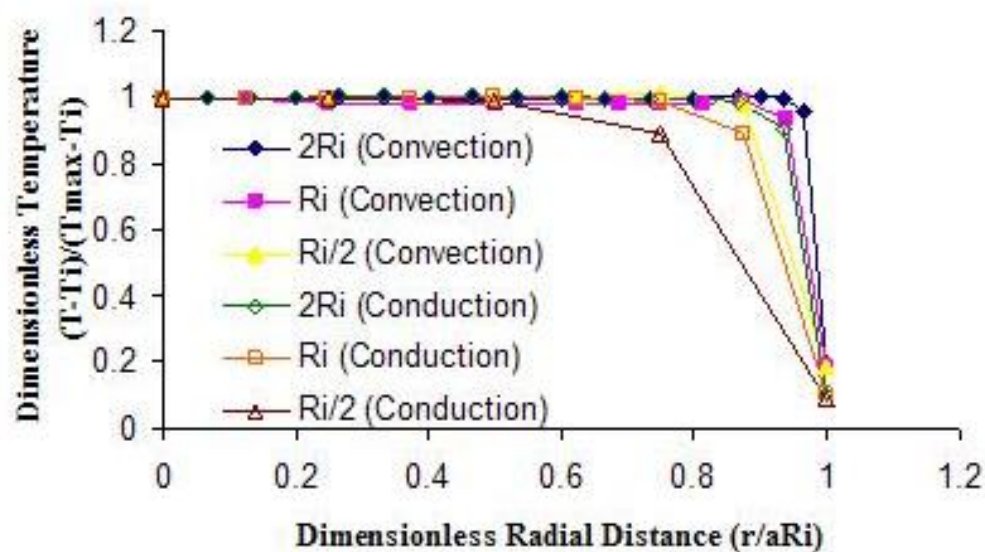
Figure 7-22: COV of *C. botulinum* inactivation plotted against time for vertical high pressure vessel with no water inlet, water inlet from top and water inlet from bottom $T_i = 368$ K, $P = 700$ MPa, $T_{inlet} = 298$ K, $Q = 860,000$ W/m³ for ($0 \leq t \leq 180$ s).

7.3.2.6 Effect of Vessel Size

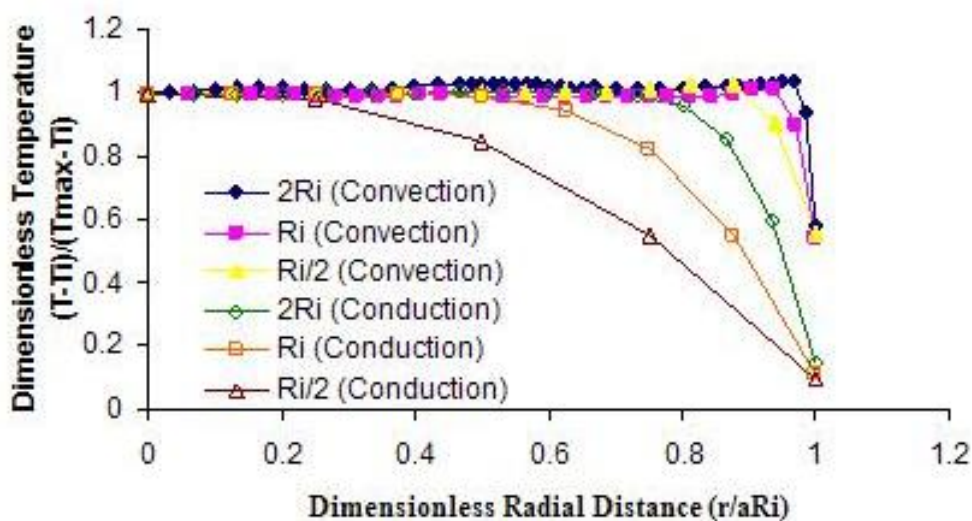
The numerical simulation program was further used to understand the effect of vessel size on the temperature distribution in water inside the vessel. Both conduction only (no gravity effects) and conjugate (conduction & convection) cases were compared. The effect of vessel size on numerically predicted temperature profiles for conduction only and conjugate cases, along the horizontal mid plane of the vessel are shown in **Figure 7-23(a)** at the end of pressurization and in **Figure 7-23(b)** at the end of pressure hold time, for three different sizes of the vessel i.e., keeping the same height but varying inner radius ($2R_i$, R_i and $R_i/2$). For numerical simulation purposes only, the thickness of the s.steel vessel was kept constant. The radial distance was non-dimensionalized with respect to aR_i where 'a' has the values 2, 1 and 0.5.

From **Figure 7-23(a)** and **Figure 7-23(b)** it can be seen that for conduction cases the distribution of the dimensionless temperature $(T-T_i)/(T_{\max}-T_i)$ becomes more uniform along dimensionless radial distance as the vessel size is increased. Similarly, during conjugate (conduction and convection) heat transfer cases it can be seen that vessel with $2R_i$ radius has the uniform distribution over a longer distance as compared to smaller radii vessels.

Between conduction only and conjugate heat transfer it was observed that the convection at the wall tends to make temperature distribution more uniform as compared to corresponding conduction case which is evident from **Figure 7-23(a)** and **Figure 7-23(b)**.



(a)



(b)

Figure 7-23: Numerically predicted dimensionless temperature variation along the horizontal mid-plane for vessels with different inner radii for $P = 700$ MPa, $T_i = 333$ K, $T_{inlet} = 298$ K, at the end of (a) pressurization (180 s), (b) hold period (780 s) for conduction only and conjugate heat transfers.

7.3.2.7 Effect of Insulating Sleeve

From the results described in the previous sections it is evident that one of the reasons for non-uniformity in temperature during high pressure process is due to heat loss to the thick metal wall of the vessel. One way to reduce the heat loss would be to add an insulating sleeve in the vessel. Therefore, the numerical simulation program was used to predict the temperature distribution in water with an insulating sleeve of certain thickness inserted in the vessel. Properties of Teflon[®] ($k = 0.2 \text{ W/m-K}$) (Tummala and Rymaszewski, 1997) as the material of the sleeve were used in the simulation model.

Numerical simulation was carried out when the initial temperature was 95°C (368 K) and vessel was pressurized to 700 MPa. The original vessel geometry was modified to include Teflon[®] insulation of 12.7 mm (=1/2 inch) thickness. A grid was regenerated with the insulation sleeve in place. The outer diameter of the sleeve was same as the inner diameter of the vessel, i.e., no gap between the sleeve and the vessel. A crude mesh was created and based on the velocity gradients in water arising during the process; the mesh was refined during simulation.

The predicted results were then compared in terms of isotherms, with and the without insulation sleeve, at initial temperature of 95°C (368 K). **Figure 7-24** and **Figure 7-25** show isotherms at the end of pressurization ($t = 180 \text{ s}$) and at the end of hold period ($t = 780 \text{ s}$), respectively. It can be seen from **Figure 7-24** that the maximum temperature of water in the vessel was 393 K when 12.7 mm thick insulation was used as compared to without insulation case in which the maximum temperature was 386 K at the end of

pressurization. Similarly, it can be seen from **Figure 7-25** that at the end of the hold period the maximum temperature in vessel with insulation was about 5K higher than the corresponding no insulation case. The average temperature in the vessel with insulation at the end of hold period was approximately 7 K higher and the region of warmer temperature extended over a longer vertical distance for the vessel with insulation as compared to the vessel with no insulation. Therefore, addition of insulation sleeve lead to warmer average temperature in the vessel. From isotherms presented in **Figures 7-24, 7-25**, it is hard to predict if insulation causes less temperature variation within the fluid (water), whether it is more uniform or not. Again, COV will be used to evaluate this.

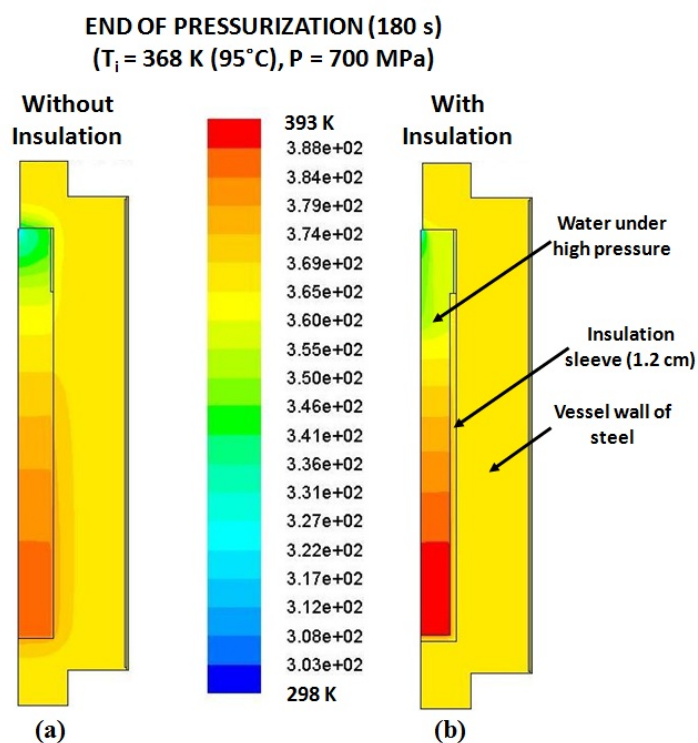


Figure 7-24: Isotherms in water and s. steel vessel for vertical vessel at $T_i = 368 \text{ K}$, $P = 700 \text{ MPa}$, $T_{\text{inlet}} = 298 \text{ K}$, $Q = 860,000 \text{ W/m}^3$ for $(0 \leq t \leq 180 \text{ s})$, (a) without insulation, & (b) with insulation (12.7 mm thick) at the end of pressurization (180 s).

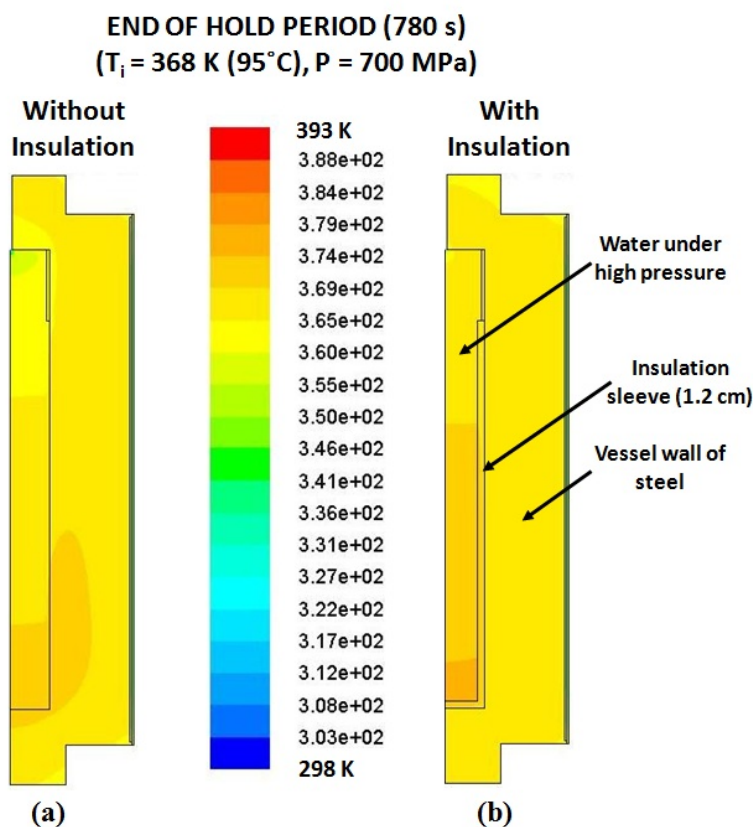


Figure 7-25: Isotherms in water and s.steel wall for vertical vessel at $T_i = 368 \text{ K}$, $P = 700 \text{ MPa}$, $T_{\text{inlet}} = 298 \text{ K}$, $Q = 860,000 \text{ W/m}^3$ for $(0 \leq t \leq 180 \text{ s})$, (a) without insulation, & (b) with insulation (12.7 mm thick) at the end of 600 s hold time (780 s).

The results presented so far show that temperature non-uniformity arises in a high hydrostatic pressure food processing vessel due to adiabatic compression heating, heat loss to the thick vessel wall, and water added to vessel to compensate for compression. As discussed, the two main sources that contribute to non-uniformity in temperature are water added for compression and heat loss at vessel wall. Therefore, the effect of adding water at temperature same as the initial temperature, at temperature same as the expected final temperature of process and effect of inserting an insulating sleeve to avoid heat loss

at wall on temperature distribution, were evaluated. **Figures 7-26, 7-27, and 7-28** shows the mean, the standard deviation and the COV of temperature, respectively, for a 10 L vertical high pressure vessel at 700 MPa and at different water inlet temperatures. It is clear from **Error! Reference source not found.** that adding the water at initial emperature of the process combined with insulation gives higher mean temperatures. **Figure 7-27** shows that the standard deviation in mean temperatures is smaller when the water added to the process was at initial or final temperature of the process. The COV of temperature (shown in **Figure 7-28**) calculated from ratio of standard deviation to mean, shows that changing the temperature of water added for compression to same as the initial temperature results in more uniformity compared to adding an insulation or even when water was added at initial temperature in presence of the insulation.

Figures 7-29, 7-30, and 7-31 show the corresponding mean, standard deviation and COV, respectively, of *C. botulinum* inactivation. **Figure 7-29** shows that although, the mean log reduction of *C. botulinum* was highest when water was added to the process at initial process temperature combined with insulation, the corresponding standard deviation was also highest, as shown in **Figure 7-30**.

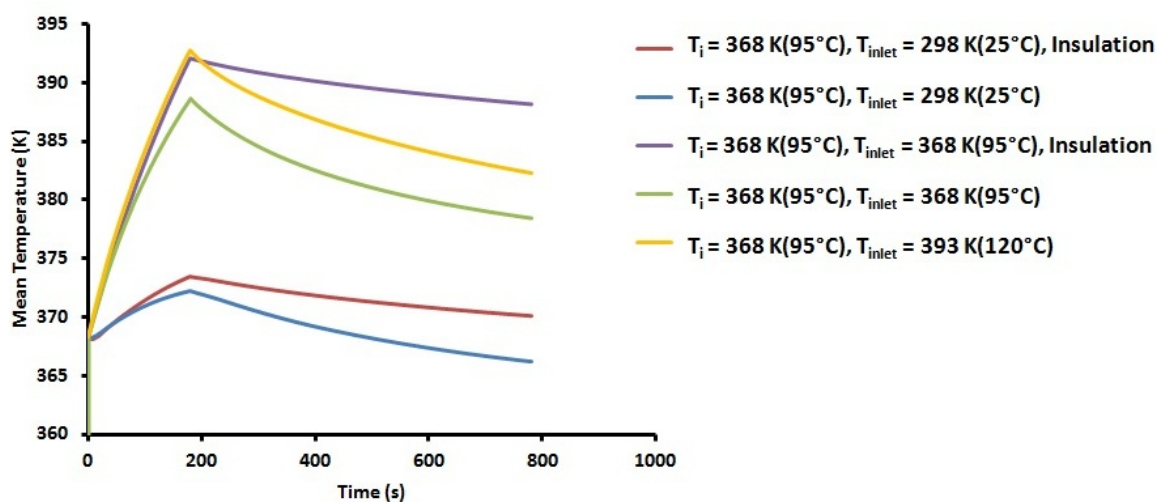


Figure 7-26: Mean (volume average) temperature for 10 L vertical vessel at $P = 700 \text{ MPa}$, $Q = 860,000 \text{ W/m}^3$ for pressurization ($0 \leq t \leq 180 \text{ s}$), 600 s hold time ($t = 780 \text{ s}$) & $T_i = 368 \text{ K}(95^\circ\text{C})$, $T_{\text{inlet}} = 298 \text{ K}(25^\circ\text{C})$, 368 K (95°C), 393 K (120°C) with or without insulation.

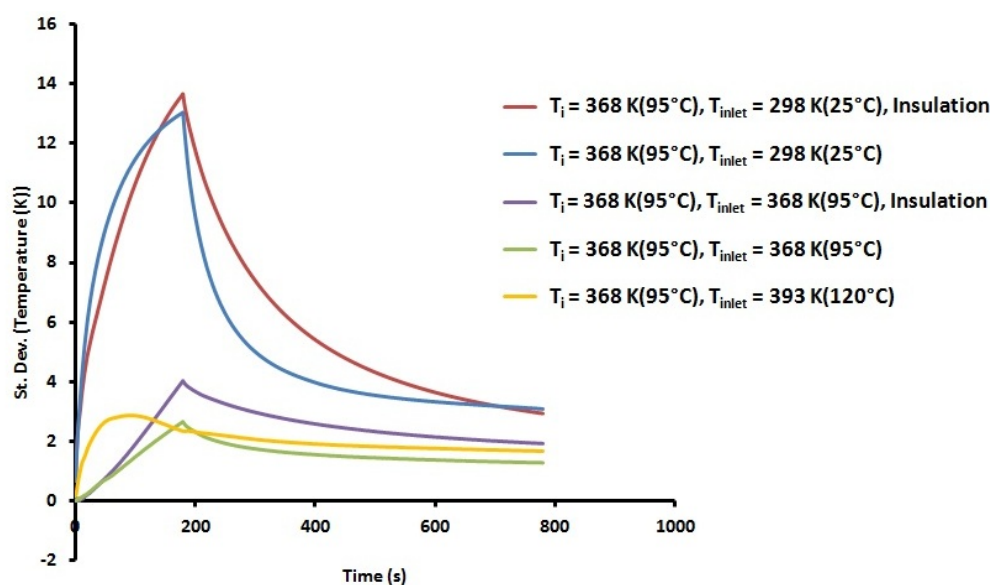


Figure 7-27: Standard deviation in mean temperatures for 10 L vertical vessel at $P = 700 \text{ MPa}$, $Q = 860,000 \text{ W/m}^3$ for pressurization ($0 \leq t \leq 180 \text{ s}$), 600 s hold time ($t = 780 \text{ s}$) & $T_i = 368 \text{ K}(95^\circ\text{C})$, $T_{\text{inlet}} = 298 \text{ K}(25^\circ\text{C})$, 368 K (95°C), 393 K (120°C) with or without insulation.

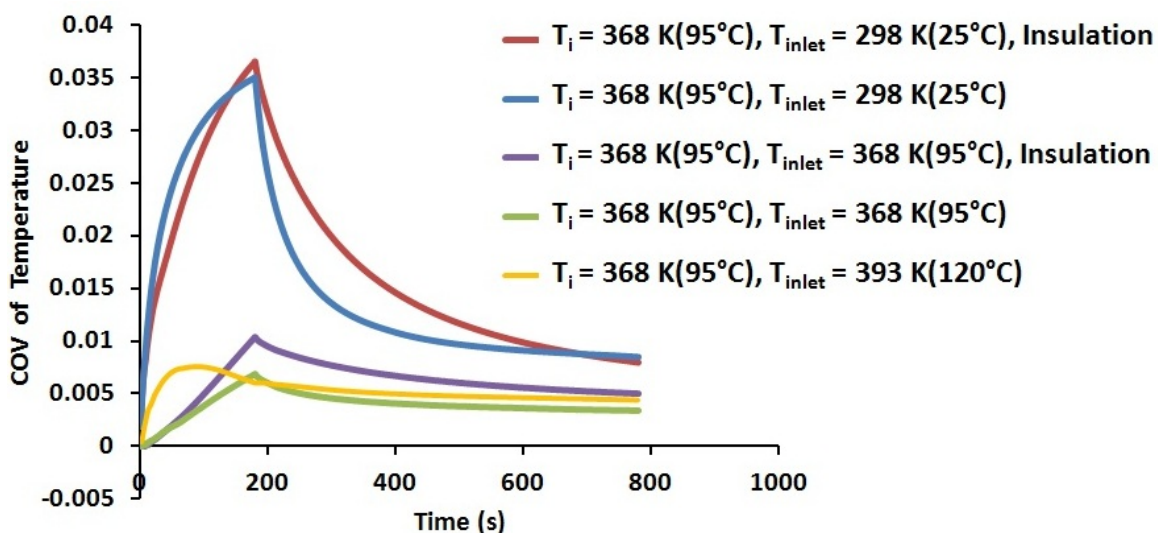


Figure 7-28: COV of temperature for 10 L vertical vessel at $P = 700$ MPa, $Q = 860,000$ W/m³ for pressurization ($0 \leq t \leq 180$ s), 600 s hold time ($t = 780$ s) & $T_i = 368$ K (95°C), $T_{inlet} = 298$ K (25°C), 368 K (95°C), 393 K (120°C) with or without insulation.

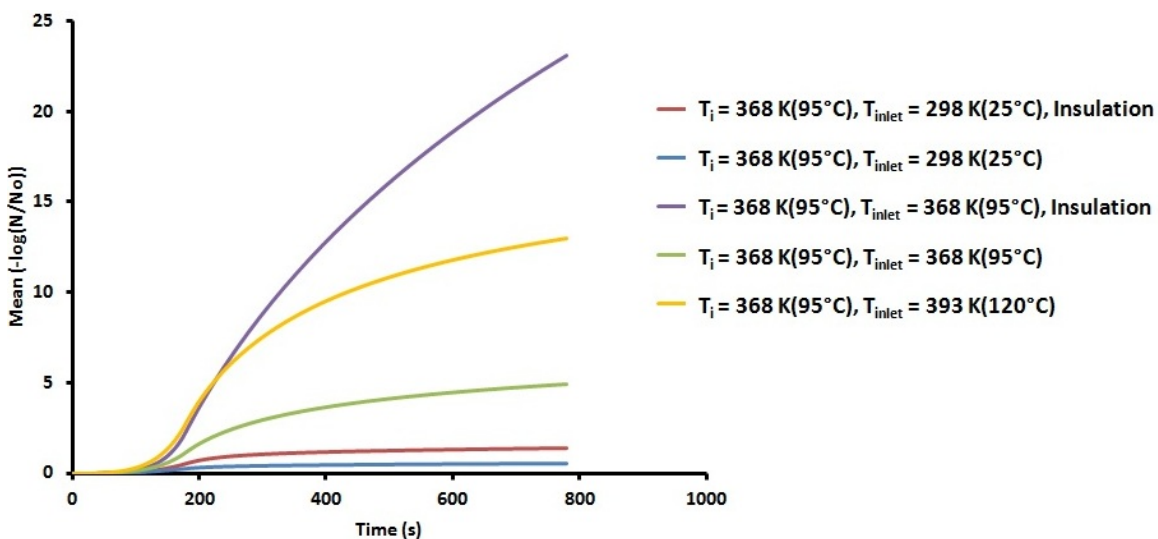


Figure 7-29: Mean log reduction of *C. botulinum* for 10 L vertical vessel at $P = 700$ MPa, $Q = 860,000$ W/m³ for pressurization ($0 \leq t \leq 180$ s), 600 s hold time ($t = 780$ s) & $T_i = 368$ K (95°C), $T_{inlet} = 298$ K (25°C), 368 K (95°C), 393 K (120°C) with or without insulation.

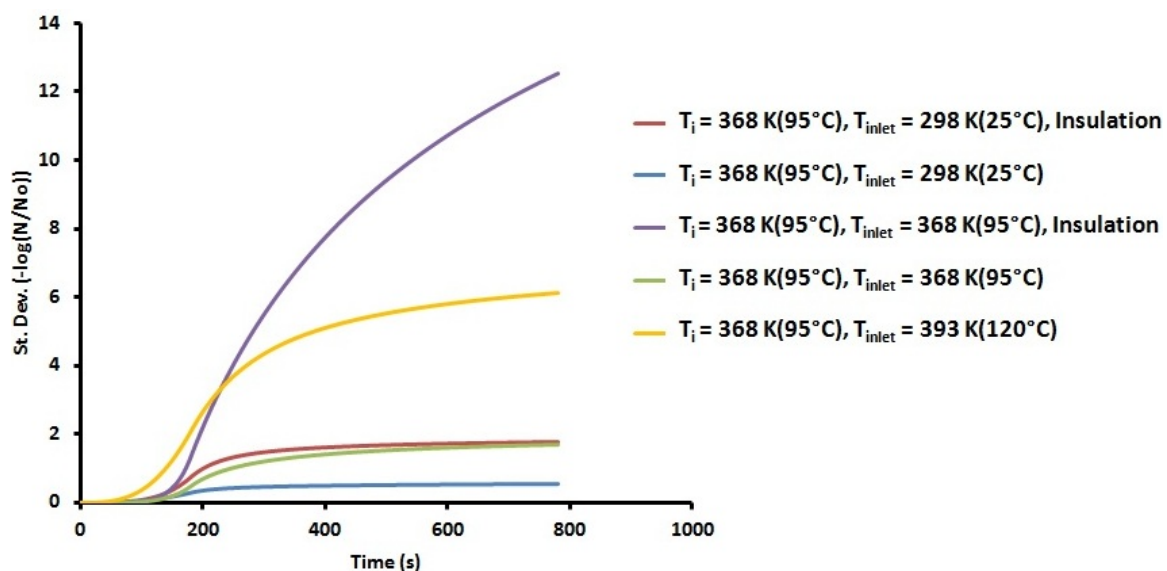


Figure 7-30: Standard deviation in mean log reduction of *C. botulinum* for 10 L vertical vessel at $P = 700 \text{ MPa}$, $Q = 860,000 \text{ W/m}^3$ for pressurization ($0 \leq t \leq 180 \text{ s}$), 600 s hold time ($t = 780 \text{ s}$) & $T_i = 368 \text{ K}$ (95°C), $T_{\text{inlet}} = 298 \text{ K}$ (25°C), 368 K (95°C), 393 K (120°C) with or without insulation.

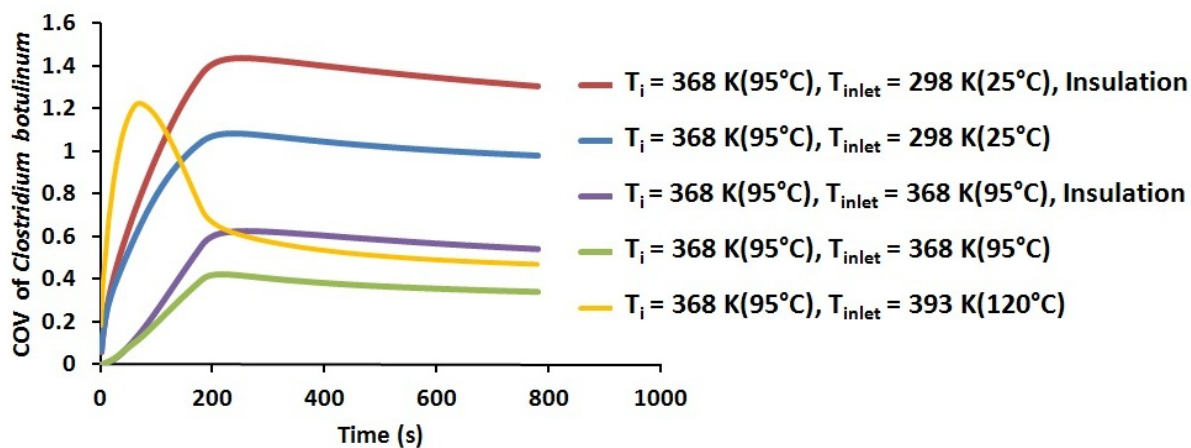


Figure 7-31: COV of *C. botulinum* inactivation for 10 L vertical vessel at $P = 700 \text{ MPa}$, $Q = 860,000 \text{ W/m}^3$ for pressurization ($0 \leq t \leq 180 \text{ s}$), 600 s hold time ($t = 780 \text{ s}$) & $T_i = 368 \text{ K}$ (95°C), $T_{\text{inlet}} = 298 \text{ K}$ (25°C), 368 K (95°C), 393 K (120°C) with or without insulation.

7.3.2.8 Effect of Inserting Pouches

The results discussed so far, were related to cases in which no food packages were present in the pressure vessel. However, from the commercial point of view, it is important to understand the temperature distribution during the high pressure process when food packages are being processed. **Figure 7-32** shows the temperature distributions inside oil pouches and in water at the end of pressurization (a) and at the end of pressure hold time (b) of 600 s when maximum pressure maintained was 700 MPa and initial temperature was 333 K. It can be seen that the temperature rise in oil pouches was more than the pressurizing medium water and, therefore, there was a simultaneous heat transfer from pouch to water and from water to the steel mass. This heat transfer results in temperature variation within each pouch and, also temperature variation from pouch to pouch. A temperature difference of approximately 8 K was observed in the individual pouches, which can lead to non-uniform inactivation of thermally labile entities such as spores in different food pouches.

7.3.2.9 Effect of Multiple Pressure Pulses (or Pressure Cycling)

Pulsed high pressure treatment has been shown to be more effective for inactivation of certain yeast, micro-organisms and enzymes compared to single pressure pulse (Meyer, 2000). In this section, the temperature non-uniformity arising during single high pressure pulse treatment at 700 MPa for 10 min pressure hold time was compared with 5 pressure pulses at 700 MPa for 2 min hold time each. The results in terms of the variation of temperature with time for each pulse are shown in **Figure 7-33**. In this case, the

depressurization (5 s) stage was also included in the simulation, as shown by small but sharp temperature drop at the end of each cycle.

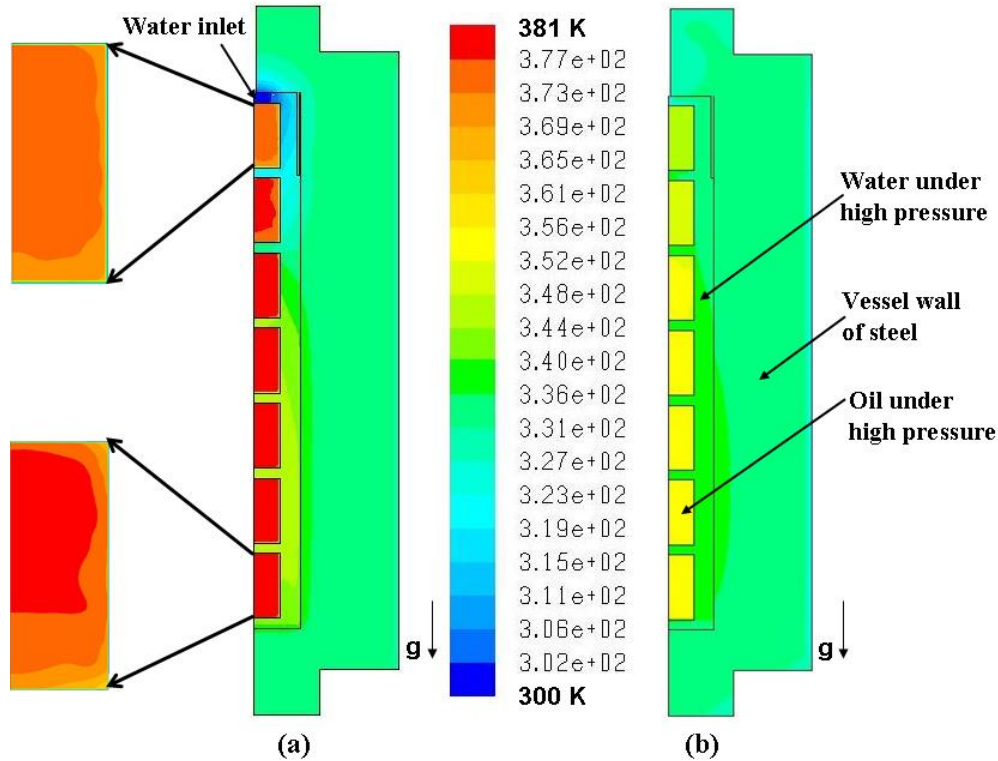


Figure 7-32: Isotherms in water, oil pouches, and s.steel wall for 10 L vertical vessel at $P = 700$ MPa, $T_i = 333$ K (60°C), $T_{\text{inlet}} = 298$ K (25°C), Q (water) = $450,000$ W/m³ for ($0 \leq t \leq 180$ s), Q (olive oil) = $750,000$ W/m³ for ($0 \leq t \leq 180$ s), at the end of (a) pressurization ($t = 180$ s), (b) pressure hold ($t = 780$ s).

Figure 7-34 shows the COV of temperature for single pressure pulse for 10 min hold time and for 5 pressure pulses of 2 min hold time each. It can be interpreted that multiple pressure pulses extend the period of temperature non-uniformity more than a single pulse of longer duration. **Figures 7-35 and 7-36** show the mean and COV, respectively, of *C. botulinum* inactivation. It is clear that multiple pulse gives higher log reduction, i.e., more inactivation of *C. botulinum*, as compared to a single pulse of longer duration.

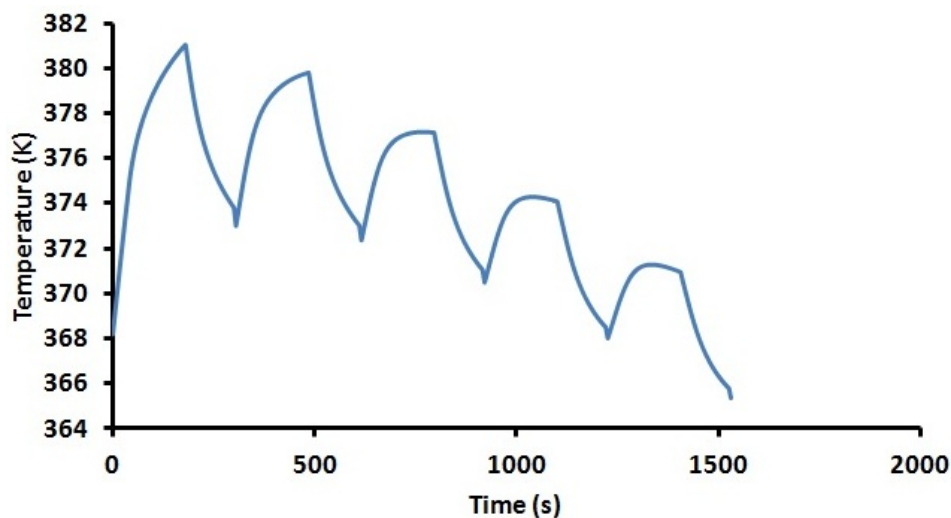


Figure 7-33: Numerically predicted time-temperature data at a selected point ($z = 546$ mm, $r = 61$ mm) in the 10 L vertical vessel for 5 pressure pulses (700 MPa) of 2 min hold time each, $T_i = 368$ K (95°C), $T_{\text{inlet}} = 298$ K (25°C) & $Q = 860,000$ W/m³ for pressurization.

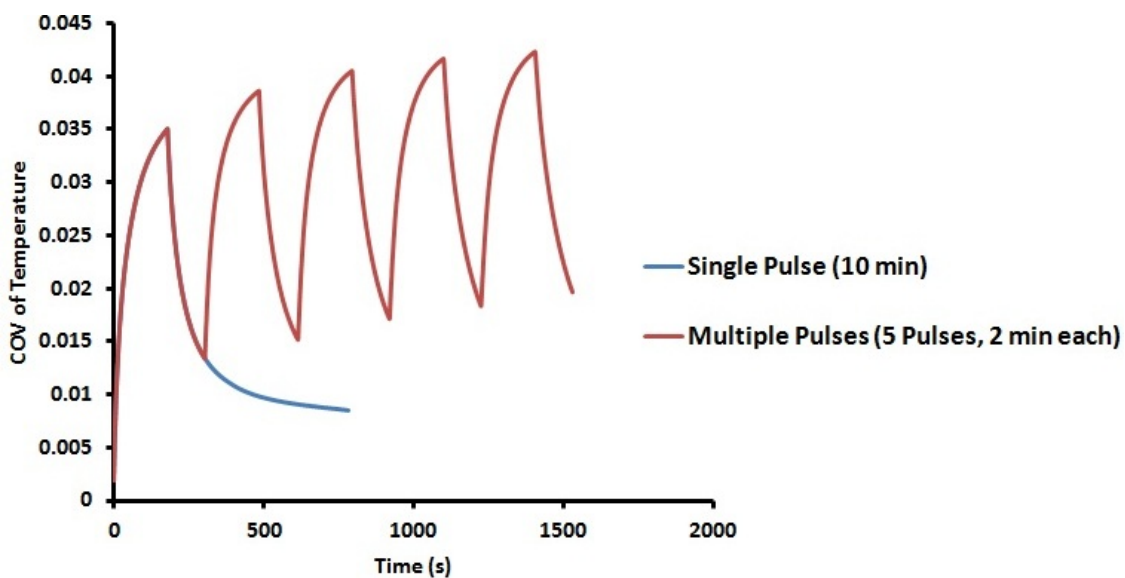


Figure 7-34: COV of temperature for 10 L vertical vessel at $T_i = 368$ K (95°C), $T_{\text{inlet}} = 298$ K (25°C), $Q = 860,000$ W/m³ for pressurization – single pressure pulse ($P = 700$ MPa) for 10 min hold time, 5 pulses (700 MPa) for 2 min hold time each.

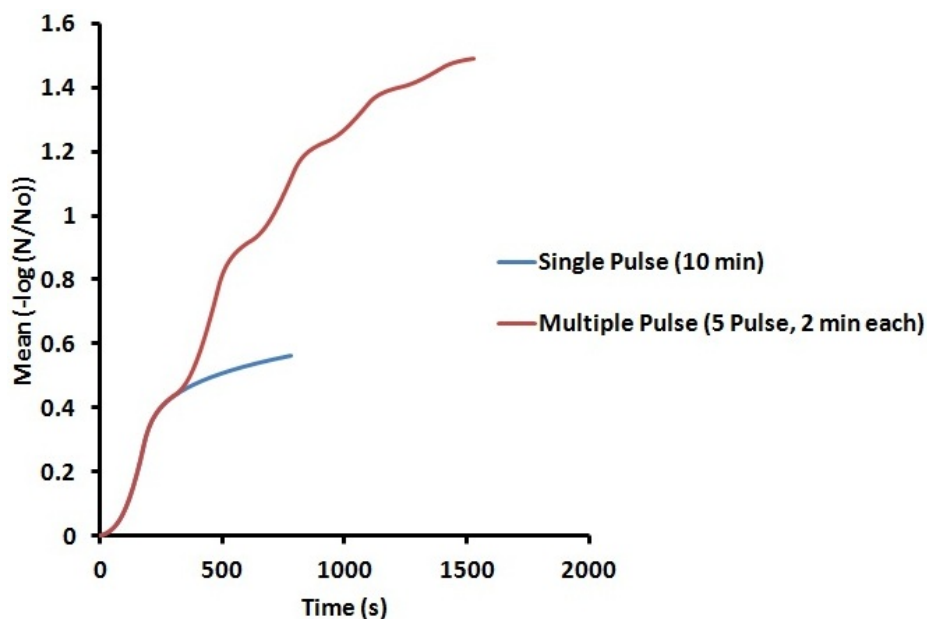


Figure 7-35: Mean of *Clostridium botulinum* inactivation for 10 L vertical vessel at $T_i = 368$ K (95°C), $T_{\text{inlet}} = 298$ K (25°C), $Q = 860,000$ W/m³ for pressurization - single pressure pulse ($P = 700$ MPa) for 10 min hold time, 5 pulses (700 MPa) for 2 min hold time each.

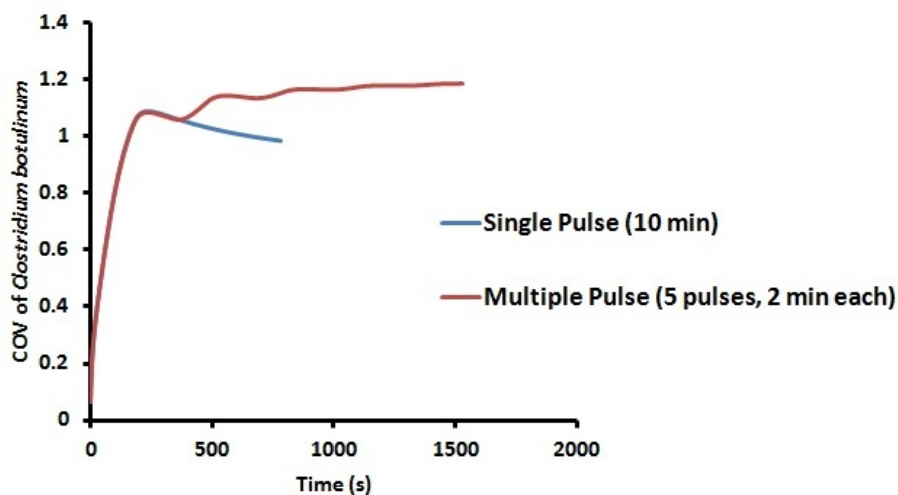


Figure 7-36: COV of *Clostridium botulinum* inactivation for 10 L vertical vessel at $T_i = 368$ K (95°C), $T_{\text{inlet}} = 298$ K (25°C), $Q = 860,000$ W/m³ for pressurization - single pressure pulse ($P = 700$ MPa) for 10 min hold time, 5 pulses (700 MPa) for 2 min hold time each.

7.3.3 Temperature and *C. botulinum* Distributions in Horizontal Vessel

As discussed in section 1.5 the commercial high pressure units are available with pressure vessels that can operate in vertical or horizontal positions, although vertical vessels came first and are more common. Horizontal vessel design was primarily built in response to the commercialization of high pressure process, i.e., demand for larger capacity vessels. From high pressure equipment design and safety point of view, in order to increase capacity, it is recommended to increase the length of the vessel than the diameter. It helps serve installations where vertical space is limited and minimum plant alteration is required. Also, horizontal vessel allows single direction in-line product flow which is favored by most regulatory agencies and is better from HACCP perspective for all food processes because it allows separation of processed and unprocessed food products. Another advantage of horizontal vessel over vertical vessel is that horizontal vessel can be run semi-continuous by keeping the next sample ready to load on the line whereas for a vertical vessel, the sample has to be completely unloaded first before loading the next sample.

To predict the temperature distribution in a horizontal high pressure vessel, the numerical simulation was carried out in a 3D meshed geometry, as shown in **Figure 6-3**. The dimensions for the 10 L vessel were assumed to be the same as the in-house vertical unit, only difference being that the horizontal vessel had water inlets from both the ends. The 350 L commercial vessel dimensions were obtained from a leading high pressure processing equipment manufacturer (see section 6.1.2 for major dimensions).

7.3.3.1 Pressure Assisted Thermal Sterilization (PATS)

Figure 7-3737 shows the isotherms in water and the s.steel wall for horizontal vessel when pressure was increased from 0.1 to 700 MPa in 180 s, the process was carried out at initial temperature of 368 K (95°C) and water inlet to the vessel was at 298 K (25°C). At the end of pressurization, the maximum temperature in the vessel reached 391 K, i.e., the temperature of water increased from 368 K to 391 K ($\Delta T_{\max} = 23$ K) due to compression heating as shown in **Figure 7-3737(b)**. The average temperature in the vessel at this point was 385 K, suggesting the heat loss occurring due to mixing of the water in the vessel with water added to compensate for compression which is at 298 K, heat loss to vessel wall and buoyancy currents. At the end of pressure hold period, the temperature in the vessel dropped to 378 K with higher temperature region on top. It was observed that the water entering the vessel from both ends to compensate for compressed water only affected the temperature of the water close to the inlets because of its low velocity and movement towards the bottom under gravity. It did not mix with the majority of the fluid in the vessel.

Similarly, **Figure 7-38(a)** and **Figure 7-38(b)** show the isotherms in water for the horizontal vessel (350 L) vertical slices at the end of pressurization (180 s) and hold time (480 s) when pressure was increased from 0.1 to 586 MPa. The maximum temperature achieved in the vessel after compression was 362 K, which dropped to 353 K at the end of 600 s of pressure hold time. Overall, a trend similar to 10 L vessel was observed.

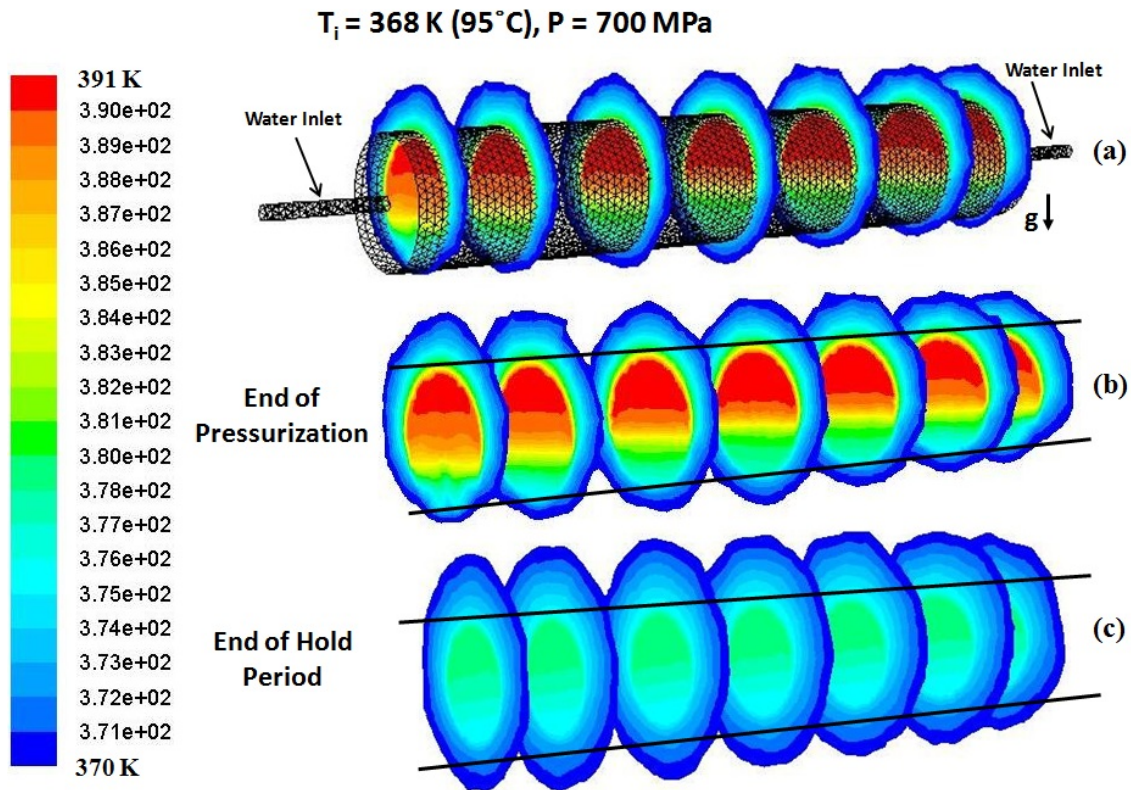


Figure 7-37: Isotherms in water and s.steel wall for 10 L horizontal vessel (vertical slices) of at $T_i = 368 \text{ K}$, $P = 700 \text{ MPa}$, $Q \text{ (water)} = 860,000 \text{ W/m}^3$ for $(0 \leq t \leq 180 \text{ s})$, with water inlet from both sides $T_{\text{inlet}} = 298 \text{ K}$, (a) location of vertical slices w.r.t. pressure cavity, (b) end of pressurization (180 s), & (c) after 600 s hold time (end of 780 s).

7.3.3.2 Effect of Vessel Size

For horizontal vessel, the effect of vessel size on temperature distribution in the vessel was predicted by carrying out numerical simulation in 2D symmetric vertical slice. The effect of vessel size on numerically predicted temperature profiles were simulated and plotted along the radial and vertical mid planes (as shown in **Figure 7-399**) of the vessel for three different sizes of the vessels ($2R_i$, R_i and $R_i/2$).

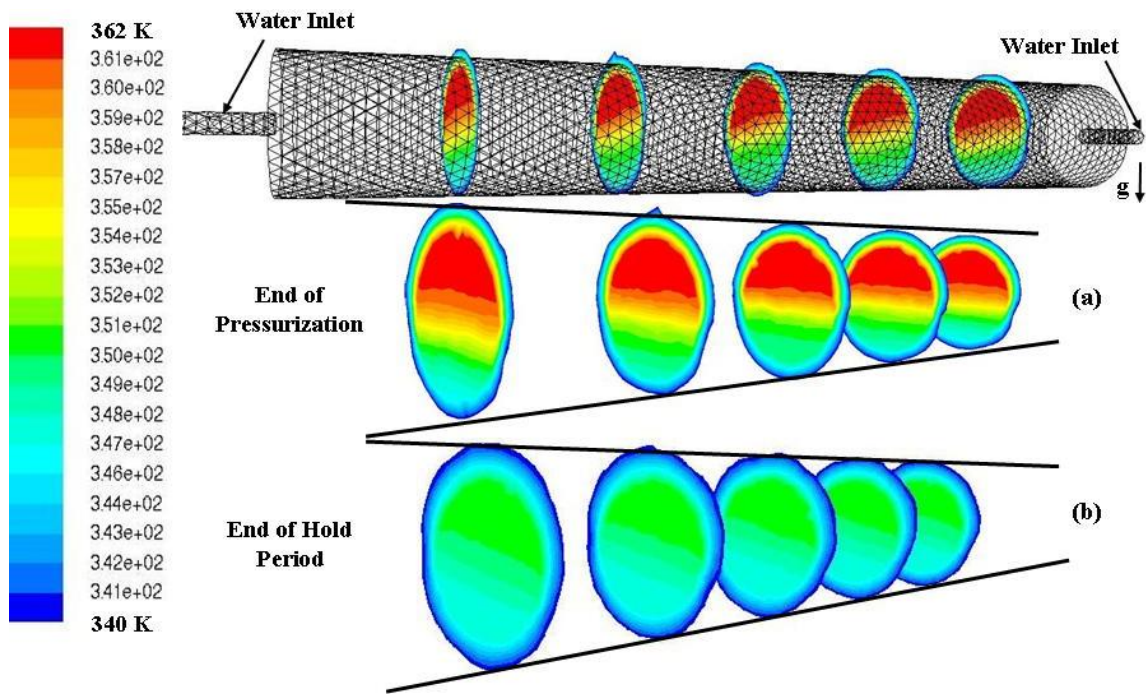


Figure 7-38: Isotherms in water and s.steel wall for horizontal vessel (vertical slices) of 350 L at $T_i = 333$ K, $P = 586$ MPa, Q (water) = $480,000$ W/m³ for ($0 \leq t \leq 180$ s), with water inlet from both sides $T_{inlet} = 298$ K, (a) end of pressurization (180 s) & (b) after 600 s hold time (end of 780 s).

7.3.3.3 Effect of Insulating Sleeve

To understand the effect of inserting a Teflon[®] ($k = 0.2$ W/m-K) insulating sleeve in the horizontal vessel on temperature distribution, the horizontal vessel geometry was modified to include an insulation (12.7 mm thick). The insulation was such that it covered the inner surface area of the cylindrical pressure cavity except the top and bottom. The outer diameter of the sleeve was same as the inner diameter of the vessel. A crude mesh was created and based on the velocity gradients arising during the process; the mesh was refined.

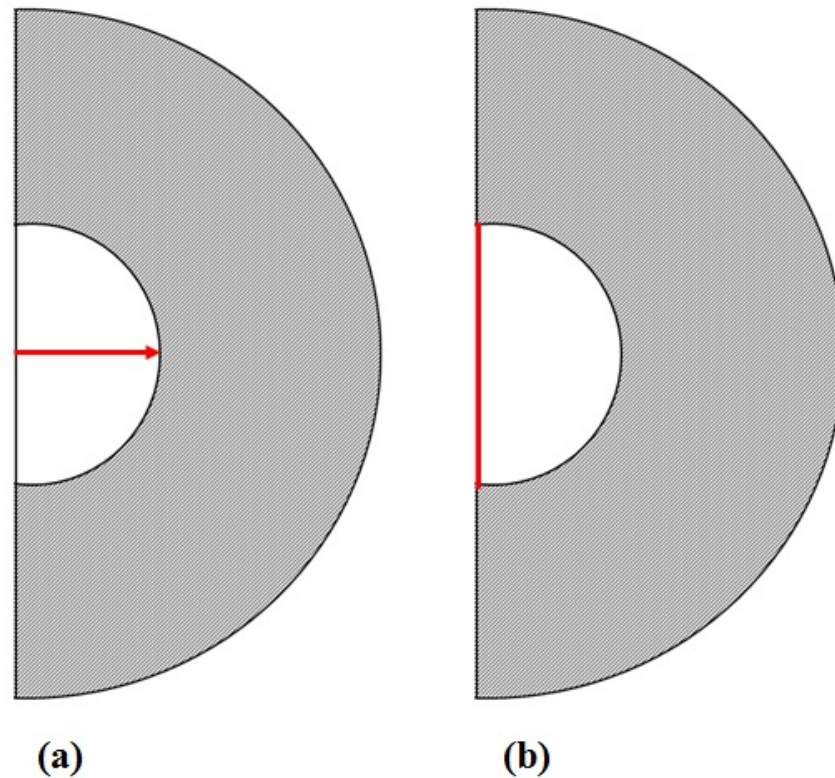


Figure 7-39: 2D symmetric slice of horizontal vessel showing (a) radial mid-plane and (b) vertical mid-plane for plotting variable radius vessel results.

Figure 7-40 and **Figure 7-41** shows the dimensionless temperature variation along the radial mid-plane and vertical plane (shown in **Figure 7-39**) of the horizontal vessel. It was observed that the dimensionless temperature $(T-T_i)/(T_{\max}-T_i)$, distribution becomes more uniform as the vessel size increases for both conduction and conjugate (including conduction and convection) cases.

Numerical simulation of horizontal vessel with insulation was carried out when the initial temperature was 95°C (368 K) and vessel was pressurized to 700 MPa with temperature of inlet water as 298 K. The predicted results were then compared with the without

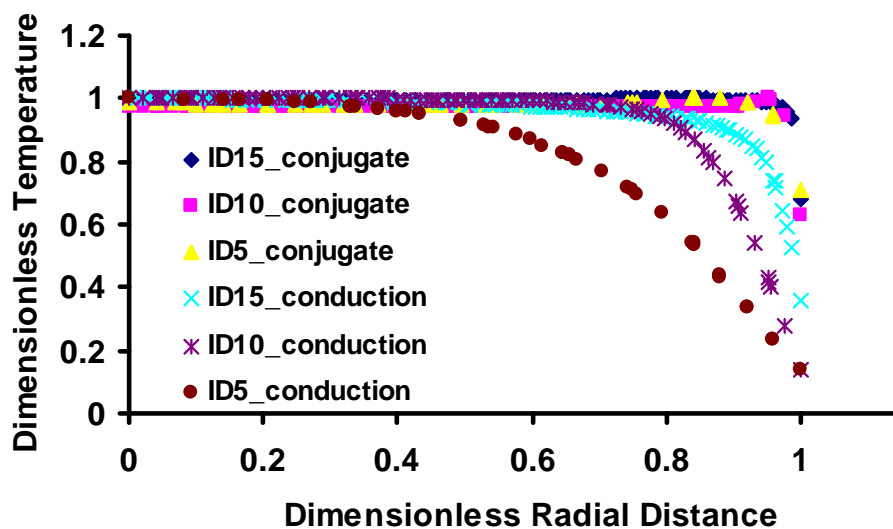


Figure 7-40: Numerically predicted dimensionless temperature variation along the radial mid plane for horizontal vessels with different inner radii, $T_i = 368$ K, $P = 700$ MPa, at the end of hold time (780 s).

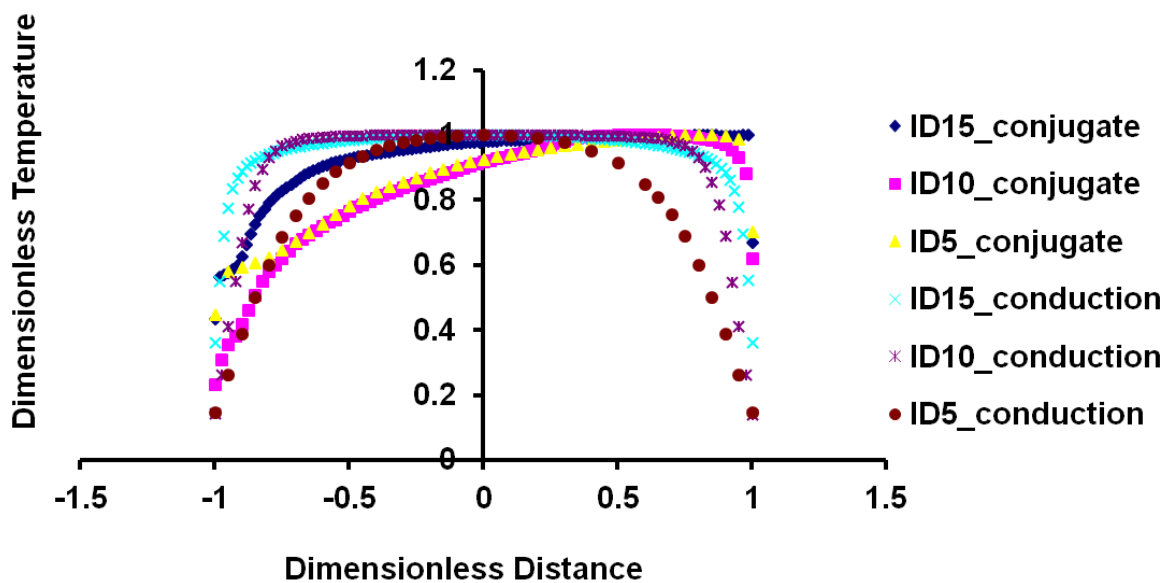


Figure 7-41: Numerically predicted dimensionless temperature variation along the vertical plane for horizontal vessels with different inner radii, $T_i = 368$ K, $P = 700$ MPa, at the end of hold time (780 s).

insulation case at same pressure and temperature conditions. **Figure 7-42** and **Figure 7-43** show isotherms at the end of pressurization (180 s) and end of hold (780 s) respectively. At the end of pressurization, the maximum temperature of water in the vessel with insulating sleeve reached 394 K as opposed to 391 K in the case with no insulation as shown in **Figure 7-42**. Here, it was observed that the average temperature of water in the vessel at end of pressurization was same (385 K) for both the cases, with and without insulation. This could be attributed to that although the temperature of water was higher for vessel with insulation but it creates a larger temperature difference in the vessel which causes faster heat transfer and thus similar average temperatures. At the end of pressure hold period, the average temperature of water in the vessel with insulation dropped to 384 K, i.e., 6 K higher than the vessel with no insulation where the average temperature was 378 K as shown in **Figure 7-43**.

To further understand and compare the temperature distribution for various initial and inlet temperatures, with and without insulation, COV values were plotted against time. From results, it was observed that the non-uniformity peaks during the end of pressurization because of the increasing temperature difference in the vessel, i.e., greater standard deviation whereas as the process goes in hold period the water inlet effects go away and temperatures try to equilibrate bringing the COV down. **Figure 7-44** shows the COV of temperature for horizontal vessel for pressure of 700 MPa, initial temperature of 368 K and temperature of water inlet of 298 K or 368 K.

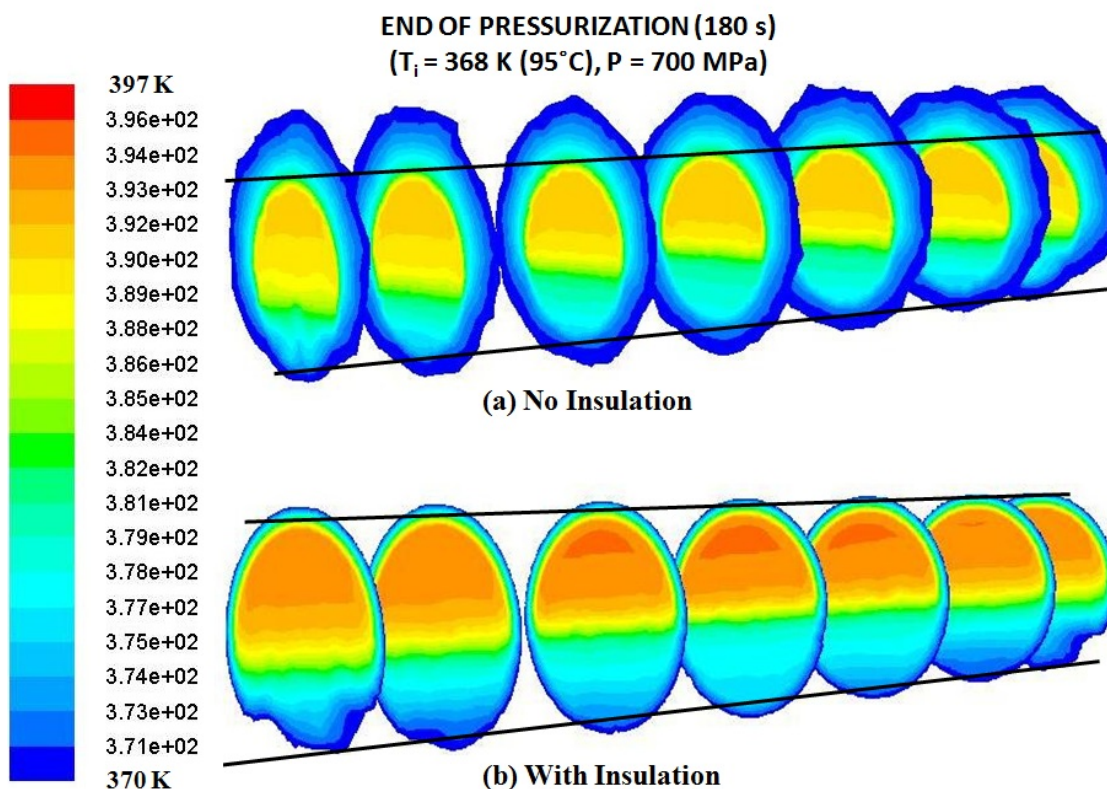


Figure 7-42: Isotherms in water and s.steel vessel for 10 L horizontal vessel (slices) at $T_i = 368 \text{ K}$, $P = 700 \text{ MPa}$, $T_{\text{inlet}} = 298 \text{ K}$, (a) no insulation, & (b) with insulation (12 mm thick) at the end of pressurization (180 s).

The results showed that the temperature distribution was most non-uniform when temperature of inlet water was 298 K and insulation was used to lessen the heat loss to the vessel wall. Therefore, it was concluded that adding insulation to the vessel lead to more non-uniform temperature distribution than without insulation. It was also observed that the temperature distribution was most uniform when the temperature of the inlet water was same as the initial temperature for the process, i.e., slightly better than combined same inlet temperature and insulation.

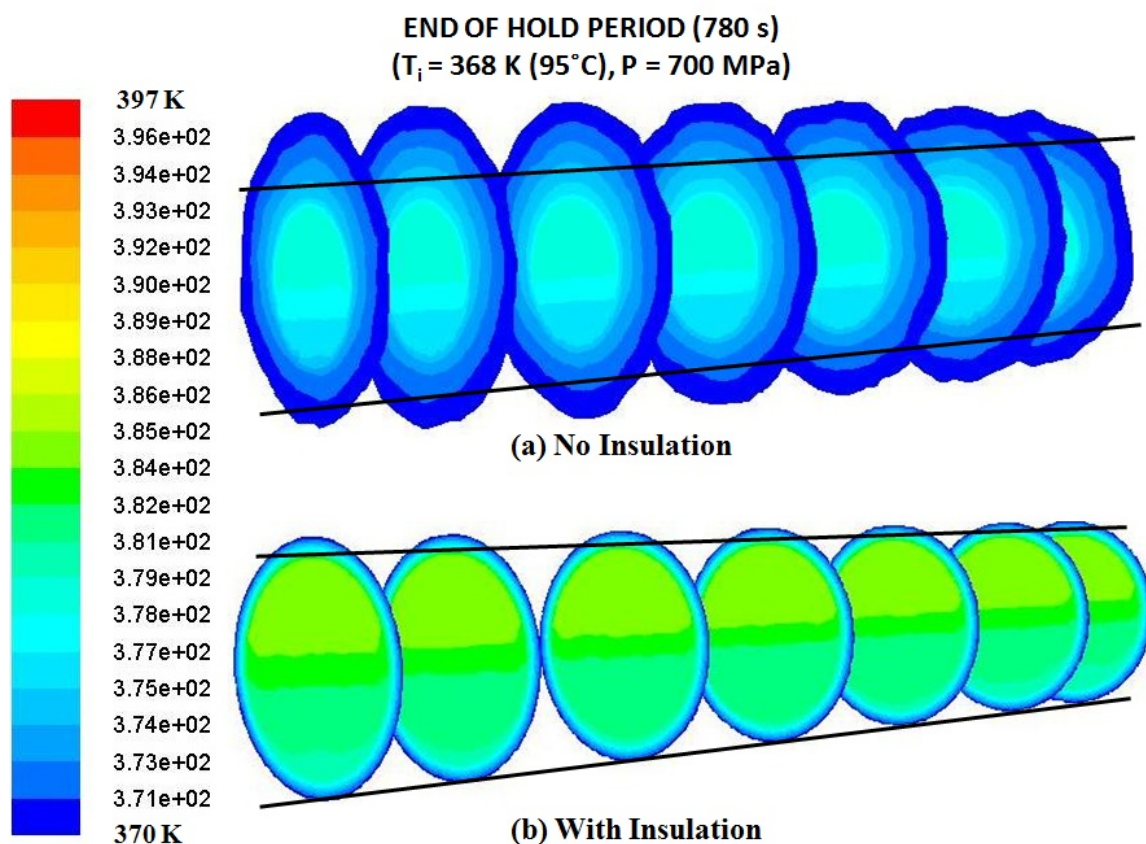


Figure 7-43: Isotherms in water and s.steel vessel for horizontal vessel (slices) at $T_i = 368 \text{ K}$, $P = 700 \text{ MPa}$, $T_{\text{inlet}} = 298 \text{ K}$, (a) no insulation, & (b) with insulation (12 mm thick) at the end of hold period (780 s).

Figure 7-45 shows the corresponding COV of *C. botulinum* inactivation where the most uniformity was achieved with the process where temperature of water inlet was same as the initial temperature of water and the s.steel mass. The inactivation was most non-uniform for the vessel when insulation was included with inlet water temperature of 298 K. This was because, in this case less heat loss from walls lead to higher maximum temperature but water inlet at 298 K results in region of comparatively lower temperature towards the bottom (**Figure 7-42** and **Figure 7-43**). Therefore, overall it gives region of

higher inactivation and lower inactivation resulting in larger standard deviation and hence higher COV.

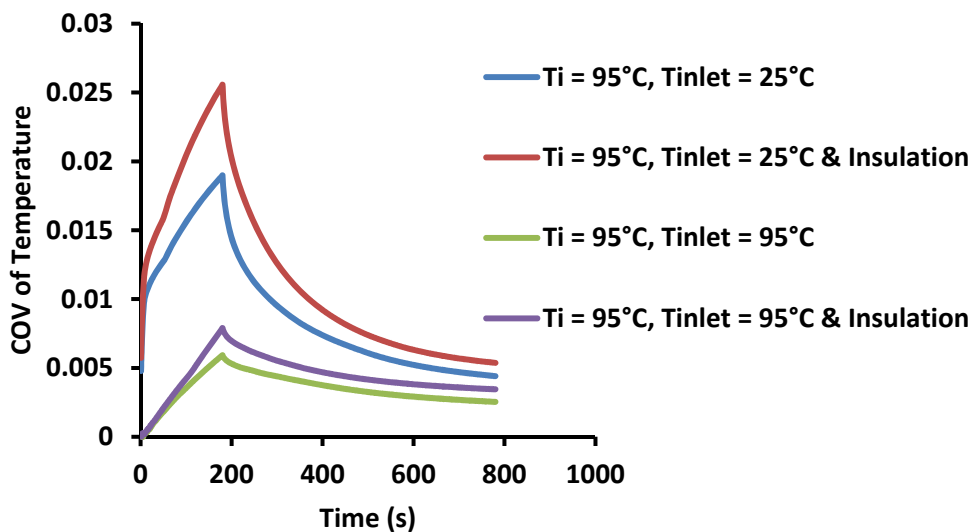


Figure 7-44: COV of temperature for horizontal vessel at $P = 700$ MPa, $T_i = 368$ K, $T_{inlet} = 298$ K (25°C), 368 K (95°C), with or without insulation.

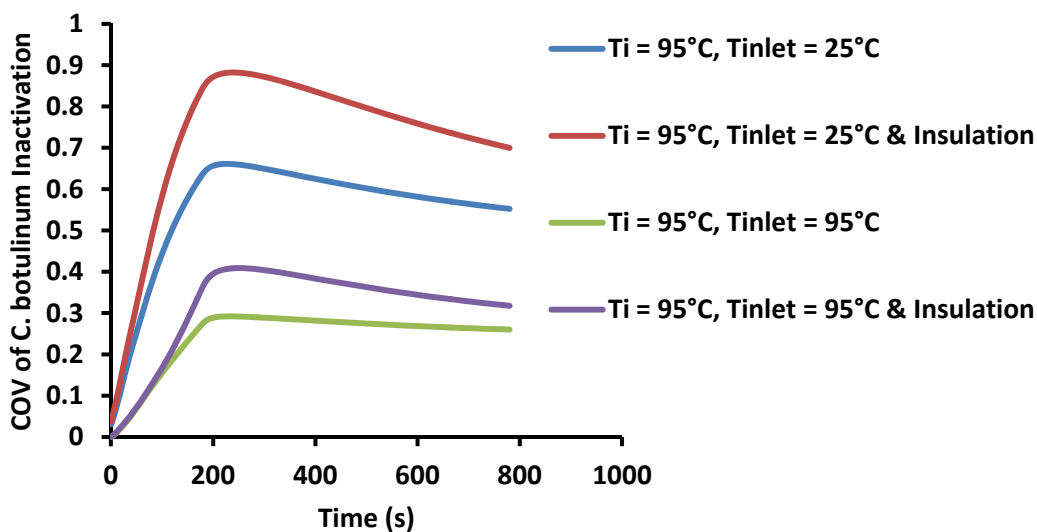


Figure 7-45: COV of *C. botulinum* inactivation for horizontal vessel at $P = 700$ MPa, $T_i = 368$ K, $T_{inlet} = 298$ K (25°C), 368 K (95°C), with or without insulation.

7.3.3.4 Effect of Inserting Pouches

As discussed in section 7.3.2.8, it is important to understand the temperature distribution when food pouches are inserted in the vessel. The horizontal vessel geometry was modified to include 5 oil pouches in the pressure cavity. Since the compression heating value for oils is higher than water, the initial temperature of 333 K was used for numerical simulation in this case.

Figure 7-46 shows the isotherms in pouches placed in the horizontal pressure cavity at the end of hold period, when initial temperature was 333 K, pressure was increased from 0.1 to 700 MPa and temperature of inlet water was 298 K. The results showed that the maximum temperature of oil increased to 375 K at the end of pressurization whereas for water (pressurizing medium) it increased to only 352 K because of lower compression heating value. It can be seen from **Figure 7-46** that at the end of hold period (600 s) the average temperature in the pouch dropped to 359 K because of the heat loss from the oil pouch to the water and convection currents within the pouch. The temperature variation was observed within the oil pouch and from one oil pouch to the other.

7.3.4 Vertical vs. Horizontal Positioned Vessel

So far, we discussed the temperature distributions in a vertical vessel and in a horizontal vessel under various conditions. In this section, we made an attempt to compare the 10 L vessel when operated in vertical position to its operation in horizontal position. Numerical simulation was carried out when pressure was increased from 0.1 to 700 MPa, initial temperature was 368 K and temperature of inlet water was 298 K.

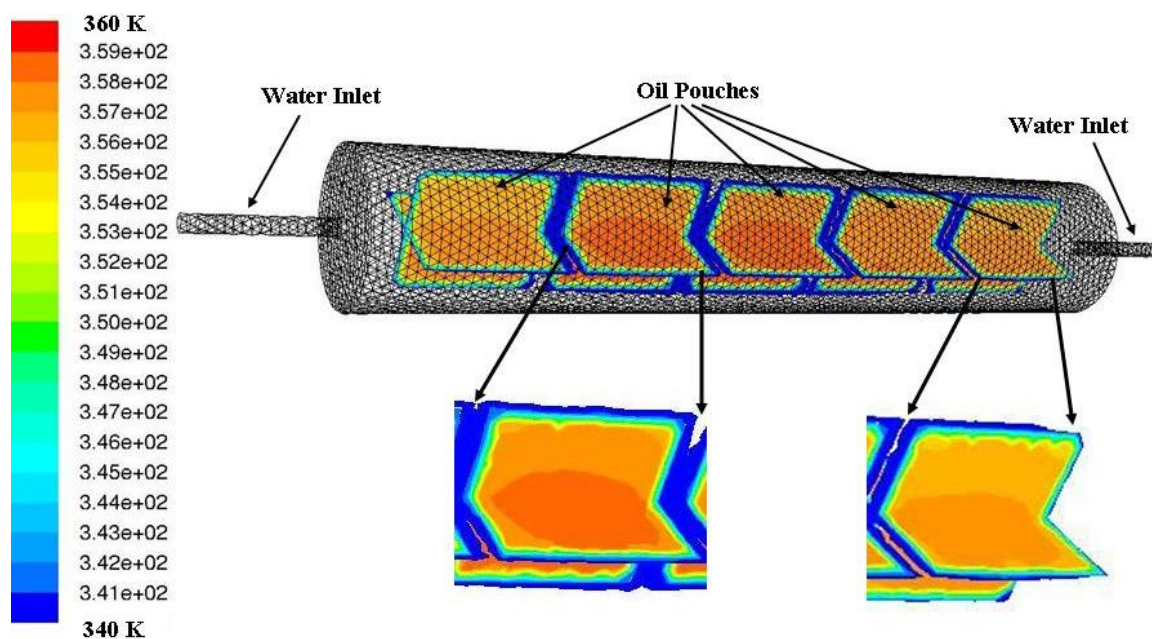


Figure 7-46: Isotherms in oil pouches and s.steel wall for horizontal vessel at $T_i = 333$ K, $P = 700$ MPa, $T_{inlet} = 298$ K, Q (water) = $450,000$ W/m³ for ($0 \leq t \leq 180$ s), Q (olive oil) = $750,000$ W/m³ for ($0 \leq t \leq 180$ s), at the end of pressure hold period (780 s).

Figure 7-47 shows the comparison in COV values in temperature for the two orientations. The COV values for vertical vessel were significantly higher than the horizontal vessel suggesting that the temperature non-uniformity is higher for the vertical vessel compared to horizontal vessel operating under the same pressure temperature conditions. In general, it was observed that the end effects due to water added for compression were lesser in case of horizontal vessel as compared to the vertical vessel. For vertical vessel with water inlet from top, the water flows down under gravity and get mixed with the bulk of the water affecting to a greater length of vessel. Whereas for the

horizontal vessel the water entering from both the sides flows down under gravity and stays very close to the inlets.

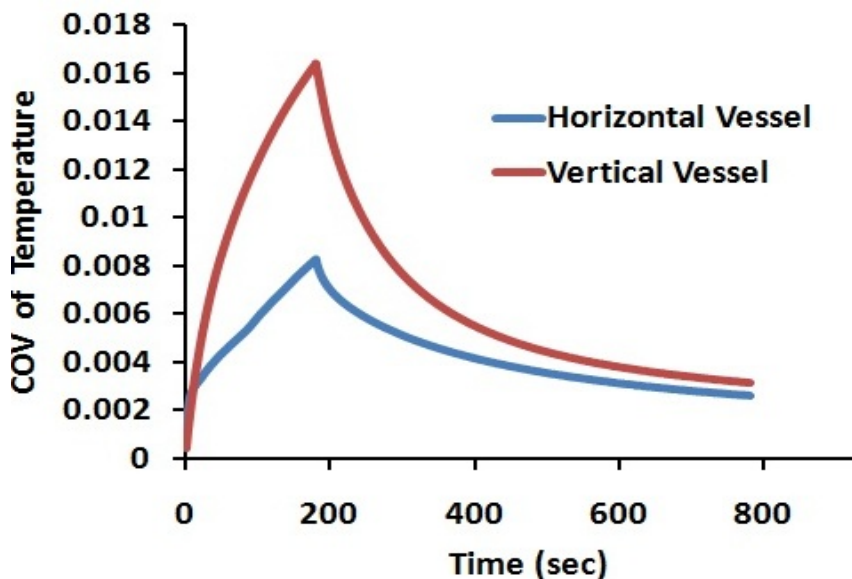


Figure 7-47: COV of temperature for 10 L high pressure vessel when operated in vertical and horizontal positions where $P = 700$ MPa, $T_i = 368$ K, and $T_{inlet} = 298$ K.

7.4 Temperature Non-Uniformity Mapping using Alkaline Phosphatase

For experimental quantification of temperature non-uniformity in vertical vessel, raw milk samples in 1.7 ml centrifuge tubes were placed at eight selected locations (See section 4.2.3 for details) in the vessel. After processing, the raw milk samples at initial temperature of 323 K (50°C), 600 MPa for 20 min, the residual activity of ALP in samples was analyzed using BioVision Alkaline Phosphatase Fluorometric Assay Kit. The residual activity was later converted to percentage inactivation.

The residual activity of ALP was measured using 4-MUP substrate. The alkaline phosphatase enzyme cleaves the substrate 4-MUP to produce highly fluorescent compound 4-MU. The amount of fluorescent signal produced is proportional to the amount of 4-MU. The rate of fluorescence represents conversion of 4-MUP to 4-MU, a measure of ALP activity. Therefore, to calculate the residual activity of ALP in combined pressure-temperature treated raw milk samples, the standard curve for 4-MU was prepared (see section 4.2.3.3 for details). The 4-MU standard curve generated to calculate activity of ALP was fitted with a linear regression line (**Figure 7-48**)

$$y = 4673.5x - 0.0476 \quad (7-22)$$

where, x is the concentration of 4-MU (nmol) and y is the relative fluorescence units.

Figure 7-49 shows the ALP inactivation at selected locations in the vertical vessel at pressure of 600 MPa, initial temperature of 328 K (55°C) and inlet temperature of 298 K (25°C). The results showed significant ($p < 0.05$) difference in inactivation of ALP for

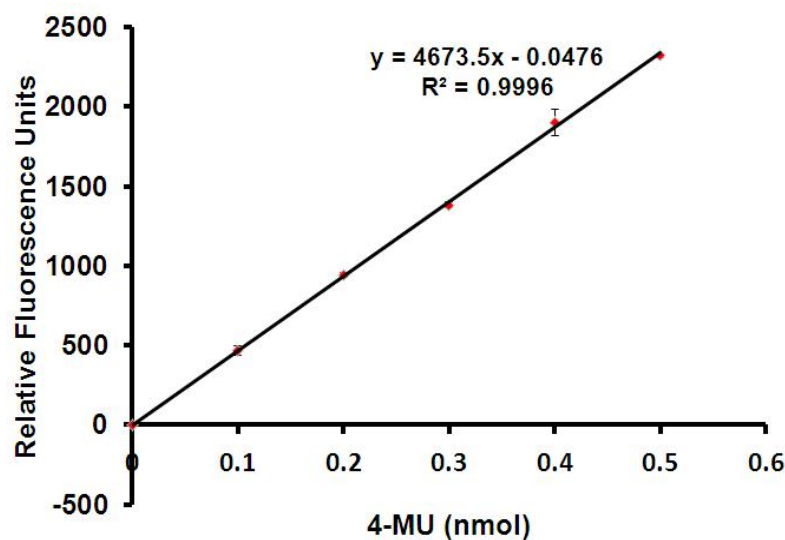


Figure 7-48: The standard curve for 4-MU, relating concentration of 4-MU to relative fluorescence units.

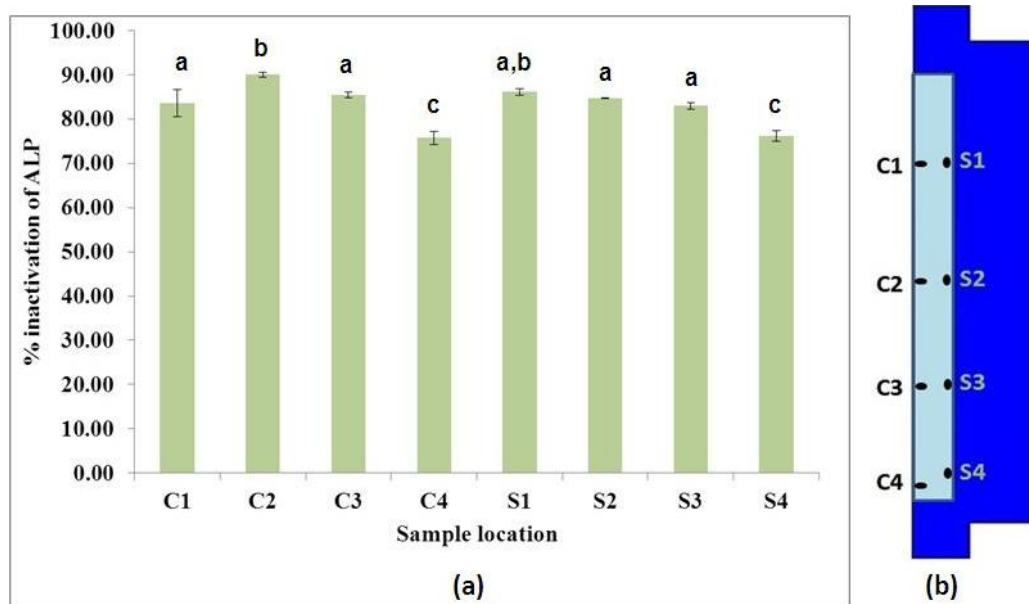


Figure 7-49: (a) Inactivation of ALP at (b) selected locations for vertical vessel at $P = 600$ MPa, $T_i = 328$ K (55°C), $T_{\text{inlet}} = 25^\circ\text{C}$. Letters a,b,c on each bar show statistical significance with $p < 0.05$.

samples placed at different locations as shown in **Figure 7-49**. One-way ANOVA was used to evaluate if there was a significant difference in means obtained at different locations. The result from one way ANOVA showed evidence of significant difference in means, therefore, further analysis was done to investigate which means were different. This was where Tukey multiple comparison test was used. The Tukey test compared the difference between each pair of means and the results for each group were presented in the form of confidence interval as shown in **Figure 7-50**.

Figure 7-50 shows that means for samples C1, C2, C3, C4, S1, S2, S3 and S4 were significantly different from the control sample, i.e., untreated raw milk sample. Also, it shows that the means for treated samples based on their significance were divided into 3 groups i.e., no significant difference between samples located at 1) C1, C3, S1, S2, S3; 2)

C2, S1, and 3) C4, S4. Letters a, b, c on each bar of **Figure 7-49(a)** show the statistical significance ($p < 0.05$) obtained using the confidence interval results from Tukey test.

In **Figure 7-49(a)**, among the samples placed along the center of the vessel, the percentage inactivation for C4 sample was the lowest which can be attributed to its location, i.e., close bottom wall of vessel. This can be explained based on our understanding from the numerical results which showed that temperature towards the bottom region of vessel is always maximum but in proximity of bottom wall the heat loss to the colder vessel wall (at 298 K) takes place throughout the process resulting in lower temperature near the bottom of the vessel. The ALP inactivation for samples placed at location C2 and C3 was found to be higher than the C4 sample, which was due to natural convection currents causing the warm water to rise towards the center. The C1 sample saw inactivation lower than C2 sample because of the colder water inlet effects during the pressurization phase. The inactivation for samples C3 and C1 was not significantly different. In the samples placed close to the side wall of the vessel, the results showed no significant difference in inactivation for samples S1, S2, S3. Whereas sample placed at location S4 showed significant difference which could be because of its proximity to the side and bottom colder vessel walls.

The above results show that non-uniformity in temperature during high pressure processing of foods can result in non-uniform inactivation of ALP.

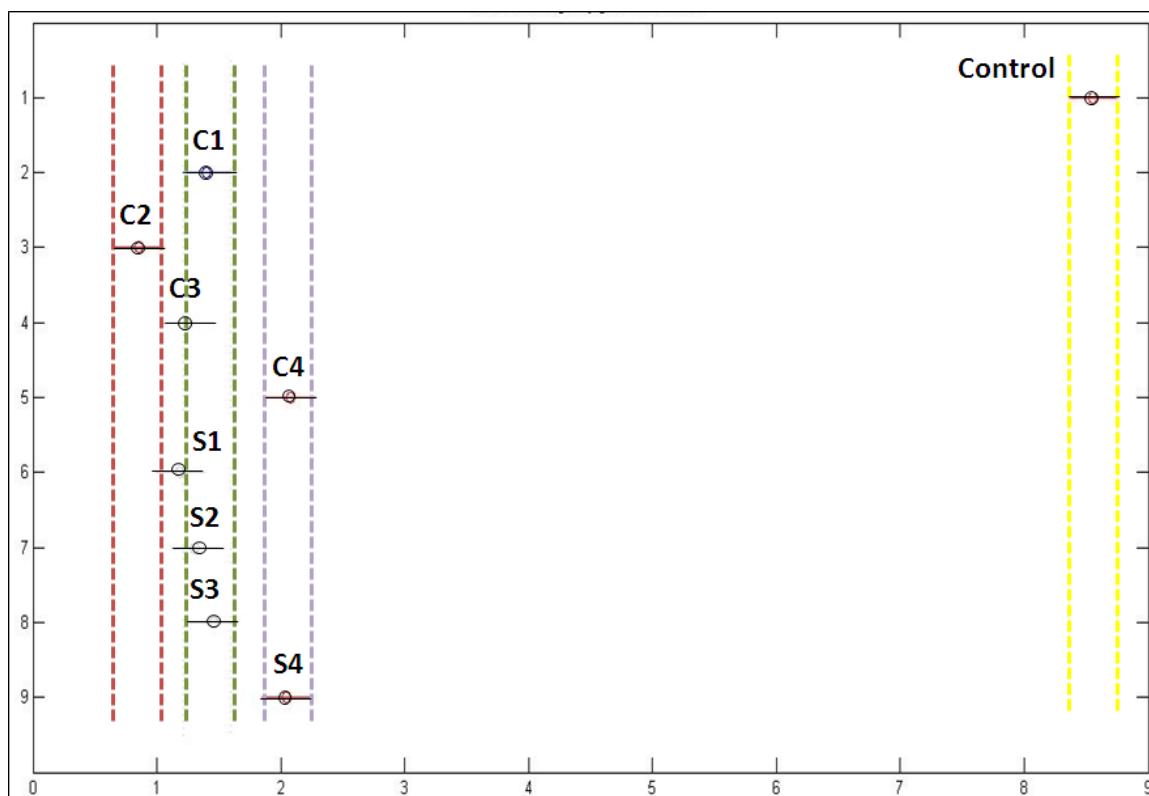


Figure 7-50: Confidence intervals for raw milk samples located at C1, C2, C3, C4, S1, S2, S3, and S4.

8. CONCLUSIONS AND IMPACT

Numerical simulations to predict temperature distribution and its impact on process safety in vertical and horizontal high hydrostatic pressure food processing vessels were carried out. For vessels of both the orientations it was observed that the temperature non-uniformity arose in the pressurizing medium (water) during high pressure processing due to adiabatic compression heating, heat loss at the vessel walls, and colder water pumped into the vessel. The non-uniformity continued during the hold time because of natural convection cooling at the vessel walls.

The predicted results showed that PATS lead to larger temperature differences ~ 18 K in the pressurizing medium in the vessel compared to PATP and cold pasteurization. The difference in temperature was influenced by the initial temperature of process and the temperature of water added to the vessel for compression. For a vertical vessel with water inlet from the top and water inlet from the bottom, the results showed that the water inlet from bottom tended to make the temperature distribution in the axial direction more uniform whereas in radial direction no difference was observed. Also, it was observed that the cooling due to the water inlet from bottom is dominated by the buoyancy forces as opposed to water inlet from the top where it is initially dominated by the water pumped into the vessel (forced convection). Also, it was observed that the hottest region in the vessel was located near the vessel bottom closure for water inlet from the top and near the top closure for water inlet from the bottom. Also, the simulation results for oil pouches in vessel showed non-uniformity in temperature within each pouch, and the variation from pouch to pouch suggesting location dependence.

For validation of the numerical program, the temperature data obtained from the numerical simulation was compared with the experimental data (corrected for lag in temperature measurement due to thermocouple) at selected locations, and a good agreement was obtained. The theoretical analysis presented for correction of measured temperature enabled accurate evaluation of lag in the temperature measurement during pressurization, pressure hold, and pressure release steps of HHPP. For our case, it was found that using the temperature variation recorded by the high pressure thermocouple assembly over predicted the F-value as compared to true temperature variation. This discrepancy in temperature measurement can be particularly of relevance when high pressure high temperature combination is used to inactivate spores as it impacts the sterilization value.

For numerical quantification of non-uniformity in temperature, the data obtained from numerical simulation were analyzed using the COV method. The comparison of high pressure process carried out with and without insulation showed that adding insulation to the vessel did not improve the overall temperature uniformity in the vessel. Whereas adding water for compression at temperature same as the initial temperature for the process resulted in more uniform temperature and more uniform *C. botulinum* inactivation compared to inserting an insulating sleeve or even combining insulating sleeve and adding water at initial temperature. Also, the comparison of vertical (water inlet from top) and horizontal vessels (water inlet from both ends) of same dimensions showed that the temperature was more uniform for the horizontal vessel under same pressure and temperature conditions, as compared to that in the vertical vessel.

For experimental quantification of the non-uniformity in temperature, Alkaline phosphatase (enzyme present in raw milk) was successfully used to detect the temperature variation inside the high pressure vessel. The results showed that the samples placed near wall of the vessel had lower inactivation compared to the samples placed at the center of the vessel due to colder wall effects. Also, the ALP inactivation was higher near the top of the vessel compared to the bottom. Non-uniform inactivation of ALP provided the experimental evidence for the existence of non-uniform temperature distribution in the vessel leading to non-uniform inactivation.

IMPACT

The non-uniform temperature distribution during combined high pressure high temperature process can lead to non-uniform inactivation of spores within the pressurizing medium and food products. The results obtained from this research will be used to determine accurate temperature distribution in vertical and horizontal high pressure vessels which will help to differentiate the effect of temperature and pressure and understand the synergy between pressure and temperature on the inactivation kinetics of enzymes, nutrients, and microorganisms. The predicted temperature distributions for vertical and horizontal vessels will add to the understanding of HHPP users to make a choice between a vertical and a horizontal vessel based on product safety requirements. Also, the knowledge gained will aid the regulating agencies like USDA and USFDA in developing guidelines to ensure safe food products. The results will also be important for food processors and equipment manufacturers to understand the effects of non-uniform thermal treatment on foods processed using PATP and PATS.

9. FUTURE WORK

Several practical solutions have been recommended by researchers to overcome the non-uniformity in temperature during high pressure process. Some of these recommendations such as inserting an insulating sleeve to minimize the heat loss to the vessel wall, adding water for pressurization at initial temperature of the process were studied as part of this research. Makita (1992) emphasized that temperature gradients in the pressure chamber are almost unavoidable, even if a thermostatic jacket is equipped around the pressure vessel. The author suggested that stirring the pressure medium could reduce the gradient but may be technically difficult under pressures higher than 300 MPa.

The next steps to this study will include:

- 1) Explore better techniques for measuring temperature in the high pressure vessels during processing
- 2) Validation of the numerical simulation program for horizontal vessel using the temperature history obtained from experiments
- 3) Carry out simulations with food packages in the vessels with more accurate pressure-temperature dependent properties such as density, viscosity, thermal conductivity
- 4) Develop the numerical model with food packages taking into account the change in volume caused due to compression based on the food sample properties and evaluate the impact on temperature and microbial distributions
- 5) Evaluate the impact of food sample to pressurizing medium ratio on the temperature and microbial distributions
- 6) Measurement of flow inside the high pressure vessels during the process if possible.

10. BIBLIOGRAPHY

1. Ahmed, J., Ramaswamy, H.S., Hiremath, N., (2005). The effect of high pressure treatment on rheological characteristics and colour of mango pulp. *International Journal of Food Science & Technology* 40(8), 885-895.
2. Ardia, A., (2004). Process Considerations on the Application of High Pressure Treatment at Elevated Temperature Levels for Food Preservation. Technische Universität Berlin.
3. Balasubramaniam, V.M., Farkas, D., Turek, E.J., (2008). Preserving foods through high-pressure processing. *Food Technology* 62(11), 32-38.
4. Balasubramaniam, S., Balasubramaniam, V.M., (2003). Compression heating influence of pressure transmitting fluids on bacteria inactivation during high pressure processing. *Food Research International* 36(7), 661-668.
5. Barbosa-Cánovas, G.V., Rodriguez, J.J., (2005). Thermodynamic aspects of high hydrostatic pressure food processing, in: Barbosa-Cánovas, G.V., Tapia, M.S., Cano, M.P. (Eds.), *Novel Food Processing Technologies*. CRC Press.
6. Bárcenas, M.E., Altamirano-Fortoul, R., Rosell, C.M., (2010). Effect of high pressure processing on wheat dough and bread characteristics. *LWT - Food Science and Technology* 43(1), 12-19.
7. Brown, P., Meyer, R., Cardone, F., Pocchiari, M., (2003). Ultra-high-pressure inactivation of prion infectivity in processed meat: A practical method to prevent human infection. *Proceedings of the National Academy of Sciences* 100(10), 6093-6097.
8. Butz, P., Fernandez, A., Fister, H., Tauscher, B., (1997). Influence of High Hydrostatic Pressure on Aspartame: Instability at Neutral pH. *Journal of Agricultural and Food Chemistry* 45(2), 302-303.
9. Butz, P., Fernández García, A., Tauscher, B., (2002). Influence of high pressure treatment on sensorial and nutritional quality of fruit and vegetables, in: Rikimaru, H. (Ed.), *Progress in Biotechnology*. Elsevier, pp. 417-421.

10. Butz, P., Tauscher, B., (2002). Emerging technologies: chemical aspects. *Food Research International* 35(2–3), 279-284.
11. Cheftel, J.C., Levy, J., Dumay, E., (2000). Pressure-assisted greazing and thawing: principles and potential applications. *Food Reviews International* 16(4), 453-483.
12. Chen, H., Hoover, D.G., (2003). Modeling the combined effect of high hydrostatic pressure and mild heat on the inactivation kinetics of *Listeria monocytogenes* Scott A in whole milk. *Innovative Food Science & Emerging Technologies* 4(1), 25-34.
13. Chevalier, D., Le Bail, A., Sequeira-Munoz, A., Simpson, B.K., Ghoul, M., (2002). Pressure shift freezing of turbot (*Scophthalmus maximus*) and carp (*Cyprinus carpio*): effect on ice crystals and drip volumes, in: Rikimaru, H. (Ed.), *Progress in Biotechnology*. Elsevier, pp. 577-582.
14. Chourot, J.-M., Boillereaux, L., Havet, M., Le Bail, A., (1997). Numerical modeling of high pressure thawing: Application to water thawing. *Journal of Food Engineering* 34(1), 63-75.
15. De Heij, B.C.W., Van Schepdael, J.M.M.L., Moezelaar, R., Hoogland, H., Master, M.A., Van Den Berg, W.R., (2003). High-pressure sterilization: maximizing the benefits of adiabatic heating. *Food Technology* 57(3), 37-41.
16. Denys, S., Ludikhuyze, L.R., Van Loey, A.M., Hendrickx, M.E., (2000a). Modeling Conductive Heat Transfer and Process Uniformity during Batch High-Pressure Processing of Foods. *Biotechnology Progress* 16(1), 92-101.
17. Denys, S., Van Loey, A.M., Hendrickx, M.E., (2000b). A modeling approach for evaluating process uniformity during batch high hydrostatic pressure processing: combination of a numerical heat transfer model and enzyme inactivation kinetics. *Innovative Food Science & Emerging Technologies* 1(1), 5-19.
18. Denys, S., Van Loey, A.M., Hendrickx, M.E., Tobback, P.P., (1997). Modeling Heat Transfer during High-Pressure Freezing and Thawing. *Biotechnology Progress* 13(4), 416-423.
19. Doona, C.J., Feeherry, F.E., (2007). *High pressure processing of foods*. Blackwell Pub.

20. Farkas, D.F., (2005). Internet site http://www.elmhurstresearch.com/hpp_history.htm.
21. Fernández, P.P., Otero, L., Guignon, B., Sanz, P.D., (2006). High-pressure shift freezing versus high-pressure assisted freezing: Effects on the microstructure of a food model. *Food Hydrocolloids* 20(4), 510-522.
22. Fryer, D.M., Harvey, J.F., (1997). *High pressure vessels*. Chapman & Hall.
23. Ghani, A.A., Mohammed, F., (2007). Modeling of High-Pressure Food Processing Using CFD, *Computational Fluid Dynamics in Food Processing*. CRC Press, pp. 537-554.
23. Ghani, A.G.A., Farid, M.M., (2007). Numerical simulation of solid–liquid food mixture in a high pressure processing unit using computational fluid dynamics. *Journal of Food Engineering* 80(4), 1031-1042.
24. Grauwet, T., Plancken, I.V.d., Vervoort, L., Hendrickx, M.E., Loey, A.V., (2010). Protein-based indicator system for detection of temperature differences in high pressure high temperature processing. *Food Research International* 43(3), 862-871.
25. Grauwet, T., Van der Plancken, I., Vervoort, L., Hendrickx, M.E., Loey, A.V., (2009). Investigating the potential of *Bacillus subtilis* α -amylase as a pressure-temperature-time indicator for high hydrostatic pressure pasteurization processes. *Biotechnology Progress* 25(4), 1184-1193.
26. Hartmann, C., (2002). Numerical simulation of thermodynamic and fluid-dynamic processes during the high-pressure treatment of fluid food systems. *Innovative Food Science & Emerging Technologies* 3(1), 11-18.
27. Hartmann, C., Delgado, A., (2002a). Numerical simulation of convective and diffusive transport effects on a high-pressure-induced inactivation process. *Biotechnology and Bioengineering* 79(1), 94-104.
28. Hartmann, C., Delgado, A., (2002b). Numerical simulation of thermofluidynamics and enzyme inactivation in a fluid food system under high hydrostatic pressure, in: Rikimaru, H. (Ed.), *Progress in Biotechnology*. Elsevier, pp. 533-540.
29. Hartmann, C., Delgado, A., (2003). The influence of transport phenomena during high-pressure processing of packed food on the uniformity of enzyme inactivation. *Biotechnology and Bioengineering* 82(6), 725-735.

30. Hartmann, C., Delgado, A., (2004). Numerical simulation of the mechanics of a yeast cell under high hydrostatic pressure. *Journal of biomechanics* 37(7), 977-987.
31. Hartmann, C., Delgado, A., Szymczyk, J., (2003). Convective and diffusive transport effects in a high pressure induced inactivation process of packed food. *Journal of Food Engineering* 59(1), 33-44.
32. Hartmann, C., Schuhholz, J.-P., Kitsubun, P., Chapleau, N., Le Bail, A., Delgado, A., (2004). Experimental and numerical analysis of the thermofluidynamics in a high-pressure autoclave. *Innovative Food Science & Emerging Technologies* 5(4), 399-411.
33. Hayakawa, I., Linko, Y.-Y., Linko, P., (1996). Novel Mechanical Treatments of Biomaterials. *LWT - Food Science and Technology* 29(5-6), 395-403.
34. Hayashi, R., (2002). High pressure in bioscience and biotechnology: pure science encompassed in pursuit of value. *Biochimica et Biophysica Acta (BBA) - Protein Structure and Molecular Enzymology* 1595(1-2), 397-399.
35. Hendrickx, M., Ludikhuyze, L., Van den Broeck, I., Weemaes, C., (1998). Effects of high pressure on enzymes related to food quality. *Trends in Food Science & Technology* 9(5), 197-203.
36. Hendrickx, M.E.G., (2001). *Ultra high pressure treatments of foods*. Kluwer Acad./Plenum Publ., New York, NY [u.a.].
37. Henry, C.J.K., Chapman, C., (2002). *The nutrition handbook for food processors*. CRC Press.
38. Heremans, K., (2002). The effects of high pressure on biomaterials, in: Hendrickx, M.E.G., Knorr, D.W. (Eds.), *Ultra high pressure treatments of foods*. Kluwer Academic/Plenum Publishers.
39. Hoover, D.G., Metrick, C., Papineau, A.M., Farkas, D.F., Knorr, D., (1989). Biological effects of high hydrostatic pressure on food microorganisms. *Food Technology* 43(3), 99-107.
40. Indrawati, I., Ludikhuyze, L.R., Van Loey, A.M., Hendrickx, M.E., (2000). Lipoxygenase Inactivation in Green Beans (*Phaseolus vulgaris* L.) Due to High

- Pressure Treatment at Subzero and Elevated Temperatures. *Journal of Agricultural and Food Chemistry* 48(5), 1850-1859.
41. Juliano, P., Knoerzer, K., Fryer, P.J., Versteeg, C., (2009). *C. botulinum* inactivation kinetics implemented in a computational model of a high-pressure sterilization process. *Biotechnology Progress* 25(1), 163-175.
 42. Kalchayanand, N., Sikes, A., Dunne, C.P., Ray, B., (1998). Factors influencing death and injury of foodborne pathogens by hydrostatic pressure-pasteurization. *Food Microbiology* 15(2), 207-214.
 43. Karatzas, K.A.G., Bennik, M.H.J., (2002). Characterization of a *Listeria monocytogenes* Scott A Isolate with High Tolerance towards High Hydrostatic Pressure. *Applied and Environmental Microbiology* 68(7), 3183-3189.
 44. Khurana, M., Karwe, M., (2009). Numerical Prediction of Temperature Distribution and Measurement of Temperature in a High Hydrostatic Pressure Food Processor. *Food and Bioprocess Technology* 2(3), 279-290.
 45. Kingsley, D.H., Hoover, D.G., Papafragkou, E., Richards, G.P., (2002). Inactivation of Hepatitis A Virus and a Calicivirus by High Hydrostatic Pressure. *Journal of Food Protection* 65(10), 1605-1609.
 46. Klotz, B., Pyle, D.L., Mackey, B.M., (2007). New Mathematical Modeling Approach for Predicting Microbial Inactivation by High Hydrostatic Pressure. *Applied and Environmental Microbiology* 73(8), 2468-2478.
 47. Knoerzer, K., Buckow, R., Chapman, B., Juliano, P., Versteeg, C., (2010a). Carrier optimisation in a pilot-scale high pressure sterilisation plant – An iterative CFD approach employing an integrated temperature distributor (ITD). *Journal of Food Engineering* 97(2), 199-207.
 48. Knoerzer, K., Buckow, R., Sanguansri, P., Versteeg, C., (2010b). Adiabatic compression heating coefficients for high-pressure processing of water, propylene-glycol and mixtures – A combined experimental and numerical approach. *Journal of Food Engineering* 96(2), 229-238.

49. Knoerzer, K., Buckow, R., Versteeg, C., (2010c). Adiabatic compression heating coefficients for high-pressure processing – A study of some insulating polymer materials. *Journal of Food Engineering* 98(1), 110-119.
50. Knoerzer, K., Juliano, P., Gladman, S., Versteeg, C., Fryer, P.J., (2007). A computational model for temperature and sterility distributions in a pilot-scale high-pressure high-temperature process. *AIChE Journal* 53(11), 2996-3010.
51. Knorr, D., (1999). Novel approaches in food-processing technology: new technologies for preserving foods and modifying function. *Current Opinion in Biotechnology* 10(5), 485-491.
52. Knorr, D., (2003). Impact of non-thermal processing on plant metabolites. *Journal of Food Engineering* 56(2–3), 131-134.
53. Knorr, D., Ade-Omowaye, B.I.O., Heinz, V., (2002). Nutritional improvement of plant foods by non-thermal processing. *Proceedings of the Nutrition Society* 61(02), 311-318.
54. Koizumi, M., Nishihara, M., (1991). *Isostatic pressing: technology and applications*. Elsevier Applied Science.
55. Krebbers, B., Matser, A.M., Hoogerwerf, S.W., Moezelaar, R., Tomassen, M.M.M., van den Berg, R.W., (2003). Combined high-pressure and thermal treatments for processing of tomato puree: evaluation of microbial inactivation and quality parameters. *Innovative Food Science & Emerging Technologies* 4(4), 377-385.
56. Kural, A.G., Chen, H., (2008). Conditions for a 5-log reduction of *Vibrio vulnificus* in oysters through high hydrostatic pressure treatment. *International Journal of Food Microbiology* 122(1–2), 180-187.
57. LeBail, A., Chevalier, D., Mussa, D.M., Ghoul, M., (2002a). High pressure freezing and thawing of foods: a review. *International Journal of Refrigeration* 25(5), 504-513.
58. LeBail, A., Mussa, D., Rouillé, J., Ramaswamy, H.S., Chapleau, N., Anton, M., Hayert, M., Boillereaux, L., Chevalier, D., (2002b). High pressure thawing. Application to selected sea-foods, in: Rikimaru, H. (Ed.), *Progress in Biotechnology*. Elsevier, pp. 563-570.

59. Lopez-Malo, A., Palou, E., Barbosa-Canovas, G.V., Swanson, B.G., Welti-Chanes, J., (2000). Minimally processed foods with high hydrostatic pressure, in: Lozano, J.E. (Ed.), *Trends in Food Engineering*. Technomic Pub.
60. Ludikhuyze, L., Hendrickx, M.E.G., (2002). Effects of High Pressure on Chemical Reactions Related to Food Quality Ultra High Pressure Treatments of Foods, in: Hendrickx, M.E.G., Knorr, D., Ludikhuyze, L., Loey, A., Heinz, V. (Eds.). Springer US, pp. 167-188.
61. Makita, T., (1992). Application of high pressure and thermophysical properties of water to biotechnology. *Fluid Phase Equilibria* 76, 87-95.
62. Messens, W., Van Camp, J., Huyghebaert, A., (1997). The use of high pressure to modify the functionality of food proteins. *Trends in Food Science & Technology* 8(4), 107-112.
63. Meyer, R.S., (2000). Ultra high pressure, high temperature food preservation process, U.S. Patent 6,017,572.
64. Meyer, R.S., (2001). Ultra high pressure, high temperature food preservation process, U.S. Patent 6,177,115 B1.
65. Molina, E., Ledward, D.A., (2003). Effects of combined high-pressure and heat treatment on the textural properties of soya gels. *Food Chemistry* 80(3), 367-370.
66. Nienaber, U., Shellhammer, T.H., (2001). High-Pressure Processing of Orange Juice: Kinetics of Pectinmethylesterase Inactivation. *Journal of Food Science* 66(2), 328-331.
67. Norton, T., Sun, D.-W., (2008). Recent Advances in the Use of High Pressure as an Effective Processing Technique in the Food Industry. *Food and Bioprocess Technology* 1(1), 2-34.
68. Otero, L., Molina-García, A.D., Ramos, A.M., Sanz, P.D., (2002a). A Model for Real Thermal Control in High-Pressure Treatment of Foods. *Biotechnology Progress* 18(4), 904-908.
69. Otero, L., Molina-García, A.D., Sanz, P.D., (2002b). Some Interrelated Thermophysical Properties of Liquid Water and Ice. I. A User-Friendly Modeling

- Review for Food High-Pressure Processing. *Critical Reviews in Food Science and Nutrition* 42(4), 339-352.
70. Otero, L., Molina, A.D., Sanz, P.D., (2002c). Thermal Control Simulation in High Pressure Treatment of Foods. *High Pressure Research* 22(3-4), 627-631.
 71. Pehl, M., Werner, F., Delgado, A., (2000). First visualization of temperature fields in liquids at high pressure using thermochromic liquid crystals. *Experiments in Fluids* 29(3), 302-304.
 72. Pehl, M., Werner, F., Delgado, A., (2002). Experimental investigation on thermofluidodynamical processes in pressurized substances, in: Rikimaru, H. (Ed.), *Progress in Biotechnology*. Elsevier, pp. 429-435.
 73. Ponce, E., Beltran, E., Sendra, E., Mor-Mur, M., Guamis, B., Pla, R., (1998). Development of a cream caramel by high hydrostatic pressure at low temperature, in: Ludwig, H. (Ed.), *Advances in High Pressure Bioscience and Biotechnology*. Springer, Germany.
 74. Rasanayagam, V., Balasubramaniam, V.M., Ting, E., Sizer, C.E., Bush, C., Anderson, C., (2003). Compression Heating of Selected Fatty Food Materials during High-pressure Processing. *Journal of Food Science* 68(1), 254-259.
 75. Rastogi, N.K., Raghavarao, K.S.M.S., Balasubramaniam, V.M., Niranjana, K., Knorr, D., (2007). Opportunities and Challenges in High Pressure Processing of Foods. *Critical Reviews in Food Science and Nutrition* 47(1), 69-112.
 76. Rauh, C., Baars, A., Delgado, A., (2009). Uniformity of enzyme inactivation in a short-time high-pressure process. *Journal of Food Engineering* 91(1), 154-163.
 77. Reddy, N.R., Solomon, H.M., Fingerhut, G.A., Rhodehamel, E.J., Balasubramaniam, V.M., Palaniappan, S., (1999). Inactivation of *Clostridium botulinum* type E spores by high pressure processing. *Journal of Food Safety* 19(4), 277-288.
 78. Riahi, E., Ramaswamy, H.S., (2004). High pressure inactivation kinetics of amylase in apple juice. *Journal of Food Engineering* 64(2), 151-160.
 79. Sánchez-Moreno, C., Plaza, L., de Ancos, B., Cano, M.P., (2002). Vitamin C, Provitamin A Carotenoids, and Other Carotenoids in High-Pressurized Orange Juice

- during Refrigerated Storage. *Journal of Agricultural and Food Chemistry* 51(3), 647-653.
80. Schauwecker, A., (2004). New technologies: under pressure, *Food Product Design*. Virgo Publishing, Online.
 81. Shigehisa, T., Ohmori, T., Saito, A., Taji, S., Hayashi, R., (1991). Effects of high hydrostatic pressure on characteristics of pork slurries and inactivation of microorganisms associated with meat and meat products. *International Journal of Food Microbiology* 12(2-3), 207-215.
 82. Simpson, R.K., Gilmour, A., (1997). The effect of high hydrostatic pressure on *Listeria monocytogenes* in phosphate-buffered saline and model food systems. *Journal of Applied Microbiology* 83(2), 181-188.
 83. Smelt, J.P.P.M., (1998). Recent advances in the microbiology of high pressure processing. *Trends in Food Science & Technology* 9(4), 152-158.
 84. Solt, M.A.A., K. , (1998). Microscopic and rheological characterization of high pressure treated starch dispersions, in: Ludwig, H. (Ed.), *International Conference on High Pressure Bioscience and Biotechnology*. Springer, Heidelberg, Germany.
 85. Spilimbergo, S., Elvassore, N., Bertucco, A., (2002). Microbial inactivation by high-pressure. *The Journal of Supercritical Fluids* 22(1), 55-63.
 86. Suzuki, A., (2002). High pressure-processed foods in Japan and the world, in: Rikimaru, H. (Ed.), *Progress in Biotechnology*. Elsevier, pp. 365-374.
 87. Ting, E.B., V. M.; & Raghubeer, E., (2002). Determining Thermal Effects in High-Pressure Processing. *Food Technology* 56(2), 31-35.
 88. Trujillo, A.J., Capellas, M., Buffa, M., Royo, C., Gervilla, R., Felipe, X., Sendra, E., Saldo, J., Ferragut, V., Guamis, B., (2000). Application of high pressure treatment for cheese production. *Food Research International* 33(3), 311-316.
 89. Venugopal, V., (2006). *Seafood processing: adding value through quick freezing, retortable packaging, and cook-chilling*. CRC/Taylor & Francis.
 90. Zhu, S., Naim, F., Marcotte, M., Ramaswamy, H., Shao, Y., (2008). High-pressure destruction kinetics of *Clostridium sporogenes* spores in ground beef at elevated temperatures. *International Journal of Food Microbiology* 126(1-2), 86-92.

11. APPENDIX I

(i) UDF for Density

```
#include "udf.h"                                /*header file udf.h*/

DEFINE_PROPERTY(cell_density,c,t) /*macro allows the function to be defined*/
{
    real rho, time;                               /* defines custom variables (rho,time) of data
                                                    type real i.e. returns real value to solver */

    real temp = C_T(c,t);                         /*returns real cell temperature*/

    time = RP_Get_Real("flow-time"); /* returns real current flow time in seconds*/

    rho = 1155 - 0.5*temp+time; /* from equation (6-7)*/

    return rho;
}
```

(ii) UDF for Thermal Conductivity

```
#include "udf.h"

DEFINE_PROPERTY(cell_thermal_conductivity,c,t)
{
    real ktc, time;

    real temp = C_T(c,t);

    time = RP_Get_Real("flow-time");

    ktc = 0.18 + 0.0014*temp+0.0011*time; /* from equation (6-8)*/

    return ktc;
}
```

(iii) UDF for Viscosity

```
#include "udf.h"

DEFINE_PROPERTY(cell_viscosity,c,t)

{

    real meu, time;

    real temp = C_T(c,t);

    time = RP_Get_Real("flow-time");

    meu = 0.0037 - 9.7*0.000001*temp+0.0000015*time; /* from equation (6-9)*/

    return meu;

}
```

(iv) UDF for log(No/N)

Also, for numerical program to calculate the cumulative log(No/N), a UDF source file was written to include the inactivation calculation for *C. botulinum*.

```
#include "udf.h"

DEFINE_EXECUTE_AT_END(logkill) /* macro is executed at the end of the time
                                step*/

{

    Domain *d; /* d is declared as a variable or domain is a structure data type that stores
                data associated with a collection of node, face and cell thread in a mesh*/

    Thread *t; /* thread is a structure data type that stores data that is common to groups
                or faces it represents*/

    real time, dt, D, Z, T, Tref;
```

```

int iter;

cell_t c; /* cell_t is a integer data type that identifies a particular cell within a cell
           thread*/

d = Get_Domain(1); /*returns fluid domain pointer*/

dt = RP_Get_Real("physical-time-step"); /*returns real current physical time step size
                                         in seconds*/

time = RP_Get_Real("flow-time");

iter = RP_Get_Integer("time-step");

Tref = 121.1; /*Reference temperature in celcius*/

Z = 10; /* Z-value for C. botulinum*/

D = 12.6; /* D-value for C. botulinum in seconds*/

Message0("Running execute at end of logkill, time-step=%i, flow-time=%fn", iter,
time);

If (iter==1)
{
Thread_loop_c(t,d)
{
Message("Initializing UDMI(0) = 0.000 prior to 1st iteration F calculation\n");

If (FLUID_THREAD_P(t))
{
begin_c_loop(c,t)

C_UDMI(c,t,0)=0.00;

end_c_loop (c,t)

```

```
}  
}  
}  
thread_loop_c(t,d)  
  
{  
if (FLUID_THREAD_P(t))  
{  
begin_c_loop(c,t)  
T = C_T(c,t);  
C_UDMI(c,t,0)= (pow(10.0,(((T-273.15)-Tref)/Z))*dt)/D + C_UDMI(c,t,0);  
end_c_loop(c,t)  
}  
}  
fflush(stdout);  
}
```